Metal-nanoparticles: synthesis and application in catalysis

Cumulative dissertation

for the attainment of the title of doctor
in the Faculty of Mathematics and Natural Sciences
at the Heinrich Heine University Düsseldorf

presented by

Raquel Marcos Esteban
from Madrid

Düsseldorf, October 2015

from the institute for Anorganische Chemie und Strukturchemie I
at the Heinrich Heine University Düsseldorf

Published by permission of the
Faculty of Mathematics and Natural Sciences at
Heinrich Heine University Düsseldorf

Supervisor: Prof. Dr. Christoph Janiak
Co-supervisor: Prof. Dr. Christian Ganter

Date of the oral examination: 20 November 2015

Declaration

I hereby declare that I wrote the present dissertation without using any other aids that those cited regarding to the “Grundsätze zur Sicherung gutter wissenschaftlicher Praxis an der Heinrich-Heine-Universität Düsseldorf”. I have clearly identified the source of the passages that are taken from other works in each individual case.

_____ _____

Date, location Signature

Acknowledgments

Firstly, I would like to express my gratitude to my supervisor, Prof. Dr. Christoph Janiak, for giving me the opportunity to work on his group. In particular, I am grateful for the continuous support during my doctoral research and for the supervision, cooperation and correction of the publications along these years.

I would also like to thank my co-supervisor Prof. Dr. Christian Ganter.

My sincere thanks goes to my *Mädelsbüro*, Anna Christin Kautz, Christina Rutz and Laure Cuignet, for making me feel at home, teaching me how to say *Röntgen* and for having a little place for this Spaniard in their *Herz*. I will never forget our long conversations and tee-time with lot of laughs (and many tears).

I would like to thank Dr. Juri Barthel and Prof. Dr. Fischer & coworkers for the cooperation's on the manuscripts.

I thank my colleagues for the good working atmosphere and for their kindness help for the different measurements and instrumentation. Specially, I would like to thank Hajo Meyer, Karsten Klauke, Dr. Kai Schütte, and Susann Wegner for their TEM and XPS measurements, and for the help and advice in our common research field; Annette Ricken for the AAS and Birgit Tommes for the IR analysis. Martin Wickenheisser for the company in our long and chaotic train travels every day with unforgettable anecdotes and snoring ☺. I would also want to thank Dr. Francisca Alberti for her kind help and tips in the first months of my work. Annika Herbst, the other sew-crafty lady in the group; Irina Gruber, Sandra Niessing, Dr. Ines Dumsch, Mike Lucka and Max Klopotowski for their conversations and their never-ending cookies. I also want to thank to my bachelor students, in particular, Ester Montoya and Philipp Brandt, and for the nice and amazing time during this almost four years I would also like to thank Sebastian Glomb, Dennis Dietrich, Thorsten Bunte, Dietmar Frunzke, Claudia Schäfer, Christian Heering, Subarna Dey, and Ilka Simon.

To my friends, Sonia, Patri, Cris, Zaira and Celia, I am very thankful for your unconditional support, it doesn't matter where or how far we are, it is a pleasure coming back to home.

Specially, I would like to thank my best friends, my mom and my sister Yolita, my dad, Bea, my little monster, Jorge, and my family and family-in-law who are supporting me wherever I go and to be there in the most difficult times, and of course, who cared about us providing *mucho jamón, chorizo y salchichón* (and love ☺) in our journey to Germany.

Last but not least, to my boyfriend Carlos. My words cannot express my gratitude to you. Your helping words in the bad moments, our long sessions of "*sofa, palomitas, tostas, manta y peli*" ☺, our unforgettable trips, our dancing moments at home with *Queen* as soundtrack and… just for making me laugh every time I get home!

¡**Muchas gracias por todo**!

to my family

This cumulative thesis was done from February 2012 to November 2015 at the Heinrich-Heine University of Düsseldorf in the working group of Prof. Dr. Christoph Janiak and is divided in three main sections: introduction, publications and unpublished results. The **publications** are already submitted or accepted for publication.

Publications (in a reverse chronological order)

1) Iridium@graphene composite nanomaterials synthesized in ionic liquid as re-usable catalysts for solvent-free hydrogenation of benzene and cyclohexene.

R. Marcos Esteban, K. Schütte, P. Brandt, D. Marquardt, H. Meyer, F. Beckert, R. Mülhaupt, H. Kölling, C. Janiak, *Nano-Structures & Nano-Objects* **2015**, *2*, 11–18. http://dx.doi.org/10.1016/j.nanoso.2015.07.001

2) Synthesis of ruthenium@graphene nanomaterials in propylene carbonate as re-usable catalysts for the solvent-free hydrogenation of benzene.

R. Marcos Esteban, K. Schütte, D. Marquardt, J. Barthel, F. Beckert, R. Mülhaupt, C. Janiak, *Nano-Structures & Nano-Objects* **2015**, *2*, 28–34.
http://dx.doi.org/10.1016/j.nanoso.2015.07.002

3) Synthesis and application of metal nanoparticle catalyst in ionic liquid media using metal carbonyl complexes as precursors.

R. Marcos Esteban, C. Janiak in *Nanocatalysis in Ionic Liquids* (Ed.: M. Prechtl) Wiley-VCH, Weinheim, **2015**, *submitted.*

4) Comparative synthesis of Cu and Cu_2O nanoparticles from different copper precursors in ionic liquid and propylene carbonate.

R. Marcos Esteban, H. Meyer, J. Kim, C. Gemel, R. A. Fischer, C. Janiak, *Eur. J. Inorg. Chem.*, *submitted*.

Poster contributions:

5) Title: “Ligand-Free” Metal- Nanoparticles in Ionic Liquids.

R. Marcos Esteban, F. M. Alberti, D. Marquardt, H. Meyer, C.Rutz, K. Schütte, C. Vollmer, C. Janiak, **13th Trends in Nanotechnology Conference**, Madrid,10. -14. September 2012.

6) Title: Hybrid iridium@graphene nanomaterials for the hydrogenation of benzene to cyclohexane.

R. Marcos Esteban, H.Meyer, K. Schütte, C. Janiak., **17. Vortragstagung für Anorganische Chemie, Wöhler Vereinigung**, Universität des Saarlandes, Saarbrücken, 24.-26. September 2014.

In addition, the following supervised B.Sc.-Thesis, which are <u>not part</u> of this cumulative thesis, are cited.

7) Copper nanoparticles as catalyst in ionic liquids.

(„Kupfer-Nanopartikel als Katalysator in ionischen Flüssigkeiten“)

S. Steckel B.Sc., Mai 2013, Düsseldorf.

8) Hydrogenation reactions with graphene supported iridium nanoparticles. (“Hydrierungsreaktionen mit„Graphen“- unterstützten Iridium Nanopartikeln“)

P. Brandt B.Sc., September 2014, Düsseldorf.

9) Synthesis of graphene supported metal nanoparticles in organic carbonates.

L. M. Lekoukenberg B.Sc., WS 2015, Düsseldorf, *in progress*.

Short summary

Metal-nanoparticles (M-NPs) are of significant interest due to their novel and characteristic properties. Their high volume area and number of active centers in comparison with bulk materials, transform the metal-nanoparticles and nanomaterials into attractive materials, in particular, in the field of catalysis. Metal-nanoparticles can be prepared using common organic solvents with the presence of an external capping ligand or stabilizers to avoid the thermodynamically favored aggregation and agglomeration due to the Ostwald ripening. Ionic liquids (ILs) are a good alternative for the stabilization of M-NPs due to their ionic nature, high polarity, high viscosity and electrostatic-steric supramolecular network, which also helps for a homogeneous nucleation and growth of M-NPs.

In this work, we were focused on the deposition of M-NPs (Ir- and Ru-) on thermally reduced graphite oxide (also named *graphene* or abbreviated as TRGO) using the ionic liquid 1-butyl-3-methyltetrafluoroborate ([BMIm][BF_4]) and propylene carbonate (PC) as solvents. Metal carbonyls, $M_x(CO)_y$, are commercially available and easy to handle, and their use as starting materials for the synthesis of M-NPs limits the formation of byproducts and the presence of reducing agents is drastically reduce due to the already zero oxidation state of the metal.

The deposition of iridium-nanoparticles (Ir-NPs) on TRGO could be achieved by the thermal decomposition of tetrairidium dodecacarbonyl, $Ir_4(CO)_{12}$, in [BMIm][BF_4]. The synthesis of Ir@TRGO nanomaterials were prepared through microwave (MWI) or electron-beam irradiation (IBA Rhodotron accelerator). Small Ir-NPs were obtained with narrow size distributions of 1.0 ± 0.4 and 2.7 ± 0.7 nm for the microwave and of 3.6 ± 1.0 nm for the e-beam irradiation experiments.

The stable Ir@TRGO nanomaterials were used for the relevant hydrogenation of benzene or cyclohexene to cyclohexane, an important intermediate in the synthesis of Nylon. The microwave-obtained Ir@TRGO nanomaterials achieved a maximal conversion of 95.9 % with a turn over frequency (TOF) up to 10000 h^{-1} after ten consecutive hydrogenation runs, meanwhile the Ir@TRGO nanomaterials from the e-beam irradiation showed a lower TOF of 4582 h^{-1} with a conversion of 96.3 % after five runs. Ir@TRGO nanomaterials were also used for the hydrogenation of cyclohexene to achieve a conversion of 85.5 with TOF of ca. 68000 h^{-1}. The size of Ir-NPs showed a slightly increment after catalysis with size

distributions of 3.6 ± 1.1 nm for the microwave irradiation and 4.6 ± 1.5 nm for the e-beam irradiation Ir@TRGO nanomaterials.

Levulinic acid (LA) is one of the products from the lignocellulosic-derived biomass feedstock, and through hydrogenation reactions could be upgraded to γ-valerolactone (GVL). The Ir@TRGO nanomaterials achieved a TOF of 1430 h^{-1} after four consecutive hydrogenation runs under solvent-free conditions. The Ir-NPs showed an increment in the size distributions to 7.8 ± 4.4 nm after the catalysis reactions.

TRGO-supported ruthenium nanoparticles (Ru@TRGO) were also obtained from the decomposition of metal carbonyls, $Ru_3(CO)_{12}$, through microwave irradiation in propylene carbonate. Small size distributions of 4.3 ± 1.4 nm were observed for Ru-NPs without the presence of agglomeration. Ru@TRGO nanomaterials were tested as catalyst for the hydrogenation of benzene, which achieved a near quantitative conversion in less than 20 min with TOF of ca. 34000 h^{-1}. The Ru@TRGO nanomaterials could be recovered and re-used for at least ten consecutives hydrogenation runs; Ru-NPs showed a slightly increment in the size distribution of 6.7 ± 2.4 nm after catalysis.

In parallel, we were focused on the synthesis of copper-nanoparticles (Cu-NPs) and cuprite-nanocubes (Cu_2O-NCs) in [BMIm][BF_4] and PC. Cu-NPs are difficult to synthetized without an external stabilizer due to their fast oxidation. Here, were chose copper salts, as $Cu(BF_4)_2$, $Cu(acac)_2$ and $Cu(AcO)_2$ monohydrate, and the organometallic compound copper(II) bis(1-(dimethylamino)propan-2-olate), $Cu(OCH(Me)CH_2NMe_2)_2$, as starting materials for the synthesis of Cu-NPs and Cu_2O-NCs. The reduction and decomposition through microwave irradiation led to the formation of Cu-NPs with sizes distributions of 45 nm from $Cu(BF_4)_2$ in PC and of 3.3 ± 0.9 nm from $Cu(acac)_2$ in [BMIm][BF_4]. The organometallic compound $Cu(dmap)_2$ achieved size distributions of 3.1 ± 0.7 nm (in PC) and 3.7 ± 1.4 nm (in [BMIm][BF_4]). The Cu_2O-nanocubes could be achieved by selecting the water content metal salt $Cu(AcO)_2$ monohydrate as starting material in [BMIm][BF_4], which led to the formation of Cu_2O-NCs with size distributions of 43 ± 15 nm.

Kurze Zussamenfassung

Metal-Nanopartikel (M-NP) sind aufgrund ihrer charakteristischen und neuartigen Eigenschaften von großem Interesse. M-NP besitzen im Vergleich zu makroskopischen Stoffen eine große Anzahl von Oberflächenatomen und aktiven Zentren, die besonders interessant für die Katalyse sind. Die Synthese von M-NP in konventionellen organischen Lösemitteln benötigt externe Substanzen, die an die Partikeloberfläche binden, um die thermodynamische Aggregation durch die Ostwald-Reifung zu vermeiden. Ionische Flüssigkeiten (ILs) sind aufgrund ihrer Ladungsdichte, hohen Polarität, hohen Viskosität und Eigenschaft um ein supramolekulares Netzwerk zu binden sehr attraktiv für die Stabilisierung der M-NP.

In dieser Arbeit wurde die Synthese von M-NP (Ir- und Ru-) und ihre weitere Immobilisierung auf das *thermally reduced graphite oxide* (TRGO) in der ionischen Flüssigekeit 1-Butyl-3-methyltetrafluoroborat ([BMIm][BF_4]) und in Propylencarbonat durchgeführt. Die Metall-Carbonyl Verbindungen sind komerziell erhältlich, leicht verarbeitbar und aufgrund der bereits vorhandenen Oxidationsstufe Null des Metalls, sind die enstandenen Nebenprodukte und die Verwendung für Reduktionsmittel drastisch reduziert.

Die Immobilisierung von Ir-NP auf TRGO (Ir@TRGO) wurde durch die Zersetzung von $Ir_4(CO)_{12}$ mit Hilfe vom Mikrowellen (MW)- oder Elektronenbestrahlung (*e-beam irradiation*) dargestellt. Die Ir-NP aus den Ir@TRGO-Nanomaterialien zeigen eine Partikelgröße von 1.0 ± 0.4 and 2.7 ± 0.7 nm aus der MW- und von 3.6 ± 1.0 nm aus der Elektronenbestrahlungsmethode.

Die stabilen Ir@TRGO-Nanomaterialien wurden als Katalysatoren für die Hydrierung von Benzol zu Cylcohexan verwendet. Die Ir@TRGO-Nanomaterialien aus der Mikrowellenmethode zeigen katalytische Aktivitäten von 10000 h^{-1} mit einer maximalen Umsetzung von Benzol zu Cyclohexan von 95.9 % nach zehn konsekutiven Durchläufen, während die Ir@TRGO-Nanomaterialien aus der Elektronenbestrahlungsmethode katalytische Aktivitäten von 4582 h^{-1} mit einer maximalen Umseztung von 96.3 % ergeben. Die Hydrierungsreaktion von Cyclohexen zu Cyclohexan erzielt eine größere katalytische Aktivität von ca. 68000 h^{-1} mit einer Umsetzung von 85.5 %. Die Ir-NP wurden nach der kataytischen Anwendung mittels TEM untesucht. Die Ir@TRGO-Nanomaterialien zeigen eine Partikelgröße von 3.6 ± 1.1 nm für die Mikrowellenbestrahlung und von 4.6 ± 1.5 nm

für die Elektronenbestrahlung.

Lävulinsäure, der Rohstoff aus der Lignocellulose-Biomasse, wurde ebenfalls durch die Hydrierung mit Wasserstoff zu γ-Valerolacton umgesetzt. Die Ir@TRGO-Nanomaterialien zeigen eine katalytische Aktivität von 1430 h^{-1} nach vier konsekutiven Durchläufen.

Ruthenium-Nanopartikel wurden auf TRGO (Ru@TRGO) in Propylencarbonat nach der Zersetzung von $Ru_3(CO)_{12}$ durch Mikrowellenbestrahlung immobilisiert. Die enstandenen Ru-NP aus den Ru@TRGO-Nanomaterialien zeigen eine Partikelgröße von 4.3 ± 1.4 nm. Die Ru@TRGO-Nanomaterialien wurden ebenfalls als Katalysator für die Hydrierung von Benzol zu Cyclohexan verwendet, welche ein katalytische Aktivität von ca. 34000 h^{-1}nach zehn Durchläufen in weniger als 20 min zeigen. Die Ru-NP zeigen eine kleine Veränderung in der Partikelgröße zu 6.7 ± 2.4 nm.

Neben der Synthese der Metall@TRGO-Nanomaterialien wurden auch Kupfer-Nanopartikel (Cu-NP) und Kupfer(I)oxid-Nanowürfel (Cu_2O-NC) in [BMIm][BF_4] und PC untersucht. Die schnelle Oxidation von Kupfer-Nanopartikeln an Luft stellen eine große Herausforderung dar. In dieser Arbeit wurde die Reduktion und die weitere Zersetzung von unterschiedlichen Kupfer-Salzen, wie $Cu(BF_4)_2$, $Cu(acac)_2$ und $Cu(AcO)_2$-Monohydrat, und der metallorganischen Verbindung Kupfer(II)-bis(1-(dimethylamino)propan-2-olat), $Cu(OCH(Me)CH_2NMe_2)_2$, durchgeführt, um Cu-NP und Cu_2O-NC durch Mikrowellenbestrahlung zu synthetisieren. Die Cu-NP aus $Cu(BF_4)_2$ in PC ergeben eine Größenverteilung von 45 nm und aus $Cu(acac)_2$ in [BMIm][BF_4] von 3.3 ± 0.9 nm. Die metallorganische Verbindung, $Cu(dmap)_2$, ergab eine Größenverteilung von 3.1 ± 0.7 nm (in PC) and 3.7 ± 1.4 nm (in [BMIm][BF_4]). Die Kupfer-Nanowürfel konnten bei der Zersetzung und Reduktion von $Cu(AcO)_2$-Monohydrat in [BMIm][BF_4] erhalten werden, die zu Cu_2O-NC mit einer Größenverteilung von 43 ± 15 nm geführt haben.

Table of abbreviations and symbols

º C	Degree Celsius
Å	Ångstrøm
a.u.	Arbitrary unit
AAS	Atomic absorption spectrometry
bar	bar, unit of pressure (1 bar ≙ 100000 Pa ≙ 100 kPa)
bp	Boiling point
CDG	Chemically derived graphene
CNT(s)	Carbon nanotube(s)
COD	Crystallographic open database
dmap	1-(Dimethylamino)propan-2-olate
DMC	Dimethyl carbonate
EDX	Energy dispersive X-ray spectroscopy
FID	Flame ionization detector
GC	Gas chromatography
GO	Graphite oxide
GVL	γ–valerolactone
h	Hour
HAADF	High Angle Annular Dark-Field
HMF	Hydroxymethylfurfural
HR-TEM	High-resolution transmission electron microscopy
IL(s)	Ionic liquid(s)
IR	Infrared spectroscopy
LA	Levulinic acid
mg	Milligram
min	Minutes
mL	Milliliter

mm	Millimeter
mol	Unit of amount of substance (1 mol ≙ 6.022·1023 particles)
mp	Melting point
MTHF	2-Methyltetrahydrofuran
MWI	Microwave irradiation
MWNTs	Multiwall carbon nanotubes
NC(s)	Nanocube(s)
nm	Nanometer
NP(s)	Nanoparticle(s)
p	Pressure
PA	Pentanoic acid
PC	Propylene carbonate
ppm	Parts per million
PXRD	Powder X-ray diffraction
rpm	Revolutions per minute
RTIL(s)	Room temperature ionic liquid(s)
SEM	Scanning electron microscopy
STEM	Scanning transmission electron microscopy
SWNTs	Single walled carbon nanotubes
T	Temperature
t	Time
TEM	Transmission electron microcospy
TOF	Turn over frequency
TON	Turn over number
TOPO	tri-n-octylphosphine
TRGO	Thermally reduced graphite oxide, *graphene*
TRGO-SH	Thiol- functionalized TRGO

VA	Valeric acid
VE	Valeric esters
wt %	Weight percent
XPS	X-ray photoelectron microscopy
θ	Theta, angle of diffracted wave in the Bragg's equation
σ	Standard deviation
λ	Lambda (wavelength, nm)
Ø	Diameter (particle size)

Table of ionic liquids*

$[BF_4]^-$ *	Tetrafluoroborate
$[BMIm]^+$ *	1-Butyl-3-methylimidazolium
$[BMPyr]^+$ *	1-Butyl-1-methylpyrrolidinium
$[CEMIm]^+$ *	1-(3-carboxyethyl)-3-methyl-imidazolium, $[CEMIm]^+$=$[CEmim]^+$
$[CF_3SO_3]^-$ *	Trifluoromethanesulfonate, triflate
$[EMIm]^+$ *	1-ethyl-3-methylimidazolium, $[EMIm]^+$= $[C_2mim]^+$
$[N(Tf)_2]^-$ *	Bis(trifluoromethylsulfonyl)imide
$[PF_6]^-$ *	Hexafluorophosphate

* There are no explicit abbreviations for ionic liquids regarding to the IUPAC. In this work, the cation will be abbreviated as $[Cation]^+$ and the anion as $[Anion]^-$.

Table of contents

1. Introduction

1.1 Ionic liquids

Ionic liquids (ILs) have been in the focus of researches in the last years due to their novel properties and wide application fields.[1,2,3,4,5,6] Ionic liquids are described as molten salts, consisting on the combination of charged inorganic and organic ions, which are known as room temperature ionic liquids (RTILs) when are liquid at room temperature (Scheme 1).[7,8,9,10] Their tunable physicochemical properties by selecting an appropriate combination of anions and cations offer many advantages of ILs as solvents, and therefore are known as “design-solvents”. The high charge density, low vapor pressure (ILs are almost non-volatile solvents), high polarity, high viscosity, dielectric constant, and the supramolecular network are some of the characteristic properties of ILs. The most used cations and anions for the formation of ILs are resumed in the Scheme 1, being the cations alkylimidazolium and tetraalkylammoniun together with the anions tetrafluoroborate ($[BF_4]^-$) or trifluoromethanesulfonate ($[CF_3SO_3]^-$) the most common combinations. The imidazolium-based ILs are likely coordinated to weekly anions ($[BF_4]^-$, $[PF_6]^-$ or $[CF_3SO_3]^-$) and had a wide liquid range of temperatures (<80 ºC), thermal stability and a negligible vapor pressures.[5,11,12,13,14,15,16,17]

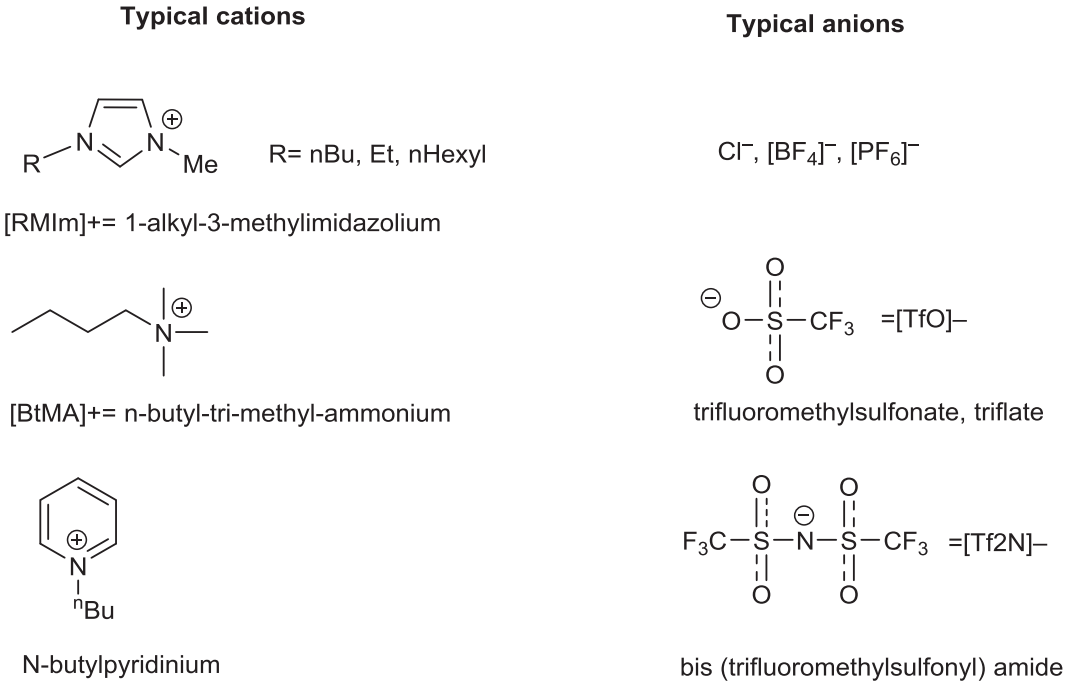

Scheme 1 Common cations and anions used for ionic liquids.

The intrinsic organization structures of ILs can be defined as “nanostructured” arrangements, stabilized by the combination of *van der Waals* interactions, Coulomb forces and hydrogen-bond interactions between the cation and anion.[13,18,19,20,21] These interactions provide a three dimensional supramolecular network, where the cations ($[RR´Im]^+$) are surrounded by the anions (A) of the type $\{[(RR´Im)_x(A)_{x-n})]^{n+}$, $[(RR´Im)_{x-n}(A)_x)]^{n-}\}$,[22,23] a structural pattern which can be observed in the solid, liquid and in gas phase. The high-organized assembly of ILs offers hydrophobic and hydrophilic domains with a high directionality (“IL-effect”) and the ionic channels and non-polar regions are adaptable to many molecules, which allows the inclusion of molecules such as metal nanoparticles in the structure of the ILs.[22]

1.2 Organic carbonates

Organic carbonates (are commonly used for the synthesis of polymers (polyurethanes or polycarbonates),[24] as solvents (in electrochemistry, as organic solvent or for Li-batteries),[25,26,27] and also in the industry for degreasing, cleaning or as additive for lubricants.[28] Organic carbonates are produced in a multitoned scale[29] and are stable polar solvents under ambient conditions with a wide range of liquid temperatures (for propylene carbonate, PC mp−49 °C, bp 243 °C).[25]

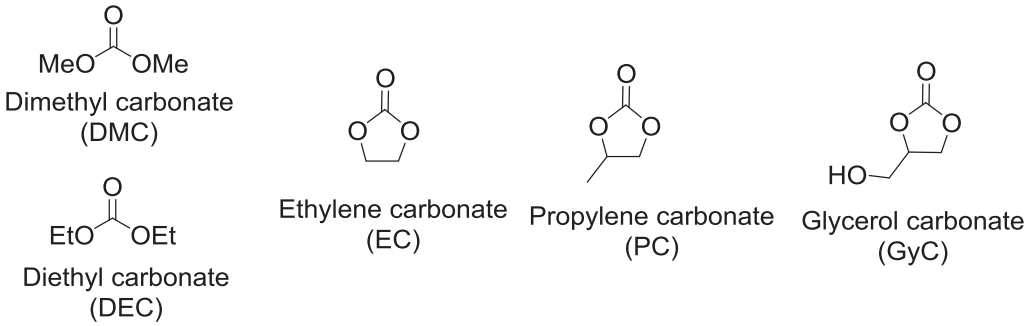

Scheme 2 Lineal (dimethyl carbonate (DMC) and diethyl carbonate (DEC)) and cyclic organic carbonates (Ethylene carbonate (EC), propylene carbonate (PC), glycerol carbonate (GyC)).

The synthesis of organic carbonates has been reported and developed in a few different strategies based on the condensation of alcohols and CO_2,[30,31] the reaction of urea and diols,[32,33] or by phosgenation reactions (reaction of hydroxy compounds with pyridine and an anhydrous solvent),[34,35] all of them techniques which have been already reviewed.[25,36,37] Among the most used organic carbonates (Scheme 2), dimethyl carbonate (DMC) and propylene carbonate (PC) are the most common. DMC is actually used for methylation reactions of aromatics (phenols, anilines or indoles)[38,39] and PC as solvent for CO_2 removal (FLUOR process).[40,41] PC is a biodegradable dipolar solvent with a low flammability, low volatility and (eco)-tocixity;[25] and due to their friendly environmental properties very attractive in homogeneous catalysis in replace to organic solvents.[25,26,42,43,44]

The use of propylene carbonate as solvent for the synthesis of M-NPs rarely appears in the literature and only a few reports have been described.[45,46,47,48] *Vollmer et al.* reported the synthesis of metal nanoparticles (M-NPs) in propylene carbonate dispersions.[49,50] Stable Mo-, W-, Re-, Fe-, Ru-, Os-, Co-, Rh-, and Ir-NPs were obtained by the thermal decomposition of metal carbonyls through microwave irradiation to achieve size

distributions of ca. 1-5 nm. The obtained M-NPs/PC dispersions showed a high catalytic activity for hydrogenation reactions reaching activities up to 1875 (mol cyclohexane) x (mol Rh)$^{-1}$ x h^{-1} with Rh-NPs/PC dispersions under milder conditions for the hydrogenation of cyclohexene (4-10 bar H_2, 90 ºC).[49] *Schütte et al.* reported the synthesis of Cu-, Zn- and Cu/Zn nanobrass alloy nanoparticles in propylene carbonate without the presence of stabilizers with the dispersions stable up to six months.[51]

1.3 Graphene

Carbon-based materials are well-known from a long time, from their allotropes as diamond or graphite to the more recently materials such as fullerenes, carbon-nanotubes (CNTs) or graphene (TRGO or CDG). *Graphene*, also named chemically derived graphene (CDG) or thermally reduced graphite oxide (TRGO), appears as a unique, versatile and interesting material, whose number of publications has particularly grown in the last years (Fig. 1).[52]

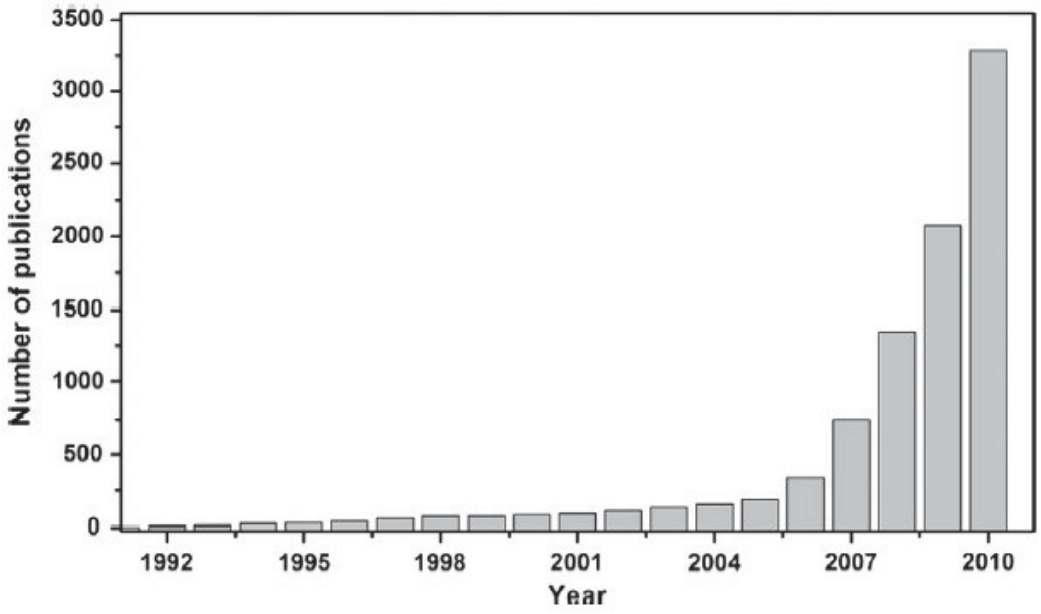

Fig. 1 Number of publications about graphene in the last years (reprinted from the Ref. [52]).

Graphene is formed by a two-dimensional layer based on the arrangement of the sp^2-bonded carbon atoms from the six-member ring (Fig. 2).[53,54] The thermally derived graphite oxide (TRGO) can be prepared in bulk quantities from the exfoliation of the 2D layers of natural graphite, whose synthesis has been already described by different methods,[55,56,57] considering the Hummers method[58] as the most used. TRGO can be prepared in a two-step oxidation/thermal reduction process from natural graphite. The oxidation to graphite oxide (GO) is done using nitric acid and potassium permanganate in concentrated sulfuric acid solutions.[58] The obtained GO has a high content of oxygen on the surface from the presence of oxygen-content functional groups (carboxyl, hydroxyl, or epoxy).[56,59,60] When GO is subjected to rapid heating above 400 °C the functional groups decompose into CO and CO_2 gas which exfoliates the layered GO structure into functionalized graphene sheets.[61] This thermal reduction of graphite oxide lends its name

to the product (TRGO). By adjusting the reduction temperature, the degree of functionalization can be controlled. At a lower reduction temperature, more oxygen atoms remain on the TRGO surface and thereby increase the degree of functionalization. This degree of functionalization influences on the dispersibility of TRGO in polar solvents[62] and its use as a support material for metal nanoparticles. A higher degree of functionalization improves the dispersibility, *e.g.* in water or acetone. Therefore, it can be expected that a TRGO-material with a high degree of functionalization has a good interaction with metal particles, and consequently represent an important application in the field of heterogeneous catalysis.[235]

Graphene is very attractive due to their chemical and physical properties such as high specific surface area (from 400 $m^2 g^{-1}$ up to 1500 $m^2 g^{-1}$), high elasticity, thermal stability or electrical transport (from the π-electron system over the C_6-rings), which permits its use in a wide scope of applications like electronics,[63,64] energy storage (Li-Batteries or solar cells),[65,66,67] sensors,[68,69] or catalysis.[66,70]

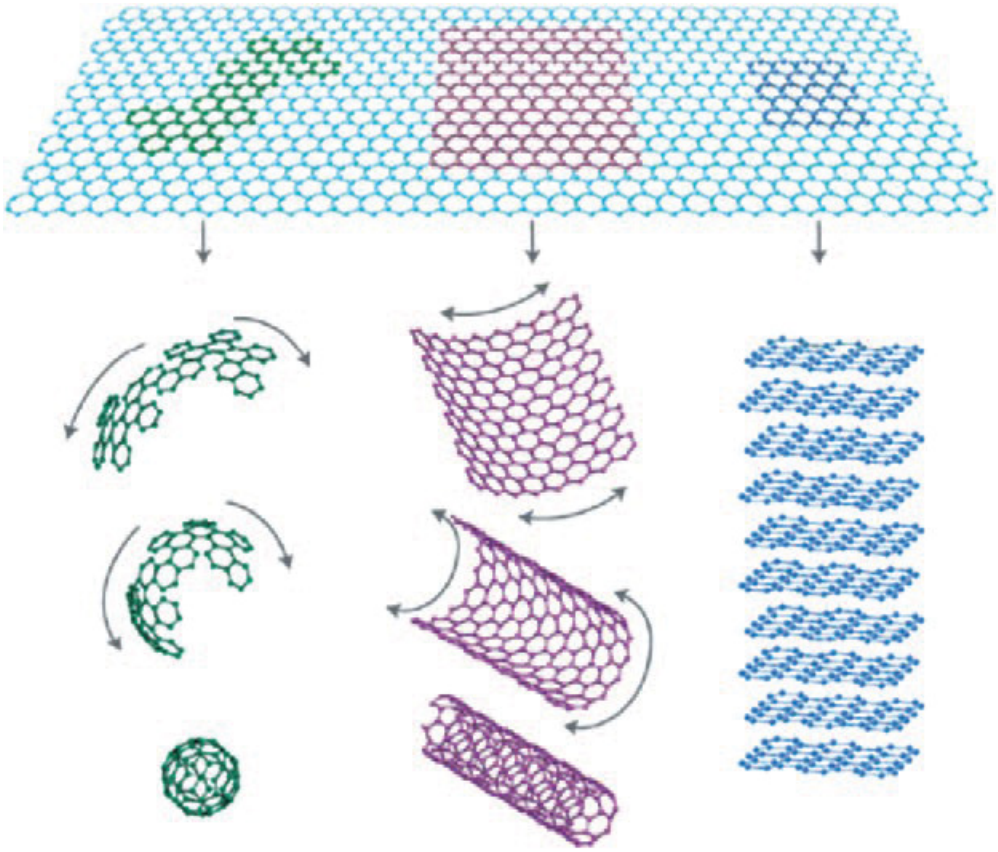

Fig. 2 Fullerenes, carbon nanotubes and graphene (reprinted from ref. [53]).

The functionalization of graphene involves a re-hybridization for the inner-carbon atoms from sp^2 to sp^3 with the resulting perturbation of the π-system and modification of the electronic and mechanical properties on graphene. In the literature are already described covalent and non-covalent approaches for the attachment of functionalized groups over the surface of graphene.[71,72,73] *Haddon et al.* reported the modification of epitaxial graphene by attaching nitrophenyl groups to the basal carbon.[74] The surface modification was achieved by the spontaneous electron transfer from the graphene layer and its substrate to the diazonium salt. The modification of the inner-carbon introduces an electron flow barrier due to the transformation of the sp^2 carbon to sp^3, which allows the formation of insulating and semiconducting domains in the graphene surface.[74] The attachment of polymers such polystyrene[75,76] or polyaniline[72] is also described in the literature. The non-covalent functionalization involves the stabilization between the substrates and the graphene layers through *van der Waals* and intramolecular interactions with the π-electron system,[53] which are significant for the research and development of nanomaterials.[71,77]

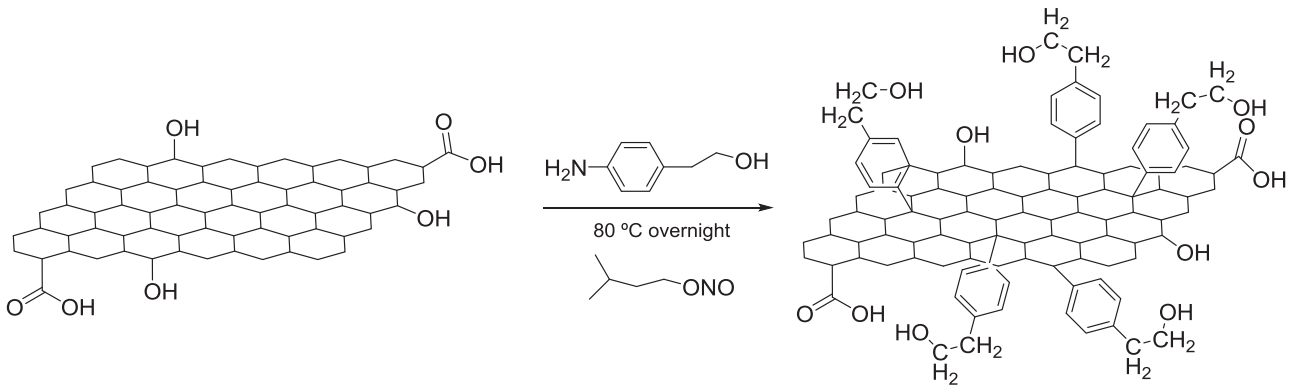

Fig. 3 Example of covalent modification of graphene by the diazonium salt (adapted from [76]).

The use of ionic liquids (ILs) as solvents for the synthesis of metal@graphene nanomaterials are very convenient, as ILs help on the growth, nucleation and further stabilization processes for the formation of M-NPs to achieve small and narrow size distributions. The dispersions of M@graphene/ILs nanomaterials can be prepared by chemical reduction,[78,79,80,81] thermal decomposition,[82] electrochemistry[83] or microwave reactions (Fig. 4).[84,85,86,117]

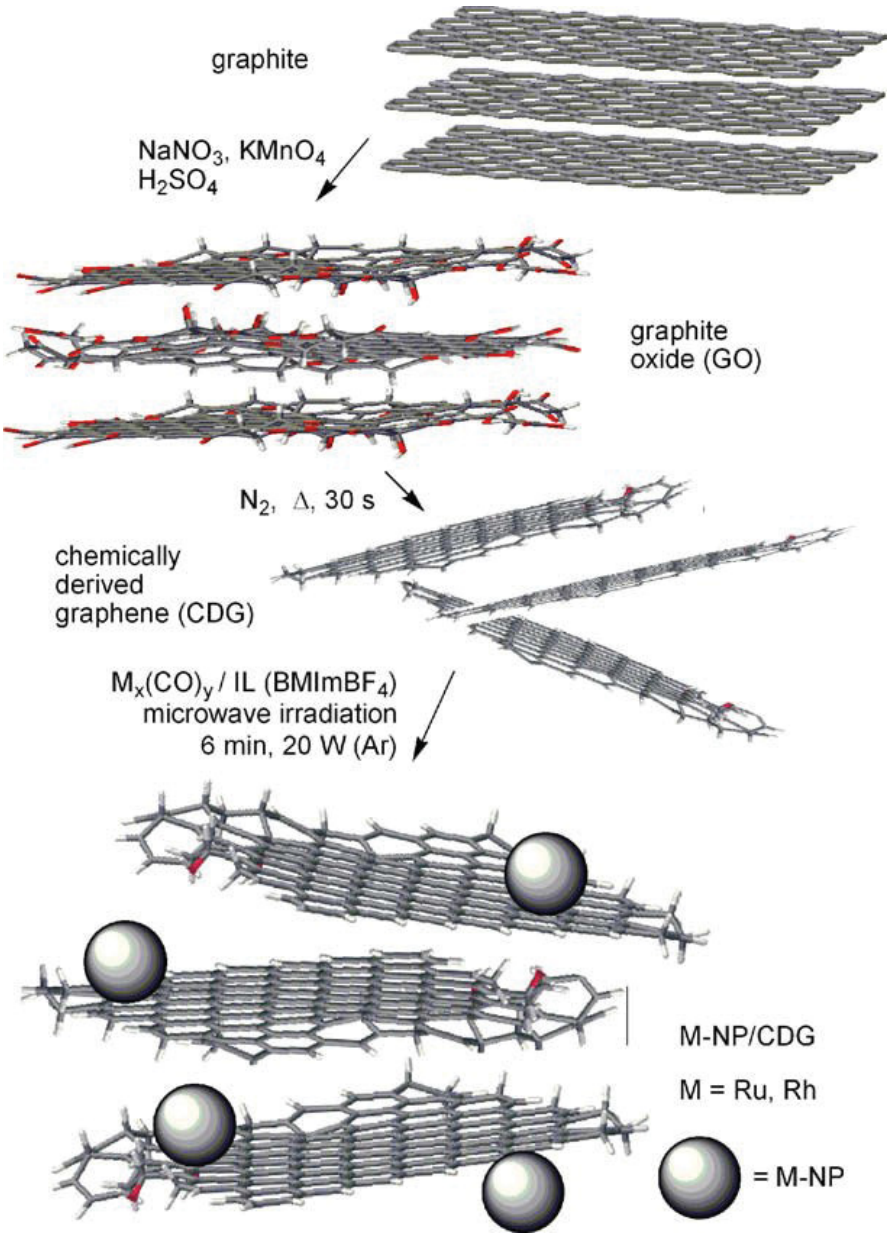

Fig. 4 Schematic synthesis of the deposition of metal nanoparticle on thermally reduced graphite oxide (reprinted from ref. [84]).

(A more detailed introduction of M@graphene as catalyst in ILs is described in the section 1.5, which is also part of the **publication 3.3**).

1.4 Synthesis of metal nanoparticles in ionic liquids

Metal nanoparticles (M-NPs) have received lot of attention in the last years due to their application in fields such as science,[87,88] medicine[89,90] or industry.[91] M-NPs can be prepared by the “top-down” or “bottom-up” approach.[92,93,94] In the “top-down” approach, M-NPs are obtained from the subdivision and degradation of bulk materials through chemical, thermal or mechanical processes.[95,96] In the “bottom-up” approach is involved a chemical, thermal or physical reduction (or decomposition) of molecular or ionic compounds (organometallic compounds or metal salts), method by which M-NPs diameters of < 10 nm can be achieved.[97] The “bottom-up” approach is the most used, because the obtained nanoparticles are commonly smaller than in the “top-down” approach, but the small size of the particles favors the formation of aggregates and agglomerates, converting the synthesis of M-NPs in a challenge and a time consuming processes.[94,97] The diameter of M-NPs can be influenced by synthesis parameters such as temperature, pressure, solvent or the character of the stabilizers and capping agents.[98]

Nanoparticles have a high ratio of surface to bulk atoms and with the decreasing of the M-NP diameter the fraction of surface atoms and the surface energy increases greatly (Fig. 5). The surface atoms with their "unsaturated bonds" dominate the chemistry and physics of nanoparticles.[99] In catalysis M-NPs or metal nanoclusters are investigated as "soluble" analogs of heterogeneous catalysts.[15,100106] The activity of (heterogeneous) nanocatalysts benefits strongly from the high surface area. Yet, small M-NPs of just a few nanometers are only kinetically stable and will agglomerate to thermodynamically more stable larger (nano)particles in a process called Ostwald ripening (Fig. 5).[107,108]

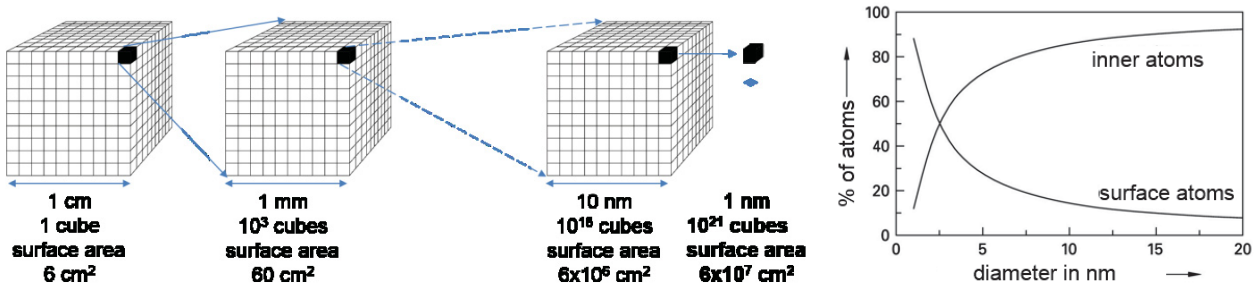

Fig. 5 Schematic representation of the increase in surface area (top) with fragmentation of a macroscopic object into nano-objects or the increase of surface atoms (bottom) relative to inner atoms with decreasing size of a nanoparticle (reprinted from the ref. [109]).

In the last years numerous methods for the synthesis of metal nanoparticles have been reported using chemical reduction,[110,111,112,113] thermal decomposition,[114,115] microwave reaction,[116,117,118,119,120] sonochemistry,[121,122,123] laser ablation,[124] photochemical reduction,[125,126] or electrochemistry,[127,128] and in order to prevent the thermodynamically favored aggregation, the use of coordinating ligands, polymers or surfactants are commonly and traditionally added during the synthesis of M-NPs to surround the M-NPs with a protective electrostatic and/or steric layer.[98,114,129,130,131]

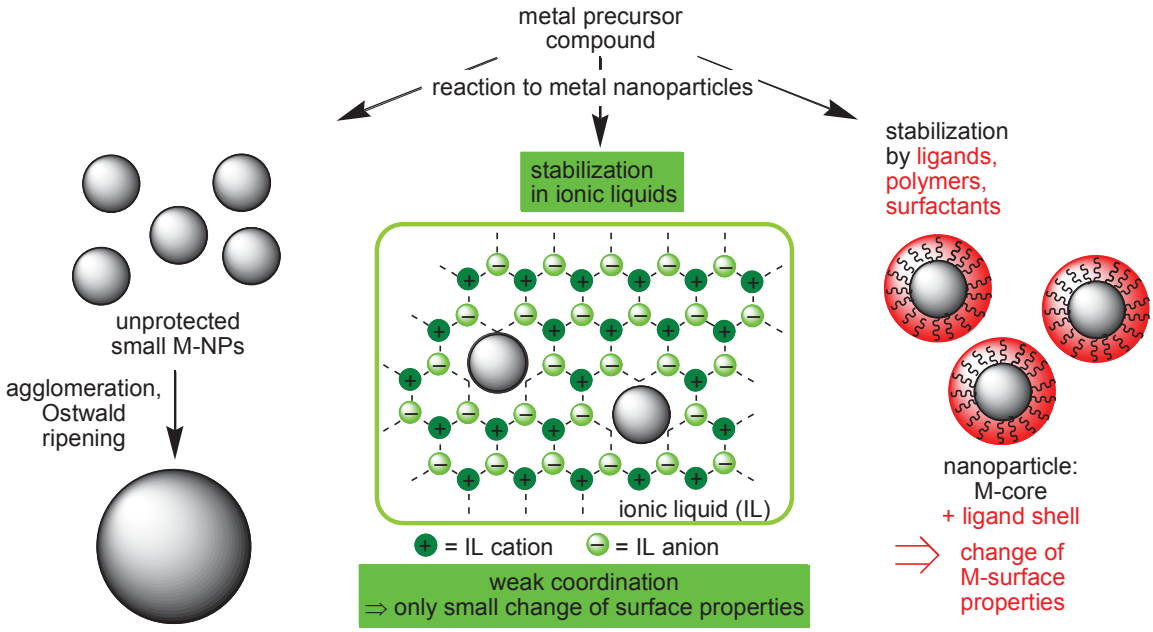

Fig. 6 Stabilization of metal nanoparticles (M-NPs) in ionic liquids (ILs) (middle) or through protective ligands (right).

Nevertheless, in catalysis the presence of a protective layer around the particle could affect to the catalytic activity of the M-NPs. Ionic liquids (ILs) are a good alternative to replace the used of common solvents and external capping ligands because the ionic nature of ILs favored the stabilization of M-NPs through their electrostatic-steric supramolecular network (Fig. 6) (see section 1.1).[13,22,23,116,132,133,134,135]

ILs are an attractive and suitable media for microwave reactions, or for microwave-induced thermal decompositions in the case of metal nanoparticle formation due to their high polarity, high ionic charge and high dielectric constant. ILs show a high dissipation factor (tan δ) for the conversion of microwave energy into heat.[136,137] Microwaves are a low-frequency energy source which induce an extremely rapid heating process in high-absorptive media.[136,138,140] Microwave irradiation directly heats the reaction mixture

and not the vessel because it is the reaction mixture which absorbs the microwave energy. This leads to localized superheating, very fast and efficient heating rates so that temperatures of 200 °C are reached within seconds.[138,141,142,144] As soon as metal particles are formed, they will also absorb the microwave radiation.

In ionic liquids metal nanoparticles can be kinetically stabilized by virtue of the ionic nature, high polarity, viscosity and electrostatic-steric supramolecular network of these molten salts without the need of external stabilizers.[3,13,22,23,116,132–135,145] The use of ionic liquids as solvents and stabilizers for metal nanoparticles should avoid the addition of external capping ligands due to the electrostatic and steric stabilization through the formation of an ion layer around the metal nanoparticles, although this type of stabilization is nowadays still a manner of discussion.[133,146] Reference is usually made to DVLO (Derjaugin-Landau-Verwey-Overbeek) theory; thereby the IL provides a “protective shell” for M-NPs.[147,148,149,150] DVLO theory predicts that the shell adjacent to the M-NP surface must be anionic and, as consequence, the IL-anion should be the primary source of stabilization of the metal nanocluster. The steric demand of the anions then also provides for a steric stabilization (or electro-steric altogether).

The synthesis of metal nanoparticles in ionic liquids[151] can generally be achieved through chemical reduction[120,152,153,154,155,156] or decomposition,[157,158,159,160] by means of electro-reduction/electro-deposition[161,162,163] or photochemical reduction[125,126] of metal salts, where the metal atom is in a formally positive oxidation state (M^{n+}). The combination of metal nanoparticles and ionic liquids is a growing field.[8,9,10,103,133,164,165,166167,168]

(This introduction section 1.5 is part of a cumulative thesis from the **publication 3.3**).

1.5 Metal carbonyls for the synthesis of metal nanoparticles

The oxidation state of the metal atom in binary carbonyls is zero. No reductant is necessary to derive at zero-valent metal from metal carbonyls $M_x(CO)_y$. Metal nanoparticles (M-NPs) can be elegantly and easily obtained by thermal, photolytic or sonolytic decomposition of binary metal-carbonyl compounds, $M_x(CO)_y$. The formation of byproducts is very limited and the liberated CO can be easily removed with the gas phase.[169,170] As pointed out above, also M-NPs from metal carbonyls need a stabilizer such as capping ligands, polymers or surfactants to avoid oxidation or aggregation.

1.5.1 Metal carbonyls – synthesis, structure and bonding

Metal complexes with carbon monoxide, CO as a ligand are called metal carbonyls or carbonyl complexes.[171] The stoichiometry in many metal carbonyls follows the 18-valence electron rule. Carbon monoxide is a two-electron donor ligand. The CO group binds with the carbon atom to the metal atom. Metal carbonyls are of structural and of theoretical interest and technically important as catalysts (e.g. Monsanto acetic acid process, hydroformylation, Fischer-Tropsch-synthesis). Carbonyl complexes occur mostly with the transition metals of d-block elements. For main group elements, lanthanoids and actinoids there are only singular examples with metal-CO bonds. The transition metals V, Cr, Mo, W, Mn, Tc, Re, Fe, Ru, Os, Co, Rh, Ir and Ni can form metal carbonyls of the general formula $M_x(CO)_y$, that is, consisting only of the metal and the CO ligand. Such carbonyl complexes are called binary metal carbonyls (Table 1).[171]

Table 1. Binary metal carbonyls.[a]

Group	5	6	7	8	9	10
Metal	V, Nb, Ta	Cr, Mo, W	Mn, Tc, Re	Fe, Ru, Os	Co, Rh, Ir	Ni, Pd, Pt
mononuclear complexes	$V(CO)_6$	**$Cr(CO)_6$** **$Mo(CO)_6$** **$W(CO)_6$**		**$Fe(CO)_5$** $Ru(CO)_5$ $Os(CO)_5$		**$Ni(CO)_4$**
polynuclear complexes			**$Mn_2(CO)_{10}$** $Tc_2(CO)_{10}$ **$Re_2(CO)_{10}$**	**$Fe_2(CO)_9$** **$Fe_3(CO)_{12}$** $Ru_2(CO)_9$ **$Ru_3(CO)_{12}$** $Os_2(CO)_9$ **$Os_3(CO)_{12}$**	**$Co_2(CO)_8$** **$Co_4(CO)_{12}$** **$Rh_4(CO)_{12}$** **$Rh_6(CO)_{16}$** **$Ir_4(CO_{12}$**	

[a] Metal carbonyls given in bold were confirmed to be commercially available, e. g., from Aldrich, ABCR or Acros.

Examples for the binary metal carbonyl structures are collected in Fig. 7. Metal carbonyls are commercially available (see Table 1) and relatively easy to handle. $Ni(CO)_4$ and $Fe(CO)_5$ are produced on a multi-ton scale.[172] Metal-carbonyl complexes $Fe(CO)_5$, $Co_2(CO)_8$ and $Ni(CO)_4$ can be prepared by direct reaction between finely dispersed metal and carbon monoxide at elevated temperature and pressure (Eq. 1).

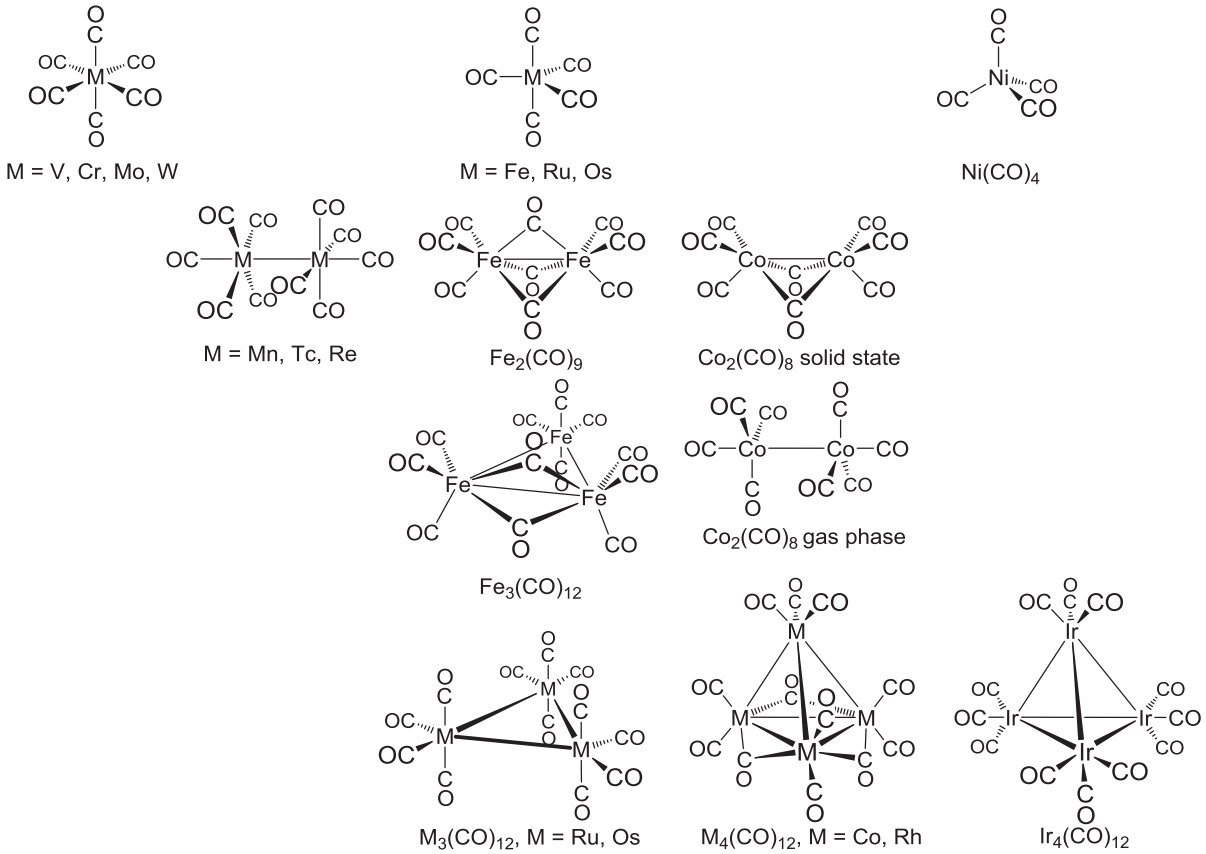

Fig. 7 Molecular structures for the binary metal carbonyl examples. $Rh_6(CO)_{16}$ where the Rh_6 atoms form an octahedra is not shown.

A more general synthesis is the reduction of metal salts in the presence of carbon monoxide (reductive carbonylation) (Eq. 2). Also, CO itself can act as a reductant (Eq. 3).

$$\begin{aligned} &Ni + 4\,CO \xrightleftharpoons[\text{(no pressure)}]{80\ ^\circ C} Ni(CO)_4 \quad \text{(Mond process)} \\ &2\,Co + 8\,CO \xrightarrow[\text{CO-pressure}]{150\text{-}200\ ^\circ C} Co_2(CO)_8 \\ &Fe + 5\,CO \xrightarrow[\text{CO-pressure}]{150\text{-}200\ ^\circ C} Fe(CO)_5 \end{aligned} \qquad (1)$$

$$CrCl_3 + Al + 6\,CO \xrightarrow[\text{300 bar CO, benzene}]{\text{140 °C}} Cr(CO)_6 + AlCl_3$$

$$2\,MnI_2 + 2\,ZnR_2 + 10\,CO \longrightarrow Mn_2(CO)_{10} + 2\,ZnI_2 + 2\,R\text{–}R$$

$$10\,RhCl_3(H_2O)_3 + 28\,CO + 15\,H_2 \longrightarrow Rh_4(CO)_{12} + Rh_6(CO)_{16} + 30\,HCl + 30\,H_2O$$

$$Ni_2^{+} + S_2O_4^{2-} + 4\,OH^- + 4\,CO \longrightarrow Ni(CO)_4 + 2\,SO_3^{2-} + 2\,H_2O \qquad (2)$$

$$Re_2O_7 + 17\,CO \longrightarrow Re_2(CO)_{10} + 7\,CO_2$$

$$[Ni(NH_3)_6]^{2+} + 5\,CO + 2\,H_2O \longrightarrow Ni(CO)_4 + (NH_4)_2CO_3 + 2\,NH_4^{+} + 2\,NH_3 \qquad (3)$$

The metal-carbonyl bond consists synergistically of a OC→metal σ-donor bond and of the important M→CO π-acceptor or back bond. The former originates from the σ-HOMO of CO into a metal orbital, the latter involves the electron transfer from an occupied metal d-orbital into the empty π*-LUMO of CO (Fig. 8).

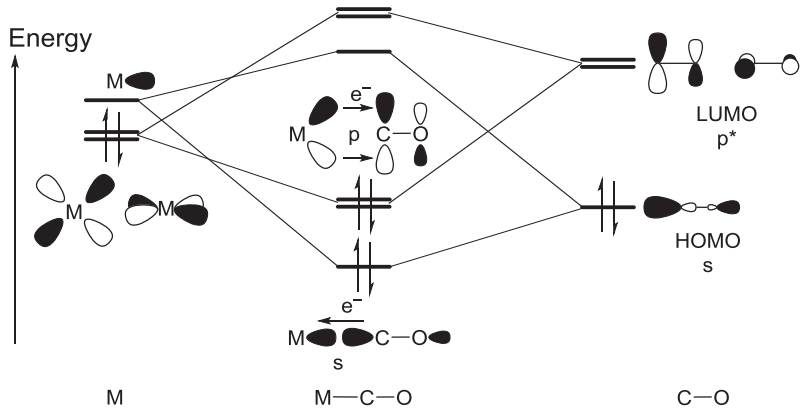

Fig. 8 Frontier orbital section of the qualitative molecular orbital (MO) diagram for the OC→metal donor σ-bond and the M→CO π-acceptor or back bond in the metal-carbonyl bond (HOMO = highest occupied MO, LUMO = lowest unoccupied MO). For clarity only one of the M→CO π-bonds is depicted.

Mononuclear metal carbonyls are formed with metal atoms possessing an even number of d-electrons (d^6: Cr, Mo, W; d^8: Fe, Ru, Os; d^{10}: Ni) such that the d-electron count plus the number of CO-ligands times two electrons (for each CO) then yields 18 valence electrons. Example: $Fe(CO)_5$ 8 d-electrons + 5 x 2 CO-electrons = 18. An exception is vanadium hexacarbonyl $V(CO)_6$ which forms a stable 17-valence-electron species. Metal atoms with an odd number of electrons have to form di- or oligonuclear carbonyl clusters

with metal-metal bonds. Sharing of metal electrons then leads to the 18-valence-electron configuration. Example: $Co_2(CO)_8$ 9 d-electrons + 4 x 2 CO-electrons + 1 metal electron = 18. The even-numbered metal atoms Fe, Ru and Os (d^8) form both mononuclear ($M(CO)_5$) and oligonuclear carbonyl complexes ($Fe_2(CO)_9$, $M_3(CO)_{12}$).

1.5.2 Metal nanoparticles from metal carbonyls in conventional organic solvents

Most of the early research on M-NPs from metal carbonyls focused on the synthesis of Fe- or Co-NPs due to their magnetic properties.[173]

In the 1960´s *Hess* and *Parker*[174] and *Thomas*[175] published the first works on the synthesis of magnetic cobalt nanoparticles (Co-NPs) by thermal decomposition of dicobalt octacarbonyl, $Co_2(CO)_8$. The Co-NPs were prepared in toluene dispersions in the presence of polymer dispersants, such as methyl methacrylate-ethylacrylate-vinylpyrrolidone terpolymers, high-purity polystyrene, styrene-acrylonitrile polymers, polyacrylonitril, chloropolyethylene sulfonamide, polyester, and polyether urethanes to from stable colloids of discrete particles which were separated by polymer coatings. The particle diameter and stability of the Co-NPs depended on a balance between the ligand and precursor concentrations, temperature, polymer molecular weight and solvent, to achieve a uniform size of Co-NPs in the 1-100 nm range.[175]

Papirer et al.[176,177] described the preparation of spherical cobalt nanoparticles as a ferrofluid by thermal decomposition at 110 ºC of $Co_2(CO)_8$ in an aromatic solvent in the presence of an alkyl sulfonate surfactant. The diameter of the particles was determined by small-angle-X-ray scattering and magnetic methods to an average diameter of 7 nm. The intermediate formation of $Co_4(CO)_{12}$ was detected.[176]

Suslick et al. prepared amorphous Fe-NPs,[178,179] FeCo alloy-NPs[180] and Mo_2C-NPs[180,181] using sonochemistry techniques. The volatile metal carbonyl precursors $Fe(CO)_5$, $Mo(CO)_6$, $[Co(CO)_3(NO)]$, were dissolved in a dry high-boiling solvent (decane or hexadecane) at 0-90 ºC and irradiated for 1-3 hours under argon. The sonochemically produced amorphous Fe-NPs were ten times more reactive per gram in the the Fischer-Tropsch conversion of carbon monoxide and hydrogen to low-molecular-weight alkanes at very low temperatures (200 ºC) than crystalline iron powder (5 µm diameter). At 250 ºC, the activity for cyclohexane dehydrogenation (to benzene) and hydrogenolysis (predominantly to methane) was over 30 times higher for the sonochemically produced amorphous Fe-NPs relative to crystalline iron.[178]

The formation of magnetic $CoPt_3$ Co_{core}-Pt_{shell} nanoparticles was reported by *Cheon* and co-workers through redox transmetalation of the reactants $Co_2(CO)_8$ and $Pt(hfac)_2$ (hfac = hexafluoroacetylacetonate), without the presence of external reductants. The composition

of the nanoparticles could be tuned by adjusting the ratio of the reactants.[182]

Lee and coworkers reported the synthesis of iron, chromium, molybdenum and tungsten metal clusters by laser decomposition of the respective metal carbonyls. The reaction was carried out using a 10.6 μm CO_2 laser in the presence of Ar and SF_6.[183] The metal clusters of Fe, Cr, Mo, and W showed an average particle diameter of 6, 3.5, 2 and ~1 nm, respectively, with narrow distribution. The presence of argon helped to increase the purity of the metal clusters by avoiding the formation of higher nuclearity metal carbonyls. SF_6 acted as infrared (IR) photosensitizer, which absorbed the 10.6 μm IR photons from the CO_2 laser and transferred the energy to a metal carbonyl via collisions. The metal clusters were formed in the body centered cubic (bcc) lattice for Fe and Cr, face centered cubic (fcc) for Mo, and in an amorphous structure in the case of W (all these bulk metals have bcc structure). Considering the cluster atom count (9630, 1870, 230 and ~30 for Fe, Cr, Mo and W clusters, respectively) which was estimated from their average diameters, it is likely that there exists a structural transition from fcc to bulk bcc with increasing cluster size in these M-NPs.[183]

Sun et al. prepared monodispersed iron-platinum (FePt) nanoparticles by thermal decomposition of $Fe(CO)_5$ at high temperatures and the reduction of $Pt(acac)_2$ (acac = acetyl acetonate) by using a long-chain 1,2-hexadecanediol. Both reactions were initiated together in the presence of oleic acid and oleylamine, to provide a controlled route to monodisperse FePt-NPs.[184] Further investigations showed that the controlled variation of the precursors $Fe(CO)_5$ and $Pt(acac)_2$ can be adjusted to obtain ferromagnetic FePt nanocrystal superlattices. Using dioctyl ether as solvent, a 3:2 molar ratio of $Fe(CO)_5$ to $Pt(acac)_2$ gave $Fe_{48}Pt_{52}$ particles, a 2:1 molar ratio yielded $Fe_{52}Pt_{48}$ and a molar ratio of 4:1 gave $Fe_{70}Pt_{30}$ particles. The FePt diameter could be tuned from 3 to 10 nm. Monodisperse FePt nanoparticles were of an average diameter of 3 nm and the consecutive addition of more reagents could enlarge the existing seeds to the desired particle size.[184]

Puntes et al. reported a pyrolysis method for the synthesis of monodisperse, stabilized and defect-free e-Co nanoparticles. The magnetic colloids (Co-NPs) were synthesized by the rapid pyrolysis of $Co_2(CO)_8$ under inert (Ar) atmosphere to give narrow diameter distributions (3-17 nm) of Co-NPs controlled by the concentration of the organic surfactants mixture (oleic acid, lauric acid, trioctylphosponic acid and oxide, pyridine, etc).[185,186]

Weller et al. synthesized $CoPt_3$ nanocrystals by reduction of $Pt(acac)_2$ and thermodecomposition of $Co_2(CO)_8$ in the presence of 1-adamantanecarboxylic acid to produce $CoPt_3$ nanoparticles. The mean particle diameter could be varied from 1.5 to 7.2 nm by the reaction conditions and the type of coordinating mixture. As-synthesized $CoPt_3$ particles represented single crystal domains and had a chemically disordered face-centered cubic (fcc) structure.[187]

Rutnakornpituk and coworkers[188] reported superparamagnetic Co-NPs from $Co_2(CO)_8$ in toluene via thermal decomposition in the presence of poly(dimethysiloxane) (PDMS) as carrier fluid and poly[dimethylsiloxane-b-(3-cyanopropyl)methylsiloxane-b-dimethylsiloxane] (PDMS-PCPMS-PDMS) triblock copolymers as steric stabilizers. These copolymers formed micelles and acted as “nanoreactors” for the thermal decomposition of the metal carbonyl. The nitrile groups on the PCPMS central blocks were thought to adsorb onto the particle surface, while the PDMS end blocks protrude into the reaction medium to provide steric stability. The particle diameter could be controlled by adjusting the cobalt to copolymer ratio and non-aggregated cobalt nanoparticles are observed in TEM.

Bönnemann et al. prepared cobalt, iron and iron-cobalt nanoparticles via thermal decomposition in the presence of aluminium alkyls (AlR_3), as air-stable magnetic metal nanoparticles. Once the metal carbonyls, $Co_2(CO)_8$, $Fe(CO)_5$ or $Co_2(CO)_8/Fe(CO)_5$, were decomposed the nanoparticle-AlR_3 dispersions were treated with synthetic air through a thin capillary (giving smooth oxidation to an Al_2O_3 shell around the M-NP core) to yield magnetic particles stable in air under ambient conditions for over a year, as confirmed by magnetic measurements.[189,190]

Yang et al.[191] synthesized magnetic nanoparticles and carbon nanotube (CNT) core-shell nanostructures, such as CoO/CNTs and Mn_3O_4/CNTs, by the non-aqueous solvothermal treatment of the corresponding metal carbonyls on CNT templates using hexane as solvent at 200 ºC in an autoclave. The hydrophobic interaction between nanoparticles and CNTs in hexane played the critical role for the formation of CNT-based core-shell nanostructures. Moreover, the CoO/CNT core-shell nanostructures showed weak ferromagnetic performance at 300 K due to the ferromagnetic Co clusters and the uncompensated surface spin states, while the Mn_3O_4/CNT core–shell nanostructures displayed an apparent transition from paramagnetic to ferromagnetic behavior with decreasing temperature.

The above examples together with the several reviews published in the last years[116,135,173,192,193,194,195] show that magnetic nanoparticles from iron or cobalt were early on investigated for application in electronics, medicine or industry, but also due to the commercial availability of $Fe(CO)_5$ or $Co_2(CO)_8$. By now, M-NPs based on metal carbonyl precursors appear studied more for catalytic uses.

Hyeon and coworkers[196] used cobalt nanoparticles for the catalysis in the inter- and intra-molecular Pauson-Khand (alkyne+alkene or enyne) reactions for the synthesis of cyclopentenone derivates. The Co-NPs were prepared from $Co_2(CO)_8$ in dioctyl ether together with oleic acid and trioctylphosphine. A transmission electron microscopic (TEM) image confirmed that the particles were well separated and that they are nearly monodisperse, having a mean diameter of 8 nm. The colloidal cobalt showed a high catalytic activity for the intramolecular reaction of an enyne, achieving a yield of 97 % at 130 ºC at a CO pressure of 5 atm in comparison with normal heterogeneous cobalt catalysts supported on silica or charcoal.[196]

Landau et al.[197] deposited nickel nanoparticles on multiwall carbon nanotubes (MWCNTs) by sonochemical decomposition of a solution of $Ni(CO)_4$ in decaline. Ni/MWCNT composites contained 25 and 51 wt% nickel, showed good dispersion and uniformity of size distribution of Ni-NPs at high loadings, together with enhanced catalytic activity in the selective carbonyl group hydrogenation of chloroacetophenone by factors of 2–18, compared with non-sonochemical decoration methods.

Zachariach et al.[198] generated iron and nickel nanoparticles for the simultaneous catalytic ignition of toluene in an aerosol reactor. Fe- and Ni-NPs were generated by gas-phase pyrolysis of $Ni(CO)_4$ and $Fe(CO)_5$, respectively. In comparison to non-catalytic homogeneous ignition, the addition of metal NPs lowered the ignition temperature of toluene by as much as 150 ºC. Iron was found to be a more active than nickel. Inspection of the catalyst indicated sintering at relatively low temperatures presumably as a result of the exothermic reaction on the particle surface. A turnover frequency of 80 s^{-1} implied greater catalyst efficiency than commonly found for substrate-stabilized catalysts. Electron microscopic analysis shows that the Fe-NPs undergo structural transformation (oxidation and sintering), which is likely initiated by the rapid heat release from the Fe-NP oxidation process. A similar oxidation process was also observed for Ni catalysts.[198]

Chamberlain, *Khlobystov*, *Bourne et al.* reported the encapsulation of metal nanoparticles into single walled carbon nanotubes (SWNT).[199,200] Metal nanoparticles

from tungsten, rhenium and osmium were inserted into single walled carbon nanotubes (SWNT) by decomposition of the corresponding metal carbonyls under heat treatment or electron beam irradiation. The nanotube host acted as an efficient template, controlling the growth of M-NPs to ~1 nm in diameter. As a result, the M-NPs stayed largely spheroidal in shape and were uniformly distributed throughout the entire length of the SWNT. The released carbon monoxide (CO) gas creates pockets of high pressure between nanoparticles, thus, preventing their collision and coalescence into larger structures. Despite their extremely small size (30-90 atoms on average) and unprotected surface, the metallic nanoparticles encapsulated in nanotubes were very stable under ambient conditions and even at elevated temperatures.[199] Ru-NPs were also deposited on SWNT (~1-2 nm diameter) in the gas phase using the volatile $Ru_3(CO)_{12}$ precursor. Thermal decomposition of $Ru_3(CO)_{12}$ generated Ru-NPs size-controlled by the nanotube diameter. TEM showed very small Ru-NPs with a narrow diameter distribution (0.92 ± 0.13 nm). The Ru@SWNT nanoparticles were also tested as catalyst for hydrogenation reactions. The extreme spatial confinement of the Ru@SWNT catalyst yielded a lower TOF for the reduction of cyclic alkenes in comparison to a Ru/C catalyst, but no drop in activity or change in structure of the Ru-NPs embedded in SWNT were observed over 24 hours at 110 ºC.[200]

Fu et al. reported the synthesis of cobalt phosphide (Co_2P) nanoparticles for photocalatytic hydrogen evolution in a system with CdS nanorods as photosensitizer and DL-mandelic acid as electron donor.[201,202] Co_2P nanoparticles were synthesized by thermal decomposition of $Co_2(CO)_8$ in 1,2-dichlorobenzene in the presence of tri-n-octylphosphine oxide (TOPO) and oleic acid. The system demonstrated an H_2 production rate of up to 19373 mmol g^{-1} h^{-1} after 10 h LED light (λ > 420 nm) irradiation. Mandelic acid was oxidized to benzoylformic acid by the holes formed in CdS.[201]

1.5.3 Metal nanoparticles from metal carbonyls in ionic liquids

The formation of M-NPs from metal carbonyls in the ILs can be achieved under inert gas atmosphere by conventional thermal decomposition (at ~180-250 ºC for 6-12 h), by UV-photolysis (e.g. with a 1000 W mercury lamp for 15 min) or by rapid (3-15 min) and energy saving (10-150 W) microwave irradiation (MWI) without the presence of any stabilizer or capping ligand (Fig. 9, Fig. 10, Table 2.).

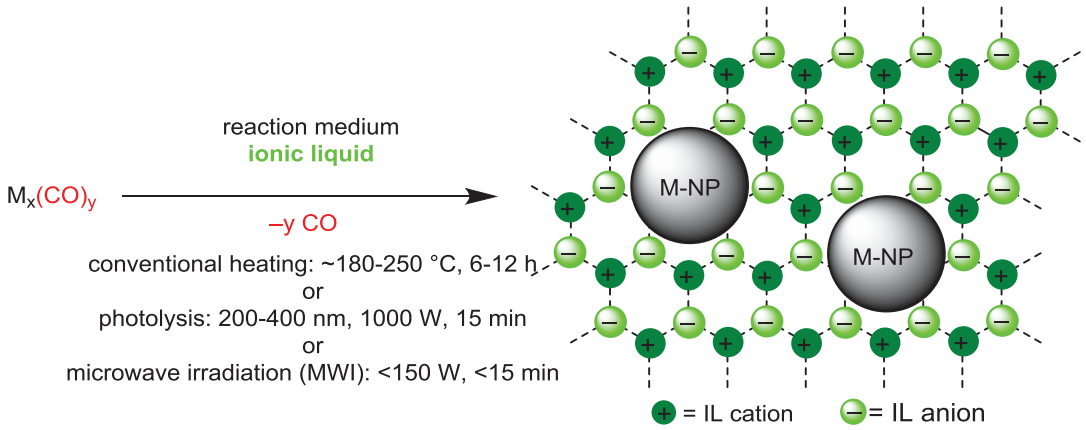

Fig. 9 Synthesis and stabilization of metal nanoparticles from metal carbonyl precursors in ionic liquids.

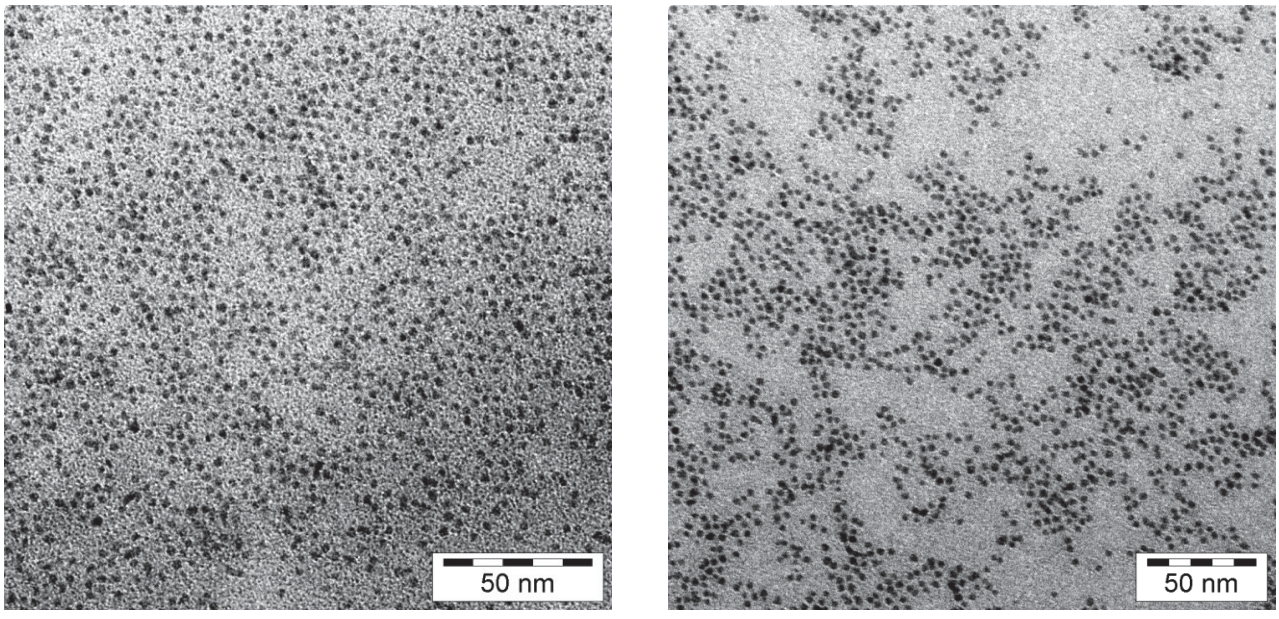

a **b**

Fig. 10 Examples of TEM images of metal nanoparticles obtained from metal carbonyl precursors in ionic liquids. (a) Os-NPs from $Os_3(CO)_{12}$by MWI in [BMIm][BF_4], Ø 2.5 ± 0.4 nm; (b) Ru-NPs from $Ru_3(CO)_{12}$ by photolysis in [BMIm][BF_4], Ø 2.0 ± 0.5 nm (reprinted from ref. [116]).

Table 2. Examples of metal nanoparticles formed from metal carbonyl precursors in ionic liquids.

Metal	Metal carbonyl precursor	Ionic liquid [a]	M-NP average diameter ± standard deviation (nm)	Remarks	Ref.
Cr	$Cr(CO)_6$	[BMIm][BF_4], [BMIm][CF_3SO_3], [BMIm][$N(Tf)_2$]	≤ 1.5 ± 0.3, MWI, thermal;[b] 4.4 ± 1.0, hν[b]	c, d, e	[120, 211]
	$Cr(CO)_6$	[EMIm]Cl	3.6 ± 0.7 nm, MWI, 2.3 ± 0.4 nm, thermal	catalyst for glucose to HMF conversion, see Fig. 17	[203]
Mo	$Mo(CO)_6$	[BMIm][BF_4], [BMIm][CF_3SO_3], [BMIm][$N(Tf)_2$]	~1 – 2, MWI, hν;[b] ≤ 1.5 ± 0.3, thermal[b]	c, d, e	[120, 211]
W	$W(CO)_6$	[BMIm][BF_4], [BMIm][CF_3SO_3], [BMIm][$N(Tf)_2$]	3.1 ± 0.8, MWI;[b] < 1, hν;[b] ≤ 1.5 ± 0.3, thermal[b]	c, d, e see Fig. 11, Fig. 12	[120, 211]
Mn	Mn_2CO_{10}	[BMIm][BF_4]	12.4 ± 3, MWI; < 1, hν 28.6 ± 11.5, MWI	b, c, d see Fig. 11	[120, 204]
	Mn_2CO_{10}	[CEMIm][BF_4] [g]	4.3 ± 1.0, MWI		[204]
Re	Re_2CO_{10}	[BMIm][BF_4]	2.4 ± 0.9, MWI; < 1, hν	c, d	[120]
Fe	$Fe_2(CO)_9$	[BMIm][BF_4]	8.6 ± 3.2, MWI;[b] 7.0 ± 3.1, hν;[b] 5.2 ± 1.6, thermal[b]	c, d, e	[132,120]
	$Fe_2(CO)_9$	[BMIm][BF_4]	thermal	cyclohexenone hydrogenat. cat., see Fig. 16	[205]
Ru	$Ru_3(CO)_{12}$	[BMIm][BF_4]	1.6 ± 0.3, MWI;[b] 2.0 ± 0.5, hν;[b] 1.6 ± 0.4, thermal[b]	c, d, e; see Fig. 10, hydrogenation cat., Fig.16	[132,120]
	$Ru_3(CO)_{12}$	[BMIm][BF_4]	2.2 ± 0.4, MWI	Ru-NPs deposited on TRGO, see text, Fig. 14, Fig. 17	[117]
	$Ru_3(CO)_{12}$	[BMIm][PF_6]	2.9 ± 0.8, thermal	cyclohexenone hydrogenat. cat., see Fig. 16	[205]
Os	$Os_3(CO)_{12}$	[BMIm][BF_4]	0.7 ± 0.2, MWI;[b] 2.0 ± 1.0, hν;[b] 2.5 ± 0.4, thermal[b]	c, d, e see Fig. 10	[132,120]
Co	$Co_2(CO)_8$	[BMIm][BF_4], [BMIm][CF_3SO_3], [BMIm][$N(Tf)_2$]	5.1 ± 0.9, MWI;[b] 8.1 ± 2.5, hν;[b] 14 ± 8, thermal[b]	c, d, e	[120,132]
	$Co_2(CO)_8$	[CEMIm][BF_4] [f]	1.6 ± 0.3, MWI		[204]
	$Co_2(CO)_8$	[BMIm][$N(Tf)_2$] [C_{10}MIm][BF_4]	7.7, thermal at 150 °C	Fischer-Tropsch catalyst giving olefins, oxygenates, and paraffins (C_7-C_{30}),	[206]

				reusable at least three times	
	$Co_2(CO)_8$	$[C_{10}MIm][N(Tf)_2]$	53 ± 22, thermal at 150 °C	Co-NPs with cubic shape together with Co-NPs of irregular shape	[207]
	$Co_2(CO)_8$	$[N_{1888}][N(Tf)_2]$, [BMPyr][N(Tf)$_2$], [BMIm][PF_6], [BMIm][N(Tf)$_2$], [BMIm][BF_4]	5.8 ± 0.9 to 16 ± 3 3.6 ± 0.7 to 21 ± 6 6 ± 1 to 7 ± 1 11 ± 3 4 ± 2	magnetic fluids, particle size varies with concentration	[208]
Rh	$Rh_6(CO)_{16}$	[BMIm][BF_4], [BMIm][CF_3SO_3], [BMIm][N(Tf)$_2$]	1.7 ± 0.3, MWI;[b] 1.9 ± 0.3, h*v*;[b] 3.5 ± 0.8, thermal[b]	[c, d, e]; see Fig. 12; hydrogenation cat., see Fig. 16	[132,120]
	$Rh_6(CO)_{16}$	[BMIm][BF_4]	2.8 ± 0.5	Rh-NPs deposited on TRGO, see text, Fig. 14; hydrogenation cat., Fig. 17	[117]
	$Rh_6(CO)_{16}$	[BMIm][BF_4]	2.1 ± 0.5	Rh-NPs deposited on Teflon-coated stirring bar, see text, Fig. 15 and Fig. 18.	[209]
Ir	$Ir_4(CO)_{12}$	[BMIm][BF_4], [BMIm][CF_3SO_3], [BMIm][N(Tf)$_2$]	0.8 ± 0.2, MWI;[b] 1.4 ± 0.3, h*v*;[b] 1.1 ± 0.2, thermal[b]	[c, d, e]; hydrogenation catalyst, see Fig. 16	[132,120]
FeRu 1:1	$Fe_2(CO)_9$, $Ru_3(CO)_{12}$	[BMIm][PF_6] [BMIm][BF_4]	1.7 ± 0.3, thermal	cyclohexenone hydrogenat. cat., see Fig. 16	[205]

[a] For selected IL cations and anions see Scheme 1; [b] in [BMIm][BF4] ;[c] median diameters and standard deviations are from TEM measurements; [d] photolytic decomposition of metal carbonyls with a 1000 W Hg lamp (200-450 nm wavelength) for 15 min; [e] thermal decomposition of metal carbonyls for 6-12 h at 180-230 °C depending on the metal carbonyl. [f] [CEMIm] = 1-(3-carboxyethyl)-3-methyl-imidazolium.

The complete decomposition of metal carbonyls under microwave irradiation occurs in a rapid and short time (3-10 min) and can be verified by vibrational spectroscopy through absence of the (metal-carbonyl bands between 1750 and 2000 cm^{-1} after microwave heating (Fig. 11).[116,120]

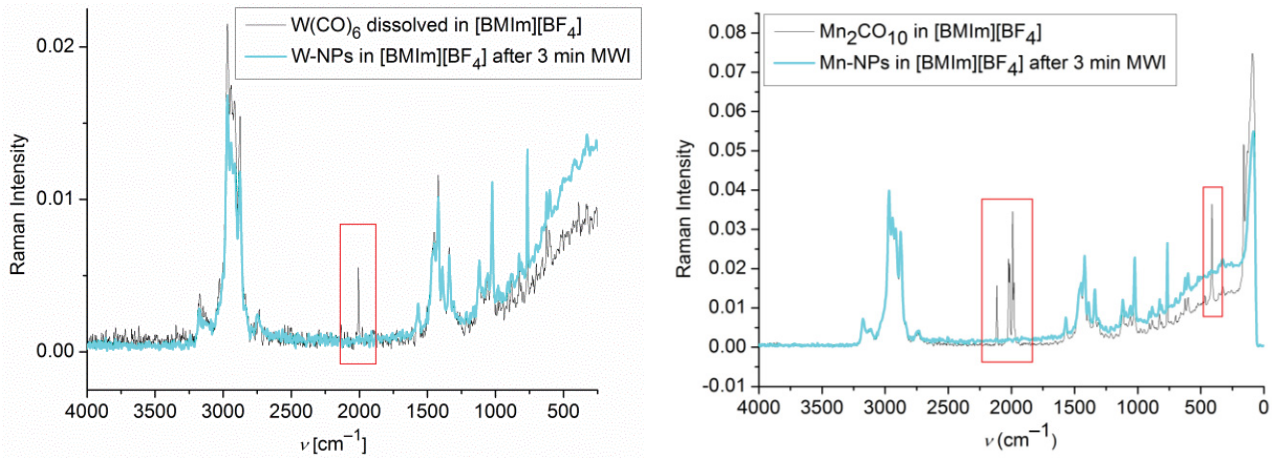

Fig. 11 Raman spectra of $W(CO)_6$ and $Mn_2(CO)_{10}$ in $[BMIm][BF_4]$ before and after microwave irradiation (MWI for 3min at 10 W). Red boxes highlight the characteristic carbonyl and metal carbonyl bands. $[BMIm]^+ = [C_4mim]^+$ (reprinted from references [116,120]).

Tungsten and rhodium nanoparticles from the corresponding metal carbonyls $W(CO)_6$ and $Rh_6(CO)_{16}$ illustrated the importance of the IL anion for stabilization by showing an increase in their diameter with the molecular volume of the ionic liquid anion (Fig. 12).[210,211,212]

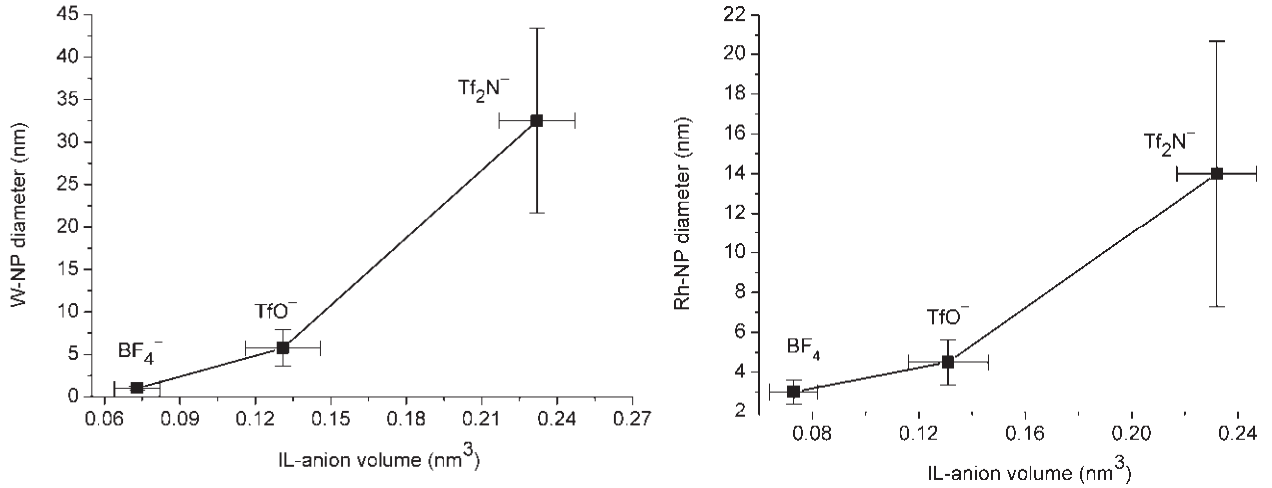

Fig. 12. Correlation between the molecular volume of the ionic liquid anion and the observed W (left) and Rh (right) nanoparticle diameter with standard deviations as error bars.[210,211] Adapted from ref. [116] with permission from the author; © 2011 Elsevier B. V.

1.5.4 Synthesis in ionic liquid with deposition on support

Ionic liquids prevent agglomeration by forming a protective layer (shell) around the particles (core). Also immobilization or deposition of nanoparticles on supports such as graphene,[117,209,213,214] carbon nanotubes[215,216] or more often Al_2O_3[217] is a means to prevent agglomeration. Furthermore, when nanoparticles are used as catalysts biphasic (liquid-liquid) homogeneous-catalytic systems[129] often exhibit leaching of metal ions to the products, making their separation and purification process economically and environmentally more complicated. To avoid these problems, the research and development of new quasi-homogeneous supported nanoparticle catalyst systems is an issue.[218,219]

In the last years, carbon-based materials such as graphene[220,221] or carbon nanotubes[222,223,224] have become substrates for the deposition of metal nanoparticles[225,226,227,228,229,230,231,232,233,234] Thermally reduced graphite oxide (TRGO, or also known as *graphene*)[225–231] has been long known[58,221] and is lately re-discovered as an extremely versatile carbon material.[220,221,235] TRGO can be prepared in a two-step oxidation/thermal reduction from natural graphite (see section 1.3.).[56,59–62,221] The functional oxygen-containing (epoxy, aldehyde, hydroxyl, carboxyl) groups still present in TRGO are an important aspect for the utilization of this material in the field of heterogeneous catalysis.[235] Surface functionalization and the high specific surface area of TRGOs of 400 $m^2 g^{-1}$ up to 1500 $m^2 g^{-1}$, make them promising support materials for catalytic applications.[230,231,235] Examples for metal-nanoparticles on carbon materials can be found in ref. [84,85,236241].

For the synthesis of M-NPs on TRGO, the IL not only acts as kinetic stabilizing template in the metal nanoparticle formation process, the IL also helps to exfoliate and separate the TRGO-“graphene" sheets in order to increase the surface area and accessibility for deposition of M-NPs. Ruthenium, rhodium or iridium nanoparticles can be supported on TRGO by decomposition through microwave irradiation of their corresponding metal carbonyl, $Ru_3(CO)_{12}$ and $Rh_6(CO)_{16}$ respectively, in an ionic liquid, e.g. [BMIm][BF_4] with small and narrow nanoparticle distribution (Ru 2.2 ± 0.4 nm and Rh 2.8 ± 0.5 nm) (Fig. 13 and Fig. 14).[117]

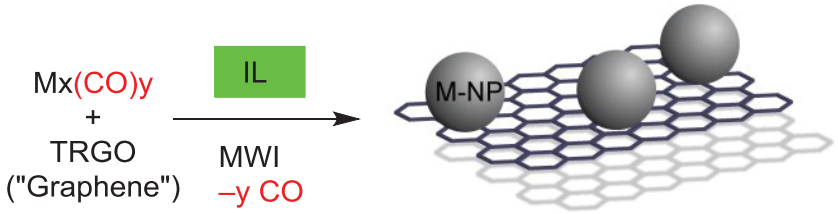

Fig. 13 Schematic synthesis of transition metal nanoparticles supported on the thermally reduced graphite oxide through microwave irradiation.[117]

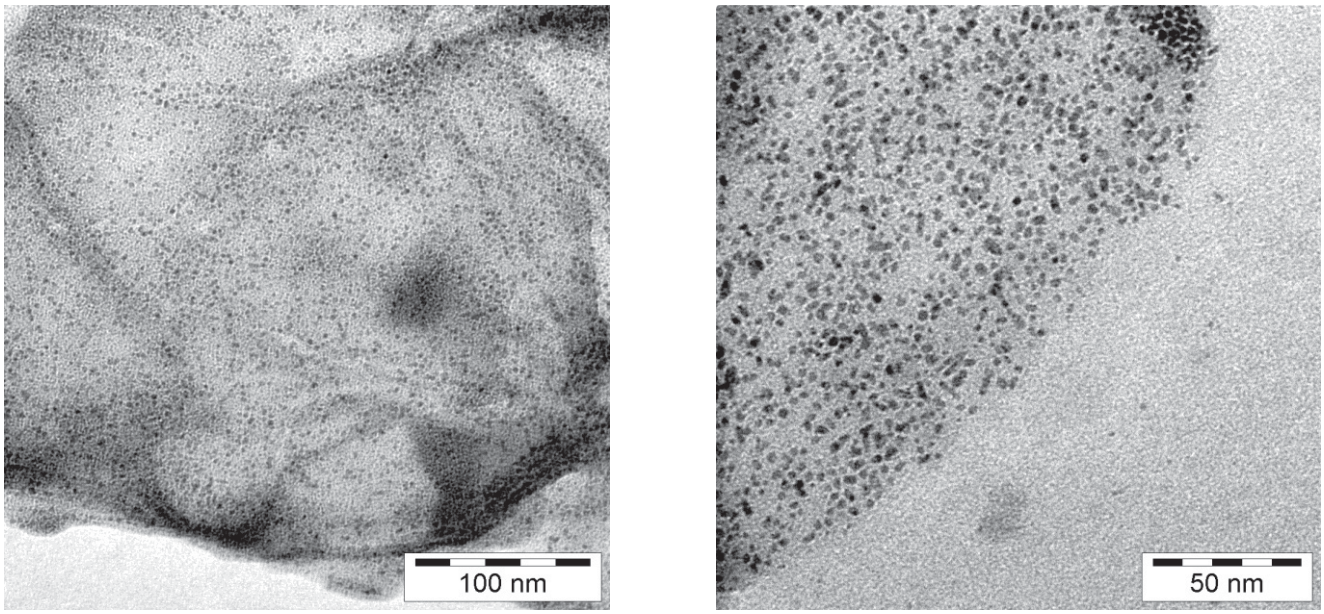

Fig. 14 TEM images of Ru-NPs (left) and Rh-NPs (right) supported on thermally reduced graphite oxide obtained upon decomposition of $Ru_3(CO)_{12}$ and $Rh_6(CO)_{16}$, respectively, by means of microwave irradiation in [BMIm][BF_4].[117] (Reprinted from ref. [117])

An example for M-NPs on a non-carbon support was reported with the deposition of Rhodium nanoparticles onto a standard Teflon-coated magnetic stirring bar which was present during microwave decomposition of $Rh_6(CO)_{16}$ in [BMIm][BF_4] (Fig. 15). The metal nanoparticle deposits could not be removed from the Teflon surface by simple washing with organic solvents. The Rh-NP/stirring bar deposits were barely visible with the naked eye and amounted to 32 µg or less Rh metal with average diameter 2.1 ± 0.5 nm on a 20 × 6 mm magnetic stirring bar.[209]

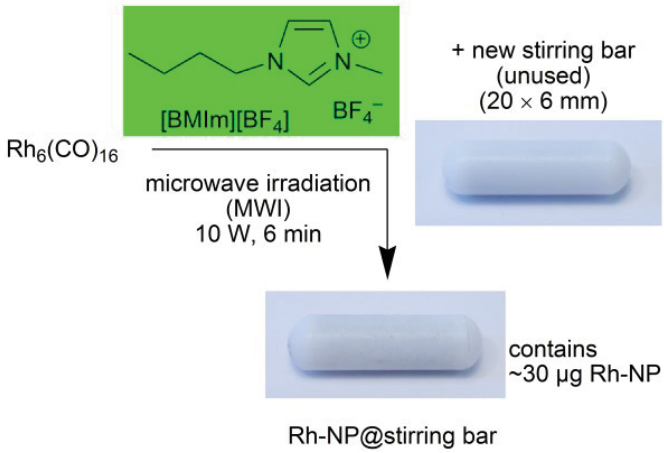

Fig. 15 Rh-NP deposition on a Teflon-coated magnetic stirring bar from an IL dispersion.[209] (Reprinted in part from ref. [209])

1.5.5 Catalytic applications of metal nanoparticles from metal carbonyls in ionic liquids

The absence of a strongly coordinating ligand layer around the metal nanoparticles in ionic liquids could represent an advantage in terms of catalytic application, because the shielding of the reactive metal surface towards the reaction substrates is drastically reduced. The ionic liquid network contains only weekly coordinating cations and anions, which should bind less strongly to the metal surface, and, hence, should be less deactivating, than commonly employed capping or protective ligands (cf. Fig. 6). In this context the system of metal nanoparticles and ionic liquids are sometimes referred to as a *green catalytic system* because it can avoid the use of organic solvents. ILs are interesting in the context of green catalysis[242] which requires that catalysts be designed for easy product separation from the reaction products and multi-time efficient reuse/ recycling[136,243,244] The very low vapor pressure of the ILs and the designable low solubility of organic substrates in ILs help for the separation of the products by distillation or removal in vacuum or by biphasic liquid-liquid separation.

Metal nanoparticles, which are stabilized on the ILs network, were shown to be recyclable and reusable catalysts, because the IL is able to retain and stabilize the M-NPs in its network.[22] The use of M-NPs/ILs dispersions (with M-NPs from non-metal-carbonyl sources) as catalyst systems for many catalytic reactions were already reviewed.[100,101,245] The higher high surface area with decreasing diameter of M-NPs provides a larger number of active sites, which generally increases the catalytic activity.[15,100,245,246,247] Generally, the catalytic properties (activity and selectivity) of dispersed M-NPs indicate that they possess pronounced surface-like (multi-site) rather than single-site-like character.[246,247]

Generally, iron,[205] ruthenium,[205] chromium,[203] palladium[248] or iridium[106] nanoparticles were used for diverse catalytic reactions in organic chemistry such as hydrogenation,[102,105,106,205] hydroformylation[105] and cross-coupling,[102,248] in multiphase conditions[103,105] and in energy-related processes such as biomass refinement.[203]

Superparamagnetic cobalt nanoparticles (Co-NPs) from $Co_2(CO)_8$ in ionic liquids, e.g. 1-alkyl-3-methylimidazolium-[$N(Tf)_2$]-ILs, with a particle diameter between 5-8 nm were catalysts for Fischer-Tropsch synthesis. The reaction of syngas was carried out at 20 atm of H_2/CO(2:1) at 210 ºC for 100 h and led mainly to hydrocarbons (Diesel-like products, C_7-C_{30} paraffins) and could be reused at least three times if they were not exposed to

air.[206,207]

Stable dispersions of Ru-, and Rh-NPs/[BMIm][BF_4] obtained by microwave irradiation from their metal carbonyls were tested as catalyst for the biphasic hydrogenation of benzene or cyclohexene to cyclohexane under organic solvent-free conditions (Fig. 16).[120,211]

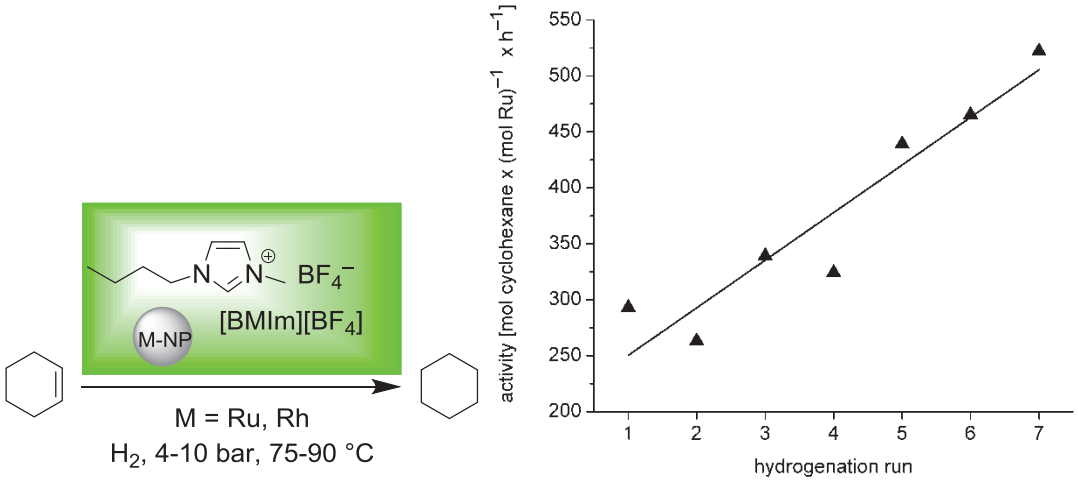

Fig. 16 Schematic hydrogenation reaction of cyclohexene to cyclohexane with Ru-, Rh- and Ir-NPs/IL dispersions (from metal carbonyls, see above) without use of an organic solvent besides IL and substrate.[117,120,211] The activity or turnover frequency (TOF) as (mol cyclohexane × (mol Ru)$^{-1}$ × h^{-1} increases with the hydrogenation run (re-use) for the Ru-NPs/IL catalyst. The hydrogenation reaction with Ru was run at 90 °C and 10 bar H_2 to 95 % conversion where the reaction was intentionally stopped as thereafter the decrease in cyclohexene concentration lowered the reaction rate.[120] It was suggested that this activity rise with each recycle could be due to surface restructuring and/or the formation of active Ru-*N*-heterocyclic carbene (NHC)[249] surface species. If the rate of restructuring or NHC-Ru formation reactions is slow then the continuous formation of defects, edges, corners, or steps on the surface, which are known to be more active sites,[250] will gradually increase the catalytic activity even after seven runs.[120] Rh/[BMIm][BF_4] catalyst yielded an activity of 400 mol product × (mol Rh)$^{-1}$ × h^{-1} with quantitative conversion at 75 °C, 4 bar H_2 pressure and 2.5 h reaction time. With the homologous Ir/[BMIm][BF_4] catalyst even higher activities up to 1,900 mol cyclohexane × (mol Ir)$^{-1}$ × h^{-1} could be obtained under the same conditions due to a shorter reaction time of 1 h for near quantitative conversion.[120] Reprinted from ref. [120].

The composite nanomaterials of Ru-NP/TRGO and Rh- NP/TRGO (obtained from metal carbonyls in ILs, see above) were catalytically active for the hydrogenation of cyclohexene or benzene with complete conversion to cyclohexane under organic-solvent-free and mild

conditions (50–100 ºC, 4–10 bar H_2) (Fig. 17).[117]

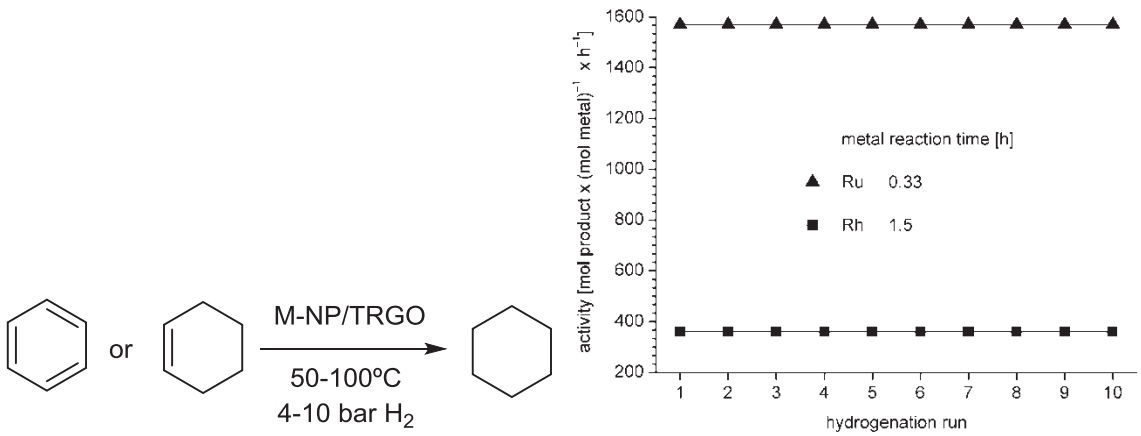

Fig. 17 Schematic hydrogenation reaction of benzene or cyclohexene to cyclohexane with Ru-, or Rh- under organic-solvent-free conditions. The constant activities for cyclohexene hydrogenation over 10 consecutive runs were achieved at 4 bar H_2 and 75 C with 0.01 mol cyclohexene, 1.89×10^{-5} mol Ru (molar substrate to metal ratio 530) or 1.82×10^{-5} mol Rh (molar ratio 550) (11 mg M-NP/TRGO with 17.4 wt% Ru or 17.0 wt% Rh, respectively).[117] Reprinted from ref. [117] with permission from the author; © 2010 Elsevier Ltd.

In addition, the Rh-NP/stirring bar could act as an easy to handle and re-usable catalyst in the organic-solvent-free hydrogenation reaction of cyclohexene with quantitative conversion and very high turnover frequencies of up to 32800 mol cyclohexene × (mol Rh)$^{-1}$ × h^{-1} (Fig. 18).[209]

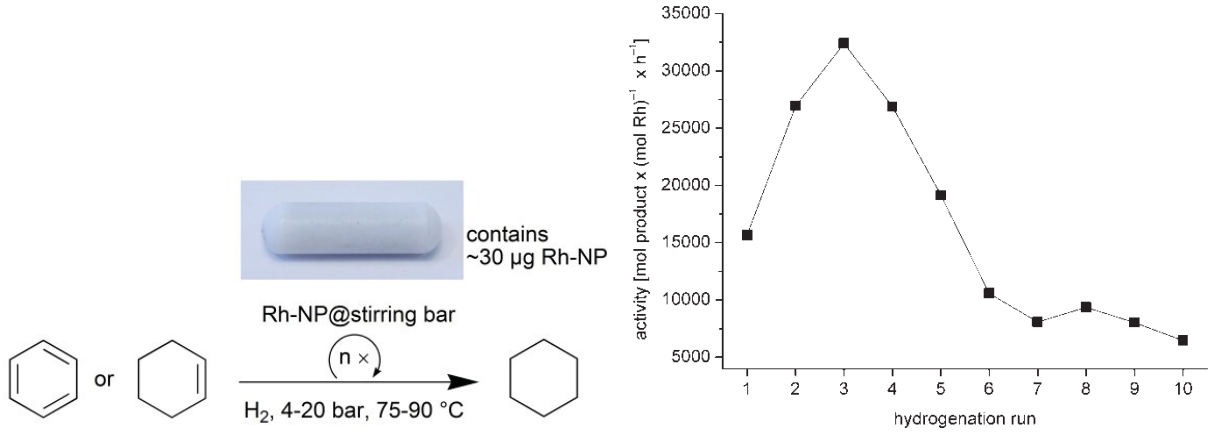

Fig. 18 Schematic benzene or cyclohexene hydrogenation by Rh-NPs deposited on a Teflon-coated magnetic stirring bar and the activity plot over 10 consecutive runs for cyclohexene hydrogenation (conditions 6.8 mmol cyclohexene, 3.1×10^{-7} mol Rh, molar ratio ~22,000; 75 °C, 4 bar H_2).[209] Reprinted in part from ref. [209] with permission from the author; © 2010 Elsevier Ltd.

Comparative activity data for related M-NP catalysts in cyclohexene and benzene hydrogenation reactions was given in the aforementioned articles.[116,117,120, 209,211]

Fe-, Ru- and bimetallic Fe-Ru-NPs were tested as catalysts in [BMIm][BF_4] and [BMIm][PF_6] for the hydrogenation of cyclohexenone to mostly cyclohexanone and partly cyclohexanol at 50 °C (Fig. 16). The bimetallic FeRu (1 : 1) alloy was most active followed by the pure Ru-NPs. Addition of CO_2 to the IL reaction mixture increased the reaction rate up to four times faster with 60 bar of CO_2 than without. At 60 bar of CO_2 a high selectivity >95 % to cyclohexanone, at a TOF of *ca.* 300 h^{-1}, was achieved and the catalyst could be reused 5 times without noticeable deactivation.[205]

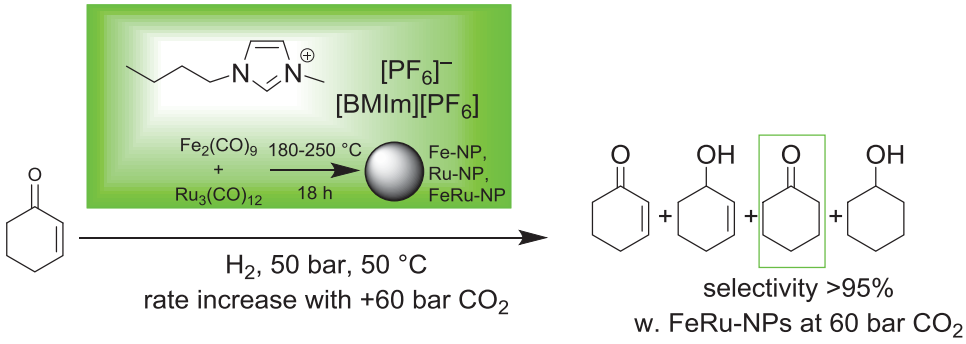

Fig. 16 Cyclohexenone hydrogenation to mostly cyclohexanone with Fe-, Ru- or FeRu-NPs obtained from (mixtures of) $Fe_2(CO)_9$ and $Ru_3(CO)_{12}$ in IL.[205]

Cr–NP catalysts from $Cr(CO)_6$ could dehydrate glucose to 5-hydroxymethylfurfural (HMF) (Fig. 17) in the IL [EMIm]Cl at T = 120 °C. Mn-, Fe- or Co-NPs from their carbonyl complexes did not catalyze this conversion.[203]

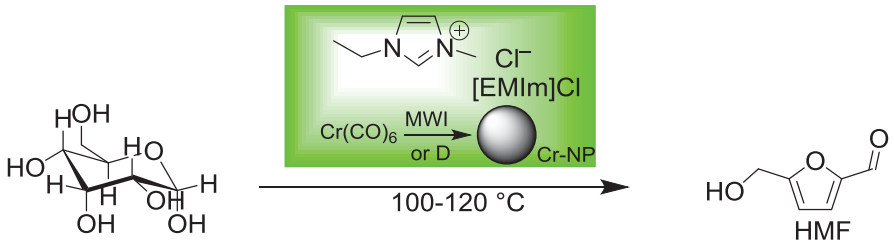

Fig. 17 Conversion of glucose to 5-hydroxymethylfurfural (HMF) by Cr-NPs (obtained from $Cr(CO)_6$ in IL).[203]

(This introduction section 1.5 is part of a cumulative thesis from the **publication 3.3**).

1.6 Biomass, a promising feedstock

In the 19th century the discovery of the crude oil or petroleum as a feedstock for the production of energy and fuels produced a worldwide impact and a huge change on the industry. However, the use of fossil fuels, especially in the petrochemical industry, contributes to the global warming, acid rain and the deterioration of the air quality because of the generation of gas emissions (nitrous acid and methane), a high consumption of heat and energy and the greenhouse effect gases through its combustion.[251] Biomass is a good alternative to fossil fuels for the production of bio-fuels, chemicals and energy, becoming a new research focus for researches in the last years (Fig. 19).[252,253,254,255]

An estimated quantity of 1.3×10^9 metric tons of dry biomass/year can be produced (from the agriculture and forest) only in the U.S. as the U.S. department of Agriculture (USDA) as the Oak Rigdest National Laboratory reported.[256] The demand of biomass is increasing in the last years, and some chemical or oil companies, as Shell[257] or Dupont[258,259] among others,[260,261] are developing the implantation of new infrastructures for the production of biofuels from the biomass.

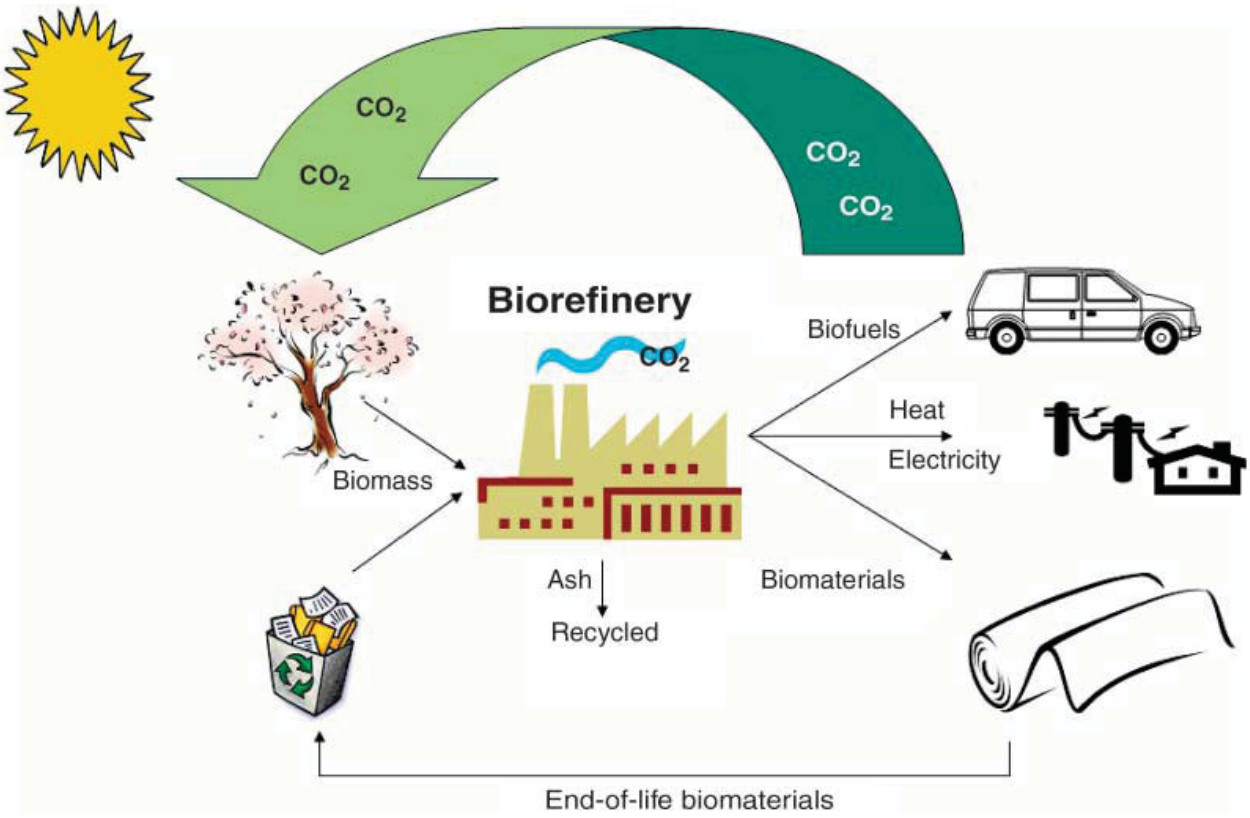

Fig. 19 Biomass to biofuels, energy and biomaterials cycle (reprinted from ref. [255]).

Biomass is a renewable source which growths from the organic waste (forest products, agricultural waste, sugar or starch crops, or water weed) and the reaction (photosynthesis) of CO_2, H_2O, sunlight and air to obtain the renewable carbon-based feedstock, lignocellulose (Fig. 20).[253] Lignocellulose is formed by lignin (10-25 %), cellulose (40-80%) and hemicellulose (15-60 %).[262,263] The lignin fraction can be removed from biomass through depolymerization/solubilization in alkaline-alcohol solutions and it is commonly destined for the synthesis of bio-fuels or burned for the production of heat and electricity.[264,265,266] Hemicellulose contains five different sugar monomers as D-xylose, L-arabinose, D-glucose, D-galactose and D-mannose, and the most common application, after their extraction and hydrolysis, is for the production of ethanol (via fermentation) or for the preparation of furfural (via dehydration).[267,268,269] Cellulose, in comparison with lignin and hemicellulose, is commonly used for the synthesis of fine chemicals. However, the hydrolysis of cellulose needs strong mineral acids solutions (H_2SO_4) and higher temperatures for the formation of hydroxymethylfurfural (HMF) and levulinic acid (LA), among other chemicals.[270,271]

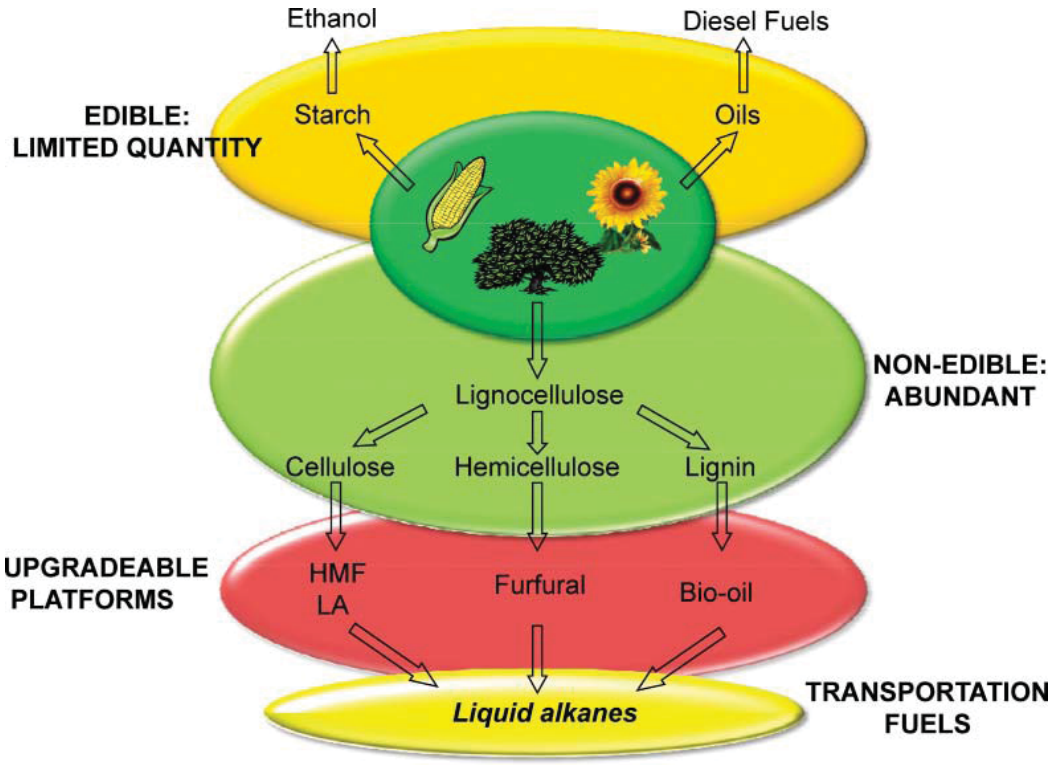

Fig. 20 Biomass based materials platform for the synthesis of biofuels (reprinted from ref. [251]).

Lignocellulosic biomass is mainly processed by thermochemical (gasification, pyrolysis or liquefaction) and hydrolysis routes.[272] The thermochemical processes involve high temperatures (up to 500 ºC) and pressures, and are normally coupled to the syn-gas

catalytic process (such as the Fischer-Tropsch, methanol or Water-Shift synthesis) for the synthesis of bio-fuels.[251,273,274,275,276,277] Meanwhile, in the hydrolysis route the biomass is treated by chemical or biological processes, which are more expensive as the thermochemical, however offer a wider selective range of chemicals and processing options.[251,264,278,279,280,281]

1.6.1 Synthesis of fine chemicals from lignocellulosic biomass

The synthesis of sugars from lignocellulosic biomass requires a previously pre-treatment to decrease the crystallinity of cellulose as well as to achieve the separation of the hemicellulose and lignin from the cellulose. Pre-treatment of lignocellulose is the most expensive process of the biomass treatment and includes chemical, physical and thermal treatments.[264] The hydrolysis of the obtained cellulose is used for the production of sugars (glucose or xylose), which can be converted into fine chemicals such as hydromethylfurfural (HMF) or levulinic acid, and fuels (for the ethanol production).

Levulinic acid (LA) can be easily and cheaply produced from the hydrolysis of cellulosic biomass.[282,283] The further chemical reactions as hydrogenation, (de)hydration or hydrogenolisis convert the levulinic acid into derivates as γ-valerolactone (GVL), valeric fuels, pentanoic acid (PA), 5-nonanone or methyltetrahydrofuran (MTHF).[251,284,285,286,287,288,289,290,291] An interesting product from the hydrogenation of levulinic acid is γ-valerolactone (GVL).[291] GVL is a colorless liquid commonly used as additive for perfumes or food due to their sweet and herbaceous odor and is stable at normal conditions with a high boiling point (207 ºC), and it is also used as solvent for the synthesis of valeric esters, butane or MTHF.[285,292,293]

Noble metals, such as Zr-, Cu-, Pt-, Ru-, or Pd-NPs, are commonly used as catalysts for the hydrogenation of levulinic acid, which are usually supported on carbon. The reduction of levulinic acid can be done using molecular hydrogen[294,295,296,297] or formic acid as reductant,[298,299] being Ru-[300,301] and Pd-NPs[302] often used.

Weckhuysen et al. reported the influence of the support for Ru-NPs in the hydrogenation of levulinic acid.[303] Non-acidic materials (Ru/TiO_2) show higher selectivities to GVL as when zeolite materials are used (Ru/H-b or H-ZSM5). However, the strongly acidic sites on the zeolite materials can upgrade the levulinic acid conversion to pentanoic acid (PA).

Supported palladium nanoparticles (Pd-NPs) on SiO_2 were also reported by *Yan et al.* achieving a turn over number (TON) of 884.7 for a 97.3 % conversion of LA to GVL.[304] Other mesoporous supports such as MCM-41, ZrMCM-41 and TiMCM-41 were also tested for supporting Pd-NPs for the hydrogenation of LA, reaching high conversions and selectivity's after several hydrogenation runs without loss of their catalytic activity.[305]

Recently, *Chieffi et al.* reported the use of FeNi-bimetallic nanomaterials to obtain GVL at 150 ºC and 50 bar H_2 in EtOH solutions to achieve conversions of 99.6 % to GVL.[306] *Yang et al.* also described the used of Ru-Ni/C bimetallic nanomaterials for the hydrogenation of LA to GVL. Ru-Ni/C nanomaterials can be recovered and re–used for at least 15 consecutive hydrogenation runs reaching activities with a turn over frequency of >2000 h^{-1}.[307]

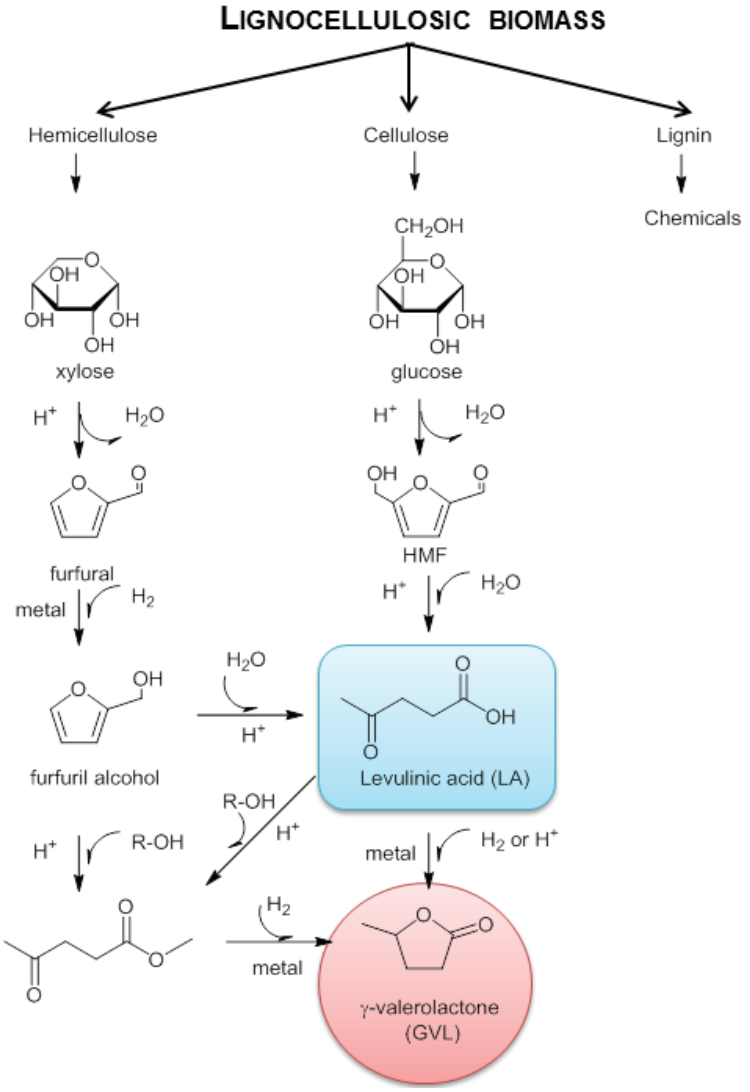

Fig. 21 Reaction routes from lignocellulosic biomass to fine chemicals (adapted from ref. [291]).

2. Aim of this work

The synthesis of metal nanoparticles is usually done using capping ligands or stabilizers to stabilize and avoid the aggregation and agglomeration of the particles. However, the presence of ligands around M-NPs could reduce the catalytic activity, and therefore the application. The aim of this thesis was based on the synthesis of “naked” metal nanoparticles in the ionic liquid 1-Butyl-3-methylimidazolium tetrafluoroborate, ([BMIm][BF_4]), and in propylene carbonate (PC) through the reduction or decomposition of metal salts or metal carbonyls by microwave irradiation without the presence of external stabilizers.

The use of metal carbonyls compounds should be investigated as starting materials. Iridium- and ruthenium-NPs should be deposited on thermally reduced graphite oxide (TRGO) by the thermal decomposition of $Ir_4(CO)_{12}$ and $Ru_3(CO)_{12}$ through microwave irradiation in [BMIm][BF_4] and PC. The obtained Ir@TRGO and Ru@TRGO nanomaterials should be investigated for hydrogenation reactions as reusable catalysts for more than 5 consecutive runs.

This work is also focused on the synthesis of copper nanoparticles (Cu-NPs), a more challenging research due to the quick oxidation and aggregation of Cu-NPs. The induced microwave-reduction of the different copper salts or organometallic compounds should be tested in both solvents, ILs and PC.

Metal-nanoparticles and metal@TRGO nanomaterials should be fully characterized by transmission electron microscopy (TEM) for an accurate size distribution of the nanoparticles, together with a further analysis by powder X-ray diffraction (PXRD), energy dispersive X-ray spectroscopy (EDX), atomic absorption spectrometry (AAS) and X-ray photoelectron spectroscopy (XPS), which gives more information about the composition, oxidation state, and the metal content on metal@TRGO nanomaterials.

3. Publications

In the following sections (3.1-3.4) are described the publications which are part of this cumulative thesis. The publications are cited by the chronological order of publication and submission, with their own references list. A brief introduction and summary of each publication is given, together with the assignments of tasks of the authors.

The unpublished results are presented in the section 4 of this work.

3.1 Iridium@graphene composite nanomaterials synthesized in ionic liquid as re-usable catalysts for solvent-free hydrogenation of benzene and cyclohexene.

R. Marcos Esteban, K. Schütte, P. Brandt, D. Marquardt, H. Meyer, F. Beckert, R. Mülhaupt, H. Kölling, C. Janiak.
Nano-Structures & Nano-Objects **2015**, *2*, 11–18.
http://dx.doi.org/10.1016/j.nanoso.2015.07.001, ref. [85].

Small iridium nanoparticles (Ir-NPs) can be easily obtained and supported on thermally reduced graphite oxide (TRGO) after decomposition of tetrairidium dodecacarbonyl, $Ir_4(CO)_{12}$, by two different heating methods such as microwave irradiation (MWI) and electron-beam irradiation (IBA Rhodotron accelerator) (Scheme 3).

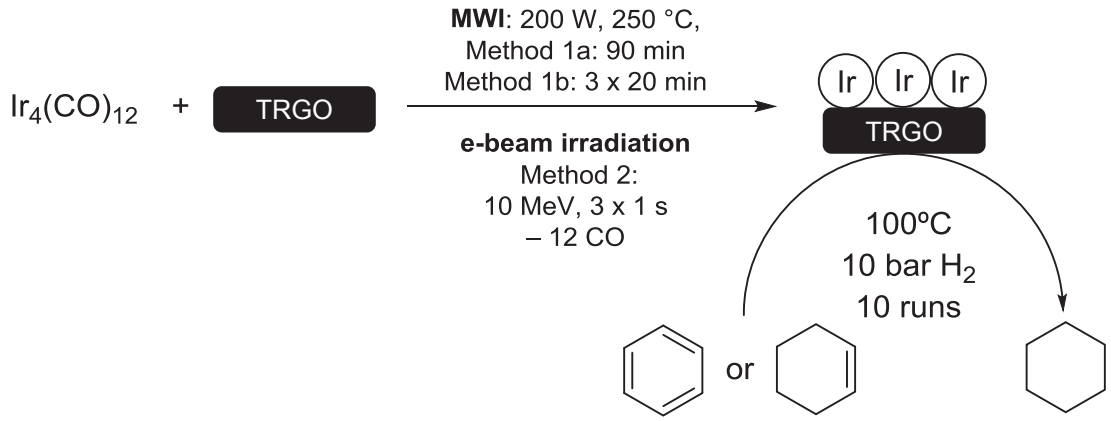

Scheme 3 Schematic synthesis of Ir@TRGO in [BMIm][BF_4] and their application as catalyst for hydrogenation reactions of benzene or cyclohexene to cyclohexane.

The stable Ir@TRGO nanomaterials were characterized by transmission electron microscopy (TEM) showing a well size distribution of the Ir-NPs on the TRGO layers with an average of 1.0 ± 0.4 and 2.7 ± 0.7 nm for the microwave reactions (method 1a and 1b respectively) and of 3.6 ± 1.0 nm for e-beam irradiation (method 2). Further analysis were done by powder X-ray diffraction (PXRD), energy dispersive X-ray spectroscopy (EDX), infrared spectroscopy (IR) and atomic absorption spectrometry (AAS) to give information about the composition and structure of the Ir@TRGO nanomaterials.

The Ir@TRGO nanomaterials were tested for the relevant hydrogenation of benzene or cyclohexene to cyclohexane, a useful feedstock for the synthesis of Nylon or caprolactam [308,309]. The hydrogenation reaction were done under mild conditions (100ºC,

10 bar H_2), where Ir@TRGO nanomaterials show a good selectivity to cyclohexane without the presence of secondary products as cyclohexene. The catalyst could be recovered and re-used for at least ten consecutive runs without loss of activity and achieving turn over frequencies up to 10000 h^{-1} (Fig. 22).

The Ir@TRGO nanocomposites seem to be very stable along the consecutive hydrogenation runs and heating processes and the Ir-NPs increases their size only ca. 1 nm after ten consecutives runs (Fig. 23).

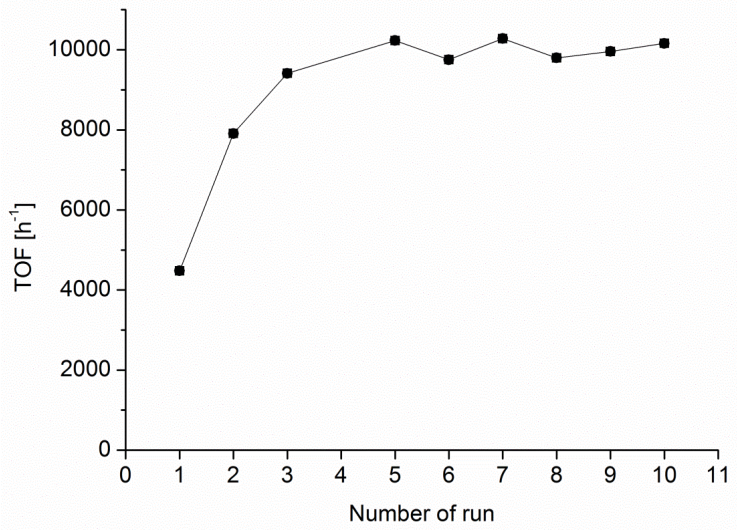

Fig. 22 Turn over frequency over number of run for the hydrogenation of benzene to cyclohexane using Ir@TRGO nanomaterials (method 1b) as catalyst (100ºC, 10 bar H_2).

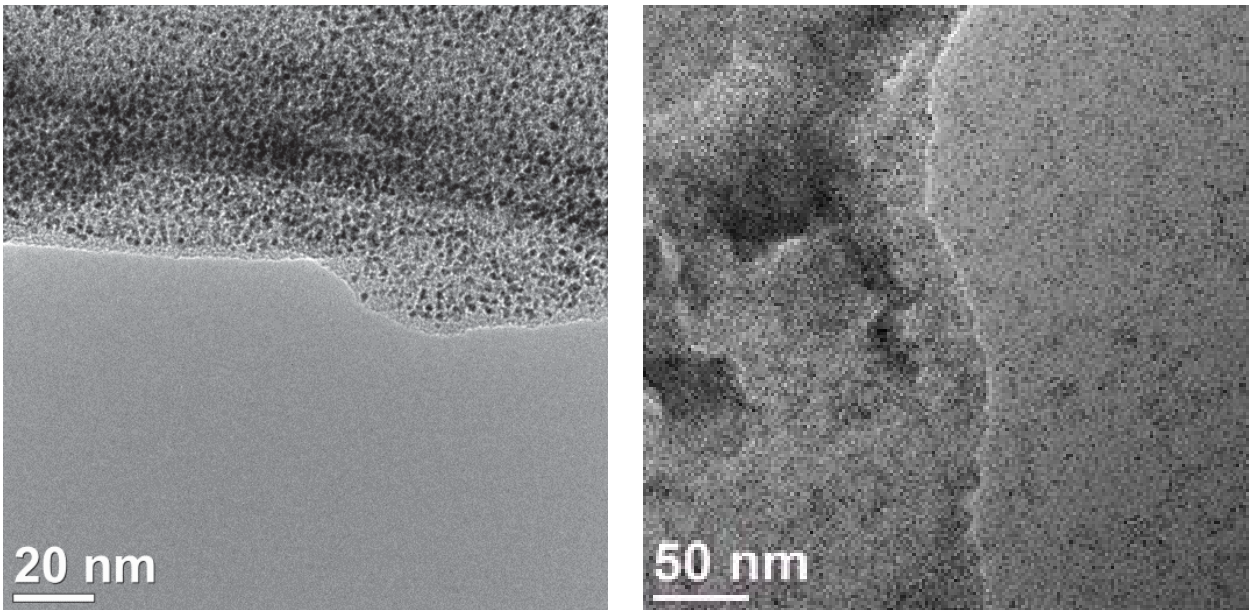

Fig. 23 TEM images of Ir@TRGO nanomaterials (left) before and (right) after the hydrogenation of benzene (method 1b).

Author's contribution to the publication:*

- Previously bibliographic research, design of the synthetic procedures and application of the methods (experimental work).[310]
- Characterization of the samples by PXRD, IR and AAS, and GC analysis for hydrogenation reactions.
- Writing of the manuscript together with the further edition according to the reviewer's comments.

* Detailed work of the co-authors in the manuscript:

-Dr. Schütte and H. Meyer: measurements of TEM and EDX.

-P. Brandt: laboratory work for the hydrogenation reactions of cyclohexene to cyclohexane during his Bachelor thesis.

-Dr. D. Marquardt: previous work on the decomposition and deposition of $Ir_4(CO)_{12}$ on TRGO.[310]

-Dr. Fabian Beckert and Prof. Dr. R. Mülhaupt: synthesis of the thermally reduced graphite oxide (TRGO).

-Hartmurth Kölling: cooperation for the electron-beam irradiation experiments.

Nano-Structures & Nano-Objects 2 (2015) 11–18

Contents lists available at ScienceDirect

Nano-Structures & Nano-Objects

journal homepage: www.elsevier.com/locate/nanoso

Iridium@graphene composite nanomaterials synthesized in ionic liquid as re-usable catalysts for solvent-free hydrogenation of benzene and cyclohexene

Raquel Marcos Esteban [a], Kai Schütte [a], Philipp Brandt [a], Dorothea Marquardt [a], Hajo Meyer [a], Fabian Beckert [b], Rolf Mülhaupt [b,c], Hartmuth Kölling [d], Christoph Janiak [a,*]

[a] Institut für Anorganische Chemie und Strukturchemie, Heinrich Heine Universität Düsseldorf, 40204 Düsseldorf, Germany

[b] Freiburger Material Forschungszentrum (FMF) and Institut für Makromolekulare Chemie, Universität Freiburg, Stefan-Meier-Str. 21-31, 79104 Freiburg, Germany

[c] FRIAS, Freiburg Institute for Advanced Studies, Albertstr. 19, 79104 Freiburg, Germany

[d] Herotron E-Beam Service GmbH, Guardianstrasse 6-10, 06766 Bitterfeld-Wolfen, Germany

HIGHLIGHTS

- Easy iridium nanoparticle synthesis and deposition on graphene in ionic liquids (ILs).
- Rapid synthesis by microwave or electron-beam irradiation of Ir-carbonyl in ILs.
- Ir-nanoparticles on graphene as stable, re-usable hydrogenation catalyst.
- Synthesis and catalytic use of stable 2–5 nm Ir-nanoparticles on graphene.
- Hydrogenation catalysis under solvent-free conditions with easy catalyst recycling.

GRAPHICAL ABSTRACT

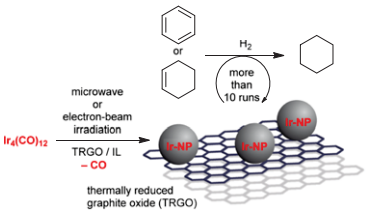

Iridium nanoparticles (Ir-NPs) can easily and quickly be prepared by microwave or electron-beam irradiation from the metal carbonyl in ionic liquids (IL), supported on graphene and show high and stable catalytic activities over several runs in benzene or cyclohexene hydrogenation reactions under organic-solvent-free and mild conditions.

ARTICLE INFO

Article history:
Received 16 July 2015
Accepted 20 July 2015

Keywords:
Iridium nanoparticles
Graphene
Thermally reduced graphite oxide, TRGO
Benzene hydrogenation
Catalysis

ABSTRACT

Synthesis of stable hybrid iridium@graphene nanomaterials in the ionic liquid (IL) 1-butyl-3-methylimidazolium tetrafluoroborate ([BMIm][BF_4] through microwave irradiation (MWI) or electron-beam (e-beam) irradiation (IBA Rhodotron accelerator) induced decomposition of $Ir_4(CO)_{12}$ in the presence of graphene provides an easy method for the generation of small iridium nanoparticles with size distributions of 1.0 ± 0.4 and 2.7 ± 0.7 nm by MWI reactions with 90 and 60 min decomposition time, respectively, and of 3.6 ± 1.0 nm for e-beam irradiation synthesis. Graphene was derived by thermal reduction of graphite oxide (TRGO). Powder X-ray diffraction (PXRD), transmission electron microscopy (TEM) and energy-dispersive X-ray spectrometry (EDX) showed the formation of Ir nanoparticles which are evenly distributed on the TRGO sheets. Ir@TRGO proved to be a highly active (~10 000 mol cyclohexane x(mol Ir)$^{-1}$x h^{-1} for benzene hydrogenation) and selective heterogeneous catalyst for the industrially relevant hydrogenation of benzene or cyclohexene to cyclohexane under mild conditions (100 °C, 10 bar H_2) with quantitative conversion. The catalyst could be re-used over 10 consecutive hydrogenation reactions with similar activities. A brief correlation between activity and particle size points to an optimal diameter or surface regime for the catalytic activity with iridium particles of 3.6 ± 1.0 nm on TRGO giving here the highest activity in benzene hydrogenation.

* Corresponding author. Tel.: +49 211 81 12286; fax: +49 211 81 12287.
E-mail address: janiak@uni-duesseldorf.de (C. Janiak).

http://dx.doi.org/10.1016/j.nanoso.2015.07.001

1. Introduction

New methods and techniques for the synthesis of metal nanoparticles (M-NPs) have increased in the last five years due to their applications in fields of medicine [1], industry [2] or science [3]. The high surface area and thereby large number of active centers make the metal nanoparticle dispersions very attractive catalysts [4,5].

Typical syntheses of metal nanoparticles in aqueous or organic solutions need the presence of capping ligands, surfactants or polymer coating as stabilizer around the metal nanoparticle to prevent their aggregation and agglomeration in Ostwald ripening processes [6–8]. In recent years ionic liquids were developed into an alternative to traditional solvents [9,10]. The electrostatic and steric properties of ionic liquids (ILs) as molten salts do not require additional stabilizing ligands around the metal nanoparticles [11–13]. The possibility to prepare ligand-free, sometimes called "naked" metal nanoparticles (M-NPs) is advantageous for catalytic applications [13]. The high ionic charge, polarity and dielectric constant of ILs gives them a very high absorption efficiency for microwave irradiation (MWI) and allows for rapid microwave heating during precursor decomposition for nanoparticle synthesis [14–20]. Nanoparticle synthesis in ILs can be achieved from metal salts with [21–24] or without reducing H_2 gas [25–27], organometallic π-complexes [28–33] and metal carbonyls [17,18, 34–39] through thermal or photochemical [40,41] decomposition or electroreduction/ electrodeposition [11,42,43].

M-NP/IL dispersions as catalytic systems can be also re-used and recycled for many times, showing no loss of efficient and catalytic activity [18,44,45]. Biphasic (liquid–liquid) homogeneous-catalytic systems [6] often exhibit leaching of metal ions to the products, making their separation and purification process economically and environmentally more complicated. To avoid these problems, the research and development of new quasi-homogeneous nanoparticle catalyst systems is growing in the last few years [46,47].

Carbon-based materials like carbon nanotubes (CNTs) [48–50] are long known substrates for the deposition of metal nanoparticles. Nowadays a novel attractive material of the carbon family is thermally reduced graphite oxide (TRGO) also commonly named "*graphene*" [51]. Its tunable properties introduce this material as a novel support material for the deposition of metal nanoparticles such as Au- [52], Cu- [53], Pt- [54], Rh- or Ru-NPs [36,55] among others.

M-NPs synthesized using electron-beam (e-beam) irradiation are already reported in the literature. Uranium dioxide (UO_2) nanoparticles were obtained by electron beam irradiation of 7 MeV [56]. Cadmium selenide nanoparticles (CdSe) could also be synthesized by electron beam irradiation of aqueous butanol solutions with equimolar amounts of $Cd(NH_3)_4SO_4$ and Na_2SeSO_3 [57,58]. Also, gold/iron oxide composite were reported using a high-energy electron-beam irradiation [59].

Here we report the synthesis of iridium nanoparticles in ionic liquids with small size and narrow size distribution and their in situ deposition on thermally derived graphite oxide (Ir@TRGO). The energy input for metal-precursor decomposition can subtly influence the decomposition kinetics, nucleation and growth processes of nanocrystals. Thus, two different methods (MWI and e-beam irradiation) are also compared here for their possible influence in the synthesis of metal nanoparticles. The hybrid materials were tested for the industrially relevant catalytic hydrogenation of benzene and cyclohexene to cyclohexane [60,61].

2. Results and discussion

2.1. Synthesis and characterization of supported iridium nanoparticles

Iridium nanoparticles were obtained through thermal decomposition of $Ir_4(CO)_{12}$ by means of microwave irradiation (MWI) or e-beam irradiation (IBA Rhodotron accelerator) in 1-butyl-3-methyl-imidazolium tetrafluoroborate ([BMIm][BF_4]). The concomitant decomposition of tetrairidium dodecacarbonyl, $Ir_4(CO)_{12}$ and exfoliation of TRGO in [BMIm][BF_4] were achieved using the energy input by microwave (200 W, 250 °C, 90 min (**1a**) or 3 × 20 min (**1b**)) or e-beam irradiation (10 MeV, 3 × 1 s (**2**)) (Scheme 1).

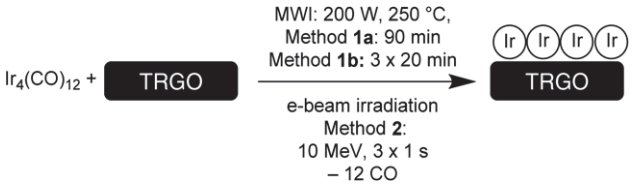

Scheme 1. Schematic synthesis of iridium@graphene nanomaterials in [BMIm][BF_4].

Powder X-ray diffractograms (PXRD) of the Ir@TRGO composites show the characteristic reflections at 2ϑ values of 40.7°, 46.8°, 68.6° and 83.3° corresponding to the (111), (002), (022) and (113) reflection of iridium metal (Fig. 1 and Fig. S2). Yet, a low intensity, high background and broad peaks indicate that the Ir-NPs are small and/or of low crystallinity. A particle-size determination by the Scherrer equation gave a diameter of 1.2 nm for the method **1a** and of 2.2 nm in the case of the method **1b** based on the most intense (111) reflection. A more accurate size and size distribution of the composites was derived from transmission electron microscopy (TEM) with the images shown in Fig. 2, and in the Supp. Info. Fig. S4 and S5. Small nanoparticles with narrow size distributions were obtained after 90 min (**1a**) and 3 × 20 min (**1b**) from microwave reaction, with a medium diameter of 1.0 ±0.4 nm (**1a**)

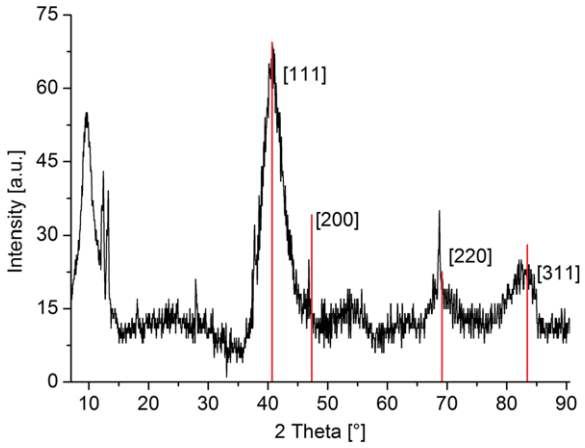

Fig. 1. Powder X-ray diffractogram of Ir@TRGO (Method **1a**) synthesized in [BMIm][BF_4]. Reference data in red for Ir metal is taken from the crystallographic open database, COD 9008470. The 2 Theta values between 5 and 25° correspond to the reflections of TRGO and in particular at 10° to residual GO (see Supp. Info. Fig. S1). (For interpretation of the references to color in this figure legend, the reader is referred to the web version of this article.)

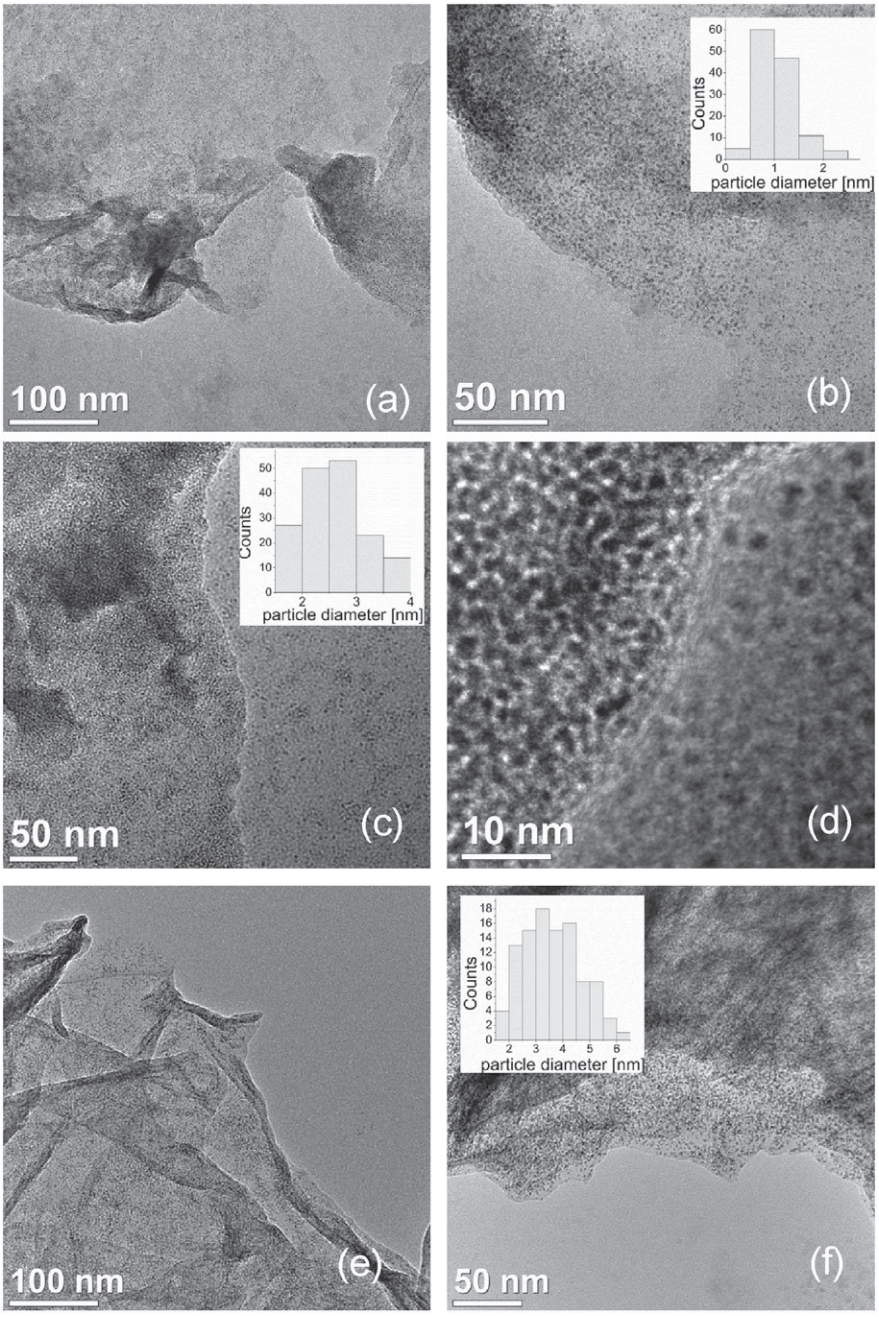

Fig. 2. TEM images of Ir@TRGO nanomaterials synthesized in [BMIm][BF_4] using microwave irradiation **1a** (a–b), **1b** (c–d) and e-beam irradiation **2** (e–f). Particle diameter distribution from 150 particles each is depicted in the inserted histograms. Additional TEM images for method **1a** and **1b** are shown in Fig. S4 and S5 in Supp. Info.

and 2.7 ±0.7 nm (**1b**), respectively (Table 1). The e-beam irradiation method (**2**) gave larger particles with a size distribution of 3.6 ±1.0 nm albeit of no crystallinity (Fig. S3).

The metal content of the Ir@TRGO composites was determined by atomic absorption spectrometry (AAS) between 3.6 and 7.2 wt%, depending on the method (Table 1). An elemental analysis by energy dispersive X-ray spectroscopy (Fig. S6 to S8 in supp. info.) only gave the expected bands for Ir metal (Ir-Lα, -Lγ, -Lλ1, -Mα, -Mγ) besides the bands for carbon and copper of the TRGO and the carbon-coated copper grid.

Infrared spectroscopy (IR) was used to follow and verify the decomposition of $Ir_4(CO)_{12}$. The IR spectra of the Ir@TRGO products in Fig. 3 still show weak absorptions for carbonyl bands at 2021 and 2058 cm^{-1}, which correspond to the CO stretching bands from the $Ir_4(CO)_{12}$ starting material. Hence, it can be concluded that either

Table 1
Ir@graphene nanomaterials synthesized in [BMIm][BF_4].

Method[a]	PXRD diameter distribution $\emptyset \pm \sigma$ (nm)[b]	TEM diameter distribution $\emptyset \pm \sigma$ (nm)[c]	Metal content (wt %)[d]
1a	1.2	1.0 ±0.4	4.9
1b	2.2	2.7 ±0.7	3.6
2	[e]	3.6 ±1.0	7.2

[a] Ir@TRGO nanomaterials were heated under microwave irradiation for 90 min (**1a**) and 3 × 20 min (**1b**) or by e-beam irradiation (**2**).
[b] From PXRD by the Scherrer equation based on the (111) reflection.
[c] Determined by TEM (cf. Fig. 2).
[d] Determined by AAS.
[e] The e-beam irradiation sample failed several times to give a PXRD.

residual $Ir_4(CO)_{12}$ precursor is still present or, more likely, that CO is bound to the surface of the iridium nanoparticles.

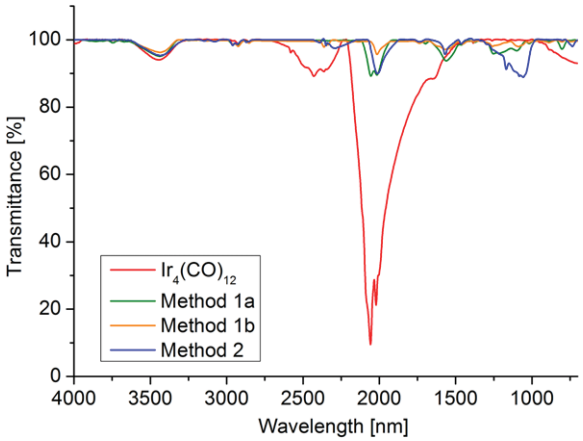

Fig. 3. Comparison of IR spectra of the Ir@TRGO composites synthesized by different methods (cf. Scheme 1) from $Ir_4(CO)_{12}$.

2.2. Hydrogenation of benzene to cyclohexane

The Ir@TRGO composite nanomaterials were tested for the industrially relevant hydrogenation of benzene to cyclohexane (Scheme 2) [60,61].

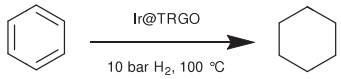

Scheme 2. Hydrogenation of benzene to cyclohexane with Ir@TRGO.

All catalytic reactions were done under inert atmosphere in a Büchi stainless-steel autoclave provided with a glass inlay to avoid any influence of the steel surface. The precursor material $Ir_4(CO)_{12}$ was also tested in 10 consecutive runs for benzene hydrogenation reaction, albeit without giving any activity.

The Ir@TRGO composite was suspended together with the benzene substrate in the autoclave. The hydrogenation reaction was carried out solvent-free at 100 °C at a constant pressure of 10 bar of H_2 with monitoring of the H_2 uptake over time (Figs. 4 and 5, Fig. S9 and S10). After one hour the reaction was stopped and cooled to room temperature. The products were condensed under vacuum in a cold trap and the composition was determined by GC. The catalyst can be recovered and re-used for at least five to ten times, without a significant loss of activity (Table 2).

For the Ir@TRGO nanocomposites synthesized by method **1b**, it could be observed that the catalyst is less active in the first runs (Table 2). The Ir@TRGO catalyst from method **1b** increased its activity to a maximum activity in about run 6 or 7 with TOF $=\sim$ 6300 or 10,300 h^{-1} depending on the experiment (Fig. S10c). The activity increase seen with Ir@TRGO **1b** may also be due to the initially still present CO coverage (cf. Fig. 3) of active sites. For Ir@TRGO synthesized by method **2** the activity was at maximum with the first run with no further increase (Fig. 5, Table 2). Catalytic tests for Ir@TRGO by method **1a** are given in the Supp. Info (Fig. S9, Tab. S1).

Conversion of benzene to cyclohexane was determined by H_2-gas uptake. Additional GC analyses also showed in all the cases cyclohexane as the only product without the presence of the cyclohexene intermediate.

In the case of the Ir@TRGO nanomaterials we found that the slightly larger nanoparticles from method **2** (3.6 ±1.0 nm diameter) gave initially a higher activity during the first and next runs (Table 2) compared to the smaller nanoparticles **1b** (2.7 ±0.7 nm diameter). The latter only increased in activity after run 4.

Table 2
Hydrogenation of benzene to cyclohexane by Ir@TRGO nanomaterials[a].

Catalyst[b]	Conversion (%)[e]		TOF (h^{-1})[f]	
$Ir_4(CO)_{12}$	None			
	–			
Ir@TRGO **1b**[c]	Exp. 1	Exp. 2	Exp. 1	Exp. 2
run 1	59.8	52.6	2210	4478
run 2	76.0	80.4	3033	7909
run 3	92.3	80.4	3325	9411
run 4[g]	87.3	40.2[g]	3358	4124
run 5[g]	69.8[g]	95.9	3668	10232
run 6	91.0	95.9	6251	9750
run 7	89.8	80.4	5104	10280
run 8	83.5	92.8	4879	9797
run 9	91.0	80.4	4678	9959
run 10	91.0	95.9	4326	10159
Ir@TRGO **2**[d]				
run 1	97.4		4861	
run 2	90.8		3870	
run 3	89.7		3723	
run 4	96.3		4582	
run 5	52.5		2194	

[a] Hydrogenation reactions were done at 100 °C, 10 bars of H_2 and using a Büchi stainless-steel autoclave with a Büchi press-flow controller for measuring the H_2-uptake over the time.
[b] Molar ratio benzene/iridium, 3790 for method **1b**, experiment 1, 4490 **1b**, experiment 2 and 3943 for method **2**; see caption of Figs. 4 and 5 for further details.
[c] Synthesis by microwave irradiation; Catalytic tests for Ir@TRGO by method **1a** are given in the Supp. Info (Fig. S9).
[d] Synthesized by e-beam irradiation.
[e] Determined by H_2-uptake.
[f] TOF = mol cyclohexane × (mol Ir)$^{-1}$ × h^{-1}.
[g] Run 5 (4) in experiment 1 (2) had an instrumental error (see Fig. S10). It is important to note, however, that the problems observed in run 5 (4) were instrumental problems with the Büchi bpc gas flow controller or the autoclave. It was not a catalyst problem as the following run gave a high conversion and TOF again.

The Ir-NPs on TRGO showed a slight increase in average diameter of ∼1 nm for both samples **1b** and **2** according to TEM investigation after the 10th or 5th catalytic hydrogenation run, respectively. The Ir@TRGO **1b** synthesized by MWI (Fig. 6) exhibited a size distribution of 3.6 ±1.1 nm after ten hydrogenation runs, compared to 2.7 ±0.7 nm before. Ir@TRGO from e-beam irradiation method **2** (Fig. 7) gave a distribution of 4.6 ±1.5 nm after five hydrogenation runs, compared to 3.6 ±1.0 nm before (cf. Table 1). This leads us to conclude that there may be an optimal diameter or surface regime for the catalytic activity. Here, particles around 3.6 nm – which is the initial size from method **2** or reached during catalysis for method **1b** – can be correlated with high catalytic activity.

The size of the nanoparticles has an influence on the turnover frequency. Cunha and co-workers [62] reported for Ir nanoparticles supported on γ-Al_2O_3, that the use of smaller nanoparticles (<2 nm) gave a decreasing activity in the hydrogenation of benzene and toluene. This size dependent behavior was also observed for other catalytic reactions using supported Pt-NPs on Al_2O_3 [63] or on activated carbon [64,65], rhodium nanoparticles [66,67] or palladium nanoparticles [68].

When comparing noble-metal nanoparticle catalysts in the hydrogenation of benzene (Table 3) supported iridium nanoparticles on TRGO (TOF ∼ 10 000 h^{-1}) or zeolite [69] (TOF 3190 h^{-1}) gave a higher catalytic activity in comparison with unsupported Ir-NPs [23] in ionic liquid dispersions (∼85 h^{-1}) or in solvent-free conditions (∼71 h^{-1}) (Table 3). When considering the lower H_2 pressure of 3 bar also Ir@zeolite [69] gave high activities (Table 3).

Cyclohexene could be hydrogenated under the same mild conditions using Ir@TRGO (investigated here for the material from method **1b**). A complete conversion was achieved in less than 5 min at 100 °C and 10 bar of H_2 pressures without any loss of activity

Table 3
Hydrogenation reactions of benzene to cyclohexane by different materials.

Nanoparticle catalyst	T (°C)	p H_2 (bar)	TOF (h^{-1})	Reference
Ir@TRGO	100	10	10 000	this work
Ir@zeolite	25	3	3190	[69]
Ir-NPs	75	4	71	[23]
Ir-NP/IL	75	4	85	[23]
Ru/SiO2	100	20	5000	[70]
Rh@CNTs	25	10	2414	[72]
Rh@TRGO	50	4	310	[36]
Rh/AlO(OH)	75	4	1700	[71]
Pt-NPs	75	4	28	[73]
Pt-NP//IL	75	4	11	[73]

Table 4
Hydrogenation of cyclohexene to cyclohexane with Ir@TRGO[a] nanomaterial **1b** as catalyst[b].

Entry	Conversion (%)[c]	TON[d]	TOF (h^{-1})[e]
run 1	76.9	3070	61390
run 2	81.8	3265	65300
run 3	84.9	3390	67770
run 4	84.9	3390	67770
run 5	85.5	3410	68250

[a] Ir@TRGO method **1b**, 14 mg containing 3.6% Ir, 2.62×10^{-3} mmol Ir.
[b] Hydrogenation reactions of 0.86 g, 1.06 mL, 10.47 mmol cyclohexene were done by 100 °C, 10 bars of H_2 and 3 min, using a Büchi stainless-steel autoclave with a molar ratio of 3991 (mol cyclohexene/ mol iridium).
[c] Determined by GC analysis;.
[d] TON = mol cyclohexane/mol Ir;.
[e] TOF = mol cyclohexane × (mol Ir)$^{-1}$ × h^{-1}.

after 5 consecutive runs (Table 4). (For TEM and PXRD analysis of Ir@TRGO after 5 runs see Supp. Info.) Much higher TOFs of over 61000 h^{-1} were found in comparison with analogous Ru@TRGO (∼1570 h^{-1}) and Rh@TRGO (360 h^{-1}) catalysts [36].

3. Conclusion

In summary, we report here easy and rapid methods for the synthesis of iridium@graphene nanomaterials by thermal decomposition of $Ir_4(CO)_{12}$ in the presence of a graphene material in the ionic liquid 1-butyl-3-methylimidazolium tetrafluoroborate. Decomposition energy was provided either by microwave irradiation (MWI) or by electron-beam irradiation. Both methods gave particles with average diameters of less than 5 nm without the need of additional stabilizers or capping ligands, Microwave heating resulted in slightly smaller nanoparticles.

The Ir@TRGO nanomaterials were re-usable catalysts for the relevant hydrogenation of benzene and cyclohexene. Benzene hydrogenation was successfully achieved under mild conditions (100 °C, 1 h, 10 bars) with turnover frequencies up to 10 000 h^{-1} over 5 to 10 consecutive runs with similar activities. The Ir-NPs were recovered with only slightly increased (less than 1 nm) average diameters after 5 or 10 hydrogenation runs.

A brief correlation between activity and particle size points to an optimal diameter or surface regime for the catalytic activity. Here iridium particles of 3.6 ±1.0 nm on TRGO gave the highest activity in benzene hydrogenation compared to smaller (2.7 ±0.7 nm diameter) and larger (4.6 ±1.5 nm) particles.

4. Experimental section

4.1. Materials and methods

All experiments were done using Schlenk techniques under inert atmosphere. Tetrairidium dodecacarbonyl [$Ir_4(CO)_{12}$] (98% purity) were purchased by ABCR chemicals and thermally reduced graphite oxide (TRGO) was prepared in to a two-step oxidation/thermal reduction process using natural graphite (type

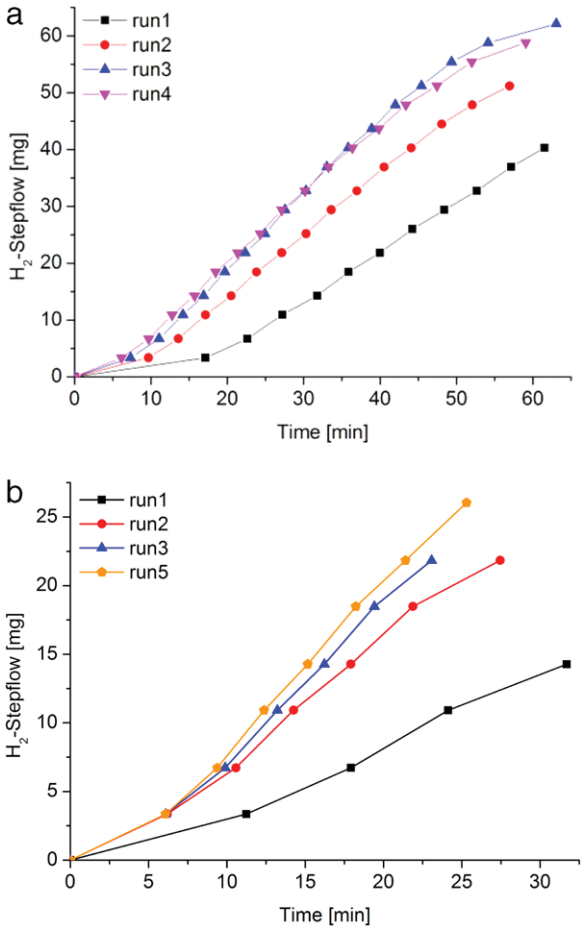

Fig. 4. H_2-uptake over time for the hydrogenation of benzene to cyclohexane with Ir@TRGO nanomaterials from method **1b** in consecutive runs with the same Ir@TRGO catalyst at 100 °C, 10 bar H_2 pressure (cf. Table 2). H_2-uptakes for the additional runs are shown in Fig. S10 in the Supporting Information. Conditions: **a** (experiment 1): benzene: 0.87 g, 1.0 mL, 11.14 mmol; Ir@TRGO catalyst: 15.7 mg, containing 3.6% Ir, 2.94×10^{-3} mmol Ir; molar benzene/metal ratio of 3790. An H_2 uptake of 67.4 mg H_2 (33.4 mmol, 802 mL) corresponds to 100% conversion. **b** (experiment 2): benzene: 0.35 g, 0.40 mL, 4.49 mmol; Ir@TRGO catalyst: 5.32 mg, containing 3.6% Ir, 1×10^{-3} mmol Ir; molar benzene/metal ratio of 4490. An H_2 uptake of 27.15 mg H_2 (13.47 mmol, 323 mL) corresponds to 100% conversion.

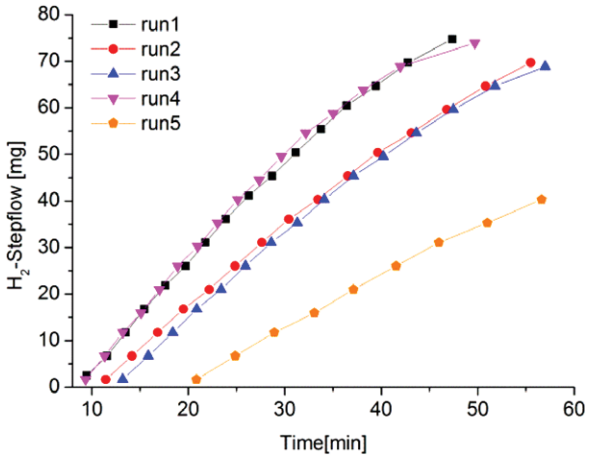

Fig. 5. H_2-uptake over time for the hydrogenation of benzene (0.99 g, 1.14 mL, 12.70 mmol) to cyclohexane with Ir@TRGO nanomaterials from method **2** in five consecutive runs with the same Ir@TRGO catalyst (8.6 mg containing 7.2% Ir, 3.22×10^{-3} mmol Ir). Molar benzene/metal ratio of 3943 at 100 °C, 10 bar H_2 pressure (cf. Table 2). An H_2 uptake of 76.8 mg (38.1 mmol, 914 mL) corresponds to 100% conversion.

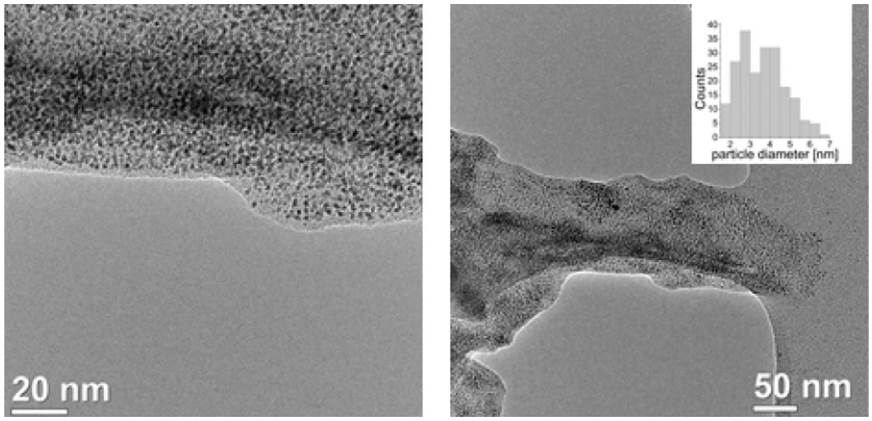

Fig. 6. TEM images of Ir@TRGO **1b** after 10 hydrogenation runs.

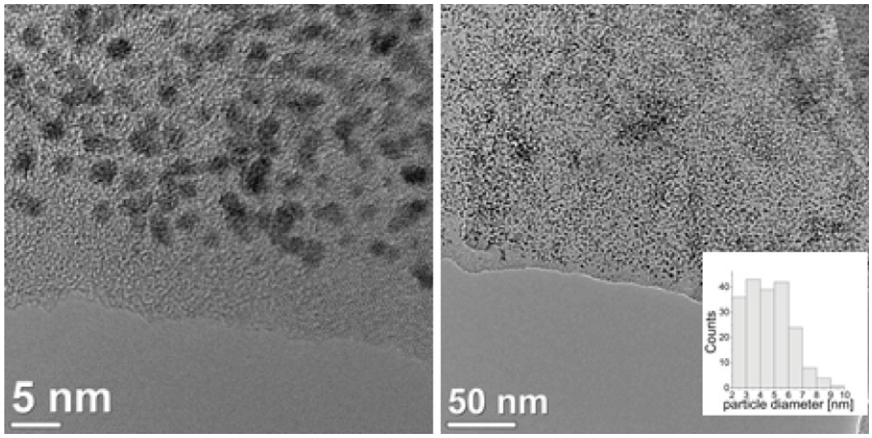

Fig. 7. TEM images of Ir@TRGO **2** after 5 hydrogenation runs.

KFL 99.5 from Kropfmühl AG, Passau, Germany) as raw material. Graphite was oxidized to graphite oxide (GO) according to the procedure described by Hummers and Offeman [74]. This oxidation incorporates functional groups like epoxy and alcohol moieties into the graphite structure. When GO is subjected to rapid heating above 400 °C the functional groups decompose into CO and CO_2 gas which exfoliates the layered GO structure into functionalized graphene sheets [75]. This thermal reduction of graphite oxide lends its name to the product (TRGO). By adjusting the reduction temperature, the degree of functionalization can be controlled. At a lower reduction temperature, more oxygen atoms remain on the TRGO surface and thereby increase the degree of functionalization. This degree of functionalization influences on the dispersibility of TRGO in polar solvents [76] and its use as a support material for metal nanoparticles. A higher degree of functionalization improves the dispersibility, e.g., in water or acetone. Therefore, it can be expected that a TRGO-material with a high degree of functionalization has a good interaction with metal particles. For these reasons we reduced GO at 400 °C and achieved an oxygen content of 21 wt% as calculated by the difference to 100e% from elemental analysis (77.9% C, 0.7% H). The benzene (VWR p.A.), and cyclohexene (Sigma Aldrich, p.A) were dried with sodium, distilled and store on 4 Å molecular sieves.

The ionic liquid, [BMIm][BF_4], was synthesized by reacting 1-methylimidazole with 1-chlorobutane to yield first [BMIm]Cl which was further reacted with HBF_4 to give [BMIm][BF_4]. The IL was dried under high vacuum (10–7 mbar) at 80 °C for several days. Quantitative anion exchange and, thus, IL purity was assessed by ion chromatography (ICS-1100, with Ion-Pac® AS22, 4 × 250 mm column) to be >99%. The water content determined by coulometric Karl Fischer titration (ECH/ANALYTIKJENA AQUA 40.00) was less than 10 ppm.

Powder X-ray diffraction patterns data were measured at on a Bruker D2 Phaser using a flat low background sample holder and Cu-Kα radiation (λ = 1.54182 Å, 35 kV) covering 2 theta angles 5–90° over a time of 8 h, that is 0.003°/s. All measurements were done at room temperature. The samples had been precipitated and washed with water and were dried under vacuum.

IR was measured on a Bruker TENSOR 37 IR spectrometer in a range from 4000 to 500 cm^{-1} in form of KBr disks.

Metal analyses were performed by flame atomic absorption spectroscopy (AAS) on a Vario 6 from Analytik Jena. Samples were digested in *aqua regia* three times, filtered and *aqua regia* was added to a final volume of 25 mL.

Transmission electron microscopy (TEM) micrographs were taken on a FEI Tecnai G20 TEM operating at an accelerating voltage of 200 kV. Samples were deposited on 200 μm carbon-coated copper grids (3.025 mm copper-grids with a 200 mesh and coated with 10 nm carbon film) from PLANO GmbH. The size distribution was determined using Gatan Digital Micrograph for 150 nanoparticles. Energy dispersive X-ray spectra were taken on a FEI Tecnai f20, detector voltage 136 kV; the exposure time for individual EDX spectra was 3 min.

Conversion of benzene to cyclohexane was determined by gas chromatography (GC) (Perkin Elmer 8500 HSB 6, equipped with a DB-5 film capillary column, 60 m × 0.32 mm, film thickness 25 μm, oven temperature 40 °C, N_2 carrier flow 120 L/min and a flame ionization detector (FID), 250 °C detector temperature). The samples were analyzed by putting a drop of the product into a GC sample vial together with 1 mL of distilled water. Also the

conversion was determined by NMR on a Bruker Avance DRX 200 (^{1}H — NMR, 200 MHz) in $CDCl_3$. Conversion of cyclohexene to cyclohexane was determined by gas chromatography (SHIMADZU, GC-2014).

4.2. Synthesis of Ir@TRGO nanoparticles in [BMIm][BF_4].

Microwave irradiation: In a typical experiment [$Ir_4(CO)_{12}$] (35.8 mg, 0.032 mmol) and TRGO (4.8 mg, 0.2 wt% related to 2.42 g [BMIm][BF_4]) were dispersed in 1-butyl-3-methylimidazolium tetrafluoroborate ([BMIm][BF_4]) (2 mL, 1.21 g/mL), sonicated at 30 ° C for 6 h and stirred at room temperature for the next 12 h.

Decomposition of the sample was done using microwave irradiation by 250 °C (200 W, 4 bars) for 90 min (Method **1a**) or 3x 20 min (Method **1b**). After heating the volatiles (CO) were removed *in vacuo*. Finally the sample was washed and centrifuged (6000 rpm × 15 min) with distilled water and dried under vacuum at 100 °C for several hours.

e-beam accelerator (Method **2**): Sample preparation and isolation were done with the same procedure as by the microwave method. The sample was decomposed by β-irradiation in a 10 MeV IBA Rhodotron e-beam accelerator as follows: energy of the electron 10 MeV; energy uptake up to 90 kGy, each run 30 kGy; radiation 30–58 kGy/s, time 3 × 1 s (Herotron E-Beam Service GmbH)[d].

4.3. Hydrogenation reactions

All catalytic processes were done using stainless-steel autoclaves under inert atmosphere. Each autoclave was equipped with a glass inlay to avoid any effect of the steel in the reaction.

The desired amount of catalyst (*Benzene*: Ir@TRGO **1b**, 15.71 mg containing 3.6% Ir, 2.94 × 10^{-3} mmol Ir; Ir@TRGO **2,** 8.6 mg containing 7.17% Ir, 3.22 × 10^{-3} mmol Ir or *cyclohexene*: Ir@TRGO **1b** 14 mg containing 3.6% Ir, 2.62 × 10^{-3} mmol Ir) and the substrate (for **1b**: benzene 0.87 g, 1.0 mL, 11.14 mmol or cyclohexene: 0.86 g, 1.06 mL, 10.47 mmol and for **2**: benzene 0.99 g, 1.14 mL, 12.70 mmol) were loaded in the autoclave under inert atmosphere. The autoclave was purged three times with H_2 and then charge with 10 bars of H_2. The stirring rate was 800 rpm and the heating temperature 100 °C. After one hour (benzene) or 3 min (cyclohexene) the process was stopped and cooled down. The organic volatile products were condensed under vacuum and condensed in a cool trap and analyzed by GC. Conversion of benzene was determined by H_2 uptake.

Re-use and recycling of the catalyst: Once the product was removed under vacuum, the autoclave was charged again with the desired amount of benzene and close properly for the next run.

All syntheses and catalytic runs were repeated at least twice to ensure reproducibility (see Fig. 4, Table 2).

Acknowledgments

Authors are thankful to the Deutsche Forschungsgemeinschaft (DFG) for grant Ja466/31-1 within SPP 1708, Herotron E-Beam Service GmbH, Bitterfeld-Wolfen for β-irradiation decomposition and to Dr. Juri Barthel and the Ernst Ruska-Centre (ER-C) for Microscopy and Spectroscopy with Electrons, Jülich Research Centre and RWTH Aachen University, 52425 Jülich (Germany) for help and access to the HR-TEM facilities. We thank Mrs. Christina Rutz for the IL-anion analysis.

Appendix A. Supplementary data

Supplementary material (additional PXRD patterns, TEM images, EDX spectra and information to catalytic hydrogenation runs of **1a** and **1b**) related to this article can be found online at http://dx.doi.org/10.1016/j.nanoso.2015.07.001.

References

[1] K. Saha, S.S. Agasti, C. Kim, X. Li, V.M. Rotello, Chem. Rev. 112 (2012) 2739–2779.
[2] H. Goesmann, C. Feldmann, Angew. Chem. Int. Ed. 49 (2010) 1362–1395.
[3] J.A. Dahl, B.L.S. Maddux, J.E. Hutchison, Chem. Rev. 107 (2007) 2228–2269.
[4] D. Astruc, Nanoparticles and Catalysis, Wiley-VCH, Weinheim, 2007.
[5] J.D. Scholten, B.C. Leal, J. Dupont, ACS Catal. 2 (2012) 184–200.
[6] D. Astruc, F. Lu, J.R. Aranzaes, Angew. Chem. Int. Ed. 44 (2005) 7852–7872.
[7] C. Pan, K. Pelzer, K. Philippot, B. Chaudret, F. Dassenoy, P. Lecante, M.J. Casanove, J. Am. Chem. Soc. 123 (2001) 7584–7593.
[8] J.D. Aiken III, R.G. Finke, J. Am. Chem. Soc. 121 (1999) 8803–8810.
[9] T. Welton, Chem. Rev. 99 (1999) 2071–2084.
[10] C. Feldmann, Introduction to special issue on ionic liquids in chemical synthesis, Z. Naturforsch. 68b (2013) 1057.
[11] C. Janiak, Z. Naturforsch. 68b (2013) 1059–1089.
[12] C. Janiak, Metal nanoparticle synthesis in ionic liquids, in: J. Dupont, L. Kollar (Eds.), Ionic Liquids (ILs) in Organometallic Catalysis, in: Topics in Organometallic Chemistry, vol. 51, Springer, Heidelberg, 2015, pp. 17–53.
[13] C. Janiak, Metal nanoparticle synthesis in ionic liquids, in: C. Hardacre, V. Parvulescu (Eds.), Catalysis in Ionic Liquids: From Catalyst Synthesis to Application, RSC Publishing, Cambridge, 2014, pp. 537–577 (chapter 11).
[14] J. Dupont, J.D. Scholten, Chem. Soc. Rev. 39 (2010) 1780–1804.
[15] P. Wasserscheid, W. Keim, Angew. Chem. Int. Ed. 39 (2000) 3773–3789.
[16] L. Taubert, Z. Li, Dalton Trans. (2007) 723–727.
[17] E. Redel, J. Krämer, R. Thomann, C. Janiak, J. Organomet. Chem. 694 (2009) 1069–1075.
[18] C. Vollmer, E. Redel, K. Abu-Shandi, R. Thomann, H. Manyar, H. Hardacre, Chem. Eur. J. 16 (2010) 3849–3858.
[19] K. Schütte, H. Meyer, C. Gemel, J. Barthel, R.A. Fischer, C. Janiak, Nanoscale 6 (2014) 3116–3126.
[20] K. Klauke, B. Hahn, K. Schütte, J. Barthel, C. Janiak, Nano-Struct. Nano-Objects 1 (2015) 24–31.
[21] G.S. Fonseca, G. Machado, S.R. Teixeira, G.H. Fecher, J. Morais, M.C.M. Alves, J. Dupont, J. Colloid Interface Sci. 301 (2006) 193–204.
[22] G.S. Fonseca, J.B. Domingos, F. Nome, J. Dupont, J. Mol. Catal. A 248 (2006) 10–16.
[23] G.S. Fonseca, A.P. Umpierre, P.F.P. Fichtner, S.R. Teixeira, J. Dupont, Chem. Eur. J. 9 (2003) 3263–3269.
[24] J. Dupont, G.S. Fonseca, A.P. Umpierre, P.F.P. Fichter, S.R. Teixeira, J. Am. Chem. Soc. 124 (2002) 4228–4229.
[25] E. Redel, M. Walter, R. Thomann, L. Hussein, M. Krüger, C. Janiak, Chem. Commun. 46 (2010) 1159–1161.
[26] E. Redel, M. Walter, R. Thomann, C. Vollmer, L. Hussein, H. Scherer, M. Krüger, C. Janiak, Chem. Eur. J. 15 (2009) 10047–10059.
[27] E. Redel, R. Thomann, C. Janiak, Inorg. Chem. 47 (2008) 14–16.
[28] P. Migowski, G. Machado, S.R. Teixeira, M.C.M. Alves, J. Morais, A. Traverse, J. Dupont, Phys. Chem. Chem. Phys. 9 (2007) 4814–4821.
[29] T. Gutel, C.C. Santini, K. Philippot, A. Padua, K. Pelzer, B. Chaudret, Y. Chauvin, J.-M. Basset, J. Mater. Chem. 19 (2009) 3624–3631.
[30] T. Gutel, J. Garcia-Anton, K. Pelzer, K. Philippot, C.C. Santini, Y. Chauvin, B. Chaudret, J.-M. Basset, J. Mater. Chem. 17 (2007) 3290–3292.
[31] G. Salas, A. Podgorsek, P.S. Campbell, C.C. Santini, A.A.H. Pádua, M.F. Costa Gomes, K. Philippot, B. Chaudret, M. Turmine, Phys. Chem. Chem. Phys. 13 (2011) 13527–13536.
[32] E.T. Silveira, A.P. Umpierre, L.M. Rossi, G. Machado, J. Morais, G.V. Soares, I.J.R. Baumvol, S.R. Teixeira, R.F.P. Fichtner, J. Dupont, Chem. Eur. J. 10 (2004) 3734–3740.
[33] D. Marquardt, J. Barthel, M. Braun, C. Ganter, C. Janiak, Cryst. Eng. Comm. 14 (2012) 7607–7615.
[34] C. Vollmer, C. Janiak, Coord. Chem. Rev. 255 (2011) 2039–2057.
[35] C. Vollmer, M. Schröder, Y. Thomann, R. Thomann, C. Janiak, Appl. Catal. A 425-426 (2012) 178–183.
[36] (a) D. Marquardt, C. Vollmer, R. Thomann, P. Steurer, R. Mülhaupt, E. Redel, C. Janiak, Carbon 49 (2011) 1326–1332;
(b) R. Marcos Esteban, K. Schütte, D. Marquardt, J. Barthel, F. Beckert, R. Mülhaupt, C. Janiak, Nano-Struct. Nano-Objects 1 (2015) http://dx.doi.org/10.1016/j.nanoso.2015.07.002.
[37] D. Marquardt, Z. Xie, A. Taubert, R. Thomann, C. Janiak, Dalton Trans. 40 (2011) 8290–8293.
[38] J. Krämer, E. Redel, R. Thomann, C. Janiak, Organometallics 27 (2008) 1976–1978.
[39] E. Redel, R. Thomann, C. Janiak, Chem. Commun. (2008) 1789–1791.
[40] J.M. Zhu, Y.H. Shen, A.J. Xie, L.G. Qiu, Q. Zhang, X.Y. Zhang, J. Phys. Chem. C. 111 (2007) 7629–7633.
[41] M.A. Firestone, M.L. Dietz, S. Seifert, S. Trasobares, D.J. Miller, N.J. Zaluzec, Small 1 (2005) 754–760.
[42] F. Endres, D. MacFarlane, A. Abbott, Electrodeposition from Ionic Liquids, Wiley-VCH, Weinheim, 2008.
[43] D. Marquardt, C. Janiak, Nachr. Chemie 61 (2013) 754–757.
[44] R. Venkatesan, M.H.G. Prechtl, J.D. Scholten, R.P. Pezzi, G. Machado, J. Dupont, J. Mater. Chem. 21 (2011) 3030- 3036–3030- 3036.
[45] K. Schütte, A. Doddi, C. Kroll, H. Meyer, C. Wiktor, C. Gemel, G. van Tendeloo, R.A. Fischer, C. Janiak, Nanoscale 6 (2014) 5532–5544.
[46] S. Schauermann, N. Nilius, S. Shaikhu, H.-J. Freund, Acc. Chem. Res. 46 (2013) 1673–1681.
[47] P.D. Kent, J.E. Mondloch, R.G. Finke, J. Am. Chem. Soc. 136 (2014) 1930–1941.
[48] H. Park, Mater. Chem. Phys. 133 (2012) 1050–1054.

[49] H. Park, J.S. Kim, B.G. Choi, S.M. Jo, D.Y. Kim, W.H. Hong, S.-Y. Jang, Carbon 48 (2010) 1325–1330.
[50] Y. Gao, S. Li, B. Zhao, Q. Zhai, A. Lita, N.S. Dalal, H.W. Kroto, S.F.A. Acquah, Carbon 77 (2014) 705–709.
[51] C.N.R. Rao, A.K. Sood, K.S. Subrahmanyam, A. Govindaraj, Angew. Chem. Int. Ed. 48 (2009) 7752–7777.
[52] Z. Wang, K. Shang, J. Dong, Z. Cheng, S. Ai, Microchim. Acta 179 (2012) 227–234.
[53] X.-Y. Yan, X.-L. Tong, Y.-F. Zhang, X.-D. Han, Y.-Y. Wang, G.-Q. Jin, Y. Qina, X.-Y. Guo, Chem. Commun. 48 (2012) 1892–1894.
[54] D. Marquardt, F. Beckert, F. Pennetreau, F. Tölle, R. Mülhaupt, O. Riant, S. Hermans, J. Barthel, C. Janiak, Carbon 66 (2014) 285–294.
[55] K. Gotoh, K. Kawabata, E. Fujii, K. Morishige, T. Kinumoto, Y. Miyazaki, H. Ishida, Carbon 47 (2009) 2112–2142.
[56] M.C. Rath, D.B. Naik, S.K. Sarkar, J. Nucl. Mater. 438 (2013) 26–31.
[57] S. Singh, M.C. Rath, A.K. Singh, S.K. Sarkar, T. Mukherjee, Mater. Chem. Phys. 124 (2010) 6–9.
[58] S. Singh, M.C. Rath, A.K. Singh, T. Mukherjee, O.D. Jayakumar, A.K. Tyagi, S.K. Sarkar, Radiat. Phys. Chem. 80 (2011) 736–741.
[59] S. Seino, T. Kinoshita, E.T. Nakagawa, T. Kojima, R. Taniguci, S. Okuda, T.A. Yamamoto, J. Nanopart. Res. 10 (2008) 1071–1076.
[60] A. Stanislaus, B.H. Cooper, Catal. Rev. 36 (1994) 75–123.
[61] R.C. Larock, Comprehensive Organic Transformations, Wiley-VCH, New-York, 1999.
[62] D.S. Cunha, G.M. Cruz, Appl. Catal. A: General 236 (2002) 55–66.
[63] H. Shi, O.Y. Gutiérrez, H. Yang, N.D. Browning, G.L. Haller, J.A. Lercher, ACS Catal. 3 (2013) 328–338.
[64] B. Meryemoglu, S. Irmak, A. Hasanoglu, O. Erbatur, B. Kaya, Fuel 134 (2014) 354–357.
[65] T. Frelink, W. Visscher, J.A.R. van Veen, J. Electroanalyt. Chem. 382 (1995) 65–72.
[66] Y. Zhang, D.A.J.M. Ligthart, X.-Y. Quek, L. Gao, E.J.M. Hensen, Int. J. Hydrog. Energy 39 (2014) 11537–11546.
[67] E. Galicia, G. Diaz, S. Fuentes, Catalysis 38 (1987) 11–19.
[68] O.M. Wilson, M.R. Knecht, J.C. Garcia-Martinez, R.M. Crooks, J. Am. Chem. Soc. 128 (2006) 4510–4511.
[69] Y. Tonbul, M. Zahmakiran, S. Ozkar, Appl. Catal. B: Environmental. 148-149 (2014) 466–472.
[70] X. Kang, J. Zhang, W. Shang, T. Wu, P. Zhang, B. Han, Z. Wu, G. Mo, X. Xing, J. Am. Chem. Soc. 136 (2014) 3768–3771.
[71] I.-S. Park, M.S. Kwon, K.Y. Kang, J.S. Lee, J. Parka, Adv. Synth. Catal. 349 (2007) 2039–2047.
[72] H.-B. Pan, C.M. Wai, J. Phys. Chem. C 113 (2009) 19782–19788.
[73] C.W. Scheeren, G. Machado, J. Dupont, P.F.P. Fichtner, S.R. Texeira, Inorg. Chem. 42 (2003) 4738–4742.
[74] W.S. Hummers, R.E. Offeman, J. Am. Chem. Soc. 80 (1958) 1339.
[75] D.R. Dreyer, S. Park, C.W. Bielawski, R.S. Ruoff, Chem. Soc. Rev. 39 (2010) 228–240.
[76] F.J. Tölle, M. Fabritius, R. Mülhaupt, Adv. Funct. Mater. 22 (2012) 1136–1144.

Supporting Information (SI)

Iridium@graphene composite nanomaterials synthesized in ionic liquid as re-usable catalysts for solvent-free hydrogenation of benzene and cyclohexene

Raquel Marcos Esteban,[a] Kai Schütte,[a] Philipp Brandt,[a] Dorothea Marquardt,[a] Hajo Meyer, [a] Fabian Beckert,[b] Rolf Mülhaupt,[b,c] Hartmuth Kölling,[d] and Christoph Janiak[*a]

[a] *Institut für Anorganische Chemie und Strukturchemie , Heinrich Heine Universität Düsseldorf, 40204 Düsseldorf. E-mail: janiak@uni-duesseldorf.de; Fax:+49-211-81-12287; Tel: +49-211-81-12286*
[b] *Freiburger Material Forschungszentrum (FMF) and Institut für Makromolekulare Chemie, Universität Freiburg, Stefan-Meier-Str. 21-31, 79104 Freiburg, Germany.*
[c] *FRIAS, Freiburg Institute for Advanced Studies, Albertstr. 19, 79104 Freiburg, Germany*
[d] *Herotron E-Beam Service GmbH, Guardianstrasse 6-10, 06766 Bitterfeld-Wolfen, Germany*

E-mail:

Raquel Marcos Esteban: raquel.marcos.esteban@hhu.de

Kai Schütte: kai.schuette@hhu.de

Philipp Brandt: P.Brandt@uni-duesseldorf.de

Dorothea Marquardt: doromarquardt@googlemail.com

Hajo Meyer: hajo.meyer@hhu.de

Fabian Beckert: fabian.beckert@fmf.uni-freiburg.de

Rolf Mülhaupt: rolf.muelhaupt@fmf.uni-freiburg.de

Hartmut Kölling: koelling@herotron.com

Christoph Janiak: janiak@hhu.de

Powder X-ray diffraction (PXRD) of the TRGO-400 and Ir@TRGO nanomaterials.

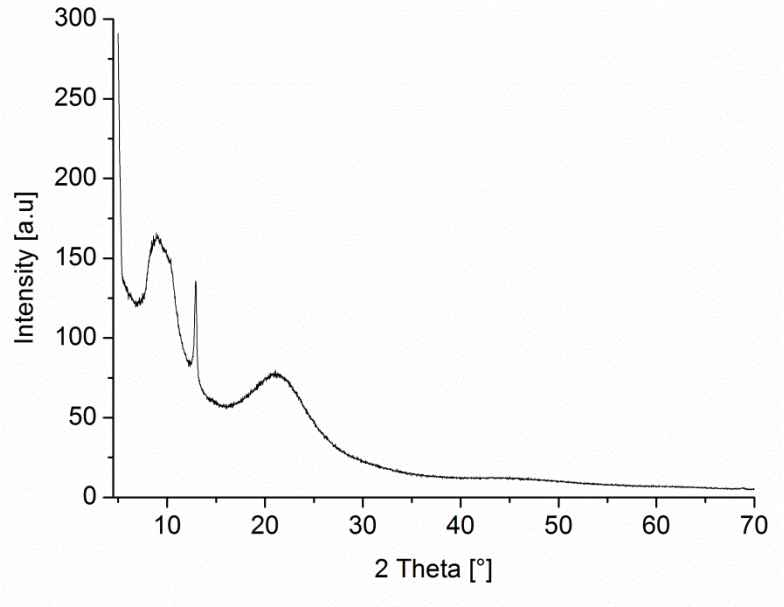

Fig. S 1 Powder X-ray diffractogram TRGO-400.

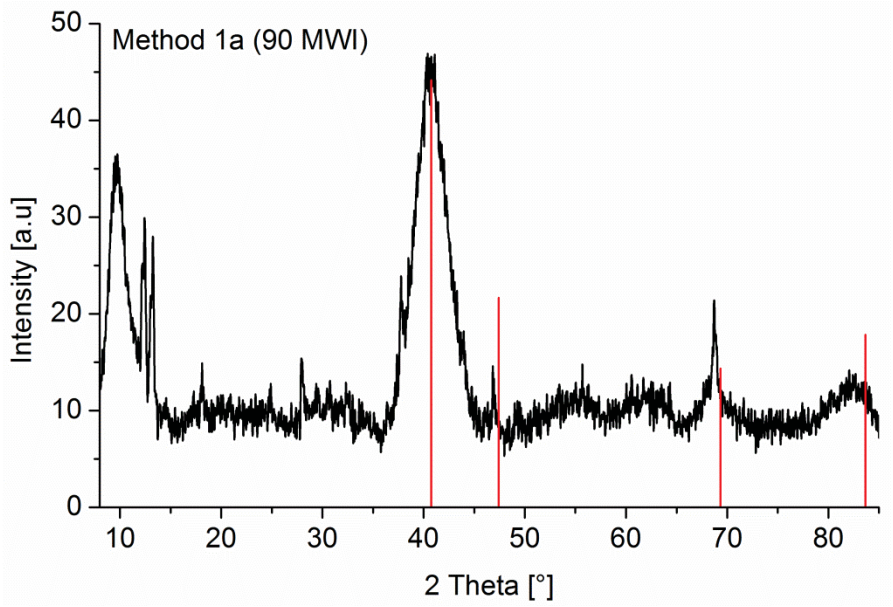

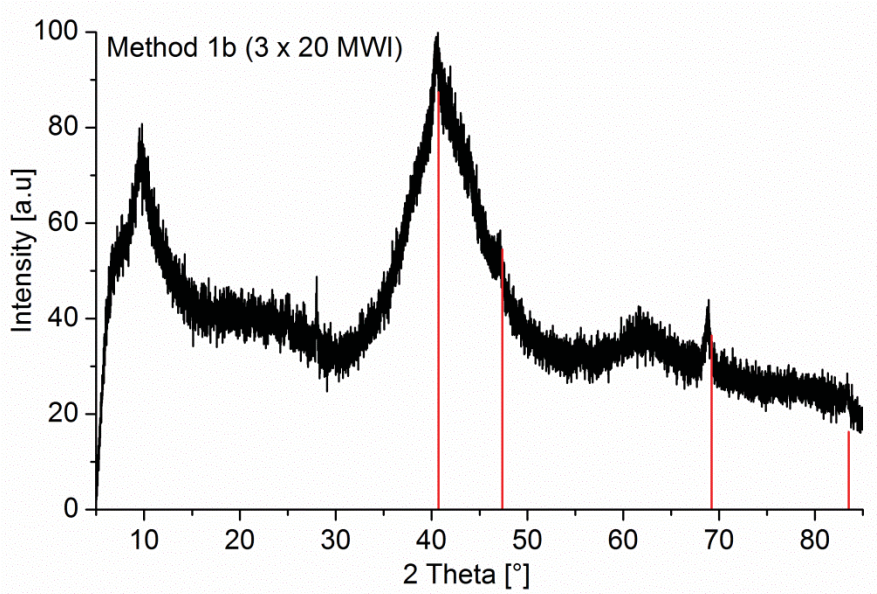

Fig. S 2 Powder X-ray diffractograms of Ir@TRGO synthesized in [BMIm][BF_4] under microwave irradiation by method 1a (MWI, 90 min) (top) and 1b (MWI, 3 x 20 min) (bottom). Reference data in red for Ir metal is taken from the crystallographic open database, COD 9008470.

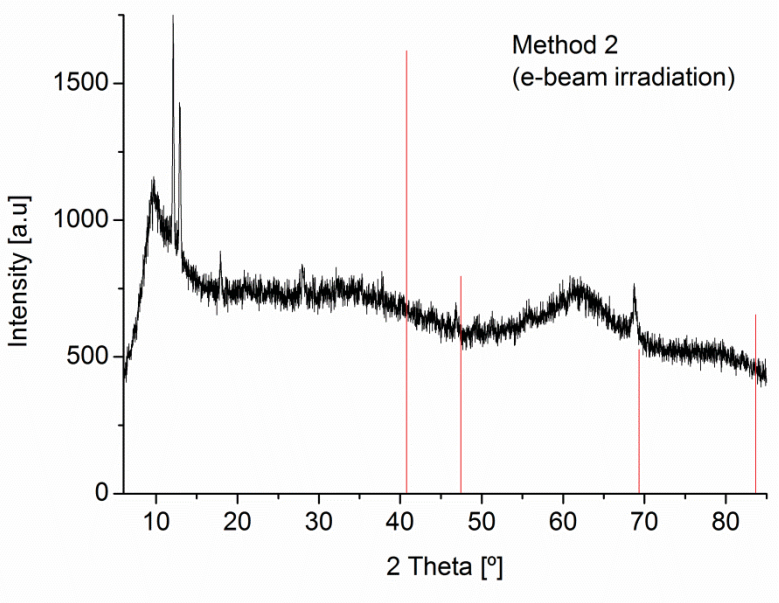

Fig. S 3 PXRD of Ir@TRGO in [BMIm][BF_4] synthesized by e-beam irradiation (IBA Rhodotron accelerator) (Method 2). Reference data in red for Ir metal is taken from the crystallographic open database, COD 9008470.

Additional TEM images of Ir@TRGO nanomaterials.

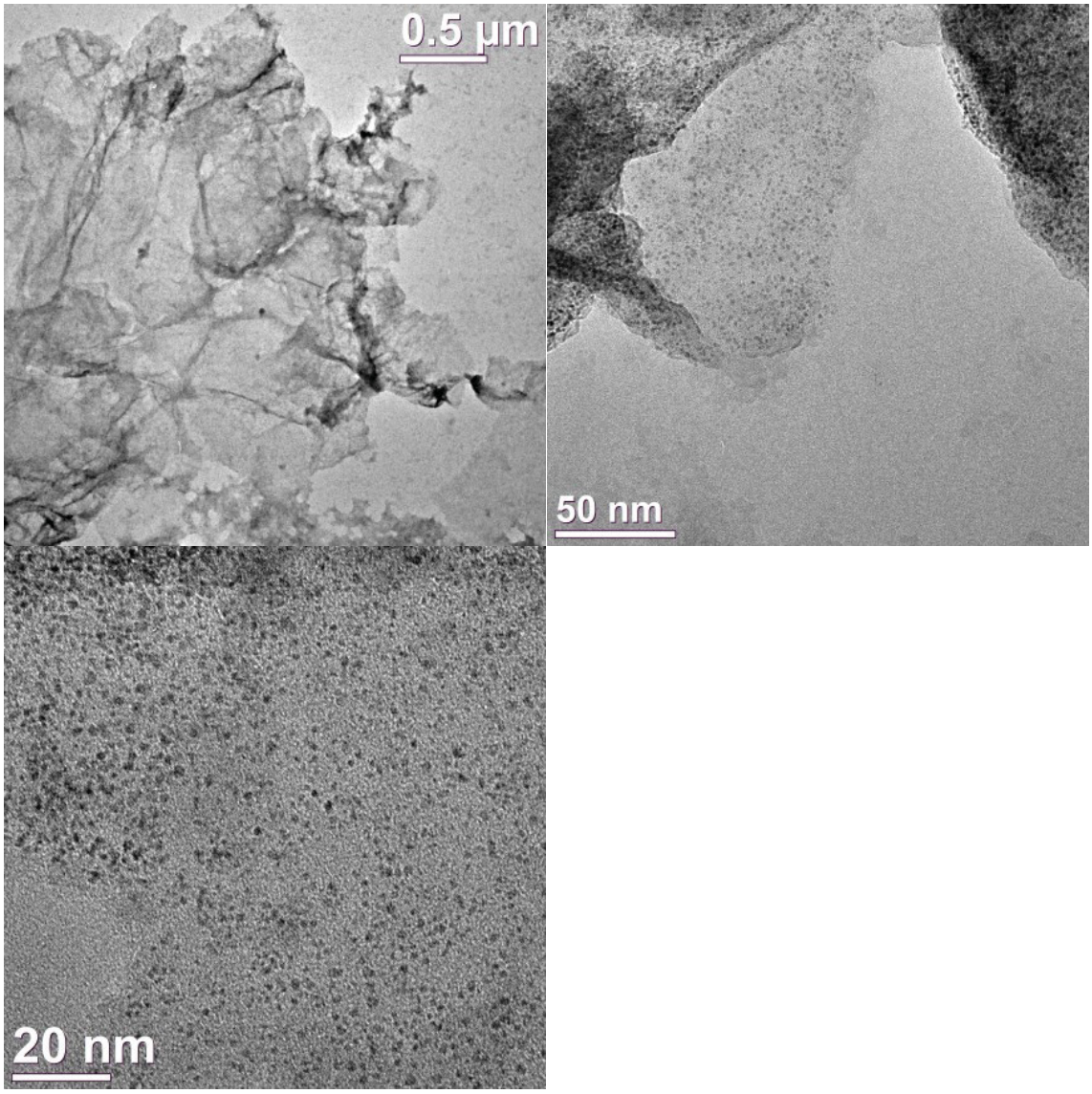

Fig. S 4 TEM images of Ir@TRGO from $Ir_4(CO)_{12}$ in [BMIm][BF_4] after 90 min MWI (Method 1a).

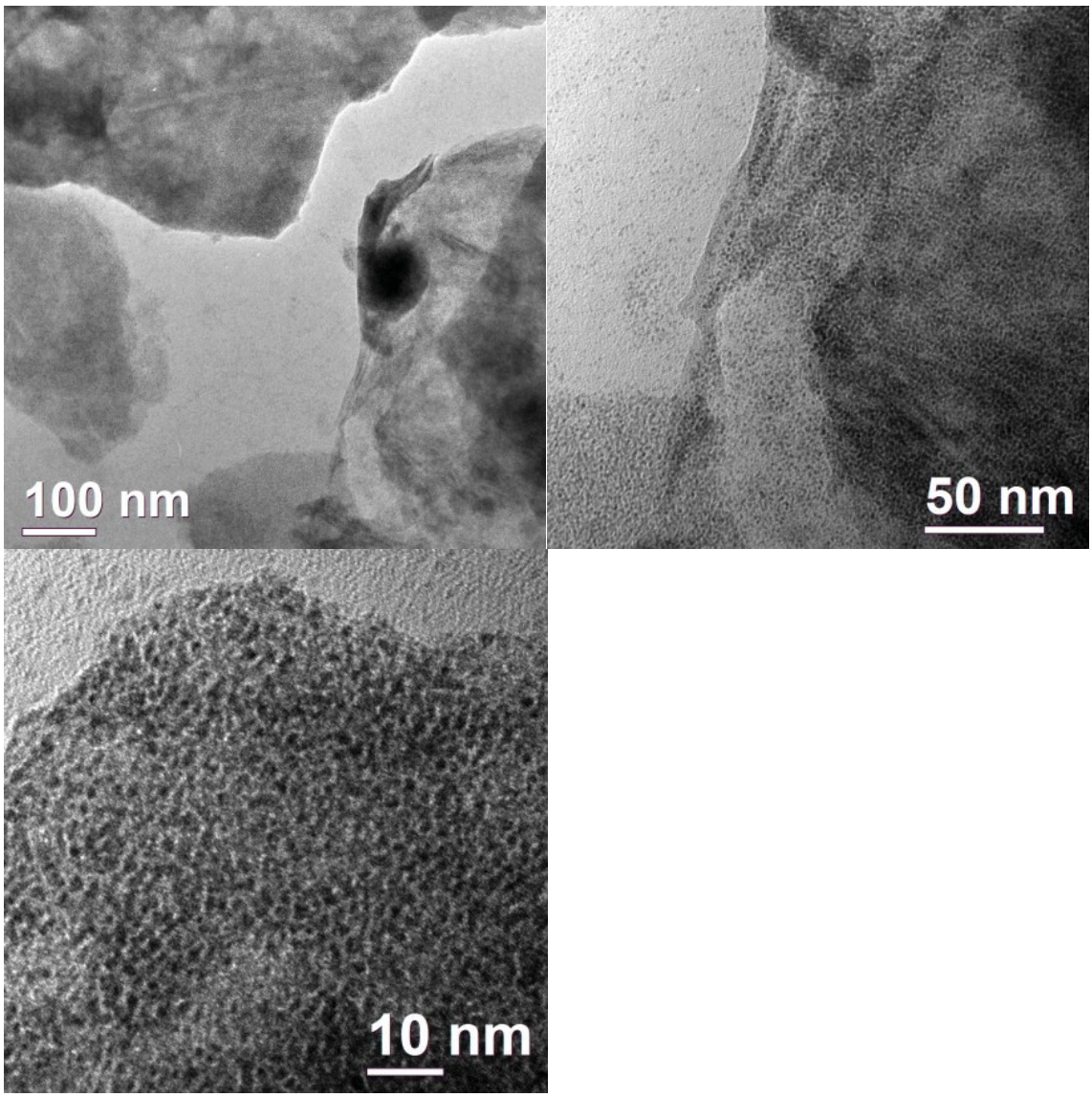

Fig. S 5 TEM images of Ir@TRGO from $Ir_4(CO)_{12}$ in [BMIm][BF_4] after 3 x 20 min MWI (Method 1b).

Energy Dispersive X-ray Spectroscopy (EDX)

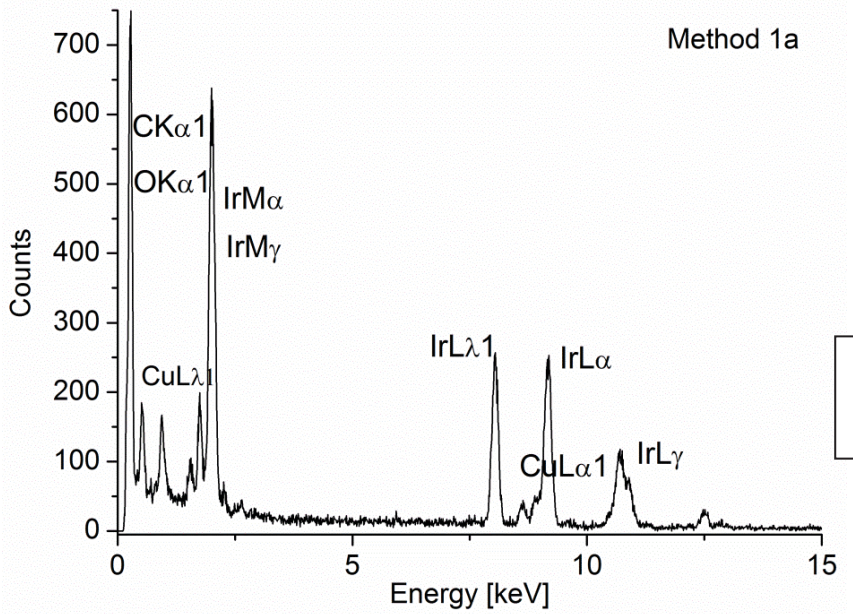

Fig. S 6 Energy dispersive X-ray spectra (EDX) of Ir@TRGO nanomaterials from method 1a.

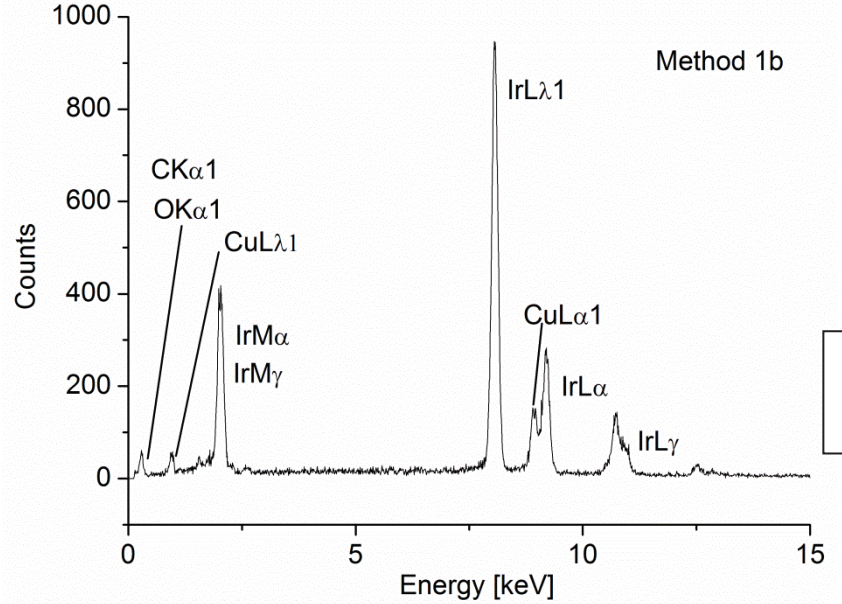

Fig. S 7 Energy dispersive X-ray spectra (EDX) of Ir@TRGO nanomaterials from method 1b.

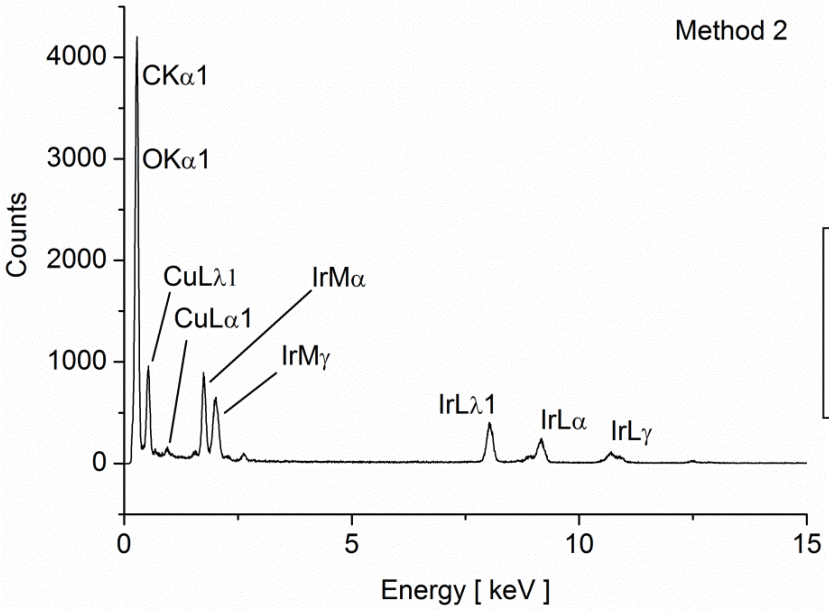

Fig. S 8 Energy dispersive X-ray spectrum (EDX) of Ir@TRGO nanomaterial synthesized by e-beam irradiation (IBA Rhodotron accelerator) (Method 2).

Hydrogenation of benzene to cyclohexane with Ir@TRGO.

Ir@TRGO from method 1a:

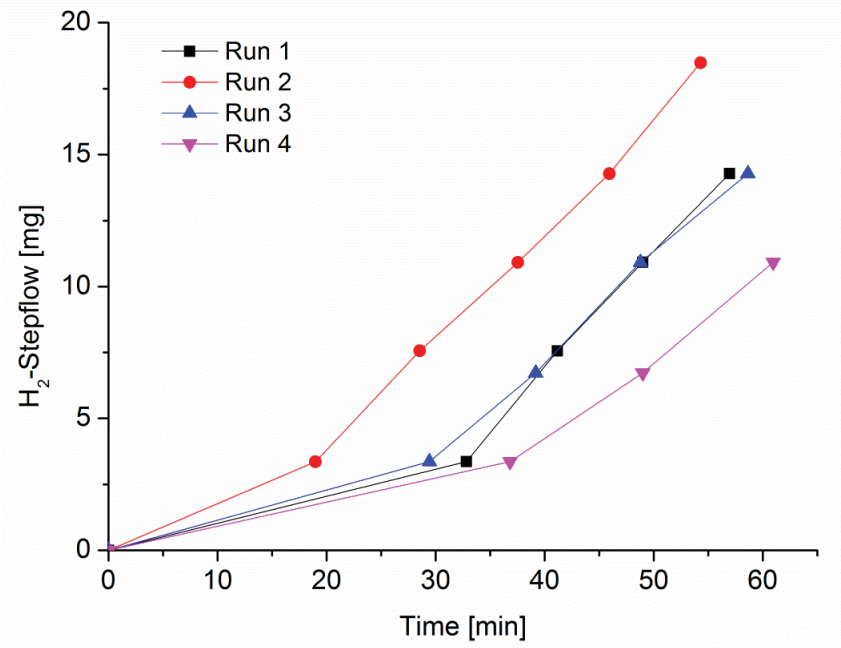

Fig. S 9 H_2-Uptake over time for the hydrogenation of benzene (1.74 g, 2 mL, 22.27 mmol) to cyclohexane by Ir@TRGO from method 1a in four consecutive runs with the same Ir@TRGO catalyst (2 mg containing 4.9 % Ir, 5.10 x 10^{-4} mmol Ir). Molar benzene/metal ratio of 43,696 at 100 °C, 10 bar H_2 pressure (cf. Table S 1). An H_2 uptake of 134.7 mg (66.81 mmol, 1.603 L) corresponds to 100% conversion.

Tab. S1 Hydrogenation of benzene to cyclohexane with the Ir@TRGO catalyst 1a.

Catalyst [a,b]	Conversion [%] [e]	TOF [h^{-1}] [f]
$Ir_4(CO)_{12}$	none	-
Ir@TRGO 1a [c]		
run 1	10.7	4966
run 2	13.9	6740
run 3	10.7	4824
run 4	8.2	3548

[a] Hydrogenation reactions were done at 100 °C, 10 bars of H_2 and using a Büchi stainless steel autoclave with a Büchi press-flow controller for measuring the H_2-uptake over the time. [b] Molar ratio benzene/iridium, 43,696 for method 1a. [c] Synthesis by microwave irradiation. [e] Determined by H_2-uptake. [f] TOF= mol cyclohexane x (mol Ir) $^{-1}$ x h^{-1}.

Ir@TRGO from method 1b;

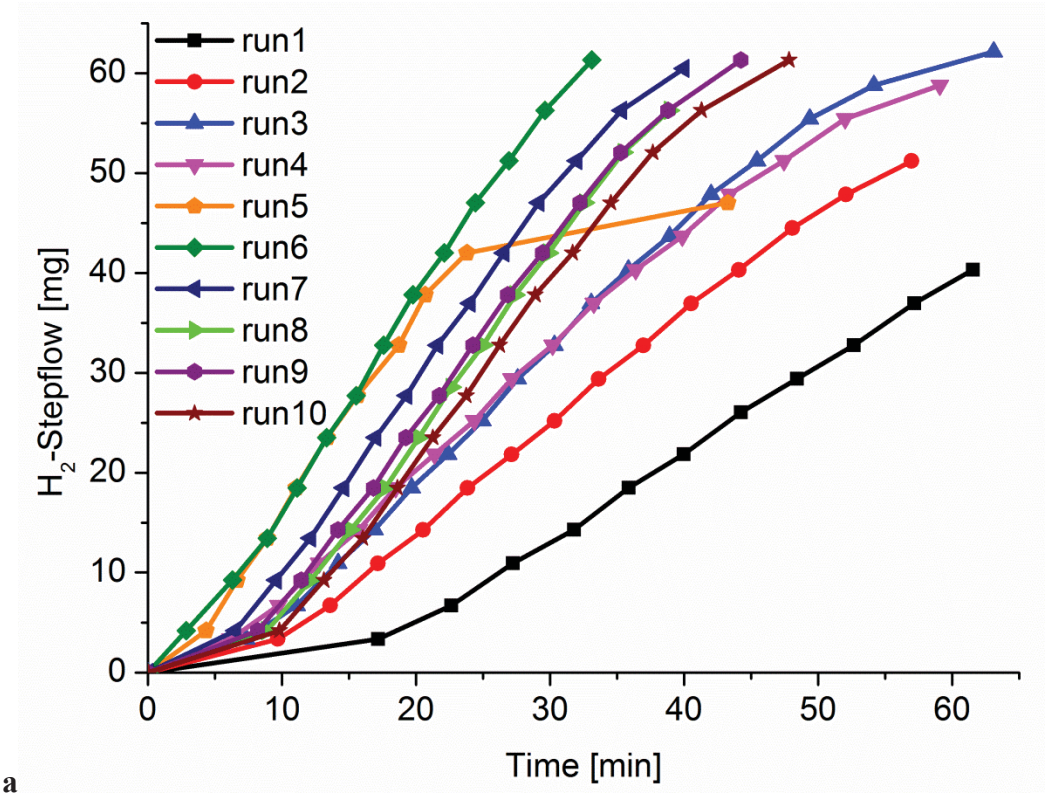

a

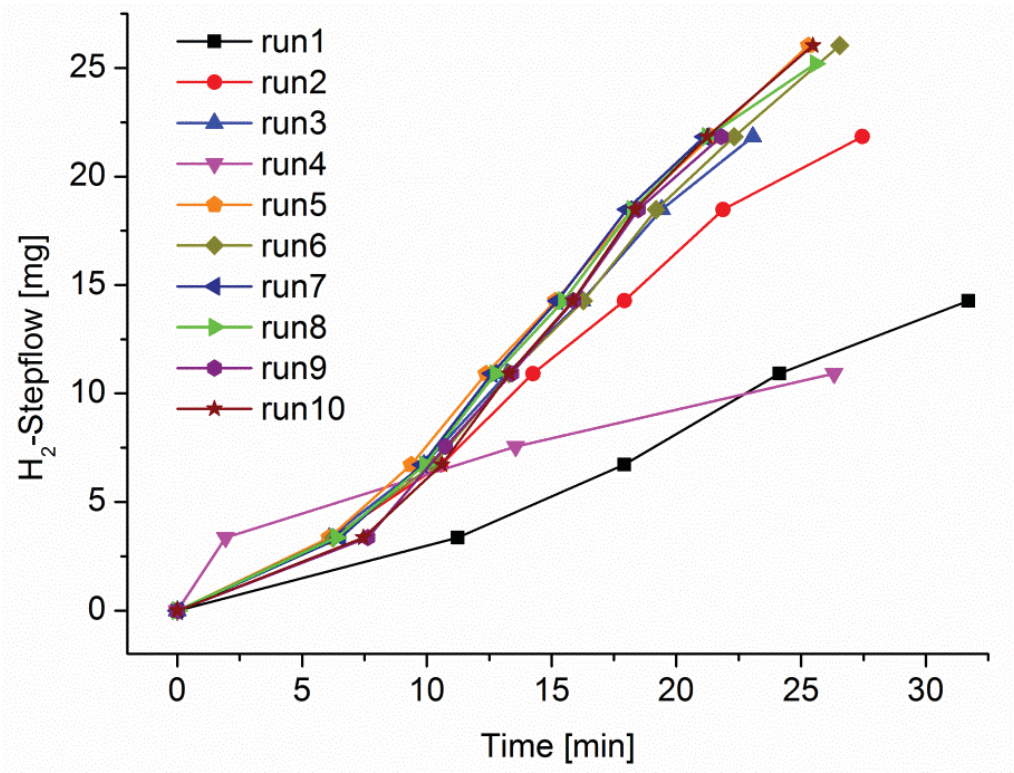

b

Fig. S 10 a and b: H_2-Uptake over time for the hydrogenation of benzene to cyclohexane by Ir@TRGO from method 1b in experiments 1 (a) and 2 (b) (see main publication for details). Run 5 in a and run 4 in b had an instrumental (but not a catalyst) error as shown here.

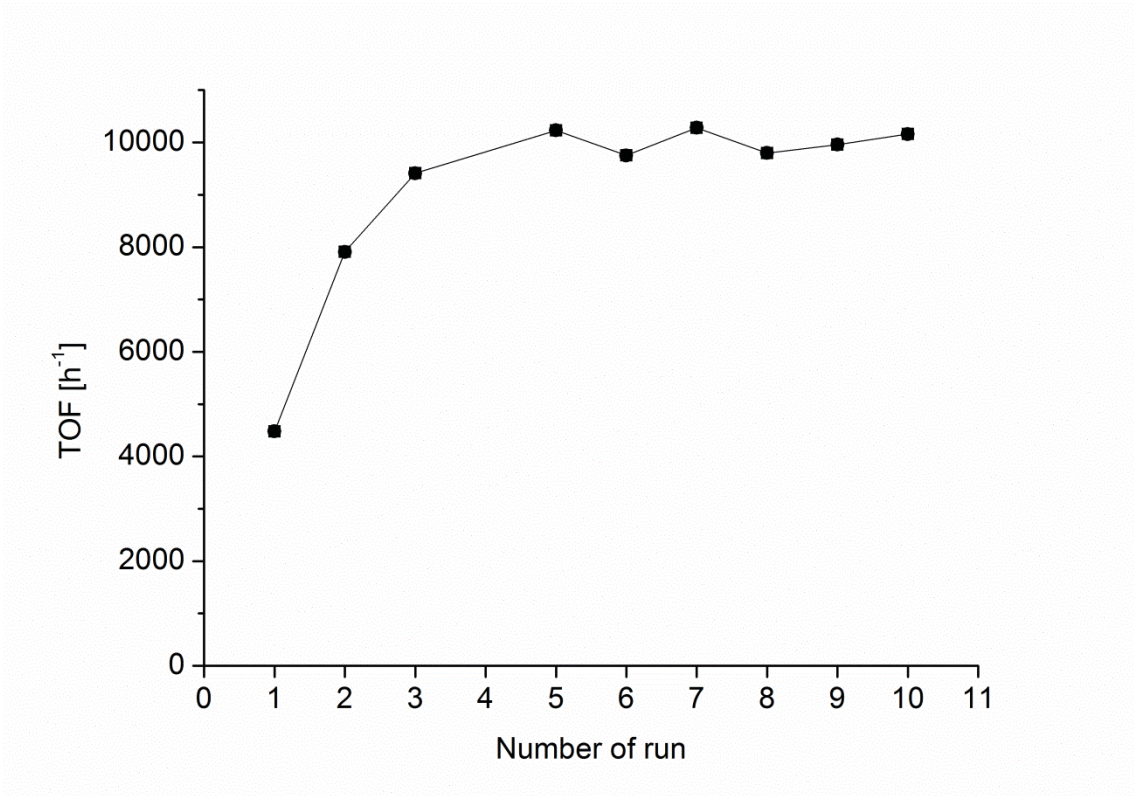

Fig. S 10 c: Activity as turnover frequency for the hydrogenation of benzene to cyclohexane by Ir@TRGO from method 1b in experiment 1 (see Table 2 in main publication for details and actual values).

Hydrogenation of cyclohexene to cyclohexane with Ir@TRGO.

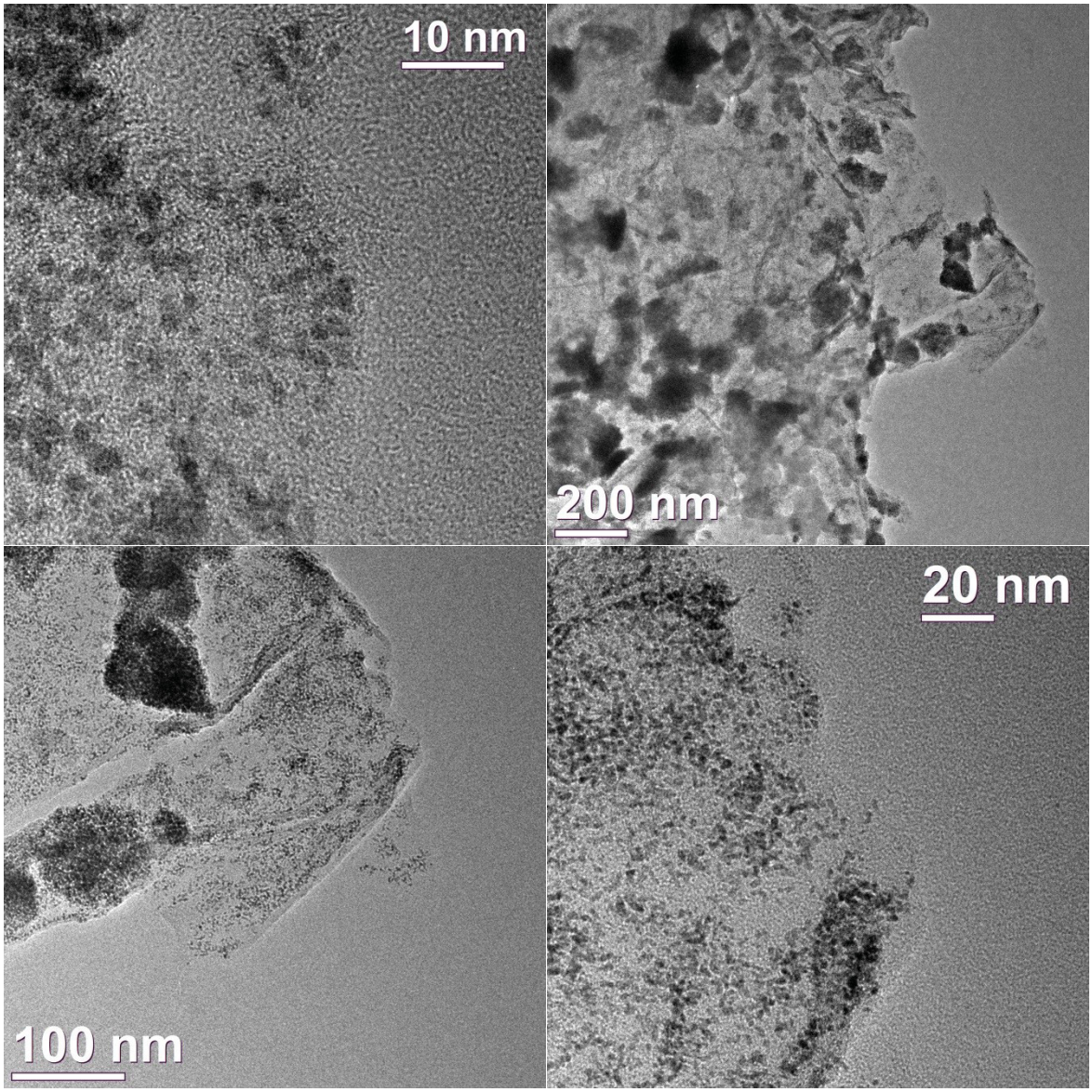

Fig. S 11 TEM from Ir@TRGO (method 1b) after 5 runs of hydrogenation of cyclohexene to cyclohexane.

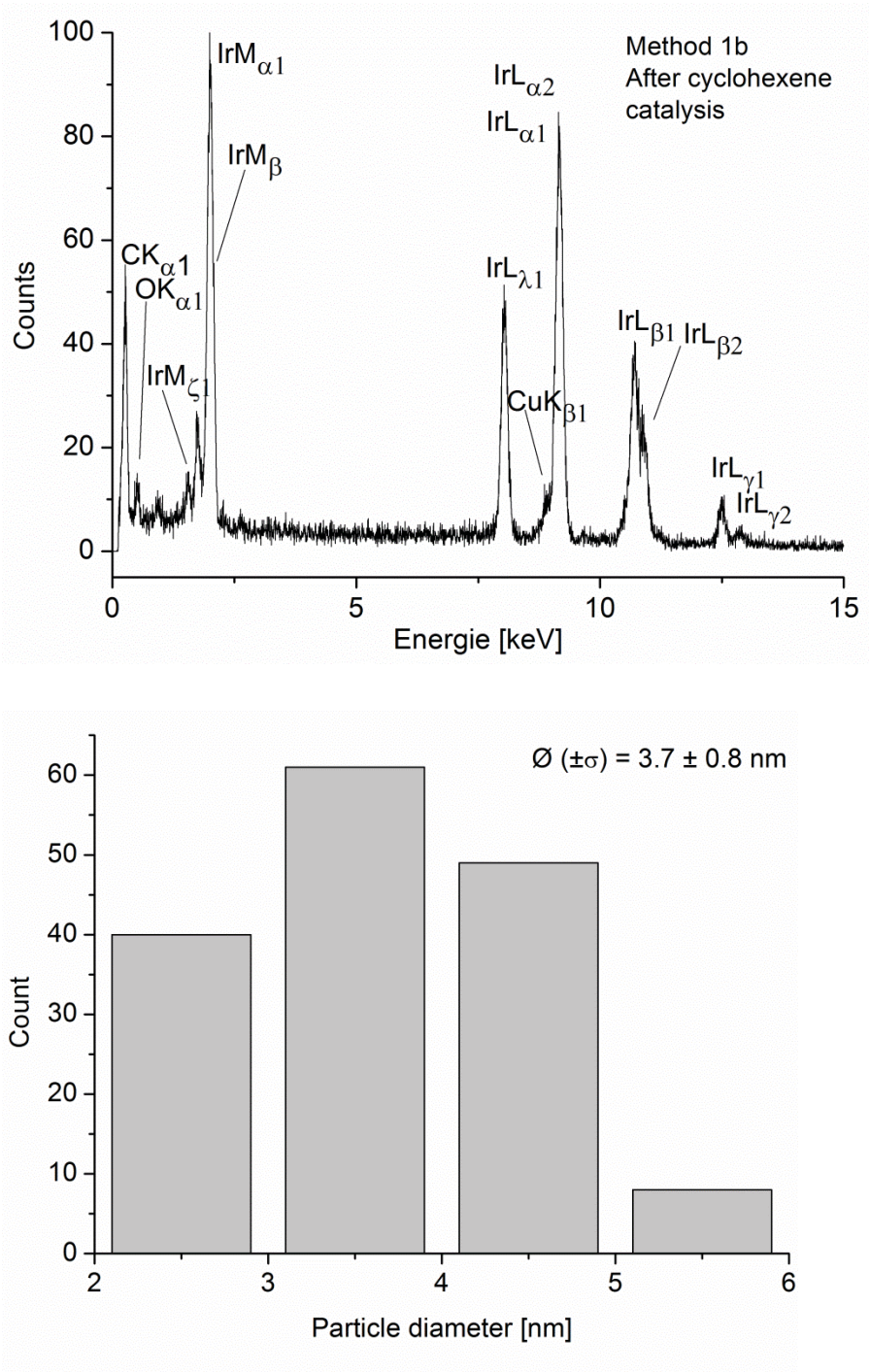

Fig. S 12 EDX from Ir@TRGO (method 1b) after 5 runs for the hydrogenation of cyclohexene to cyclohexane (top). Size distribution of Ir-NPs from the Ir@TRGO nanocomposite (bottom).

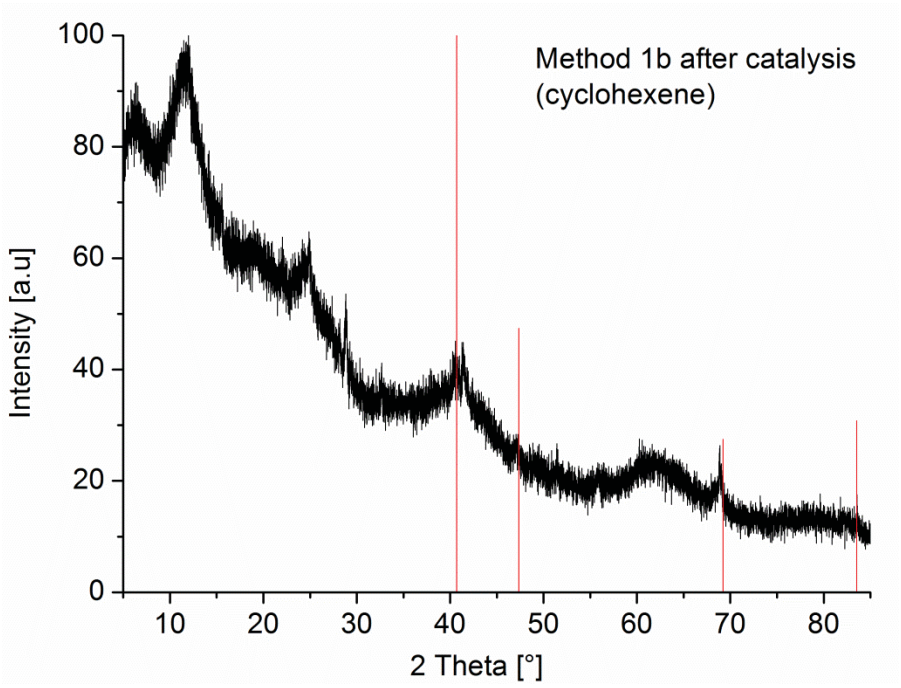

Fig. S 13 PXRD of Ir@TRGO in [BMIm][BF_4] (Method 1b) after five runs for the cyclohexene hydrogenation. Reference data in red for Ir metal is taken from the crystallographic open database, COD 9008470.

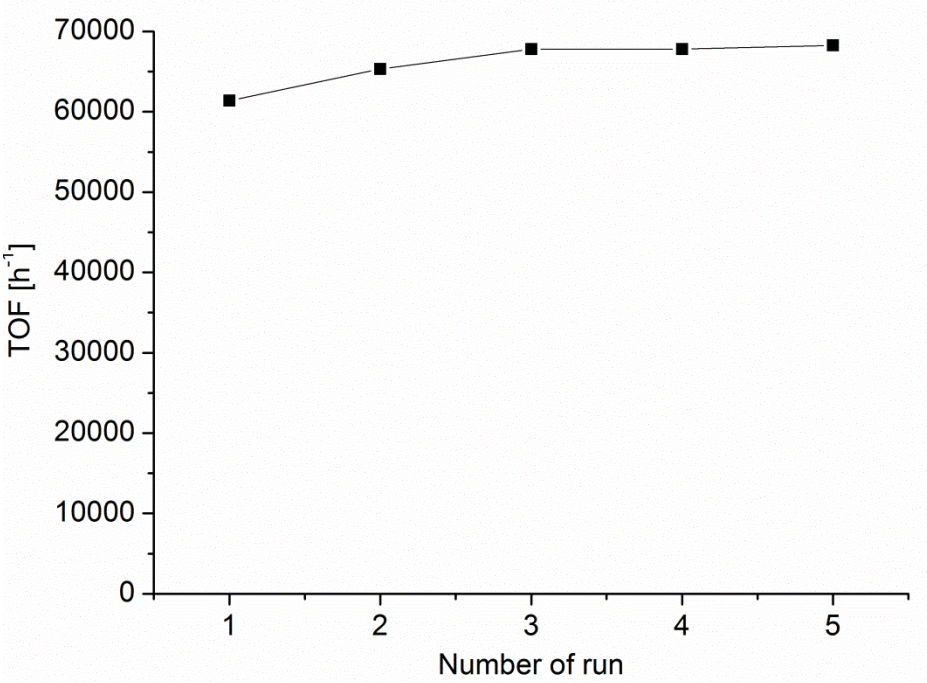

Fig. S 14 TOF vs. run number of the hydrogenation of cyclohexene to cyclohexane using Ir@TRGO (method 1b) as a catalyst.

3.2 Synthesis of ruthenium@graphene nanomaterials in propylene carbonate as re-usable catalysts for the solvent-free hydrogenation of benzene

R. Marcos Esteban, K. Schütte, D. Marquardt, J. Barthel, F. Beckert, R. Mülhaupt, C. Janiak.

Nano-Structures & Nano-Objects **2015**, *2*, 28–34.

http://dx.doi.org/10.1016/j.nanoso.2015.07.002; ref. [50].

Heterogeneous catalysis is usually a cleaner and cheaper method in comparison with homogenous catalysis, and they also reduce the cost of solvents, time and energy. Here we report the synthesis of supported ruthenium nanoparticles on the thermally reduced graphite oxide (Ru@TRGO) as new nanomaterials for the heterogeneous hydrogenation of benzene to cyclohexane (Scheme 4).

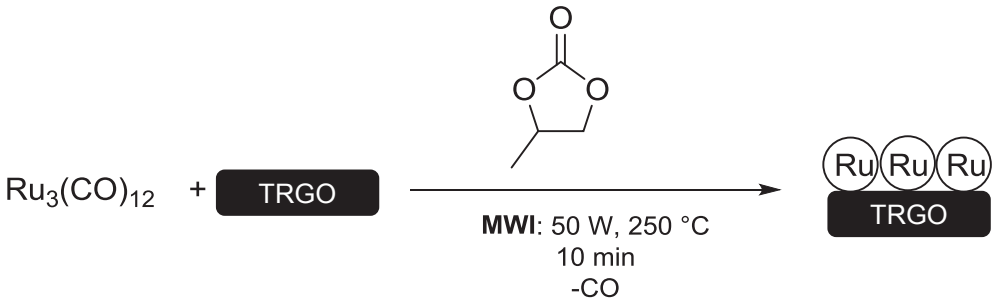

Scheme 4 Synthesis of Ru@TRGO in propylene carbonate by microwave irradiation.

The Ru@TRGO nanomaterials can be obtained by the thermal decomposition of the triruthenium dodecacarbonyl compound, $Ru_3(CO)_{12}$, in propylene carbonate (PC). Propylene carbonate is an aprotic solvent with a low (eco-)toxicity and flammability solvent very suitable for the synthesis of M-NPs and microwave reactions (section 1.2), helping to the decomposition of metal carbonyls and to achieve narrow size distributions of Ru–NPs. The Ru@TRGO nanomaterials were fully characterized by HR–TEM, TEM, PXRD, IR and XPS. PC helps to the growth and nucleation of the Ru-NPs and the TRGO allow the deposition of Ru-NPs to obtain a well distributed nanomaterials with a Ru-NPs size distributions of 4.3 ± 1.4 nm (Scheme 4, Fig. 24).

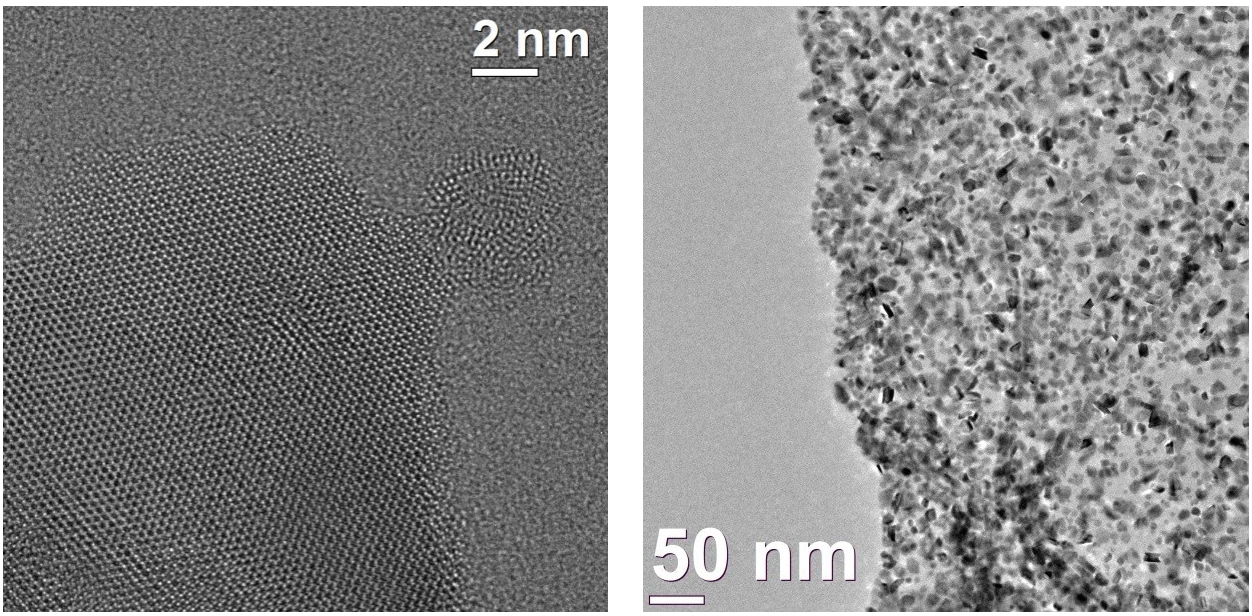

Fig. 24 HR–TEM (left) and TEM (right) images of Ru@TRGO nanomaterials. The left image shows the graphite mesh.

The hydrogenation of benzene to cyclohexane using Ru@TRGO nanomaterials was carried under solvent-free and mild conditions (100º C, 10 bar H_2), achieving in less than 20 min. a selectivity near to 100 % to cyclohexane. The recovery of Ru@TRGO nanomaterials were also tested, and the catalyst could be recycled and re-used for at least ten consecutive hydrogenation runs without loss of activity (TOF = 34000 h^{-1}) (Fig. 25). After ten consecutive hydrogenation runs, the Ru-NPs show a slightly increase in the size distribution of ca. 2–3 nm (6.7 ± 2.4 nm) (Fig. 25).

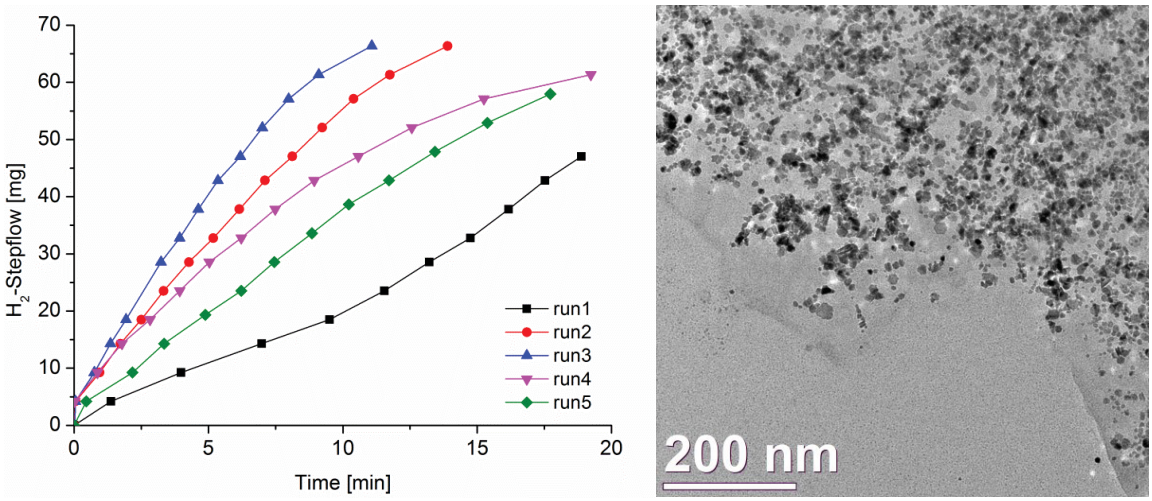

Fig. 25 (Left) H_2-uptake over time for the hydrogenation of benzene to cyclohexane with Ru@TRGO nanomaterials; (right) TEM images of Ru@TRGO nanomaterials after 10 consecutive catalysis runs with a size distribution of 6.7 ± 2.4 nm.

Author's contribution of the publications:*

- Previously research, design of the synthetic procedures and application of the methods (laboratory work).
- Characterization of the samples by PXRD, IR, and GC analysis for the hydrogenation reactions.
- Writing of the manuscript together with the further edition according to the reviewer's comments.

* Detailed work and cooperation's of the co-authors in the manuscript:

-Dr. Schütte: measurements of TEM, EDX and XPS.

-Dr. J. Barthel: measurements of HR-TEM

-Dr. D. Marquardt: first try of the decomposition and deposition of $Ru_3(CO)_{12}$ on TRGO.[310]

-Dr. Fabian Beckert and Prof. Dr. R. Mülhaupt: synthesis of the thermally reduced graphite oxide (TRGO).

Nano-Structures & Nano-Objects 2 (2015) 28–34

Contents lists available at ScienceDirect

Nano-Structures & Nano-Objects

journal homepage: www.elsevier.com/locate/nanoso

Synthesis of ruthenium@graphene nanomaterials in propylene carbonate as re-usable catalysts for the solvent-free hydrogenation of benzene

Raquel Marcos Esteban [a], Kai Schütte [a], Dorothea Marquardt [a], Juri Barthel [b], Fabian Beckert [c], Rolf Mülhaupt [c,d], Christoph Janiak [a,*]

[a] Institut für Anorganische Chemie und Strukturchemie, Heinrich Heine Universität Düsseldorf, 40204 Düsseldorf, Germany

[b] Ernst Ruska-Centre for Microscopy and Spectroscopy, Forschungszentrum Jülich GmbH and RWTH Aachen University, 52425 Jülich, Germany

[c] Freiburger Material-forschungszentrum (FMF) and Institut für Makromolekulare Chemie, Universität Freiburg, Stefan-Meier-Str. 21-31, 79104 Freiburg, Germany

[d] FRIAS, Freiburg Institute for Advanced Studies, Albertstr. 19, 79104, Freiburg, Germany

HIGHLIGHTS

- Deposition of ruthenium nanoparticles (Ru-NPs) on graphene material.
- Propylene carbonate as non-toxic and biodegradable solvent for the synthesis of Ru-NPs.
- Quick and easy method for the preparation of Ru-NPs by microwave irradiation.
- Synthesis of stable, small (~4 nm diameter) and catalytic active Ru-NPs.
- Hydrogenation catalysis of benzene under solvent-free conditions.

GRAPHICAL ABSTRACT

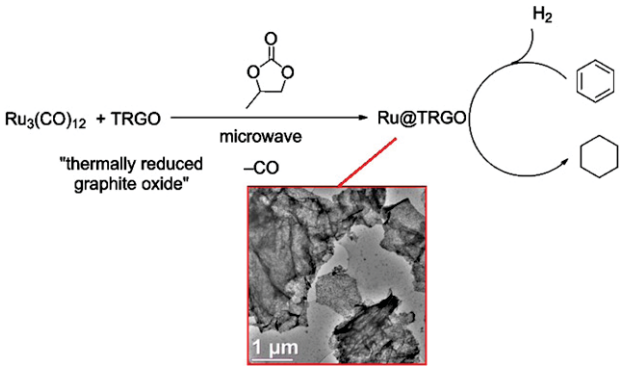

ARTICLE INFO

Article history:
Received 1 June 2015
Received in revised form
16 July 2015
Accepted 20 July 2015

Dedicated to Prof. Ekkehard Hahn on the occasion of his 60th birthday

Keywords:
Ruthenium nanoparticles
Graphene
Thermally reduced graphite oxide, TRGO
Benzene hydrogenation
Catalysis

ABSTRACT

Ruthenium nanoparticles (Ru-NPs) can be deposited on thermally reduced graphite oxide (TRGO) in propylene carbonate (PC). Propylene carbonate is a biodegradable and non-toxic solvent. Synthesis of Ru-NPs and deposition on TRGO were achieved by decomposition of ruthenium dodecacarbonyl, $Ru_3(CO)_{12}$, by microwave irradiation. Ru@graphene nanomaterials were identified and characterized by high resolution transmission electron microscopy (TEM, HR-TEM), energy-dispersive X-ray diffraction (EDX), selected area electron diffraction (SAED), X-ray photoelectron spectroscopy (XPS) and powder X-ray diffraction (PXRD) with a small diameter and size distribution of 7 ± 4 nm Ru-NPs on TRGO. These Ru@graphene nanomaterials are active catalysts for the solvent-free hydrogenation of benzene to cyclohexane under mild conditions (100 °C, 10 bar) with activities of 34,000 (mol cyclohexane) · (mol Ru)$^{-1}$ · h^{-1} and over 90% conversion in at least ten consecutive runs.

* Corresponding author. Tel.: +49 211 81 12286; fax: +49 211 81 12287.
E-mail address: janiak@uni-duesseldorf.de (C. Janiak).

http://dx.doi.org/10.1016/j.nanoso.2015.07.002

1. Introduction

Properties of the transition metal nanoparticles (M-NPs) are of general interest due to their various applications in science and technology [1–3]. The small size together with a large surface area of M-NPs offers a wide range of opportunities in the field of catalysis [4–8].

Ruthenium is an attractive catalytic metal because of its lower economical price compared to other noble metals such as palladium or rhodium. The selectivity of Ru-NP catalysts for the hydrogenation of C=C carbon double bonds in alkenes or arenes [9–12] allows for their possible application in hydrogenation processes such as the relevant hydrogenation of benzene or cyclohexene to cyclohexane [13], or in the Fischer–Tropsch synthesis [14,15] for the production of hydrocarbons.

Synthesis of ruthenium nanoparticles [4] is possible by simple reduction of common salts, $RuCl_3$ [16,17], or by decomposition of zero-valent compounds, such as $Ru_3(CO)_{12}$ [18–20] or [Ru(cyclooctadiene)(cyclooctatetraene)] [21–25].

For small M-NPs agglomeration and aggregation due to the Ostwald ripening [26,27] needs to be prevented and a stabilizing ligand shell is often needed. Such stabilizers can be organic donor ligands or polymers, [5,22,28–30] or ionic liquids, [31–35] which form a protective layer (shell) around the particles (core). Also immobilization or deposition of nanoparticles on supports such as graphene [36–39], carbon nanotubes [40,41] or more often Al_2O_3 [13] is a means to prevent agglomeration.

Over the last years, thermally reduced graphite oxide [42–48] also simply called "graphene", has been rediscovered as an extremely versatile carbon material [49–51]. Because of the functional groups present in TRGO (Fig. S1 in Supporting Information), the sorption of ions and molecules is possible [49]. This and the high specific surface area of TRGO of 400 $m^2\ g^{-1}$ up to 1500 $m^2\ g^{-1}$, make them promising materials for catalytic applications [49]. Metal-nanoparticles on carbon materials are of recent interest [52–60].

Organic carbonates (Fig. 1) are used in industry for degreasing, gas treating or cleaning [62]. Organic carbonates are polar solvents with a wide range of liquid temperature range (for propylene carbonate, PC mp −49 °C, bp 243 °C), and with a low flammability, low volatility and low (eco)toxicity [61]. Biodegradable PC is used as solvent in the FLUOR process for CO_2 removal [63,64], in the research on lithium-ion batteries [65–67] or as co-solvent for cosmetics due to its low toxicity and irritability [68,69].

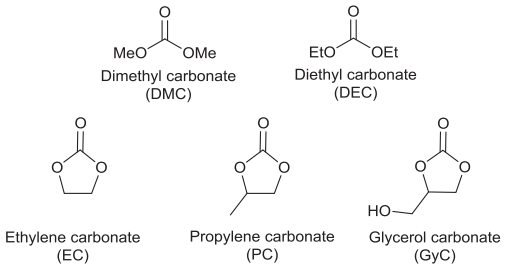

Fig. 1. Selected organic carbonates: dimethyl carbonate (DMC); diethyl carbonate (DEC); ethylene carbonate (EC); propylene carbonate (PC); glycerol carbonate (GyC) [61].

There appear to be only few reports on metal nanoparticle synthesis in organic carbonates in the literature [70–73]. The role of propylene carbonate is not fully clear yet. Its carbonate oxygen functionality may coordinate to the metal surface and thereby play the role of a capping agent. Only recently a more comprehensive report on the synthesis of Mo-, W-, Re-, Fe-, Ru-, Os-, Co-, Rh-, or Ir-metal-nanoparticles in propylene carbonate has appeared. These M-NPs were obtained (without TRGO support) from their metal carbonyls by means of microwave irradiation as small particles with narrow diameter distributions (*e.g.*, for Ru-NPs 2.7 ± 0.5 nm from $Ru_3(CO)_{12}$ or for Os-NPs 3.0 ± 1.5 nm from $Os_3(CO)_{12}$) [20]. When 3-mercaptopropionic acid, HS-$(CH_2)_2$-COOH was added post-synthetically to this Ru-NP/PC dispersion, the isolated ligand-capped nanoparticles were significantly larger (13 (±4) nm diameter). Thus, the introduction of a protic organic thiol ligand more than doubles the size of the resulting capped metal nanoparticles. Therefore, the thiol ligand addition must perturb and weaken the stabilizing property of propylene carbonate towards the M-NPs so that further M-NP agglomeration is driven by the surface–surface interactions [20]. Cu-, Zn- and Cu/Zn nanobrass alloy nanoparticles were also obtained in PC without the use of extra-stabilizers and dispersions seemed to be stable up to six months [74]. The M-NP/PC dispersions have been tested for the hydrogenation of cyclohexene for Rh-NPs under mild conditions (4–10 bar H_2, 25–90 °C), to give turnover frequencies up to 1875 mol h^{-1} [20].

Here we report the deposition of Ru-NPs on thermally reduced graphite oxide (TRGO) by decomposition of $Ru_3(CO)_{12}$ in PC, and the use of the Ru@TRGO composite as catalyst for the hydrogenation of benzene.

2. Results and discussion

2.1. TRGO-supported Ru-NPs in propylene carbonate

Deposition of Ru-NPs on graphene (TRGO) can be achieved from the corresponding metal carbonyl, $Ru_3(CO)_{12}$, by the rapid and saving-energy method of microwave irradiation (MWI, 250 °C, 50 W, 10 min) with TRGO in propylene carbonate (PC) (Scheme 1).

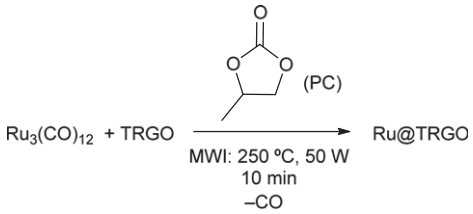

Scheme 1. Synthesis of Ru@TRGO nanomaterials by means of decomposition from $Ru_3(CO)_{12}$ in the presence of TRGO using the energy input of microwave irradiation.

TRGO as support can allow for the synthesis (nucleation and growth) and stabilization of metal nanoparticles because of the functional groups on its surface, where the metal nanoparticles adsorb (bind) and consequently their agglomeration is limited [49,51].

Decomposition of $Ru_3(CO)_{12}$ was followed by infrared spectroscopy (IR) and no bands for the carbonyl bonds at 2020 and 2060 cm^{-1} were found after MWI, indicating full conversion of the metal carbonyl precursor to Ru-NPs (Fig. S3). Of course, our spectroscopic measurement was not sensitive enough to rule out some CO coordination to the surface of the formed Ru nanoparticles.

The resulting Ru@TRGO nanomaterials were characterized by powder X-ray diffraction (PXRD) (Fig. 2). The characteristic reflections at 2θ values of 38.1°, 42.2°, 43.7°, 58.3°, 69.1°, 78.3°, 82.4°, 84.5°, and 86.1° correspond to the indicated [010], [002], [011], [012], [110], [013], [020], [122], and [021] reflections, respectively, of bulk ruthenium metal (Fig. 2). Reflections in the 2θ region between 5 and 25° are derived from TRGO (see Fig. S2 in Supp. Info). The average diameter of the Ru-NPs was calculated by the Debye–Scherrer equation to 10.5 nm from the half-width of the [010] reflection. Characterization of the Ru@TRGO nanomaterials

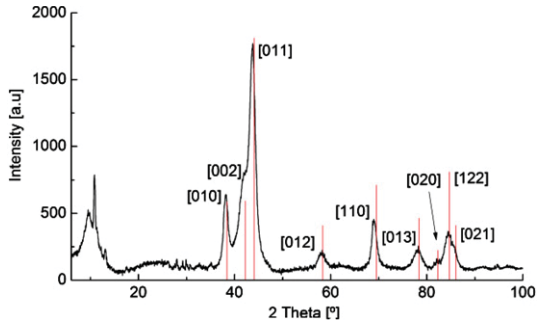

Fig. 2. PXRD of Ru-NPs deposited on TRGO after decomposition by means of microwave irradiation in comparison with the literature (Crystallographic open database COD. 9008513, red bars). Reflections between 5 and 25° are due to TRGO (cf. Fig. S2 in Supp. Info.). (For interpretation of the references to colour in this figure legend, the reader is referred to the web version of this article.)

by transmission electron microscopy (TEM) (Fig. 3) and high-resolution transmission electron microscopy (HR-TEM) with selected area electron diffraction (SAED) (Fig. 4) yielded a diameter and distribution of 7 ± 4 nm for the Ru-NPs (see TEMs with histograms in Fig. S4) and illustrated the nanocrystalline nature. High-resolution TEM images in Fig. 3 (at 10 nm) and Fig. 4 (at 2 nm) showed facetted Ru nanoparticles of presumably cuboctahedral nature. The shape of a crystalline cuboctahedron most closely approaches those of a sphere. From interference of the electron beam with the Ru atoms the highly crystalline, symmetrical most likely cuboctahedral structure of the Ru nanoparticles became visible in the form of their lattice planes (Fig. 4). Energy-dispersive X-ray spectroscopy (EDX) (Fig. S5) only gave the expected bands for Ru metal (Ru-Kα, -Lα1, -Lβ1, -Lγ1, -Mα, -Mγ) besides the bands for carbon and copper of the TRGO and the carbon-coated copper grid.

X-ray photoelectron spectroscopy (XPS) measurements yielded composition of the Ru@TRGO nanomaterials (Fig. 5 and Fig. S6). A content of 3.5 wt% Ru was calculated based on the peaks at 460.9 eV (Ru $3p_{3/2}$) and at 283.4 eV (C 1s). A zero-valent oxidation state of ruthenium is verified from the peak at 279.4 eV, which corresponds to Ru $3d_{5/2}$ [75]. The C 1s and O 1s peak at 283.4 and 530.9 eV, respectively, are associated to graphene and its functional oxygen groups. The O 1s band corresponds to C=O and O=C–OH groups [76].

2.2. Hydrogenation of benzene

Ru@TRGO was tested as heterogeneous catalyst for the hydrogenation of benzene to cyclohexane (Scheme 2).

In a typical hydrogenation reaction Ru@TRGO (5.0 mg, containing 3.5 wt% Ru, 1.73×10^{-3} mmol), and the substrate (benzene, 1.0 mL, 11.14 mmol) were loaded in a stainless-steel autoclave, equipped with a glass inlay to avoid any interference from the steel surface. The autoclave was purged with H_2 at least three times and

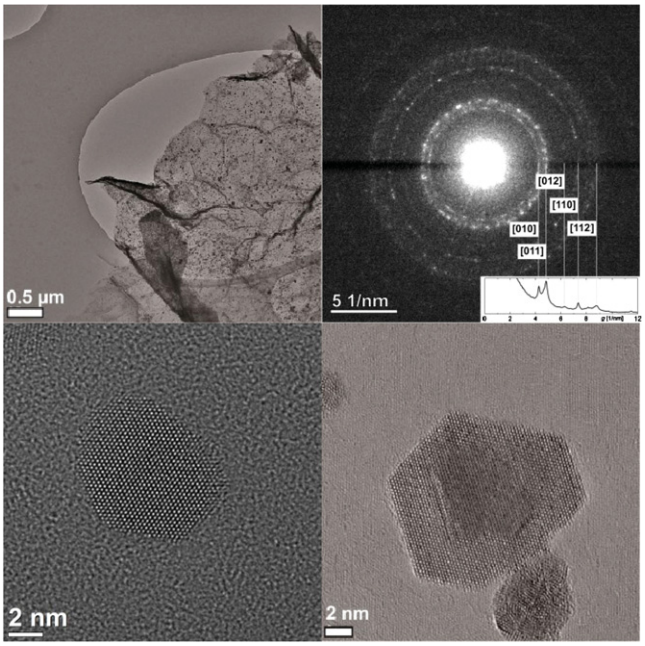

Fig. 4. HR-TEM and electron diffraction of Ru@TRGO synthesized in propylene carbonate. The upper row shows a TRGO flake with many Ru nanoparticles attached, and an electron diffraction pattern taken from this area. The inset diagram shows the average diffraction intensity depending on spatial frequencies in the diffraction pattern. The lower row displays two high-resolution TEM images of single Ru nanoparticles revealing their nano-crystalline and presumably cuboctahedral nature.

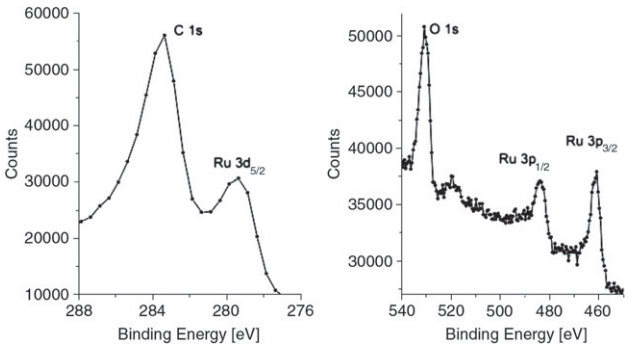

Fig. 5. Enlarged regions of the XPS spectrum (see Fig. S6 in Supp. Info. for full spectrum) of Ru@TRGO nanomaterial with a calculated 3.5 wt% loading of Ru on TRGO.

pre-heated to 100 °C. Once the desired temperature was reached the autoclave was pressurized to 10 bars of H_2 and the reaction mixture stirred (800 rpm) for 20 min. After this time the autoclave was cooled down and the substrate/product mixture was

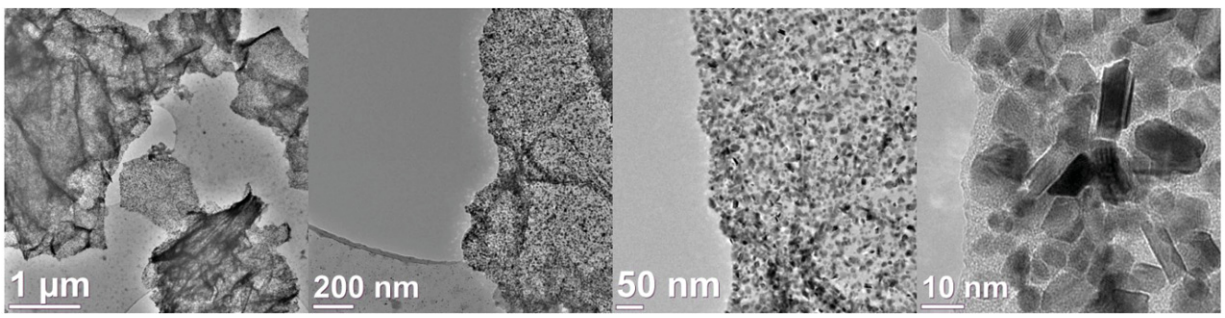

Fig. 3. TEM images of Ru@TRGO nanomaterials synthesized in propylene carbonate.

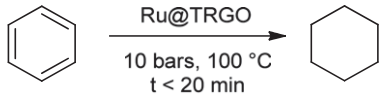

Scheme 2. Hydrogenation of benzene to cyclohexane with Ru@TRGO nanocomposites under solvent-free conditions.

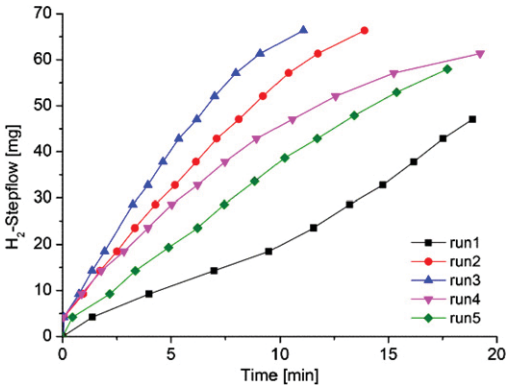

Fig. 6. H_2-uptake over time for the hydrogenation of benzene (0.87 g, 1.0 mL, 11.14 mmol) with Ru@TRGO (5.0 mg, containing 3.5 wt% Ru, 1.73×10^{-3} mmol) at a benzene/metal ratio of 6436, 100 °C and 10 bars H_2. A 100% conversion corresponds to an H_2-uptake of 67.4 mg (33.4 mmol, 802 mL). For clarity the runs 6–10 are given in Fig. S7 in the Supporting Information.

condensed under vacuum into a cold trap. The H_2 uptake was monitored over time by a Büchi bpc press-flow controller (Fig. 6 and Fig. S7).

Conversion of benzene to cyclohexane was calculated based on the consumption of H_2 (Fig. 6 and Fig. S7). Additional measurements by gas chromatography, GC, show no formation of other products such as cyclohexene. The catalyst Ru@TRGO remained in the autoclave and could be re-used at least 10 times without significant loss of activity.

The Ru@TRGO catalyst increased its activity up to the third run to reach a turnover frequency (TOF) of ~34,330 (molcyclohexane) · (mol Ru)$^{-1}$ · h^{-1} (Table 1) near quantitative conversion in about 11 min (Fig. 6). Afterwards, the conversion decreased to 92.3% to stay constant between run 6 to 10 with activities (TOF) around 22,000 (mol cyclohexane) · (mol Ru)$^{-1}$ · h^{-1}.

Heterogeneous catalytic reactions are extremely complex and defects, the surface topology, and surface atom sites (edges, corners, steps) rather than the sole amount of surface atoms strongly influence the catalytic activity. We therefore suggest that the activity increase upon recycling is due to surface reconstruction creating more and more active sites. Increase in activity could also result from surface cleaning of adsorbed and deactivating solvent, carbon or oxygen species. Because of the TRGO support also further exfoliation could occur which would expose more Ru-NPs. The TOF calculation was based on the total quantity of Ru present in the nanomaterial. We note that only surface atoms and among them only a fraction will be catalytically active. If less than 5% of the metal atoms of the Ru-NPs are active surface sites then the activity would be more than 20-times higher on a per-active-metal-atom basis.

Graphene-supported metal nanoparticles were already investigated in our group for Ru- and Rh-NPs and synthesized in the ionic liquid (IL) 1-butyl-3-methylimidazolium tetrafluoroborate [36]. Lower activities were found for Ru- and Rh-NP@graphene in IL than here in propylene carbonate (Table 2). Apparently the remaining IL coating around the nanoparticles presents a diffusion barrier for the substrate species (benzene and H_2). Using M@TRGO/IL (M=Ru or Rh) at 50 or 75 °C with 4 bar of H_2 the time to achieve a

Table 1
Hydrogenation of benzene to cyclohexane with Ru@TRGO nanomaterials[a].

Run	Conversion (%)[b]	Time (min)[c]	TOF (h^{-1})[d]	TON[e]
1	69.8	18.9	14282	4494
2	98.5	13.9	27366	6340
3	98.5	11.1	34331	6340
4	91.0	19.2	18279	5858
5	86.0	17.7	18749	5537
6	92.3	16.9	21059	5939
7	92.3	15.9	22367	5939
8	92.3	16.2	22035	5939
9	92.3	15.7	22767	5939
10	84.4	11.2	29286	5457

[a] Hydrogenation reaction at 100 °C, 10 bars H_2 using Ru@TRGO (mol benzene/mol Ru = 6436).
[b] Calculated based on the H_2-consumption.
[c] Time needed for the given maximum conversion.
[d] Turnover frequency = activity as (mol cyclohexane) · (mol Ru)$^{-1}$ · h^{-1}; with total quantity of Ru present in the nanomaterial.
[e] Turnover number as (mol cyclohexane) · (mol Ru)$^{-1}$.

conversion near 98% was almost four hours (even when cyclohexene was used instead of benzene). The reason to run the catalysis in this work at 100 °C and 10 bar of H_2 was the desire to achieve a conversion of 80%–90% in less than 30 min. Although not tested here, we can assume that the Ru@TRGO/PC system will also be active under milder conditions.

Table 2
Metal@graphene nanomaterials as catalyst for the hydrogenation reaction of benzene[a] or cyclohexene[b] to cyclohexane.

M-NPs/Solvent[c]	pH_2 (bar)	T (°C)	Time[d] (h)	TOF[e] (h^{-1})	Ref.
Ru@TRGO/PC	10	100	<0.33	34330[a]	This work
Ru@TRGO/IL	4	75	4	1570[b]	[37]
Rh@TRGO/IL	4	50	4	310[a]	

[a] Hydrogenation of benzene or.
[b] cyclohexene to cyclohexane.
[c] PC = propylene carbonate or IL = 1-butyl-3-methyltetrafluoroborate [BMIm][BF_4].
[d] For near quantitative conversion.
[e] Turnover frequency as (mol cyclohexane) · (mol metal)$^{-1}$ · h^{-1}.

A wide range of supports for the immobilization of Ru-NPs has been tested for the hydrogenation of benzene (Table 3). Dupont et al. recently reported the deposition of Ru-NPs on modified Al_2O_3 supports with anchored imidazolium-ILs achieving a TOF of 9180 h^{-1} for the hydrogenation of benzene to cyclohexene [13]. Carbon-based supports are also suitable for the stabilization of Ru-NPs and their application in catalysis, Ru-NPs deposited on carbon nanotubes [40] show activities up to ~6900 h^{-1}, and activities around ~35,000 h^{-1} were found for embedded ruthenium nanoparticles on ordered mesoporous carbon [77].

After ten consecutive hydrogenation runs the Ru@TRGO catalyst was analyzed by TEM and SAED (Fig. 7). The nanoparticles retained their crystallinity as is evident from their facets in the TEM and the reflections in the SAED. The average diameters of the Ru-NPs essentially did not change with now 7.2 ± 3.4 nm (for histogram and EDX see Fig. S8 in Supp. Info.).

Concerning leaching we note that even in solution or dispersion, that is, without the TRGO support, the Ru-NP will be catalytically active. This was shown by their use as hydrogenations catalysts for cyclohexene as Ru-nanoparticle/IL dispersion [18]. A leaching process would not have led to removal from the catalyst dispersion here as we removed the products and starting materials by evaporation under vacuum so that no catalyst part could be removed.

Table 3
Hydrogenation reaction for benzene with supported Ru-NPs.

Catalyst[a]	H_2 pressure (bar)	T (°C)	TOF[b] (h^{-1})	Ref.
Ru/HEA-16-Cl	30	20	600[c]	[7,78]
Ru/MMT	8	110	4000	[79]
Ru/CNTs	4	80	6983	[40]
Ru/SiO_2	20	100	5000	[80]
Ru/IL-Al_2O_3	4	75	9180[d]	[77]
Ru-OMC	4	110	35,112	[77]

[a] HEA-16-Cl = *N*,*N*-dimethyl-N-cetyl-N-(2-hydroxyethyl)ammonium chloride, MMT = montmorillonite, CNT = carbon nanotubes, IL = ionic liquid, OMC = ordered mesoporous ruthenium containing carbon.
[b] Turnover frequency = activity as (mol cyclohexane) · (mol total Ru)$^{-1}$ h^{-1} unless noted otherwise.
[c] TOF as (mol consumed H_2) · (mol total Ru)$^{-1}$ h^{-1}.
[d] TOF as (mol benzene conversion) · (mol surface Ru)$^{-1}$ h^{-1}.

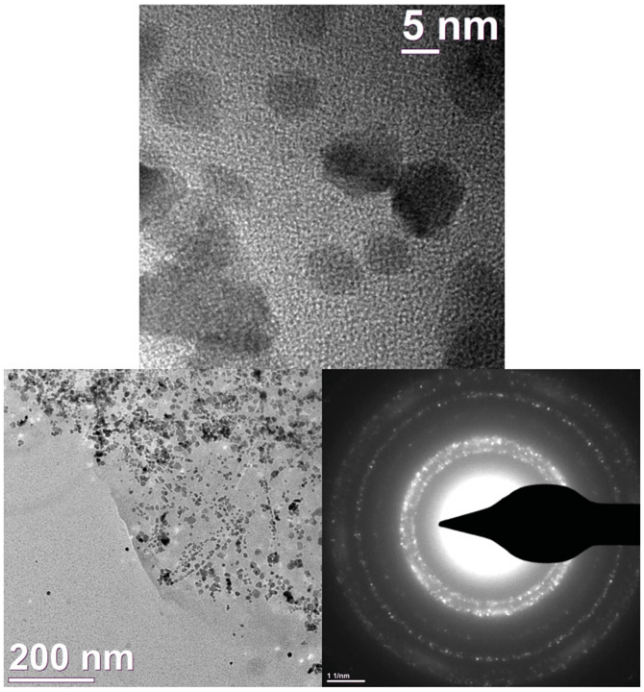

Fig. 7. TEM and SAED of Ru@TRGO after ten consecutive runs in the hydrogenation of benzene to cyclohexane. The black line corresponds to the beam stopper. (For more HR-TEM images see Fig. S9 in Supp. Info.)

3. Conclusion

We describe a straightforward method for the deposition of ruthenium nanoparticles (Ru-NPs) on thermally reduced graphite oxide (TRGO) using propylene carbonate as solvent. The formed Ru-NPs have a size distribution of 7 ± 4 nm and no extra capping ligand or stabilizer is needed for their immobilization and stabilization.

The Ru@TRGO nanomaterials show higher catalytic activities for the hydrogenation of benzene in comparison with their Rh- or Ir-@TRGO analogs, which were synthesized in ionic liquids instead of in organic carbonates. Propylene carbonate, PC, can readily and more completely be removed from the Ru@TRGO composite so as to avoid a diffusion barrier which is otherwise given by a remaining IL layer around the nanoparticles. As a consequence the Ru@TRGO catalysts achieve near quantitative conversion in less than 20 min with turnover frequencies over 18,000 and up to 34,000 (mol cyclohexane) · (mol Ru)$^{-1}$ · h^{-1} for at least 10 consecutive runs under solvent-free conditions. Ru@TRGO nanomaterials exhibit also higher activities than other reported immobilized Ru-NPs.

4. Experimental section

4.1. Materials and methods

All experiments were done using Schlenk techniques under inert atmosphere. Triruthenium dodecacarbonyl $Ru_3(CO)_{12}$ (99% purity) was purchased from ABCR chemicals and thermally reduced graphene oxide (TRGO) was prepared in a two steps oxidation/thermal reduction process using natural graphite (type KFL 99.5 from AMG Mining AG, former Kropfmühl AG, Passau, Germany) as raw material. The graphite oxidation process of Hummers and Offeman [81] was employed. Benzene was purchased by VWR (p.A.), dried with sodium, distilled and stored over 4 Å molecular sieve.

Propylene carbonate was dried under vacuum at 100 °C (10^{-3} mbar) for at least three days. IR spectra were measured on a Bruker TENSOR 37 IR spectrometer in the range from 4000 to 500 cm^{-1} as KBr disks.

The X-ray photoelectron spectroscopy, XPS- (ESCA-) measurement was performed with a Fisons/VG Scientific ESCALAB 200X xp-spectrometer, operating at room temperature, a pressure of $1.0 \cdot 10^{-8}$ bar and a sample angle of 30°. Photoelectron spectra were recorded using polychromatic Al-K_α excitation (14 kV, 20 mA) and an emission angle of 0°. Calibration of the XPS was carried out by recording spectra, using Al K_α X-rays, from clean samples of copper, silver and gold, at 20 eV and 10 eV pass energies and comparison with reference values.

TEM micrographs were recorded with an FEI Tecnai g2 f20 operated at 200 kV accelerating voltage. High-resolution TEM images were recorded with an FEI Titan 80–300 image CS-corrected electron microscope at an accelerating voltage of 300 kV. Samples were prepared using 200 μm carbon-coated copper grids. The size distribution was determined manually and using Gatan Digital Micrograph for at least 150 nanoparticles. For the automatic selection of the nanoparticles we introduced a threshold in the picture, where the nanoparticles will have a different intensity as the background. Noteworthy the automatic determination gave a smaller average diameter than the manual measurement.

High angle energy dispersive X-ray (EDX) detector with a resolution of 136 eV or better for Mn K-alpha radiation, the exposure time for individual EDX spectra was 3 min.

4.2. Synthesis of Ru@TRGO nanomaterials in propylene carbonate

$Ru_3(CO)_{12}$ (25.4 mg, 3.97×10^{-3} mmol) together with 4.7 mg of TRGO (0.2 wt% related to 2.41 g of PC) were dispersed and sonicated for 6 h at 30 °C in PC (2 mL, 2.41 g).

Metal carbonyl decomposition was done by means of microwave irradiation (CEM Discover) at 250 °C, 50 W, 4 bar and 10 min. The volatiles (CO) were removed under vacuum and the black dispersion washed with distilled water (5 × 6 mL) and centrifuged. Finally the Ru@TRGO nanomaterials were dried under vacuum at 100 °C for several hours.

4.3. Hydrogenation of benzene to cyclohexane

All catalytic processes were done using stainless-steel autoclaves under inert atmosphere. Each autoclave was equipped with a glass inlay to avoid any effect of the steel in the reaction.

The desired amount of catalyst (Ru@TRGO, 5 mg containing 3.5% Ru, 1.73×10^{-3} mmol Ru) together with the substrate (benzene, 1 mL, 0.87 g, 11.14 mmol) were loaded in the autoclave. The autoclave was purged three times with H_2 and heated to 100 °C. Once the set temperature was achieved, the autoclave was charged with 10 bars of H_2 and the reaction mixture was stirred (800 rpm) for 20 min. After this time the autoclave was cooled down and

depressurized. The organic volatile were isolated by evaporation and condensation under vacuum in a cold trap. The products were analyzed by GC and conversion was calculated in relation to the H_2 consumption.

Conversion of benzene to cyclohexane was determined by gas chromatography (GC) (Perkin Elmer 8500 HSB 6, equipped with a DB-5 film capillary column, 60 m × 0.32 mm, film thickness 25 μm, oven temperature 40 °C, N2 carrier flow 120 L/min and a flame ionization detector (FID), 250 °C detector temperature). The samples were analyzed by putting a drop of the product into a GC sample vial together with 1 mL of distilled water.

H_2-uptake measurements were followed with a Büchi bpc pressflow controller.

The catalyst could be recovered and re-used for at least 10 times. All procedures were repeated at least twice to evaluate the reproducibility of the process.

Acknowledgment

Authors are thankful to the Deutsche Forschungsgemeinschaft (DFG) for grant Ja466/31-1 within priority program SPP 1708.

Appendix A. Supplementary data

Supplementary material (PXRD pattern of TRGO-400, IR of Ru@TRGO, diameter distribution histogram, EDX-spectrum, full XPS, all H_2-stepflow curves in benzene hydrogenation and additional TEM micrographs) related to this article can be found online at http://dx.doi.org/10.1016/j.nanoso.2015.07.002.

References

[1] J.A. Dahl, B.L.S. Maddux, J.E. Hutchison, Chem. Rev. 107 (2007) 2228–2269.
[2] K. Saha, S.S. Agasti, C. Kim, X. Li, V.M. Rotello, Chem. Rev. 112 (2012) 2739–2779.
[3] H. Goesmann, C. Feldmann, Angew. Chem. Int. Ed. 49 (2010) 1362–1395.
[4] A. Roucoux, J. Schluz, H. Patin, Chem. Rev. 102 (2002) 3757–3778.
[5] D. Astruc, F. Lu, J.R. Aranzaes, Angew. Chem. Int. Ed. 44 (2005) 7852–7872.
[6] D. Wang, Y. Li, Adv. Mater. 23 (2011) 1044–1060.
[7] D. Astruc, Nanoparticles and Catalysis, Wiley-VCH, Weinheim, 2007.
[8] J.D. Scholten, B.C. Leal, J. Dupont, ACS Catal. 2 (2012) 184–200.
[9] T. Naota, H. Takaya, S.-I. Murahashi, Chem. Rev. 98 (1998) 2599–2660.
[10] A. Gual, C. Godard, S. Castillón, C. Claver, Dalton Trans. 39 (2010) 11499–11512.
[11] Y. Huang, Y. Mao, Y. Cheng, L. Wang, X. Li, Appl. Catal. A: General 495 (2015) 124–130.
[12] J. Aguilera, I. Favier, M. Sans, A. Mor, A. Álvarez-Larena, O. Illa, M. Gómez, R.M. Ortuño, Eur. J. Org. Chem. 4 (2015) 810–819.
[13] L. Foppa, L. Luza, A. Gua, D.E. Weibel, D. Eberhardt, S.R. Texeira, J. Dupont, Dalton Trans. 44 (2015) 2827–2834.
[14] V.R.R. Pendyala, W.D. Shafer, G. Jacobs, U.M. Graham, S. Khalid, B.H. Davis, Catal. Lett. 145 (2015) 893–904.
[15] A. Haghtalab, A. Mosayebi, Int. J. Hydrog. Energy 39 (2014) 18882–18893.
[16] G. Viau, R. Brayner, L. Poul, N. Chakroune, E. Lacze, F. Fiévet-Vicent, F. Fiévet, Chem. Mater. 15 (2003) 486–494.
[17] N. Chakroune, G. Viaiu, S. Ammar, L. Poul, D. Veautier, M.M. Chehimi, C. Mangeney, F. Villain, F. Fiévet, Langmuir 21 (2005) 6788–6796.
[18] C. Vollmer, E. Redel, K. Abu-Shandi, R. Thomann, H. Manyar, H. Hardacre, C. Janiak, Chem. Eur. J. 16 (2010) 3849–3858.
[19] C. Vollmer, C. Janiak, Coord. Chem. Rev. 255 (2011) 2039–2057.
[20] C. Vollmer, R. Thomann, C. Janiak, Dalton Trans. 41 (2012) 9722–9727.
[21] K. Pelzer, O. Vidoni, K. Philippot, B. Chaudret, V. Collière, Adv. Funct. Mater. 13 (2003) 118–126.
[22] C. Pan, K. Pelzer, K. Philippot, B. Chaudret, F. Dassenoy, P. Lecante, M.-J. Casanove, J. Am. Chem. Soc. 123 (2001) 7584–7593.
[23] T. Gutel, J. Garcia-Anton, K. Pelzer, K. Philippot, C.C. Santini, Y. Chauvin, B. Chaudret, J.-M. Basset, J. Mater. Chem. 17 (2007) 3290–3292.
[24] G. Salas, A. Podgorsek, P.S. Campbell, C.C. Santini, A.A.H. Pádua, M.F. Costa Gomes, K. Philippot, B. Chaudret, M. Turmine, Phys. Chem. Chem. Phys. 13 (2011) 13527–13536.
[25] E.T. Silveira, A.P. Umpierre, L.M. Rossi, G. Machado, J. Morais, G.V. Soares, I.J.R. Baumvol, S.R. Teixeira, R.F.P. Fichtner, J. Dupont, Chem. Eur. J. 10 (2004) 3734–3740.
[26] W. Ostwald, Z. Phys. Chem. 37 (1901) 385.
[27] W. Ostwald, Lehrbuch der Allgemeinen Chemie, Vol. 2, Part 1, Leipzig, Germany, 1896.
[28] H. Bönnemann, R.M. Richards, Eur. J. Inorg. Chem. 10 (2001) 2455–2480.
[29] L.D. Pachón, G. Rothenberg, Appl. Organomet. Chem. 22 (2008) 288–299.
[30] P. Graf, A. Mantion, A. Foelske, A. Shkilnyy, A. Măsić, A.F. Thünemann, A. Taubert, Chem. Eur. J. 15 (2009) 5831–5844.
[31] (a) C. Janiak, Z. Naturforsch. B 68 (2013) 1056–1089;
(b) K. Klauke, B. Hahn, K. Schütte, J. Barthel, C. Janiak, Nano-Struct. Nano-Objects 1 (2015) 24–31.
[32] C. Janiak, Metal nanoparticle synthesis in ionic liquids, in: J. Dupont, L. Kollar (Eds.), Ionic Liquids (ILs) in Organometallic Catalysis, in: Topics in Organometallic Chemistry, vol. 51, Springer, Heidelberg, 2015, pp. 17–53.
[33] C. Janiak, Metal nanoparticle synthesis in ionic liquids, in: C. Hardacre, V. Parvulescu (Eds.), Catalysis in Ionic Liquids: From Catalyst Synthesis to Application, RSC Publishing, Cambridge, 2014, pp. 537–577, Chapter 11.
[34] J. Dupont, J.D. Scholten, Chem. Soc. Rev. 39 (2010) 1780–1804.
[35] J. Dupont, J. Brazil, Chem. Soc. 15 (2004) 341–350.
[36] R. Fernandes, N. Patel, E. Edla, N. Bazzanella, D.C. Kothari, A. Miotello, Appl. Catal. A: General 495 (2015) 23–29.
[37] D. Marquardt, C. Vollmer, R. Thomann, P. Steurer, R. Mülhaupt, E. Redel, C. Janiak, Carbon 49 (2011) 1326–1332.
[38] C. Vollmer, M. Schröder, Y. Thomann, R. Thomann, C. Janiak, Appl. Catal. A: General 425–426 (2012) 178–183.
[39] N. Cao, W. Luo, G. Cheng, Int. J. Hydrog. Energy 38 (2013) 11964–11972.
[40] Y. Ma, Y. Huang, Y. Cheng, L. Wang, X. Li, Appl. Catal. A: General 484 (2014) 154–160.
[41] L. Wang, J. Chen, L. Ge, V. Rudolph, Z. Zhu, J. Phys. Chem. C. 117 (2013) 4141–4151.
[42] G.M. Scheuermann, L. Rumi, P. Steurer, W. Bannwarth, R. Mülhaupt, J. Am. Chem. Soc. 131 (2009) 8262–8270.
[43] S. Stankovich, D.A. Dikin, G.H.B. Dommett, K.M. Kohlhaas, E.J. Zimney, E.A. Stach, R.D. Piner, S.T. Nguyen, R.S. Ruoff, Nature 442 (2006) 282–286.
[44] A.K. Geim, K.S. Novoselov, Nature Mater. 6 (2007) 183–191.
[45] D. Li, R.B. Kaner, Science 320 (2008) 1170–1171.
[46] P. Steurer, R. Wissert, R. Thomann, R. Mülhaupt, Macromol. Rapid Commun. 30 (2009) 316–327.
[47] M.J. McAllister, J.L. Li, D.H. Adamson, H.C. Schniepp, A.A. Abdala, J. Liu, M. Herrera-Alonso, D.L. Milius, R. Car, R.K. Prud'homme, I.A. Aksay, Chem. Mater. 19 (2007) 4396–4404.
[48] H.C. Schniepp, J.L. Li, M.J. McAllister, H. Sai, M. Herrera-Alonso, D.H. Adamson, R.K. Prud'homme, R. Car, D.A. Saville, I.A. Aksay, J. Phys. Chem. B 110 (2006) 8535–8539.
[49] G. Goncalves, P.A.A.P. Marques, C.M. Granadeiro, H.I.S. Nogueira, M.K. Singh, J. Grácio, Chem. Mater. 21 (2009) 4796–4802.
[50] C.N.R. Rao, A.K. Sood, R. Voggu, K.S. Subrahmanyam, J. Phys. Chem. Lett. 1 (2010) 572–580.
[51] H.P. Boehm, E. Stumpp, Carbon 45 (2007) 1381–1383.
[52] H.B. Li, W.J. Kang, B.J. Xi, Y. Yan, H.Y. Bi, Y.C. Zuhu, Y.T. Qian, Carbon 48 (2010) 464–469.
[53] H. Park, J.S. Kim, B.G. Choi, S.M. Jo, D.Y. Kim, W.H. Hong, S.-Y. Jang, Carbon 48 (2010) 1325–1330.
[54] D.N. Ventura, R.A. Stone, K.S. Chen, H.H. Hariri, K.A. Riddle, T.J. Fellers, C.S. Yun, G.F. Strouse, H.W. Kroto, S.F.A. Acquah, Carbon 48 (2010) 987–994.
[55] S. Kudo, T. Maki, K. Miura, K. Mae, Carbon 48 (2010) 1186–1195.
[56] K. Scholz, J. Scholz, A.J. McQuilla, G. Wagner, O. Klepel, Carbon 48 (2010) 1788–1798.
[57] Y.H. Kim, Y.T. Kim, H. Kim, D. Lee, Carbon 48 (2010) 2072–2084.
[58] V. Tzitzios, V. Georgakilas, E. Oikonomou, M. Karakassides, D. Petridis, Carbon 44 (2006) 848–853.
[59] D. Marquardt, F. Beckert, F. Pennetreau, F. Tölle, R. Mülhaupt, O. Riant, S. Hermans, J. Barthel, C. Janiak, Carbon 66 (2014) 285–294.
[60] R. Marcos Esteban, K. Schütte, P. Brandt, H. Marquardt, D. Meyer, F. Beckert, R. Mülhaupt, H. Kölling, C. Janiak, Nano-Struct. Nano-Objects 1 (2015) http://dx.doi.org/10.1016/j.nanoso.2015.07.001.
[61] B. Schäffner, F. Schäffner, S.P. Verevkin, A. Börner, Chem. Rev. 110 (2010) 4554–4581.
[62] J.H. Clements, Ind. Eng. Chem. Res. 42 (2003) 663–674.
[63] J. Mak, D. Nielsen, D. Schulte, LRGCC Conf. Proc. 57 (2007) 267–280.
[64] A.L. Kohl, P.A. Buckingham, Oil Gas J. 58 (1960) 146.
[65] G.G. Eshetu, J.-P. Bertrand, A. Lecocq, S. Grugeon, S. Laurelle, M. Armand, G. Marlair, J. Power Sources 269 (2014) 804–811.
[66] R. Jasinski, J. Electroanal. Chem. 15 (1967) 89–91.
[67] K.K.D. Ehinon, S. Naille, R. Dedryvère, P.-E. Lippens, J.-C.Jumas D. Gonbeau, Chem. Mater. 20 (2008) 5388–5398.
[68] H. Cheng, R.R. Gadde, J. Pharm. Sci. 74 (1986) 695–696.
[69] A. Ansmann, B. Boutty, M. Dierker, Chem. Abstr. 149 (2008) 17219.
[70] M. Reetz, G. Lohmer, Chem. Commun. 16 (1996) 1921–1922.
[71] A. Behr, H. Schmidke, Chem. Ing. Tech. 65 (1993) 568–569.
[72] A. Behr, N. Döring, S. Durowicz-Heil, B. Ellenberg, C. Kozik, C. Lohr, H. Schmidke, Fat Sci. Technol. 95 (1993) 2–12.
[73] J. Demel, J. Čejka, S. Bakardjieva, P. Štěpnička, J. Mol. Catal. A 263 (2007) 259–265.
[74] K. Schütte, H. Meyer, C. Gemel, J. Barthel, R.A. Fischer, C. Janiak, Nanoscale 6 (2014) 3116–3126.
[75] J.F. Moulder, W.F. Stickle, P.E. Sobol, K.D. Bombem, Handbook of X-ray Photoelectron Spectroscopy: a Reference Book of Standard Spectra for Identification and Interpretation of XPS Data, 1992, Published by Physical Electronics Division.
[76] D. Yang, A. Velamakanni, G. Bozoklu, S. Park, M. Stoller, R.D. Piner, S. Stankovich, I. Jung, D.A. Field, C.A. Ventrice Jr., R.S. Ruoff, Carbon 47 (2009) 145–152.

[77] Y. Li, G. Lan, H. Wang, H. Tang, X. Yan, H. Liu, Catal. Commun. 20 (2012) 29–35.
[78] A. Nowicki, V. Le Boulaire, A. Roucoux, Adv. Synth. Catal. 349 (2007) 2326–2330.
[79] S. Miao, Z. Liu, B. Han, J. Huang, Z. Sun, J. Zhang, T. Jiang, Angew. Chem. Int. Ed. 45 (2006) 266–269.
[80] X. Kang, J. Zhang, W. Shang, T. Wu, P. Zhang, B. Han, Z. Wu, G. Mo, X. Xing, J. Am. Chem. Soc. 136 (2014) 3768–3771.
[81] W.S. Hummers, R.E. Offeman, J. Am. Chem. Soc. 80 (1958) 1339–1339.

Synthesis of ruthenium@graphene nanomaterials in propylene carbonate as re-usable catalysts for the solvent-free hydrogenation of benzene

Raquel Marcos Esteban,[a] Kai Schütte,[a] Dorothea Marquardt,[a] Juri Barthel,[b] Fabian Beckert,[c] Rolf Mülhaupt,[c,d] and Christoph Janiak*[a]

[a] *Institut für Anorganische Chemie und Strukturchemie, Heinrich Heine Universität Düsseldorf, 40204 Düsseldorf. E-mail: janiak@uni-duesseldorf.de; Fax: +49-211-81-12287; Tel: +49-211-81-12286.*
[b] *Ernst Ruska-Centre for Microscopy and Spectroscopy, Forschungszentrum Jülich GmbH and RWTH Aachen University, 52425 Jülich, Germany*
[c] *Freiburger Material-forschungszentrum (FMF) and Institut für Makromolekulare Chemie, Universität Freiburg, Stefan-Meier-Str. 21-31, 79104 Freiburg, Germany*
[d] *FRIAS, Freiburg Institute for Advanced Studies, Albertstr. 19, 79104, Freiburg, Germany.*

Email:
Raquel Marcos Esteban: raquel.marcos.esteban@hhu.de
Kai Schütte: kai.schuette@hhu.de
Dorothea Marquardt: doromarquardt@googlemail.com
Fabian Beckert: fabian.beckert@fmf.uni-freiburg.de
Rolf Mülhaupt: rolf.muelhaupt@fmf.uni-freiburg.de
Juri Barthel: Ju.Barthel@fz-juelich.de
Christoph Janiak: janiak@hhu.de

1. TRGO

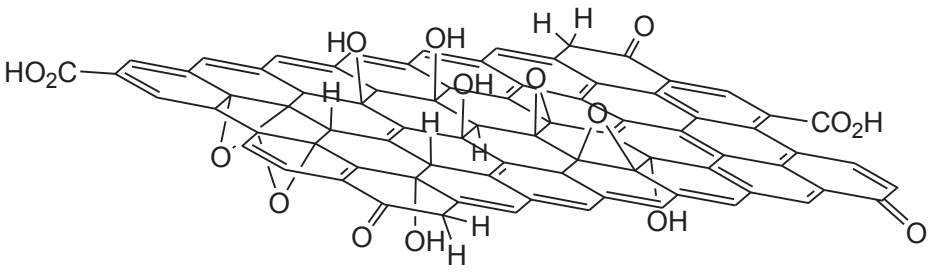

Fig. S 1 Suggested structure of TRGO with epoxy, hydroxyl, carbonyl and carboxyl functionalities.

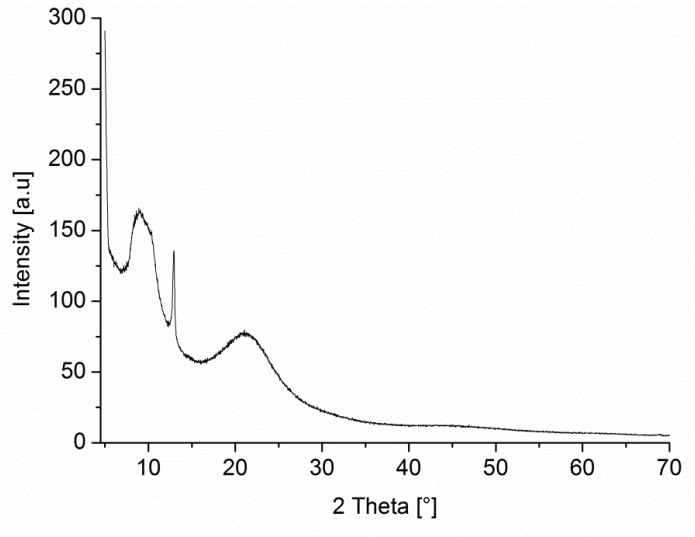

Fig. S 2 Powder X-ray diffractogram of TRGO-400.

2. Synthesis and characterization of Ru@TRGO nanomaterials.
2.1 Chracterization or Ru@TRGO before hydrogenation of benzene to cyclohexane.

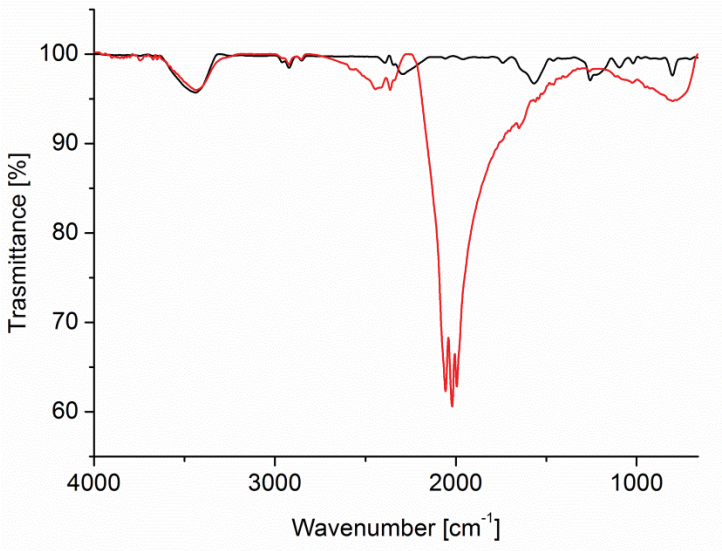

Fig. S 3 IR spectrum of Ru@TRGO (KBr, black curve) in comparison with the starting material $Ru_3(CO)_{12}$ (KBr, red curve).

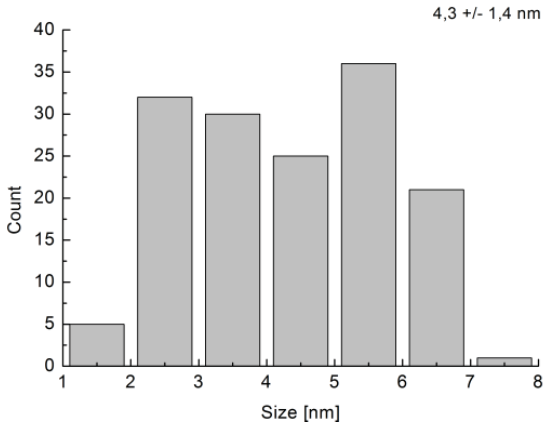

Fig. S 4 Diameter distribution histogram from TEM of Ru@TRGO nanoparticles before catalysis, measured with the programm GATAN for 150 nanoparticles in relation to the Fig.3 (50 nm scale)..

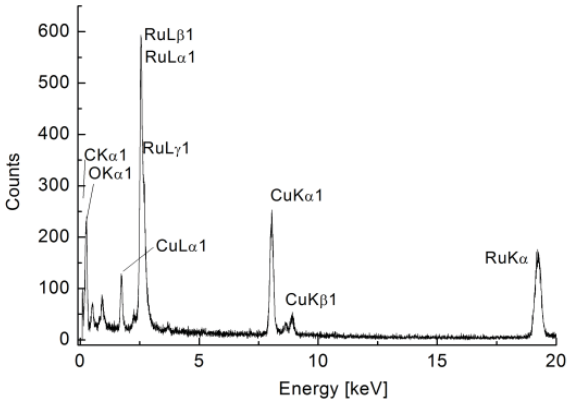

Fig. S 5 Energy-dispersive X-ray spectrum (EDX) of Ru@TRGO nanoparticles before catalysis

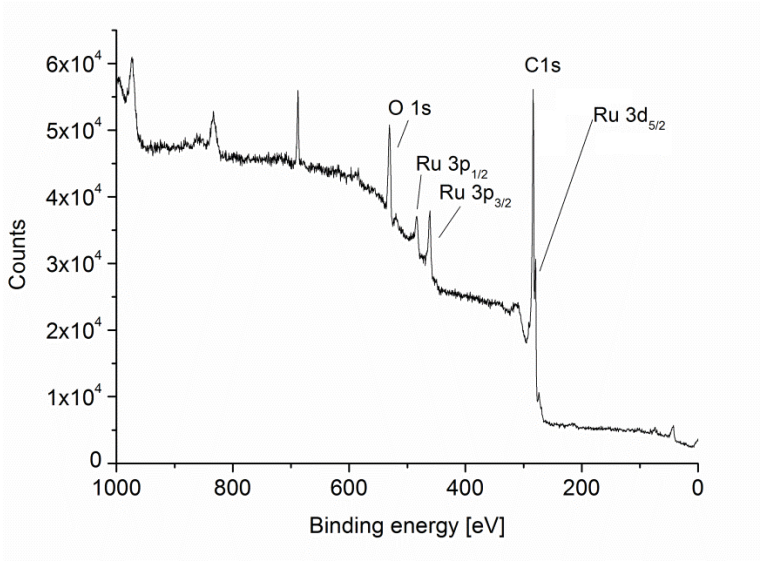

Fig. S 6 X-ray photoelectron spectrum, XPS of Ru@TRGO before catalysis.

3. Hydrogenation reactions

3.1 Hydrogenation of benzene to cyclohexane.

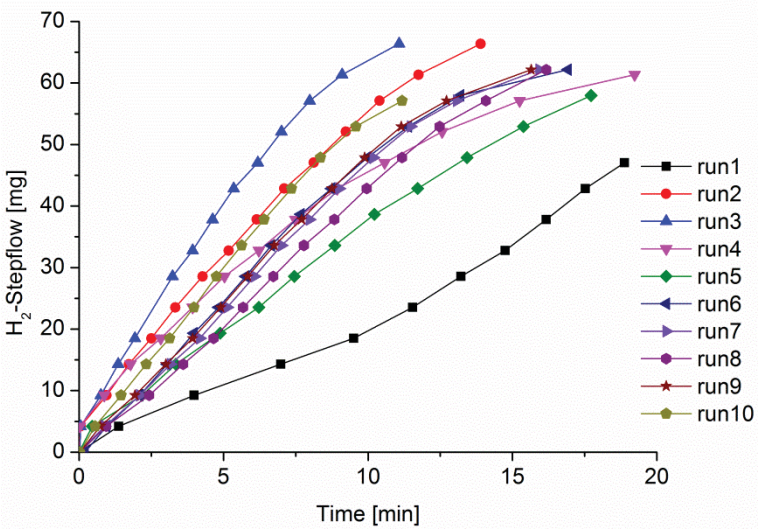

Fig. S 7 H_2-Stepflow over time for the hydrogenation of benzene to cyclohexane with Ru@TRGO nanomaterials.

3.2 Characterization of Ru@TRGO nanomaterials after catalysis reactions.

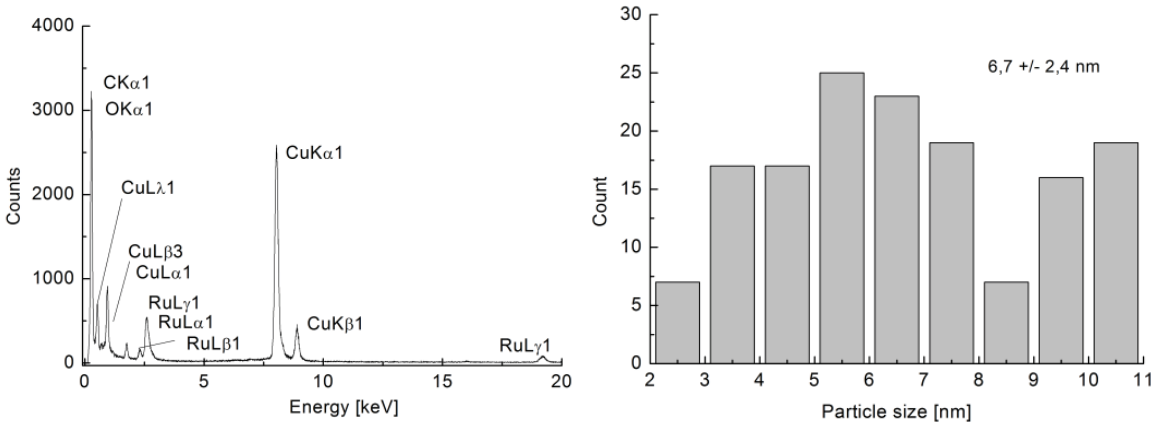

Fig. S 8 EDX (left) and diameter distribution histogram (right) of Ru@TRGO nanoparticles after hydrogenation of benzene to cyclohexane (ten runs), measured by the program GATAN for 150 nanoparticles.

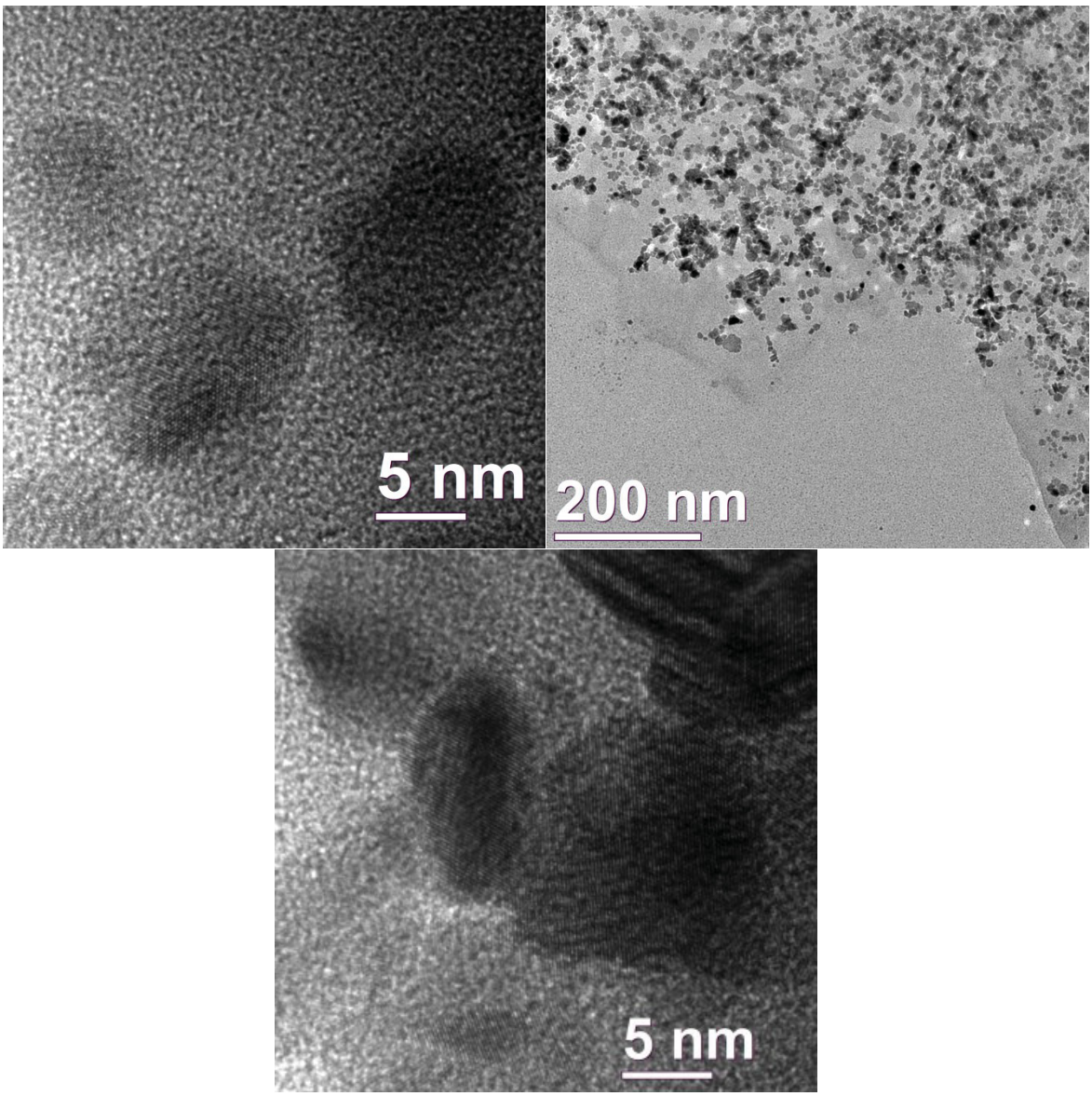

Fig. S 9 TEM micrographs of Ru@TRGo after ten consecutives runs for the hydrogenation of benzene to cyclohexane.

3.3 Synthesis and application of metal nanoparticles catalyst in ionic liquid media using metal carbonyl complexes as precursors.

R. Marcos Esteban, C. Janiak.

Nanocatalysis in Ionic Liquids (M. Prechtl Ed.), Wiley-VCH, Weinheim, **2015**, *submitted*

ref. [86]

In the last years, the research in the nanoscience has significantly grown and a myriad of different methods and techniques for the synthesis of M-NPs have been reported. The synthesis of M-NPs should be reproducible and easy to handle to achieve small size distributions and stable nanoparticles. The properties of the M-NPs can be influenced for many factors as solvents, temperature or capping agents (section 1.4). M-NPs can be obtained from two different approaches: the “top-down” approach, where bulk material is reduced to the nanometer size scale, and the “bottom-up” approach, where molecular or ionic compounds are used. The chemical “bottom-up” approach is often used for the synthesis of M-NPs by different heating methods such as chemical reduction, thermal decomposition or sonochemistry.

Metal carbonyls are commercially available and easy to handle and due to the already zero oxidation state of the metal offer an elegant and clean method for the synthesis of M-NPs, in which external reducing agents are not necessary and only byproducts (-CO) can be removed under vacuum. Ionic liquids prevent the thermodynamically favored aggregation and agglomeration of M-NPs without the presence of stabilizers. In the synthesis of M-NPs from metal carbonyls using ILs the absence of capping ligands around the M-NPs represents an advantage for catalysis, because secondary reactions are drastically reduced.

.

Author’s contribution of the publications:

- Bibliographic research, organization and classification of the publications.
- Writing the first draft and further edition of the manuscript
- My contribution as co-author of this review is approximately 60%.

SYNTHESIS AND APPLICATION OF METAL NANOPARTICLE CATALYSTS IN IONIC LIQUID MEDIA USING METAL CARBONYL COMPLEXES AS PRECURSORS

Raquel Marcos Esteban and Christoph Janiak*

Institut für Anorganische Chemie und Strukturchemie, Heinrich-Heine-Universität Düsseldorf, Universitätsstrasse 1, D-40225 Düsseldorf (Germany),
E-mail: janiak@uni-duesseldorf.de, phone: int+49-(0)211-81-12286

1. Introduction

Metal nanoparticles (M-NPs) are an important class of materials in nanoscience and nanotechnology [1,2,3,4]. M-NPs should be reproducibly synthesized with control of the topology, the particle diameter and size distribution as well as other parameters which are relevant for many applications [5,6,7,8,9]. The diameter of metal-nanoparticles, for example, can be influenced by synthesis parameters such as temperature, pressure, solvent or the character of the stabilizers and capping agents [10]. In a chemical “bottom-up” approach the decomposition or reduction of metal precursor compounds is often used which is assisted by thermal energy, photolysis or ultrasound to obtain metal nanoparticles [11].

Nanoparticles have a high ratio of surface to bulk atoms. With decreasing nanoparticle diameter the fraction of surface atoms and the surface energy increases greatly (**Figure 1**). The surface atoms with their "unsaturated bonds" dominate the chemistry and physics of nanoparticles [12]. In catalysis M-NPs or metal nanoclusters are investigated as "soluble" analogs of heterogeneous catalysts [1319]. The activity of (heterogeneous) nanocatalysts benefits strongly from the high surface area. Yet, small M-NPs of just a few nanometers are only kinetically stable and will agglomerate to thermodynamically more stable larger (nano)particles in a process called Ostwald ripening (**Figure 2**) [20,21].

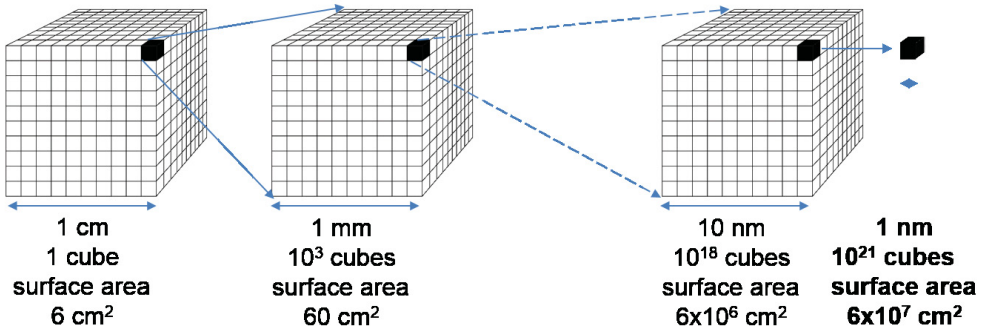

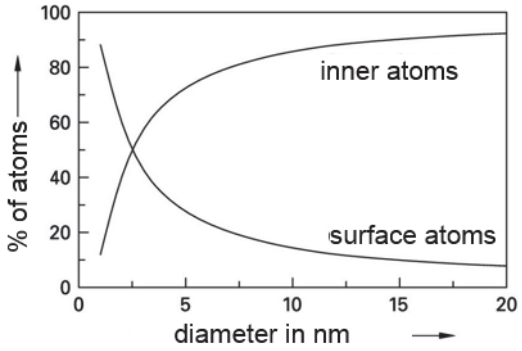

Figure 1. Schematic representation of the increase in surface area (top) with fragmentation of a macroscopic object into nanoobjects or the increase of surface atoms (bottom) relative to inner atoms with decreasing size of a nanoparticle. Graphics adapted from ref. [22].

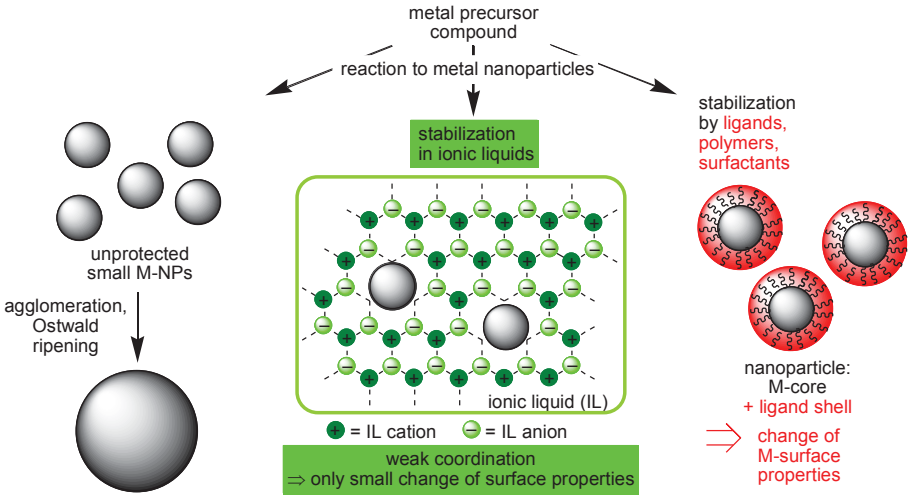

Figure 2. Stabilization of metal nanoparticles (M-NPs) in ionic liquids (ILs) (middle) or through protective ligands (right).

In order to prevent the thermodynamically favored aggregation, coordinating ligands, polymers or surfactants are commonly and traditionally added during the synthesis of M-NPs to surround the M-NPs with protective electrostatic and/or steric layer (Figure 2) [10,23,24,25,26]. As an alternative, ionic liquids (ILs) can stabilize M-NPs without added capping ligands (Figure 2). By definition, ionic liquids are salts, which are liquid below 100 °C. To achieve such a low lattice energy, the charge is distributed over a larger surface area of the cations and anions. Typical ionic liquid cations and anions are depicted in **Figure 3.**

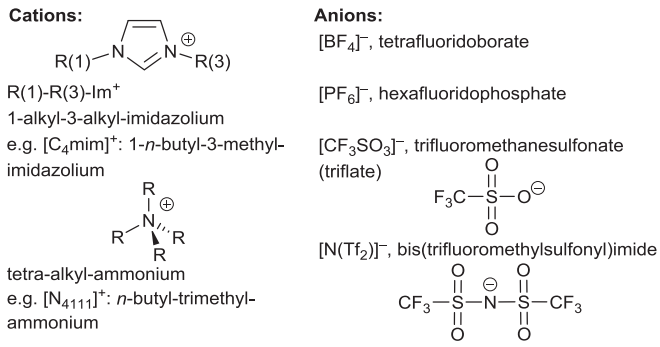

Figure 3. Cations and anions of common ILs. $[C_4mim]^+$ is also abbreviated as $[BMIm]^+$, $[BMI]^+$ or $[C_4C_1Im]^+$, $[CF_3SO_3]^-$ as $[OTf]^-$.

Ionic liquids are an attractive and suitable media for microwave reactions, or for microwave-induced thermal decompositions in the case of metal nanoparticle formation due to their high polarity, high ionic charge and high dielectric constant. ILs show a high dissipation factor (tan δ) for the conversion of microwave energy into heat [27,28]. Microwaves are a low-frequency energy source which induce an extremely rapid heating process in high-absorptive media [27,2931]. Microwave irradiation directly heats the reaction mixture and not the vessel because it is the reaction mixture which absorbs the microwave energy. This leads to localized superheating, very fast and efficient heating rates so that temperatures of 200 °C are reached within seconds [29,32,3335]. As soon as metal particles form they will also absorb the microwave radiation.

In ionic liquids metal nanoparticles can be kinetically stabilized by virtue of the ionic nature, high polarity, viscosity and electrostatic-steric supramolecular network of these molten salts without the need of external stabilizers [36,37,38,39,40,41,42,43,44,45]. The use of ionic liquids as solvents and stabilizers for metal nanoparticles should avoid the addition of external capping ligands due to the electrostatic and steric stabilization through the formation of an ion layer around the metal nanoparticles, although this type of stabilization is nowadays still a manner of discussion [39,46]. Reference is usually made to DVLO (Derjaugin-Landau-Verwey-Overbeek) theory thereby the IL provides a “protective shell” for M-NPs [47,48]. DVLO theory predicts that the shell adjacent to the M-NP surface must be anionic and as consequence, the IL-anion should be the primary source of stabilization of the metal nanocluster. The steric demand of the anions then also provides for a steric stabilization (or electro-steric altogether).

Before focusing on metal carbonyl precursors we note that the synthesis of metal nanoparticles in ionic liquids [49] can generally be achieved through chemical reduction [50,51,52,53,54,55] or decomposition [56,57,58,59], by means of electro-reduction/electro-deposition [60,61,62] or

photochemical reduction [63,64] of metal salts where the metal atom is in a formally positive oxidation state (M^{n+}). The combination of metal nanoparticles and ionic liquids is a growing field [17,37,39,43,65,66,67,68,69,70].

2. Metal carbonyls – synthesis, structure and bonding

Metal complexes with carbon monoxide, CO as a ligand are called metal carbonyls or carbonyl complexes [71]. The stoichiometry in many metal carbonyls follows the 18-valence electron rule. Carbon monoxide is a two-electron donor ligand. The CO group binds with the carbon atom to the metal atom. Metal carbonyls are of structural and of theoretical interest and technically important as catalysts (e.g. Monsanto acetic acid process, hydroformylation, Fischer-Tropsch-synthesis). Carbonyl complexes occur mostly with the transition metals of d-block elements. For main group elements, lanthanoids and actinoids there are only singular examples with metal-CO bonds. The transition metals V, Cr, Mo, W, Mn, Tc, Re, Fe, Ru, Os, Co, Rh, Ir and Ni can form metal carbonyls of the general formula $M_x(CO)_y$, that is, consisting only of the metal and the CO ligand. Such carbonyl complexes are called binary metal carbonyls (**Table 1**) [71].

Table 1. Binary metal carbonyls.[a]

Group	5	6	7	8	9	10
Metal	V, Nb, Ta	Cr, Mo, W	Mn, Tc, Re	Fe, Ru, Os	Co, Rh, Ir	Ni, Pd, Pt
mononuclear complexes	$V(CO)_6$	**$Cr(CO)_6$** **$Mo(CO)_6$** **$W(CO)_6$**		**$Fe(CO)_5$** $Ru(CO)_5$ $Os(CO)_5$		**$Ni(CO)_4$**
polynuclear complexes			**$Mn_2(CO)_{10}$** $Tc_2(CO)_{10}$ **$Re_2(CO)_{10}$**	**$Fe_2(CO)_9$** **$Fe_3(CO)_{12}$** $Ru_2(CO)_9$ **$Ru_3(CO)_{12}$** $Os_2(CO)_9$ **$Os_3(CO)_{12}$**	**$Co_2(CO)_8$** **$Co_4(CO)_{12}$** **$Rh_4(CO)_{12}$** **$Rh_6(CO)_{16}$** **$Ir_4(CO_{12}$**	

[a] Metal carbonyls given in bold were confirmed to be commercially available, e. g., from Aldrich, ABCR or Acros.

Examples for the binary metal carbonyl structures are collected in **Figure 4**. Metal carbonyls are commercially available (see Table 1) and relatively easy to handle. $Ni(CO)_4$ and $Fe(CO)_5$ are produced on a multi-ton scale [72]. Metal-carbonyl complexes $Fe(CO)_5$, $Co_2(CO)_8$ and $Ni(CO)_4$ can be prepared by direct reaction between finely dispersed metal and carbon monoxide at elevated temperature and pressure (**Eq. 1**).

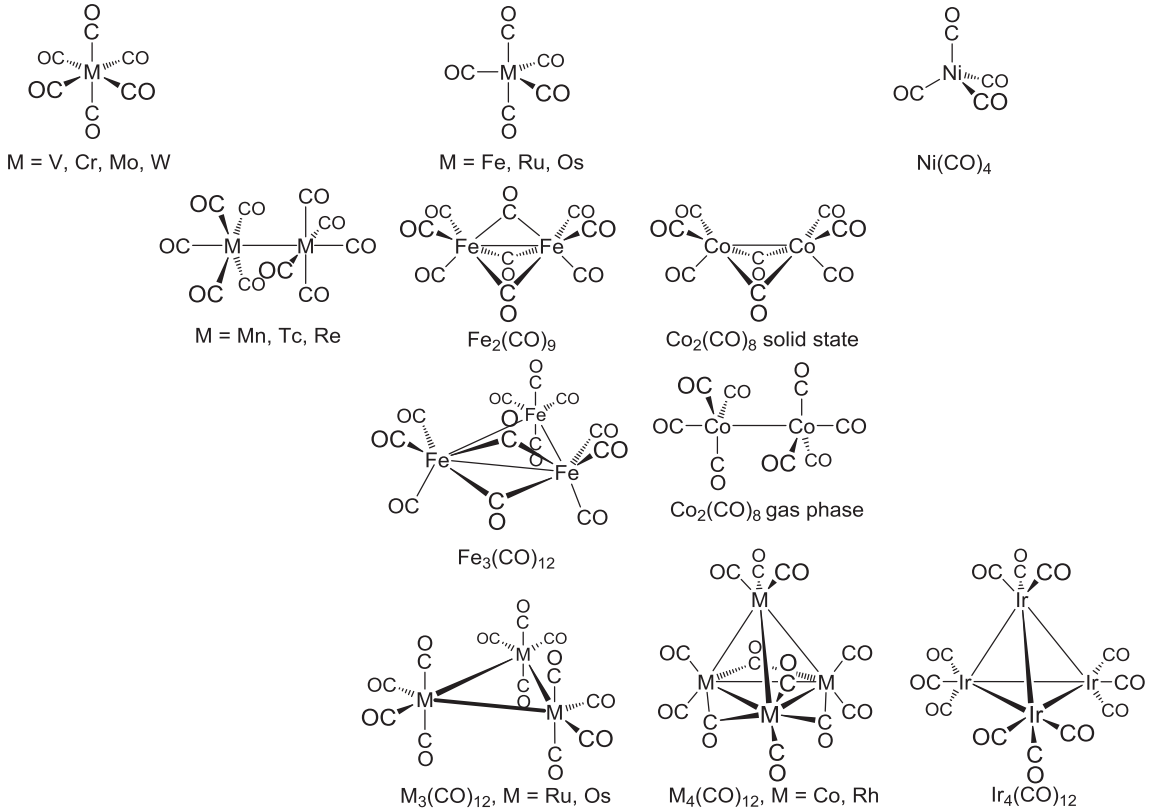

Figure 4. Molecular structures for the binary metal carbonyl examples. $Rh_6(CO)_{16}$ where the Rh_6 atoms form an octahedra is not shown.

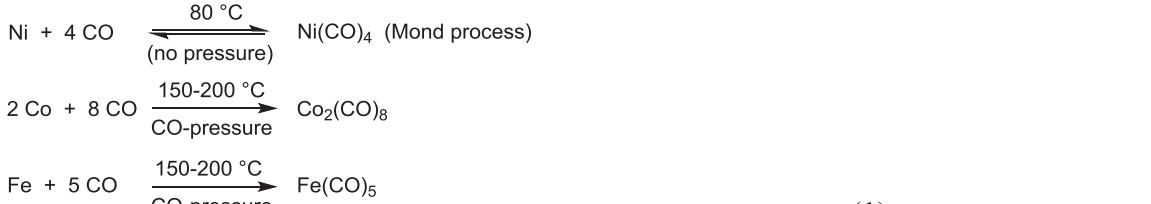

(1)

A more general synthesis is the reduction of metal salts in the presence of carbon monoxide (reductive carbonylation) (**Eq. 2**). Also, CO itself can act as a reductant (**Eq. 3**).

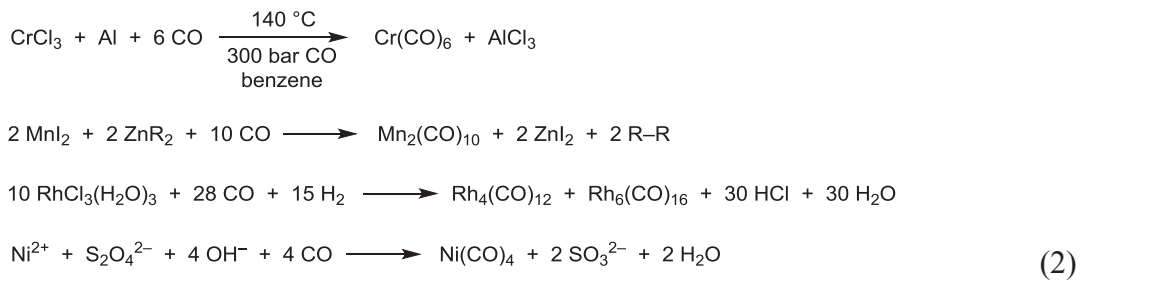

(2)

$$Re_2O_7 + 17\ CO \longrightarrow Re_2(CO)_{10} + 7\ CO_2$$

$$[Ni(NH_3)_6]^{2+} + 5\ CO + 2\ H_2O \longrightarrow Ni(CO)_4 + (NH_4)_2CO_3 + 2\ NH_4^+ + 2\ NH_3 \qquad (3)$$

The metal-carbonyl bond consists synergistically of a OC→metal σ-donor bond and of the important M→CO π-acceptor or back bond (**Figure 5**). The former originates from the σ-HOMO of CO into a metal orbital, the latter involves the electron transfer from an occupied metal d-orbital into the empty π*-LUMO of CO (Figure 5).

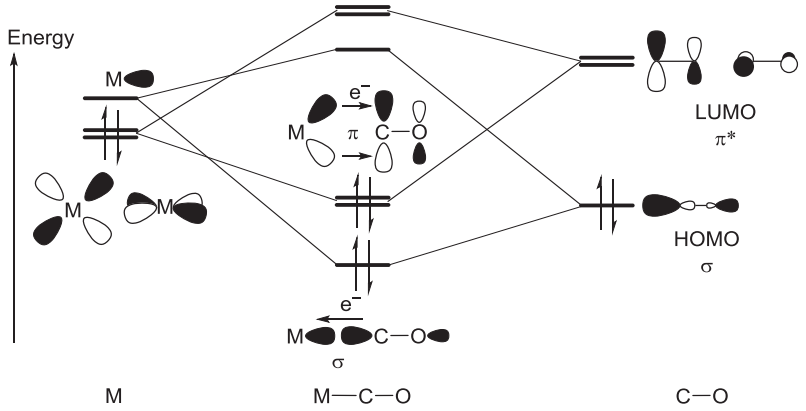

Figure 5. Frontier orbital section of the qualitative molecular orbital (MO) diagram for the OC→metal donor σ-bond and the M→CO π-acceptor or back bond in the metal-carbonyl bond (HOMO = highest occupied MO, LUMO = lowest unoccupied MO). For clarity only one of the M→CO π-bonds is depicted.

Mononuclear metal carbonyls are formed with metal atoms possessing an even number of d-electrons (d^6: Cr, Mo, W; d^8: Fe, Ru, Os; d^{10}: Ni) such that the d-electron count plus the number of CO-ligands times two electrons (for each CO) then yields 18 valence electrons. Example: $Fe(CO)_5$ 8 d-electrons + 5 x 2 CO-electrons = 18. An exception is vanadium hexacarbonyl $V(CO)_6$ which forms a stable 17-valence-electron species. Metal atoms with an odd number of electrons have to form di- or oligonuclear carbonyl clusters with metal-metal bonds. Sharing of metal electrons then leads to the 18-valence-electron configuration. Example: $Co_2(CO)_8$ 9 d-electrons + 4 x 2 CO-electrons + 1 metal electron = 18. The even-numbered metal atoms Fe, Ru and Os (d^8) form both mononuclear ($M(CO)_5$) and oligonuclear carbonyl complexes ($Fe_2(CO)_9$, $M_3(CO)_{12}$).

3. Metal carbonyls for the synthesis of metal nanoparticles (M-NPs)

The oxidation state of the metal atom in binary carbonyls is zero. No reductant is necessary to derive at zero-valent metal from metal carbonyls $M_x(CO)_y$. Metal nanoparticles (M-NPs) can be elegantly and easily obtained by thermal, photolytic or sonolytic decomposition of binary metal-carbonyl compounds, $M_x(CO)_y$. The formation of byproducts is very limited and the liberated CO can be easily removed with the gas phase [73,74]. As pointed out above, also M-NPs from metal carbonyls need a stabilizer such as capping ligands, polymers or surfactants to avoid oxidation or aggregation.

3.1. Synthesis in conventional organic solvents

Most of the early research on M-NPs from metal carbonyls focused on the synthesis of Fe- or Co-NPs due to their magnetic properties [75].

In the 1960´s Hess and Parker [76] and Thomas [77] published the first works on the synthesis of magnetic cobalt nanoparticles (Co-NPs) by thermal decomposition of dicobalt octacarbonyl, $Co_2(CO)_8$. The Co-NPs were prepared in toluene dispersions in the presence of polymer dispersants, such as methyl methacrylate-ethylacrylate-vinylpyrrolidone terpolymers, high-purity polystyrene, styrene-acrylonitrile polymers, polyacrylonitril, chloropolyethylene sulfonamide, polyester, and polyether urethanes to from stable colloids of discrete particles which were separated by polymer coatings. The particle diameter and stability of the Co-NPs depended on a balance between the ligand and precursor concentrations, temperature, polymer molecular weight and solvent, to achieve a uniform size of Co-NPs in the 1-100 nm range [77].

Papirer et al. [78,79] described the preparation of spherical cobalt nanoparticles as a ferrofluid by thermal decomposition at 110 ºC of $Co_2(CO)_8$ in an aromatic solvent in the presence of an alkyl sulfonate surfactant. The diameter of the particles was determined by small-angle-X-ray scattering and magnetic methods to an average diameter of 7 nm. The intermediate formation of $Co_4(CO)_{12}$ was detected [78].

Suslick et al. prepared amorphous Fe-NPs [80,81], FeCo alloy-NPs [82] and Mo_2C-NPs [82,83] using sonochemistry techniques. The volatile metal carbonyl precursors $Fe(CO)_5$, $Mo(CO)_6$, $[Co(CO)_3(NO)]$, were dissolved in a dry high-boiling solvent (decane or hexadecane) at 0-90 ºC and irradiated for 1-3 hours under argon. The sonochemically produced amorphous Fe-NPs were ten times more reactive per gram in the the Fischer-Tropsch conversion of carbon monoxide and hydrogen to low-molecular-weight alkanes at very low temperatures (200 ºC) than crystalline iron powder (5 μm diameter). At 250 ºC, the activity for cyclohexane dehydrogenation (to benzene) and hydrogenolysis (predominantly to methane) was over 30 times higher for the sonochemically produced amorphous Fe-NPs relative to crystalline iron [80].

The formation of magnetic $CoPt_3$ Co_{core}-Pt_{shell} nanoparticles was reported by Cheon and co-workers through redox transmetalation of the reactants $Co_2(CO)_8$ and $Pt(hfac)_2$ (hfac = hexafluoroacetylacetonate), without the presence of external reductants. The composition of the nanoparticles could be tuned by adjusting the ratio of the reactants [84].

Lee and coworkers reported the synthesis of iron, chromium, molybdenum and tungsten metal clusters by laser decomposition of the respective metal carbonyls. The reaction was carried out using a 10.6 μm CO_2 laser in the presence of Ar and SF_6 [85]. The metal clusters of Fe, Cr, Mo, and W showed an average particle diameter of 6, 3.5, 2 and ~1 nm, respectively, with narrow distribution. The presence of argon helped to increase the purity of the metal clusters by avoiding the formation of higher nuclearity metal carbonyls. SF_6 acted as infrared (IR) photosensitizer, which absorbed the 10.6 μm IR photons from the CO_2 laser and transferred the energy to a metal carbonyl via collisions. The metal clusters were formed in the body centered cubic (bcc) lattice for Fe and Cr, face centered cubic (fcc) for Mo, and in an amorphous structure in the case of W (all these bulk metals have bcc structure). Considering the cluster atom count (9630, 1870, 230 and ~30 for Fe, Cr, Mo and W clusters, respectively) which was estimated from their average diameters, it is likely that there exists a structural transition from fcc to bulk bcc with increasing cluster size in these M-NPs [85].

Sun et al. prepared monodispersed iron-platinum (FePt) nanoparticles by thermal decomposition of $Fe(CO)_5$ at high temperatures and the reduction of $Pt(acac)_2$ (acac = acetyl acetonate) by using a long-chain 1,2-hexadecanediol. Both reactions were initiated together in the presence of oleic acid and oleylamine, to provide a controlled route to monodisperse FePt-NPs [86]. Further investigations showed that the controlled variation of the precursors $Fe(CO)_5$ and $Pt(acac)_2$ can be adjusted to obtain ferromagnetic FePt nanocrystal superlattices. Using dioctyl ether as solvent, a 3:2 molar ratio of $Fe(CO)_5$ to $Pt(acac)_2$ gave $Fe_{48}Pt_{52}$ particles, a 2:1 molar ratio yielded $Fe_{52}Pt_{48}$ and a molar ratio of 4:1 gave $Fe_{70}Pt_{30}$ particles. The FePt diameter could be tuned from 3 to 10 nm. Monodisperse FePt nanoparticles were of an average diameter of 3 nm and the consecutive addition of more reagents could enlarge the existing seeds to the desired particle size [86].

Puntes et al. reported a pyrolysis method for the synthesis of monodisperse, stabilized and defect-free ε-Co nanoparticles. The magnetic colloids (Co-NPs) were synthesized by the rapid pyrolysis of $Co_2(CO)_8$ under inert (Ar) atmosphere to give narrow diameter distributions (3-17 nm) of Co-NPs controlled by the concentration of the organic surfactants mixture (oleic acid, lauric acid, trioctylphosponic acid and oxide, pyridine, etc) [87].

Weller et al. synthesized $CoPt_3$ nanocrystals by reduction of $Pt(acac)_2$ and thermodecomposition of $Co_2(CO)_8$ in the presence of 1-adamantanecarboxylic acid to produce $CoPt_3$ nanoparticles. The

mean particle diameter could be varied from 1.5 to 7.2 nm by the reaction conditions and the type of coordinating mixture. As-synthesized $CoPt_3$ particles represented single crystal domains and had a chemically disordered face-centered cubic (fcc) structure [88].

Rutnakornpituk and coworkers [89] reported superparamagnetic Co-NPs from $Co_2(CO)_8$ in toluene via thermal decomposition in the presence of poly(dimethysiloxane) (PDMS) as carrier fluid and poly[dimethylsiloxane-b-(3-cyanopropyl)methylsiloxane-b-dimethylsiloxane] (PDMS-PCPMS-PDMS) triblock copolymers as steric stabilizers. These copolymers formed micelles and acted as "nanoreactors" for the thermal decomposition of the metal carbonyl. The nitrile groups on the PCPMS central blocks were thought to adsorb onto the particle surface, while the PDMS end blocks protrude into the reaction medium to provide steric stability. The particle diameter could be controlled by adjusting the cobalt to copolymer ratio and non-aggregated cobalt nanoparticles are observed in TEM.

Bönnemann et al. prepared cobalt, iron and iron-cobalt nanoparticles via thermal decomposition in the presence of aluminium alkyls (AlR_3), as air-stable magnetic metal nanoparticles. Once the metal carbonyls, $Co_2(CO)_8$, $Fe(CO)_5$ or $Co_2(CO)_8/Fe(CO)_5$, were decomposed the nanoparticle-AlR_3 dispersions were treated with synthetic air through a thin capillary (giving smooth oxidation to an Al_2O_3 shell around the M-NP core) to yield magnetic particles stable in air under ambient conditions for over a year, as confirmed by magnetic measurements [90,91].

Yang et al. [92] synthesized magnetic nanoparticles and carbon nanotube (CNT) core–shell nanostructures, such as CoO/CNTs and Mn_3O_4/CNTs, by the non-aqueous solvothermal treatment of the corresponding metal carbonyls on CNT templates using hexane as solvent at 200 ºC in an autoclave. The hydrophobic interaction between nanoparticles and CNTs in hexane played the critical role for the formation of CNT-based core-shell nanostructures. Moreover, the CoO/CNT core-shell nanostructures showed weak ferromagnetic performance at 300 K due to the ferromagnetic Co clusters and the uncompensated surface spin states, while the Mn_3O_4/CNT core–shell nanostructures displayed an apparent transition from paramagnetic to ferromagnetic behavior with decreasing temperature.

The above examples together with the several reviews published in the last years [5,6,42,43,75,93,94] show that magnetic nanoparticles from iron or cobalt were early on investigated for application in electronics, medicine or industry, but also due to the commercial availability of $Fe(CO)_5$ or $Co_2(CO)_8$. By now, M-NPs based on metal carbonyl precursors appear studied more for catalytic uses.

Hyeon and coworkers [95] used cobalt nanoparticles for the catalysis in the inter- and intra-molecular Pauson-Khand (alkyne+alkene or enyne) reactions for the synthesis of cyclopentenone

derivates. The Co-NPs were prepared from $Co_2(CO)_8$ in dioctyl ether together with oleic acid and trioctylphosphine. A transmission electron microscopic (TEM) image confirmed that the particles were well separated and that they are nearly monodisperse, having a mean diameter of 8 nm. The colloidal cobalt showed a high catalytic activity for the intramolecular reaction of an enyne, achieving a yield of 97% at 130 ºC at a CO pressure of 5 atm in comparison with normal heterogeneous cobalt catalysts supported on silica or charcoal [95].

Landau et al. [96] deposited nickel nanoparticles on multiwall carbon nanotubes (MWCNTs) by sonochemical decomposition of a solution of $Ni(CO)_4$ in decaline. Ni/MWCNT composites contained 25 and 51 wt% nickel, showed good dispersion and uniformity of size distribution of Ni-NPs at high loadings, together with enhanced catalytic activity in the selective carbonyl group hydrogenation of chloroacetophenone by factors of 2–18, compared with non-sonochemical decoration methods.

Zachariach et al. [97] generated iron and nickel nanoparticles for the simultaneous catalytic ignition of toluene in an aerosol reactor. Fe- and Ni-NPs were generated by gas-phase pyrolysis of $Ni(CO)_4$ and $Fe(CO)_5$, respectively. In comparison to non-catalytic homogeneous ignition, the addition of metal NPs lowered the ignition temperature of toluene by as much as 150 ºC. Iron was found to be a more active than nickel. Inspection of the catalyst indicated sintering at relatively low temperatures presumably as a result of the exothermic reaction on the particle surface. A turnover frequency of 80 s^{-1} implied a greater catalyst efficiency than commonly found for substrate-stabilized catalysts. Electron microscopic analysis shows that the Fe NPs undergo structural transformation (oxidation and sintering), which is likely initiated by the rapid heat release from the Fe NP oxidation process. A similar oxidation process was also observed for Ni catalysts [97].

Chamberlain, Khlobystov, Bourne et al. reported the encapsulation of metal nanoparticles into single walled carbon nanotubes (SWNT) [98,99]. Metal nanoparticles from tungsten, rhenium and osmium were inserted into single walled carbon nanotubes (SWNT) by decomposition of the corresponding metal carbonyls under heat treatment or electron beam irradiation. The nanotube host acted as an efficient template, controlling the growth of M-NPs to ~1 nm in diameter. As a result, the M-NPs stayed largely spheroidal in shape and were uniformly distributed throughout the entire length of the SWNT. The released carbon monoxide (CO) gas creates pockets of high pressure between nanoparticles, thus, preventing their collision and coalescence into larger structures. Despite their extremely small size (30–90 atoms on average) and unprotected surface, the metallic nanoparticles encapsulated in nanotubes were very stable under ambient conditions and even at elevated temperatures [98]. Ru-NPs were also deposited on SWNT (~1-2 nm diameter) in the gas phase using the volatile $Ru_3(CO)_{12}$ precursor. Thermal decomposition of $Ru_3(CO)_{12}$ generated Ru-

NPs size-controlled by the nanotube diameter. TEM showed very small Ru-NPs with a narrow diameter distribution (0.92 ±0.13 nm). The Ru@SWNT nanoparticles were also tested as catalyst for hydrogenation reactions. The extreme spatial confinement of the Ru@SWNT catalyst yielded a lower TOF for the reduction of cyclic alkenes in comparison to a Ru/C catalyst, but no drop in activity or change in structure of the Ru-NPs embedded in SWNT were observed over 24 hours at 110 ºC [99].

Fu *et al.* reported the synthesis of cobalt phosphide (Co_2P) nanoparticles for photocalatytic hydrogen evolution in a system with CdS nanorods as photosensitizer and DL-mandelic acid as electron donor [100,101]. Co_2P nanoparticles were synthesized by thermal decomposition of $Co_2(CO)_8$ in 1,2-dichlorobenzene in the presence of tri-n-octylphosphine oxide (TOPO) and oleic acid. The system demonstrated an H_2 production rate of up to 19 373 mmol g^{-1} h^{-1} after 10 h LED light ($\lambda > 420$ nm) irradiation. Mandelic acid was oxidized to benzoylformic acid by the holes formed in CdS [100].

3.2. Synthesis in ionic liquids

The formation of M-NPs from metal carbonyls in the ILs can be achieved under inert gas atmosphere by conventional thermal decomposition (at ~180-250 ºC for 6-12 h), by UV-photolysis (e.g. with a 1000 W mercury lamp for 15 min) or by rapid (3-15 min) and energy saving (10-150 W) microwave irradiation (MWI) without the presence of any stabilizer or capping ligand (**Figure 6, Figure 7**, **Table 2.**).

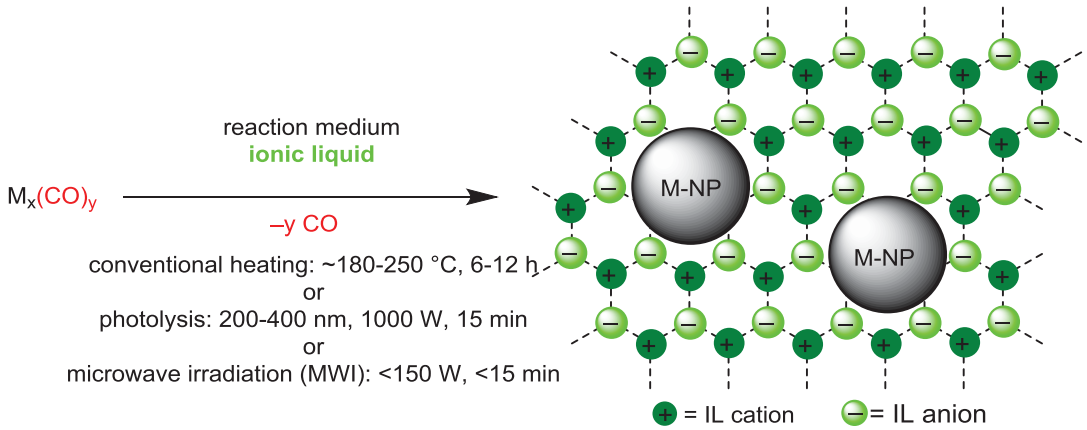

Figure 6. Synthesis and stabilization of metal nanoparticles from metal carbonyl precursors in ionic liquids.

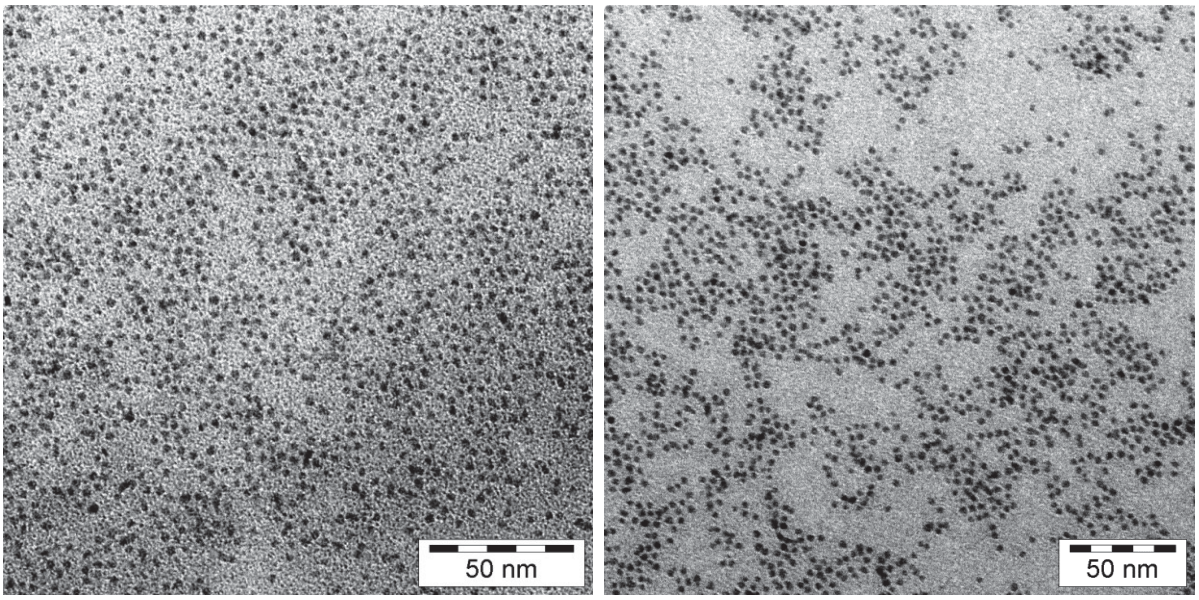

a b

Figure 7. Examples of TEM images of metal nanoparticles obtained from metal carbonyl precursors in ionic liquids. (a) Os-NPs from $Os_3(CO)_{12}$by MWI in $[C_4mim][BF_4]$, Ø 2.5 ± 0.4 nm; (b) Ru-NPs from $Ru_3(CO)_{12}$ by photolysis in $[C_4mim][BF_4]$, Ø 2.0 ± 0.5 nm. Reprinted from ref. [42] with permission from the author.

Table 2. Examples of metal nanoparticles formed from metal carbonyl precursors in ionic liquids.

Metal	Metal carbonyl precursor	Ionic liquid [a]	M-NP average diameter ± standard deviation (nm)	Remarks	Ref.
Cr	$Cr(CO)_6$	$[C_4mim][BF_4]$, $[C_4mim][CF_3SO_3]$, $[C_4mim][N(Tf)_2]$	≤ 1.5 ± 0.3, MWI, thermal;[b] 4.4 ± 1.0, hν[b]	[c, d, e, f]	[55, 111]
	$Cr(CO)_6$	$[C_2mim]Cl$	3.6 ± 0.7 nm, MWI, 2.3 ± 0.4 nm, thermal	catalyst for glucose to HMF conversion, see Figure 17	[102]
Mo	$Mo(CO)_6$	$[C_4mim][BF_4]$, $[C_4mim][CF_3SO_3]$, $[C_4mim][N(Tf)_2]$	~1 – 2, MWI, hν;[b] ≤ 1.5 ± 0.3, thermal[b]	[c, d, e, f]	[55, 111]
W	$W(CO)_6$	$[C_4mim][BF_4]$, $[C_4mim][CF_3SO_3]$, $[C_4mim][N(Tf)_2]$	3.1 ± 0.8, MWI;[b] < 1, hν;[b] ≤ 1.5 ± 0.3, thermal[b]	[c, d, e, f] see Figure 8, Figure 9	[55, 111]
Mn	Mn_2CO_{10}	$[C_4mim][BF_4]$	12.4 ± 3, MWI; < 1, hν 28.6 ± 11.5, MWI	[b, c, d] see Figure 8	[55, 103]
	Mn_2CO_{10}	$[CEmim][BF_4]$ [g]	4.3 ± 1.0, MWI		[103]
Re	Re_2CO_{10}	$[C_4mim][BF_4]$	2.4 ± 0.9, MWI; < 1, hν	[c, d, e]	[55]
Fe	$Fe_2(CO)_9$	$[C_4mim][BF_4]$	8.6 ± 3.2, MWI;[b] 7.0 ± 3.1, hν;[b] 5.2 ± 1.6, thermal[b]	[c, d, e, f]	[36, 55]
	$Fe_2(CO)_9$	$[C_4mim][BF_4]$	thermal	cyclohexenone hydrogenat. cat., see	[104]

				Figure 16	
Ru	$Ru_3(CO)_{12}$	$[C_4mim][BF_4]$	1.6 ± 0.3, MWI;[b] 2.0 ± 0.5, h*v*;[b] 1.6 ± 0.4, thermal[b]	[c, d, e, f]; see Figure 7, hydrogenation cat., Figure 13	[36, 55]
	$Ru_3(CO)_{12}$	$[C_4mim][BF_4]$	2.2 ± 0.4, MWI	Ru-NPs deposited on TRGO, see text, Figure 11, Figure 14	[105]
	$Ru_3(CO)_{12}$	$[C_4mim][PF_6]$	2.9 ± 0.8, thermal	cyclohexenone hydrogenat. cat., see Figure 16	[104]
Os	$Os_3(CO)_{12}$	$[C_4mim][BF_4]$	0.7 ± 0.2, MWI;[b] 2.0 ± 1.0, h*v*;[b] 2.5 ± 0.4, thermal[b]	[c, d, e, f] see Figure 7	[36, 55]
Co	$Co_2(CO)_8$	$[C_4mim][BF_4]$, $[C_4mim][CF_3SO_3]$, $[C_4mim][N(Tf)_2]$	5.1 ± 0.9, MWI;[b] 8.1 ± 2.5, h*v*;[b] 14 ± 8, thermal[b]	[c, d, e, f]	[36, 55]
	$Co_2(CO)_8$	$[CEmim][BF_4]$[g]	1.6 ± 0.3, MWI		[103]
	$Co_2(CO)_8$	$[C_4mim][N(Tf)_2]$ $[C_{10}mim][BF_4]$	7.7, thermal at 150 °C	Fischer-Tropsch catalyst giving olefins, oxygenates, and paraffins (C_7-C_{30}), reusable at least three times	[106]
	$Co_2(CO)_8$	$[C_{10}mim][N(Tf)_2]$	53 ± 22, thermal at 150 °C	Co-NPs with cubic shape together with Co-NPs of irregular shape	[107]
	$Co_2(CO)_8$	$[N_{1888}][N(Tf)_2]$, $[C_4mPyr][N(Tf)_2]$, $[C_4mim][PF_6]$, $[C_4mim][N(Tf)_2]$, $[C_4mim][BF_4]$	5.8 ± 0.9 to 16 ± 3 3.6 ± 0.7 to 21 ± 6 6 ± 1 to 7 ± 1 11 ± 3 4 ± 2	magnetic fluids, particle size varies with concentration	[108]
Rh	$Rh_6(CO)_{16}$	$[C_4mim][BF_4]$, $[C_4mim][CF_3SO_3]$, $[C_4mim][N(Tf)_2]$	1.7 ± 0.3, MWI;[b] 1.9 ± 0.3, h*v*;[b] 3.5 ± 0.8, thermal[b]	[c, d, e, f]; see Figure 9; hydrogenation cat., see Figure 13	[36, 55]
	$Rh_6(CO)_{16}$	$[C_4mim][BF_4]$	2.8 ± 0.5	Rh-NPs deposited on TRGO, see text, Figure 11; hydrogenation cat., Figure 14	[105]
	$Rh_6(CO)_{16}$	$[C_4mim][BF_4]$	2.1 ± 0.5	Rh-NPs deposited on Teflon-coated stirring bar, see text, Figure 12; hydrogenation cat., see Figure 15.	[109]
Ir	$Ir_4(CO)_{12}$	$[C_4mim][BF_4]$, $[C_4mim][CF_3SO_3]$, $[C_4mim][N(Tf)_2]$	0.8 ± 0.2, MWI;[b] 1.4 ± 0.3, h*v*;[b] 1.1 ± 0.2, thermal[b]	[c, d, e, f]; hydrogenation catalyst, see Figure 13	[36, 55]
	$Ir_4(CO)_{12}$	$[C_4mim][BF_4]$,	2.7 ± 0.7 nm	Ir-NPs deposited on TRGO, see text; hydrogenation cat., see Figure 14	[144]
FeRu 1:1	$Fe_2(CO)_9$, $Ru_3(CO)_{12}$	$[C_4mim][PF_6]$ $[C_4mim][BF_4]$	1.7 ± 0.3, thermal	cyclohexenone hydrogenat. cat., see Figure 16	[104]

[a] For selected IL cations and anions see Figure 3; [b] in $[C_4mim][BF_4]$;[c] median diameters and standard deviations are from TEM measurements; [e] photolytic decomposition of metal carbonyls

with a 1000 W Hg lamp (200-450 nm wavelength) for 15 min; [f] thermal decomposition of metal carbonyls for 6-12 h at 180-230 °C depending on the metal carbonyl. [g] [CEmim] = 1-(3-carboxyethyl)-3-methyl-imidazolium.

The complete decomposition of metal carbonyls under microwave irradiation occurs in a rapid and short time (3-10 min) and can be verified by vibrational spectroscopy through absence of the (metal-)carbonyl bands between 1750 and 2000 cm^{-1} after microwave heating (**Figure 8**) [42, 55].

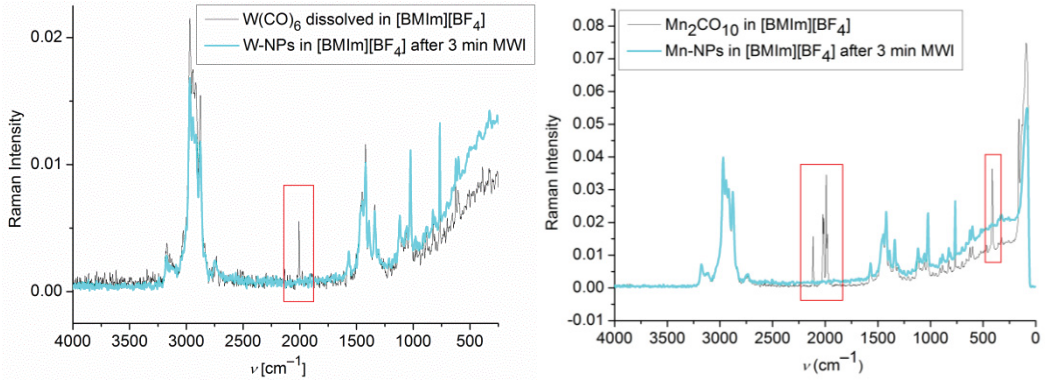

Figure 8. Raman spectra of $W(CO)_6$ and $Mn_2(CO)_{10}$ in $[C_4mim][BF_4]$ before and after microwave irradiation (MWI for 3min at 10 W). Red boxes highlight the characteristic carbonyl and metal carbonyl bands. $[BMIm]^+ = [C_4mim]^+$. Reprinted from references [42, 55] with permission from the author; © 2011 Elsevier B.V.

Tungsten and rhodium nanoparticles from the corresponding metal carbonyls $W(CO)_6$ and $Rh_6(CO)_{16}$ illustrated the importance of the IL anion for stabilization by showing an increase in their diameter with the molecular volume of the ionic liquid anion (**Figure 9**) [110,111,112].

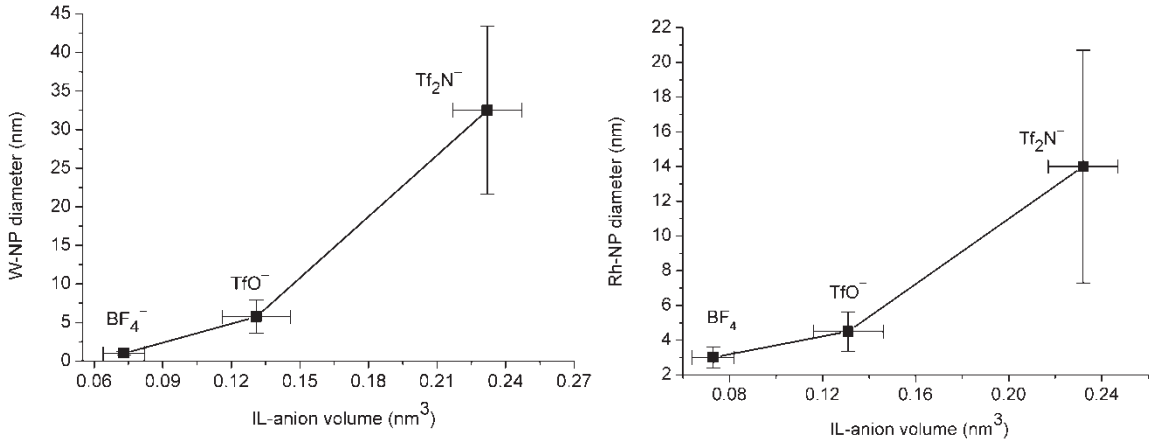

Figure 9. Correlation between the molecular volume of the ionic liquid anion and the observed W (left) and Rh (right) nanoparticle diameter with standard deviations as error bars [110, 111]. Adapted from ref. [42] with permission from the author; © 2011 Elsevier B. V.

3.3. Synthesis in ILs with deposition on support

Ionic liquids prevent agglomeration by forming a protective layer (shell) around the particles (core). Also immobilization or deposition of nanoparticles on supports such as graphene [105,109,113,114], carbon nanotubes [115,116] or more often Al_2O_3 [117] is a means to prevent agglomeration. Furthermore, when nanoparticles are used as catalysts biphasic (liquid-liquid) homogeneous-catalytic systems [24] often exhibit leaching of metal ions to the products, making their separation and purification process economically and environmentally more complicated. To avoid these problems, the research and development of new quasi-homogeneous supported nanoparticle catalyst systems is an issue [118,119].

Carbon-based support materials such as graphene [120,121] or carbon nanotubes [122,123,124] have become substrates for the deposition of metal nanoparticles. Thermally reduced graphite oxide (TRGO) [125,126,127,128,129,130,131] now also simply called "graphene", has been long known [121,132] and is lately re-discovered as an extremely versatile carbon material [120,121,133]. TRGO can be prepared in bulk quantities from graphite by oxidation with $KMnO_4$ and $NaNO_3$ in concentrated sulfuric acid (so-called graphite oxidation process of Hummers and Offeman) [132]. This oxidation incorporates functional oxygen-containing groups moieties into the graphite structure and yields the even older material graphite oxide [134]. When GO is subjected to rapid heating above 400 °C the functional groups decompose into CO and CO_2 gas which exfoliates the layered GO structure into functionalized graphene sheets [135]. This thermal reduction of graphite oxide lends its name to the product (TRGO). By adjusting the reduction temperature, the degree of functionalization can be controlled. At a lower reduction temperature, more oxygen atoms remain

on the TRGO surface and thereby increase the degree of functionalization. This degree of functionalization influences on the dispersibility of TRGO in polar solvents [136] and its use as a support material for metal nanoparticles. A higher degree of functionalization improves the dispersibility, *e.g.*, in water or acetone. Therefore, it can be expected that a TRGO-material with a high degree of functionalization has a good interaction with metal particles. The functional oxygen-containing (epoxy, aldehyde, hydroxyl, carboxyl) groups still present in TRGO are an important aspect for the utilization of this material in the field of heterogeneous catalysis [133]. Surface functionalization and the high specific surface area of TRGOs of 400 $m^2\ g^{-1}$ up to 1500 $m^2\ g^{-1}$, make them promising support materials for catalytic applications [131,133]. Examples for metal-nanoparticles on carbon materials can be found in ref. [137142,143,144,145].

For the synthesis of M-NPs on TRGO, the IL not only acts as kinetic stabilizing template in the metal nanoparticle formation process, the IL also helps to exfoliate and separate the TRGO-"graphene" sheets in order to increase the surface area and accessibility for deposition of M-NPs.

Ruthenium, rhodium or iridium nanoparticles can be supported on TRGO by decomposition through microwave irradiation of their corresponding metal carbonyl, $Ru_3(CO)_{12}$, $Rh_6(CO)_{16}$ and $Ir_4(CO)_{12}$ respectively, in an ionic liquid, e.g. $[C_4mim][BF_4]$ with small and narrow nanoparticle distribution (Ru 2.2 ± 0.4 nm, Rh 2.8 ± 0.5 nm and Ir 2.7 ± 0.7 nm) (**Figure 10** and **Figure 11**) [105,144].

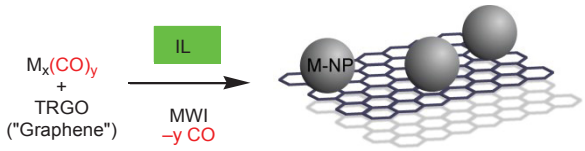

Figure 10. Schematic synthesis of transition metal nanoparticles supported on the thermally reduced graphite oxide through microwave or electron beam irradiation [105,144].

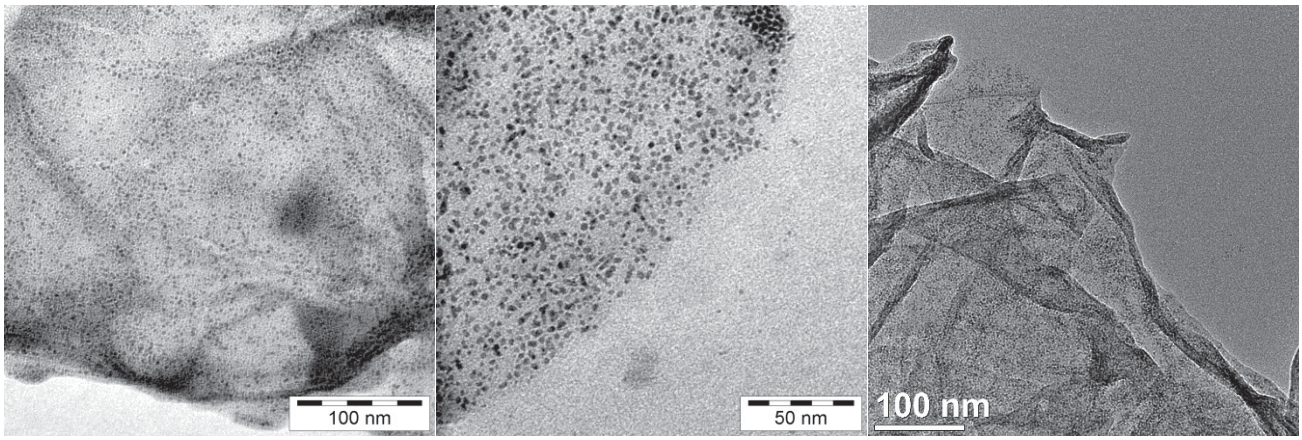

Figure 11. TEM images of Ru-NPs (left), Rh-NPs (middle) and in high resolution (HR) a single Ru-NP (encircled) (right) supported on thermally reduced graphite oxide obtained upon decomposition of $Ru_3(CO)_{12}$, $Rh_6(CO)_{16}$ and $Ir_4(CO)_{12}$, respectively, by means of microwave irradiation in $[C_4mim][BF_4]$ [105]. Left and middle image reprinted from ref. [105], right image from ref. [144] with permission from the author; © 2010, 2015 Elsevier Ltd.

An example for M-NPs on a non-carbon support was reported with the deposition of Rhodium nanoparticles onto a standard Teflon-coated magnetic stirring bar which was present during microwave decomposition of $Rh_6(CO)_{16}$ in $[C_4mim][BF_4]$ **(Figure 12**). The metal nanoparticle deposits could not be removed from the Teflon surface by simple washing with organic solvents. The Rh-NP/stirring bar deposits were barely visible with the naked eye and amounted to 32 µg or less Rh metal with average diameter 2.1 ± 0.5 nm on a 20 × 6 mm magnetic stirring bar [109].

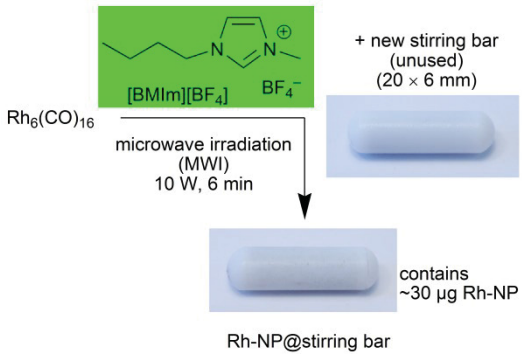

Figure 12. Rh-NP deposition on a Teflon-coated magnetic stirring bar from an IL dispersion [109]. Reprinted in part from ref. [109] with permission from the author; © 2010 Elsevier Ltd.

4. Catalytic applications of metal nanoparticles from metal carbonyls in ILs.

The absence of a strongly coordinating ligand layer around the metal nanoparticles in ionic liquids could represent an advantage in terms of catalytic application, because the shielding of the reactive metal surface towards the reaction substrates is drastically reduced. The ionic liquid network contains only weekly coordinating cations and anions, which should bind less strongly to the metal surface, and, hence, should be less deactivating, than commonly employed capping or protective ligands (cf. Figure 2). In this context the system of metal nanoparticles and ionic liquids are sometimes referred to as a *green catalytic system* because it can avoid the use of organic solvents. ILs are interesting in the context of green catalysis [146] which requires that catalysts be designed for easy product separation from the reaction products and multi-time efficient reuse/ recycling

[27,147,148]. The very low vapor pressure of the ILs and the designable low solubility of organic substrates in ILs help for the separation of the products by distillation or removal in vacuum or by biphasic liquid-liquid separation.

Metal nanoparticles, which are stabilized on the ILs network, were shown to be recyclable and reusable catalysts, because the IL is able to retain and stabilize the M-NPs in its network [37]. The use of M-NPs/ILs dispersions (with M-NPs from non-metal-carbonyl sources) as catalyst systems for many catalytic reactions were already reviewed [13,14,149]. The higher high surface area with decreasing diameter of M-NPs provides a larger number of active sites, which generally increases the catalytic activity [13,15,149,150,151]. Generally, the catalytic properties (activity and selectivity) of dispersed M-NPs indicate that they possess pronounced surface-like (multi-site) rather than single-site-like character [150,151].

Generally, iron [104], ruthenium [104], chromium [102], palladium [152] or iridium [19] nanoparticles were used for diverse catalytic reactions in organic chemistry such as hydrogenation [16,18,19,104], hydroformylation [18] and cross-coupling [16,152], in multiphase conditions [17,18] and in energy-related processes such as biomass refinement [102].

Superparamagnetic cobalt nanoparticles (Co-NPs) from $Co_2(CO)_8$ in ionic liquids, e.g., 1-alkyl-3-methylimidazolium-$[N(Tf)_2]$-ILs, with a particle diameter between 5-8 nm were catalysts for Fischer-Tropsch synthesis. The reaction of syngas was carried out at 20 atm of H_2/CO(2:1) at 210 ºC for 100 h and led mainly to hydrocarbons (Diesel-like products, C_7-C_{30} paraffins) and could be reused at least three times if they were not exposed to air [106,107].

Stable dispersions of Ru-, Rh- and Ir-NPs/$[C_4mim][BF_4]$ obtained by microwave irradiation from their metal carbonyls were tested as catalyst for the biphasic hydrogenation of benzene or cyclohexene to cyclohexane under organic solvent-free conditions (**Figure 13**) [42,55,111].

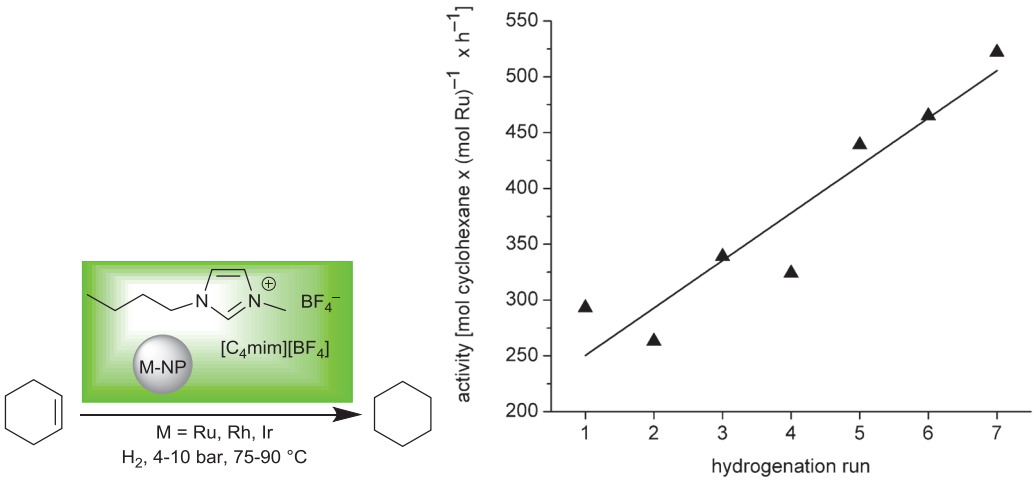

Figure 13. Schematic hydrogenation reaction of cyclohexene to cyclohexane with Ru-, Rh- and Ir-NPs/IL dispersions (from metal carbonyls, see above) without use of an organic solvent besides IL and substrate [42,55,111]. The activity or turnover frequency (TOF) as (mol cyclohexane × (mol Ru)$^{-1}$ × h^{-1} increases with the hydrogenation run (re-use) for the Ru-NPs/IL catalyst. The hydrogenation reaction with Ru was run at 90 °C and 10 bar H_2 to 95% conversion where the reaction was intentionally stopped as thereafter the decrease in cyclohexene concentration lowered the reaction rate [55]. It was suggested that this activity rise with each recycle could be due to surface restructuring and/or the formation of active Ru-*N*-heterocyclic carbene (NHC) [153] surface species. If the rate of restructuring or NHC-Ru formation reactions is slow then the continuous formation of defects, edges, corners, or steps on the surface, which are known to be more active sites [154], will gradually increase the catalytic activity even after seven runs [55]. Rh/[C_4mim][BF_4] catalyst yielded an activity of 400 mol product × (mol Rh)$^{-1}$ × h^{-1} with quantitative conversion at 75 °C, 4 bar H_2 pressure and 2.5 h reaction time. With the homologous Ir/[C_4mim][BF_4] catalyst even higher activities up to 1,900 mol cyclohexane × (mol Ir)$^{-1}$ × h^{-1} could be obtained under the same conditions due to a shorter reaction time of 1 h for near quantitative conversion [55].

The composite nanomaterials of Ru-NP/TRGO, Rh- NP/TRGO and Ir- NP/TRGO (obtained from metal carbonyls in ILs, see above) were catalytically active for the hydrogenation of cyclohexene or benzene with complete conversion to cyclohexane under organic-solvent-free and mild conditions (50-100ºC, 4-10 bar H_2) (**Figure 14**) [105,144]. For the Ir/TRGO composites, the activity was largely increasing during the first runs, which was explained by an initially still present CO coverage of active sites [144].

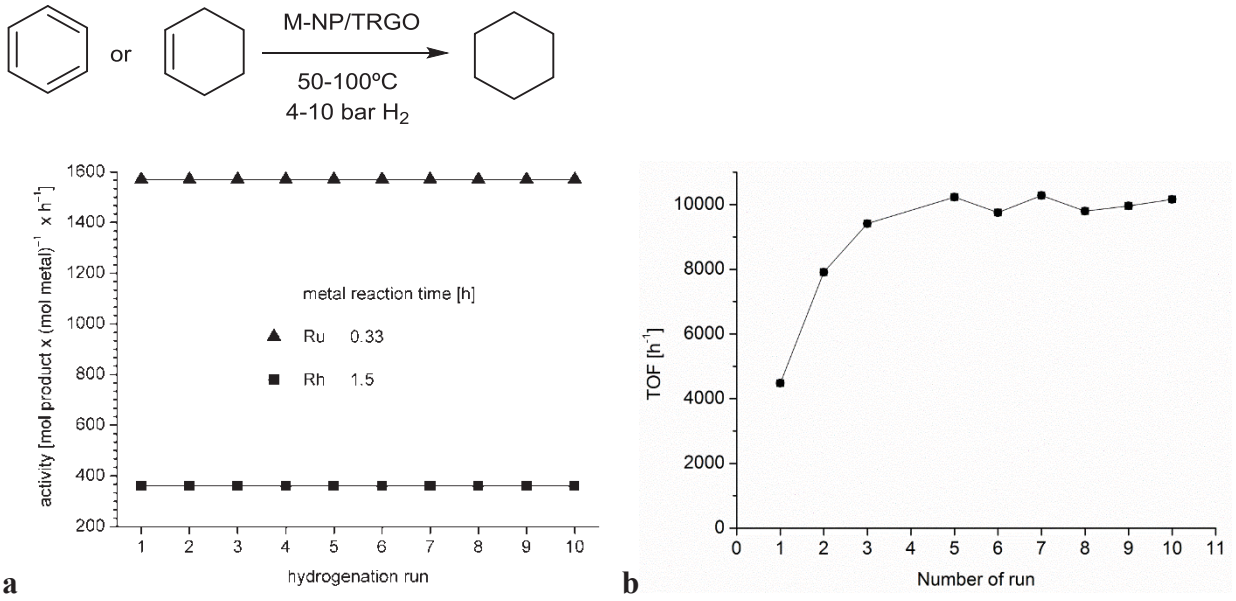

Figure 14. Schematic hydrogenation reaction of benzene or cyclohexene to cyclohexane with Ru-, Rh- or Ir-NP/TRGO under organic-solvent-free conditions.

a: The constant activities for cyclohexene hydrogenation over 10 consecutive runs were achieved at 4 bar H_2 and 75 C with 0.01 mol cyclohexene, 1.89×10^{-5} mol Ru (molar substrate to metal ratio 530) or 1.82×10^{-5} mol Rh (molar ratio 550) (11 mg M-NP/TRGO with 17.4 wt% Ru or 17.0 wt% Rh, respectively) [105]. Reprinted from ref. [105] with permission from the author; © 2010 Elsevier Ltd.

b: The increasing activity as TOF (= mol cyclohexane x $(\text{mol Ir})^{-1}$ x h^{-1}) for the hydrogenation of benzene by Ir/TRGO was monitored at 100 °C, 10 bars of H_2 with 4.49 mmol benzene, 1×10^{-3} mmol Ir (molar benzene to Ir ratio 4,490) (5.32 mg Ir/TRGO with 3.6 % Ir) [144]. Reprinted from ref. [144] with permission from the author; © 2010 Elsevier Ltd.

In addition, the Rh-NP/stirring bar could act as an easy to handle and re-usable catalyst in the organic-solvent-free hydrogenation reaction of cyclohexene with quantitative conversion and very high turnover frequencies of up to 32,800 mol cyclohexene × $(\text{mol Rh})^{-1}$ × h^{-1} (**Figure 15**) [109].

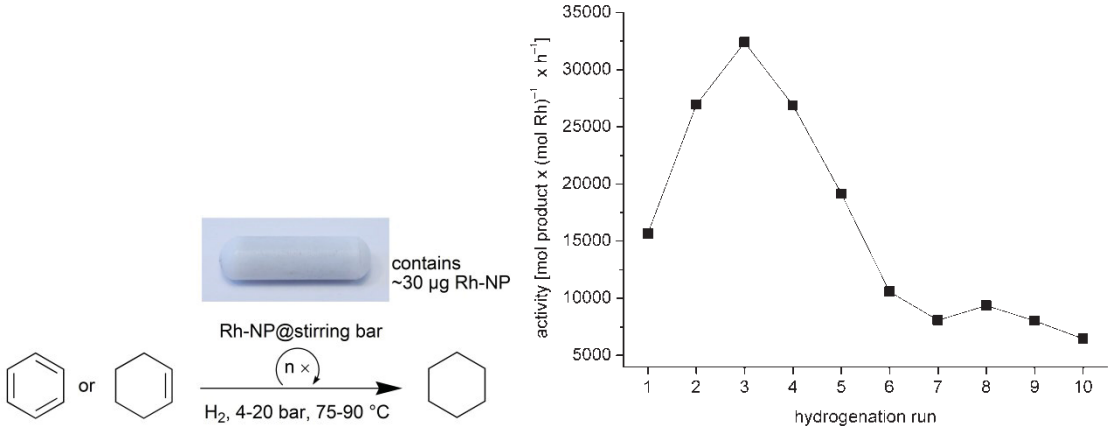

Figure 15. Schematic benzene or cyclohexene hydrogenation by Rh-NPs deposited on a Teflon-coated magnetic stirring bar and the activity plot over 10 consecutive runs for cyclohexene hydrogenation (conditions 6.8 mmol cyclohexene, 3.1×10^{-7} mol Rh, molar ratio ~22,000; 75 °C, 4 bar H_2) [109]. Reprinted in part from ref. [109] with permission from the author; © 2010 Elsevier Ltd.

Comparative activity data for related M-NP catalysts in cyclohexene and benzene hydrogenation reactions was given in the aforementioned articles [42,55,105, 109,111,144,145].

Fe-, Ru- and bimetallic Fe-Ru-NPs were tested as catalysts in $[C_4mim][BF_4]$ and $[C_4mim][PF_6]$ for the hydrogenation of cyclohexenone to mostly cyclohexanone and partly cyclohexanol at 50 °C (**Fig. 16**). The bimetallic FeRu (1 : 1) alloy was most active followed by the pure Ru-NPs. Addition of CO_2 to the IL reaction mixture increased the reaction rate up to four times faster with 60 bar of CO_2 than without. At 60 bar of CO_2 a high selectivity >95 % to cyclohexanone, at a TOF of *ca.* 300 h^{-1}, was achieved and the catalyst could be reused 5 times without noticeable deactivation [104].

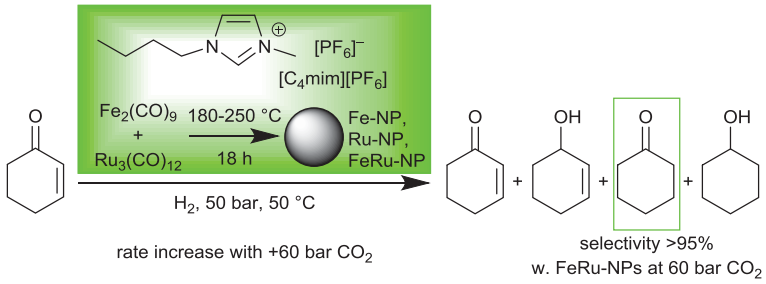

Figure 16. Cyclohexenone hydrogenation to mostly cyclohexanone with Fe-, Ru- or FeRu-NPs obtained from (mixtures of) $Fe_2(CO)_9$ and $Ru_3(CO)_{12}$ in IL [104].

Cr-NP catalysts from $Cr(CO)_6$ could dehydrate glucose to 5-hydroxymethylfurfural (HMF) (**Fig. 17**) in the IL [EMIm]Cl at T = 120 °C. Mn-, Fe- or Co-NPs from their carbonyl complexes did not catalyze this conversion [102].

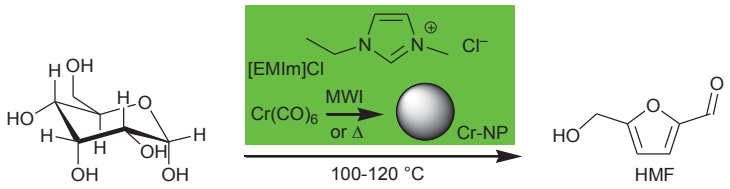

Figure 17. Conversion of glucose to 5-hydroxymethylfurfural (HMF) by Cr-NPs (obtained from $Cr(CO)_6$ in IL) [102].

5. Conclusions

Binary metal carbonyls are versatile and elegant precursors for the synthesis of a wide range of transition metal nanoparticles from group 6, 7, 8 and 9. No reducing agent is necessary and CO as the only byproduct can easily be removed with the gas phase. In ionic liquids there is no need for additional stabilizers, surfactants or capping ligands to kinetically stabilize the obtained metal nanoparticles. The supramolecular three-dimensional electrostatic and in part hydrogen-bonded network of the IL provides the needed electrostatic and steric stabilization of the metal nanoparticles and prevents for a certain time further agglomeration or aggregation. The synthesis of M-NPs from metal carbonyls in ILs can generally be carried out by thermal decomposition through conventional heating or through microwave irradiation or by photochemical decomposition. Microwave irradiation is an especially fast and easy method due to the high absorption efficiency of ILs for microwave energy due to their high ionic charge, high polarity and high dielectric constant. The synthesis of M-NPs from metal carbonyls in ILs can also be used for the *in situ* deposition of the metal nanoparticles on supports, such as thermally reduced graphite oxide (TRGO, "graphene") or polytetrafluoroethylene (Teflon). The M-NP dispersions, derived from metal carbonyls in ILs or on supports were active catalysts for Fischer-Tropsch reaction [106], hydrogenation [42,55,104,105,109,111,144], dehydration [102]. Hydrogenation reactions of cyclohexene or benzene with M-NP/IL dispersions or M-NP/support composites could be run under organic-solvent-free conditions and the catalysts could be re-used over several catalytic runs [105,144].

Acknowledgement

Much of our work on M-NP/IL systems was supported by the Deutsche Forschungsgemeinschaft (DFG) through grant Ja466/17-1. At present we thank the DFG for grant Ja466/31-1 within the priority project SPP 1708.

References

[1] Yu, S.-H., MacGillivray, L. R., Janiak, C., *CrystEngComm* **2012**, *14*, 7531-7534.

[2] Dahl, J.A., Maddux, B.L.S., Hutchison, J.E., *Chem. Rev.* **2007**, *107*, 2228-2269.

[3] Hervés, P., Pérez-Lorenzo, M., Liz-Marzán, L.M., Dzubiella, J., Lub, Y., Ballauff, M., *Chem. Soc. Rev.* **2012**, *41*, 5577–5587.

[4] Wildgoose, G.G., Banks, C.E., Compton, R.G., *Small* **2006**, *2*, 182-193.

[5] Lu, A. H., Salabas, E. L., Schüth, F., *Angew. Chem. Int. Ed*. **2007**, *46*, 1222-1244.

[6] Gedanken, A., *Ultrasonics Sonochemistry* **2004**, *11*, 47-55.

[7] Rao, C.N.R., Vivekchand, S.R.C., Biswas, K., Govindaraj, A., *Dalton Trans.* **2007**, 3728-3749.

[8] Mastai, Y., and Gedanken, A., in *Chemistry of Nanomaterials*, Vol. 1 (Eds.: C. N. R. Rao, A. Müller, A. K. Cheetham), Wiley-VCH, Weinheim, **2004**, pp. 113.

[9] Park, J., Joo, J., Kwon, S.G., Jang, Y., Hyeon, T., *Angew. Chem. Int. Ed*. **2007**, *46*, 4630-4660.

[10] An, K., Alayoglu, S., Ewers, T., Somorjai, G. A., *J. Colloid Interface Sci.* **2012**, *373*, 1-13.

[11] Peng, Z., and Yang, H., *Nano Today* 2009, **4**, 143-164.

[12] Kim, M., Phan, V.N., Lee, K., *CrystEngComm* **2012**, *14*, 7535-7548.

[13] Scholten, J. D., Leal, B. C., Dupont, J., *ACS Catal.* **2012**, *2*, 184-200.

[14] Yan, N., Xiao, C., Kou, Y., *Coord. Chem. Rev.* **2010**, *254*, 1179-1218.

[15] Pârvulescu, V. I., and Hardacre, C., *Chem. Rev.* **2007**, 107, 2615-2665.

[16] a) Welther, A., Jacobi von Wangelin, J., *Curr. Organic Chem.* **2013**, *17*, 326-335; b) Gieshoff, T.N., Welther, A., Kessler, M.T., Prechtl, M.H.G., Jacobi von Wangelin, A., *Chem. Commun.* **2014**, *50*, 2261-2264.

[17] Campbell, P.S., Prechtl, M.H.G., Santini, C.C., Haumesser, P.H., *Curr. Organic Chem.* **2013**, *17*, 414-429.

[18] Guerrero, M., Than-Chau, N. T., Noël, S., Denicourt-Nowicki, A., Hapiot, F., Roucoux, A., Monflier, E., Philippot, K., *Curr. Organic Chem.* **2013**, *17*, 364-399.

[19] Scholten, J.D., *Curr. Organic Chem.* **2013**, *17*, 348-363.

[20] Ostwald, W., *Phys. Chem.* **1901**, *37*, 385.

[21] Ostwald, W., in *Lehrbuch der Allgemeinen Chemie*, Vol. 2, Part 1. Leipzig, Germany, 1896.

[22] Goesmann, H., and C. Feldmann, *Angew. Chem.* **2010**, *122*, 1402–1437.

[23] Bönnemann, H., Richards, R.M., *Eur. J. Inorg. Chem.* **2001**, 2455-2480.

[24] Astruc, D., Lu, F., Aranzaes, J.R., *Angew. Chem. Int. Ed.* **2005**, *44*, 7852-7872.

[25] Pan, C., Pelzer, K., Philippot, K., Chaudret, B., Dassenoy, F., Lecante, P., Casanove, M.-J., *J. Am. Chem. Soc.* **2001**, *123*, 7584-7593.

[26] Aiken III, J. D., Finke, R. G., *J. Am. Chem. Soc.* **1999**, *121*, 8803-8810.

[27] Wasserscheid, P. and Keim, W., *Angew. Chem. Int. Ed.* **2000**, *39*, 3772-3789.

[28] Larhed, M., Moberg, C., Hallberg, A., *Acc. Chem. Res.* **2002**, *35*, 717-727.

[29] Bogdal, D., in *Microwave-Assisted Organic Synthesis*, *Tetrahedon Organic Chemistry Series*, Vol. 25, Elsevier , New York, USA, **2006**, pp. 47-189.

[30] Mingos, D.M.P, and Baghurst, D.R., *Chem. Soc. Rev.* **1991**, *20*, 1-47.

[31] Galema, S. A., *Chem. Soc. Rev.* **1997**, *26*, 233-238.

[32] Groh, M.F., Heise, M., Kaiser, M., Ruck, M., *Nachr. Chemie* **2013**, *61*, 26-29.

[33] Buchachenko, A. L., and Frankevich, E. L., *Chemical Generation and Reception of Radio- and Microwaves*, Wiley-VCH, Weinheim, Germany, **1993**, pp. 41-56.

[34] Ahluwulia, V.K., *Alternative Energy Processes in Chemical Synthesis*, Alpha Science International LTD, Oxford, United Kingdom, **2008**.

[35] Bilecka, I., and Niederberger, M., *Nanoscale* **2010**, *2*, 1358-1374.

[36] Krämer, J., Redel, E., Thomann, R., Janiak, C., *Organometallics* **2008**, *27*, 1976-1978.

[37] Dupont, J., and Scholten, J.D., *Chem. Soc. Rev.* **2010**, *39*, 1780-1804.

[38] Dupont, J., *J. Brazil Chem. Soc.* **2004**, *15*, 341-350.

[39] Neouze, M.-A., *J. Mater. Chem.* **2010**, *20*, 9593-9607.

[40] Consorti, C. S., Suarez, P.A.Z., de Souza, R.F., Burrow, R.A., Farrar, D.H., Lough, A.J, Loh, W., da Silva, L.H.M., Dupont, J., *J. Phys. Chem. B*. **2005**, *109*, 4341-4349.

[41] Dupont, J., Suarez, P.A.Z., de Souza, R.F., Burrow, R.A., Kintzinger, J.-P., *Chem. Eur. J.*, **2000**, *6*, 2377-2381.

[42] Vollmer, C., and Janiak, C., *Coord. Chem. Rev.* **2011**, *255*, 2039-2057.

[43] Janiak, C., *Z. Naturforsch. B* 2013, **68**, 1056-1089.

[44] Janiak, C., in *Topics in Organometallic Chemistry*, Vol. 51 (Eds. J. Dupont, L. Kollar), Springer, Heidelberg, **2015**, pp. 17-53.

[45] Janiak, C., in *Catalysis in Ionic Liquids: From Catalyst Synthesis to Application* (Eds. C. Hardacre, V. Parvulescu), RSC Publishing, Cambridge, 2014, chapter 11, pp. 537-577.

[46] Zhang, H., and Cui, H., *Langmuir* **2009**, *25*, 2604-2612.

[47] a) Verwey, E.J.W., and Overbeek, J.T.G., in *Theory of the Stability of Lyophobic Colloids*, Dover Publications Mineola, New York **1999**, pp. 1-218; b) Verwey E.J.W., and Overbeek J.T.G. *Theory of Stability of Lyophobic Colloids,* Elsevier, Amsterdam **1948**; Hansen J.-P., and Löwen H., *Annu. Rev. Phys. Chem.* **2000**, *51*, 209-242.

[48] Ninham, B.W., *Adv. Colloid Interface Sci*. **1999**, *83*, 1-17.

[49] Taubert, A., and Li Z., *Dalton Trans.* **2007**, 723-727.

[50] Redel, E., Thomann, R., Janiak C., *Inorg. Chem.* **2008**, *47*, 14-16.

[51] Ott, L.S., and Finke, R.G., *Inorg. Chem.* **2006**, *45*, 8382-8393.

[52] Fonseca, G.S., Umpierre, A.P., Fichtner, P.F.P., Teixeira, S.R., Dupont, J., *Chem. Eur. J.* **2003,** *9*, 3263-3269.

[53] Li, Z., Friedrich, A., Taubert, A., *J. Mater. Chem.* **2008**, *18*, 1008-1014.

[54] Migowski, P., Zanchet, D., Machado, G., Gelesky, M.A., Teixeira, S.R., Dupont, J., *Phys. Chem. Chem. Phys.* **2010**, *12*, 6826-6833.

[55] Vollmer, C., Redel, E., Abu-Shandi, K., Thomann, R., Manyar, H., Hardacre, C., Janiak, C., *Chem. Eur. J.* **2010**, *16*, 3849-3858.

[56] Migowski, P., Machado, G., Teixeira, S.R., Alves, M.C.M., Morais, J., Traverse, A., Dupont J., *Phys. Chem. Chem. Phys.*, **2007**, *9*, 4814-4821.

[57] Ruta, M., Laurenczy, G., Dyson, P.J., Kiwi-Minsker, L., *J. Phys. Chem. C* **2008**, *112*, 17814-17819.

[58] Deshmukh, R.R., Rajagopal, R., Srinivasan, K.V., *Chem. Commun.* **2001**, 1544-1545.

[59] Anderson, K., Fernández, S.C., Hardacre, C., Marr, P.C., *Inorg. Chem. Commun.* **2004**, *7*, 73-76.

[60] Peppler, K., Polleth, M., Meiss, S., Rohnke, M., Janek, J., Z. *Phys. Chem.* **2006**, *220*, 1507-1527.

[61] Safavi, A., Maleki, N., Tajabadi, F., Farjami, E., *Electrochem. Commun.* **2007**, *9*, 1963-1968.

[62] Kim, K., Lang, C., Kohl, P.A., *J. Electrochem. Soc.* **2005**, *152*, E9.

[63] Zhu, J.M., Shen, Y.H., Xie, A.J., Qiu, L.G., Zhang, Q., Zhang, X.Y., *J. Phys. Chem. C* **2007**, *111*, 7629-7633.

[64] Firestone, M.A., Dietz, M.L., Seifert, S., Trasobares, S., Miller, D. J., Zaluzec, N. J., *Small* **2005**, *1*, 754-760.

[65] Freudenmann, D., Wolf, S., Wolff, M., Feldmann, C., *Angew. Chem. Int. Ed.* **2011**, *50*, 11050-11060.

[66] a) Ahmed, E., Breternitz, J., Groh, M. F., Ruck, M., *CrystEngComm* **2012**, *14*, 4874-4885; b) Ahmed E., and Ruck M., *Dalton Trans.* **2011**, *40*, 9347-9357; c) Groh, M. F., Müller, U., Ahmed, E., Rothenberger, A., Ruck, M., *Z. Naturforsch.* **2013**, *68b*, 1108-1122

[67] Morris, R.E., *Chem. Commun.* **2009**, 2990-2998.

[68] Parnham, E.R., and Morris, R.E., *Acc. Chem. Res.* **2007**, *40*, 1005-1013.

[69] Cooper, E.R., Andrews, C.D., Wheatley, P.S., Webb, P.B., Wormald, P., Morris, R.E., *Nature* **2004**, *430*, 1012-1016.

[70] Rao, C.N.R., Matte, H.S.S.R., Voggu, R., Govindaraj, A., *Dalton Trans.*, 2012, **41**, 5089-5120.

[71] Janiak, C., in *Moderne Anorganische Chemie*, Vol. 4 (eds. H.-J. Meyer) Walter de Gruyter, Berlin, **2012**, chapter. 3-4, pp. 645-661.

[72] Kerfoot, D.G.E., Nickel, X., Wildermuth, E., Stark, H., Friedrich, G., Ebenhöch, F. L., Kühborth, B., Silver, J., Rituper, R., in *Ullmann's Encyclopaedia of Industrial Chemistry*, 5th ed., Wiley (online), **2008**.

[73] Gutel, T., Garcia-Anton, J., Pelzer, K., Philippot, K., Santini, C. C., Chauvin, Y., Chaudret, B., Basset, J.-M., *J. Mater. Chem.* **2007**, *17*, 3290-3292.

[74] Salas, G., Podgorsek, A., Campbell, P.S., Santini, C.C., Pádua, A.A.H., Costa-Gomes, M.F., Philippot, K., Chaudret, B., Turmine, M., *Phys. Chem. Chem. Phys.* **2011**, *13*, 13527-13536.

[75] Hyeon, T., *Chem. Commun.*, **2003**, 927-934.

[76] Hess, P.H., and Parker Jr., P.H., *J. Appl. Polym. Sci.* **1966**, *10*, 1915-1927.

[77] Thomas, J.R., *J. Appl. Phys.* **1966**, *37*, 2914-2915.

[78] Papirer, E., Horny, P., Balard, H., Anthore, R., Petipas, C., Martinet, A., *J. Colloid Interface Sci.* **1983,** *94*, 207-219. http://www.sciencedirect.com/science/article/pii/0021979783902515

[79] Papirer, E., Horny, P., Balard, H., Anthore, R., Petipas, C., Martinet, A., *J. Colloid Interface Sci.* **1983**, *94*, 220-228. http://www.sciencedirect.com/science/article/pii/0021979783902527

[80] Suslick, K. S., Choe, S.-B., Cichowlas, A.A., Grinstaff, M.W., *Nature* **1991**, *353*, 414-416.

[81] Suslick, K.S., Fang, M., Hyeon, T., *J. Am. Chem. Soc.* **1996**, *118* ,11960-11961.

[82] Suslick, K.S., Hyeon, T., Fang, M. *Chem. Mater.* **1996**, *8,* 2172-2179.

[83] Hyeon, T., Fang, M., Suslick, K.S., *J. Am. Chem. Soc.* **1996,** *118,* 5492-5493.

[84] Park, J.-I., and Cheon, J., *J. Am. Chem. Soc.* **2001**, *123*, 5743-5746.

[85] Lee, G.H., Huh, S.H., Jung, H.I., *J. Mol. Struct.* **1998**, *440*, 141-145

[86] Sun, S., Murray, C.B., Weller, D., Folks, L., Moser, A., *Science* **2000**, *287*, 1989-1991.

[87] a) Puntes, V.F., Krishnan, K.M., Alivisatos, A.P., *Appl. Phys. Lett.* **2001**, *78*, 2187-2189; b) Puntes, V.F., Gorostiza, P., Aruguete, D.M., Bastus, N.G., Alivisatos, A.P., *Nature Materials* **2004**, *3*, 263-268.

[88] Shevchenko, E. V., Talapin, D. V., Rogach, A. L., Kornowski, A., Haase, M, Weller, H., *J. Am. Chem. Soc.* **2002**, *124*, 11480-11485.

[89] Rutnakornpituk, M., Thompson, M.S., Harris, L.A., Farmer, K.E., Esker, A.R., Riffle, J.S., Connolly, J., Pierre, T.G.St., *Polymer* **2002**, *43*, 2337-2348.

[90] Bönnemann, H., Brijoux, W., Brinkmann, R., Matoussevitch, N., Waldöfner, N., Palina, N., Modrow, H., *Inorg. Chim. Acta* **2003**, *350*, 617-624.

[91] Matoussevitch, N., Gorschinski, A., Habicht, W., Bolle, J., Dinjus, E., Bönnemann, H., Behrens S., *Journal of Magnetism and Magnetic Materials* **2001**, *311*, 92-96.

[92] Zhang, H., Du, N., Wu, P., Chen, B., Yang, D., *Nanotechnology* **2008**, *19*, 315604/1-315604/6.

[93] Kodama, R.H., *Journal of Magnetism and Magnetic Materials* **1999**, *200*, 359-372.

[94] Laurent,S., Forge, D., Port, M., Roch, A., Robic, C., Elst, L.V., Muller, R.N., *Chem. Rev.* **2008**, *108*, 2064-2110.

[95] Kim, S.-W., Son, S.U., Lee, S.S., Hyeon, T., Chung, Y.K., *Chem. Commun*. **2001**, 2212-2213.

[96] Landau, M.V., Savilov, S.V., Kirikova, M.N., Cherkasov, N.B., Ivanov, A.S., Lunin, V.V., Koltypinc, Y., Gedanken, A., *Mendeleev Commun*. **2011**, *21*, 125-128.

[97] Ma, X., Liu, L., Aronhime, N., Zachariah, M.R., *Energy Fuels* **2011**, *25*, 3925-3933.

[98] Chamberlain, T.W., Zoberbier, T., Biskupek, J., Botos, A., Kaiser, U., Khlobystov, A. N., *Chem. Sci.* **2012**, *3*, 1919-1924.

[99] Chamberlain, T.W., Earley, J. H., Anderson, D.P., Khlobystova, A. N., Bourne, R. A., *Chem. Commun.* **2014**, *50*, 5200-5202.

[100] Cao, S., Chen, Y., Hou, C.-C., Lva, X.-J., Fu, W.-F., *J. Mater. Chem. A* **2015**, *3*, 6096-6101.

[101] Cao, S., Chen, Y., Wang, C. J., He P., Fu W. F., *Chem.Commun*. **2014**, *50*, 10427-10429.

[102] He, J., Zhang, Y., Chen, E.Y.-X., *ChemSusChem* **2013**, *6*, 61-64.

[103] Marquardt, D., Xie, Z., Taubert, A., Thomann, R., Janiak, C., *Dalton Trans.* **2011**, *40*, 8290-8293.

[104] Andanson, J.-M., Marx, S., Baiker, A., *Catal. Sci. Technol.* **2012**, *2*, 1403-1409.

[105] Marquardt, D., Vollmer, C., Thomann, R., Steurer, P., Mülhaupt, R., Redel, E., Janiak, C., *Carbon* **2011**, *49*, 1326-1332.

[106] Silva, D. O., Scholten, J. D., Gelesky, M. A., Teixeira, S. R., Dos Santos, A.C.B., Souza-Aguiar, E.F., Dupont, J., *ChemSusChem* **2008**, *1*, 291-294.

[107] Scariot, M., Silva, D.O., Scholten, J.D., Machado, G., Teixeira, S.R., Novak, M.A., Ebeling, G., Dupont, J., *Angew. Chem. Int. Ed.* **2008**, *47*, 9075-9078.

[108] Behrens, S., Essig, S., *J. Mater. Chem.* **2012**, *22*, 3811-3816.

[109] Vollmer, C., Schröder, M., Thomann, Y., Thomann, R., Janiak, C., *Appl. Catal. A* **2012**, *425-426*, 178-183.

[110] Redel, E., Thomann, R., Janiak, C., *Chem. Commun.* **2008**, 1789-1791.

[111] Redel, E., Krämer, J., Thomann, R., Janiak, C., *J. Organomet. Chem.* **2009**, *694*, 1069-1075.

[112] Lignier, P., in *Topics in Organometallic Chemistry*, Vol. 51 (Eds. J. Dupont, L. Kollar), Springer, Heidelberg, **2015**, pp. 55-78.

[113] Fernandes, R., Patel, N., Edla, E., Bazzanella, N., Kothari, D.C., Miotello, A., *Appl. Catal. A: General* **2015**, *495*,23-29.

[114] Cao, N., Luo, W., Cheng, G., *Int. J. Hydrogen Energy* **2013**, *38*, 11964-11972.

[115] Ma, Y., Huang, Y., Cheng, Y., Wang, L., Li, X., *Appl. Catal. A: General* **2014**, *484*, 154-160.

[116] Wang, L., Chen, J., Ge, L., Rudolph, V., Zhu, Z., *J. Phys. Chem. C.* **2013**,*117*, 4141-4151.

[117] Foppa, L., Luza, L., Gua, A., Weibel, D.E., Eberhardt, D., Texeira, S.R., Dupont, J., *Dalton Trans.* **2015**, *44*, 2827-2834.

[118] Schauermann, S., Nilius, N., Shaikhu, S., Freund, H.-J., *Acc. Chem. Res.* **2013**, *46*, 1673-1681.

[119] Kent, P.D., Mondloch, J.E., Finke, R.G., *J. Am. Chem. Soc.* **2014**, *136*, 1930-1941.

[120] Rao, C.N.R., Sood, A.K., Voggu, R., Subrahmanyam, K.S., *J. Phys. Chem. Lett.* **2010**, *1*, 572-580.

[121] Boehm, H.P., and Stumpp, E., *Carbon* **2007**, *45*, 1381-1383.

[122] Park, H., *Mater. Chem. Phys.* **2012**, *133*, 1050-1054.

[123] Park, H., Kim, J.S., Choi, B.G., Jo, S.M., Kim, D.Y., Hong, W.H., Jang, S.-Y., *Carbon* **2010**, *48*, 1325-1330.

[124] Gao, Y., Li, S., Zhao, B., Zhai, Q., Lita, A., Dalal, N.S., Kroto, H.W., Acquah, S.F.A., *Carbon* **2014**, *77*, 705-709.

[125] Scheuermann, G.M., Rumi, L., Steurer, P., Bannwarth, W., Mülhaupt, R., J. *Am. Chem. Soc.* **2009**, *131*, 8262–8270.

[126] Stankovich, S., Dikin, D.A., Dommett, G.H.B., Kohlhaas, K.M., Zimney, E.J., Stach, E.A., Piner, R.D., Nguyen, S.T., Ruoff, R.S., *Nature* **2006**, *442*, 282-286.

[127] Geim, A.K., and Novoselov, K.S., *Nature Mater.* **2007**, *6*, 183-191.

[128] Li, D., and Kaner, R.B., *Science* **2008**, *320*, 1170-1171.

[129] Steurer, P., Wissert, R., Thomann, R., Mülhaupt, R., *Macromol. Rapid Commun*. **2009**, *30*, 316-327.

[130] McAllister, M.J., Li, J.L., Adamson, D.H., Schniepp, H.C., Abdala, A.A., Liu, J., Herrera-Alonso, M., Milius, D.L., Car, R., Prud'homme, R.K., Aksay, I.A., *Chem. Mater.* **2007**, *19*, 4396-4404.

[131] Schniepp, H.C., Li, J.L., McAllister, M.J., Sai, H., Herrera-Alonso, M., Adamson, D.H., Prud'homme, R.K., Car, R., Saville, D.A., Aksay, I.A., *J. Phys. Chem. B* **2006**, *110*, 8535–8539.

[132] Hummers, W.S, and Offeman, R.E., *J. Am. Chem. Soc.* **1958**, *80*, 1339-1339.

[133] Goncalves, G., Marques, P.A.A.P., Granadeiro, C.M., Nogueira, H.I.S., Singh, M.K., Grácio J., *Chem. Mater.* **2009**, *21*, 4796-4802.

[134] a) Brodie, B.C., *Liebigs Ann. Chem.* **1860**, *114*, 6-24; b) Brodie, B. C., *Phil. Trans. Roy. Soc. London, Ser. A* **1859**, *149***,** 249; c) Boehm, H.-P., and Scholz, W., *Liebigs Ann. Chem.* **1965**, *691*, 1-8.

[135] Dreyer, D.R., Park, S., Bielawski, C.W., Ruoff, R.S., *Chem. Soc. Rev.* 2010, 39, 228-240.

[136] Tölle, F.J., Fabritius, M., Mülhaupt, R., *Adv. Funct. Mater.* **2012**, *22*, 1136-1144.

[137] Li, H.B., Kang, W.J., Xi, B.J., Yan, Y., Bi, H.Y., Zuhu, Y.C., Qian, Y.T., *Carbon* **2010**, *48*, 464-469.

[138] Ventura, D.N., Stone, R.A., Chen, K.S., Hariri, H.H., Riddle, K.A., Fellers, T.J., Yun, C.S., Strouse, G.F., Kroto, H.W., Acquah, S.F.A., *Carbon* **2010**, *48*, 987-994.

[139] Kudo, S., Maki, T., Miura, K., Mae, K., *Carbon* **2010**, *48*, 1186-1195.

[140] Scholz, K., Scholz, J., McQuilla, A.J., Wagner, G., Klepel, O., *Carbon* **2010**, *48*, 1788-1798.

[141] Kim, Y.H., Kim, Y.T., Kim, H., Lee, D., *Carbon* **2010**, *48*, 2072-2084.

[142] Tzitzios, V., Georgakilas, V., Oikonomou, E., Karakassides, M., Petridis, D., *Carbon* **2006**, *44*, 848-853.

[143] Marquardt, D., Beckert, F., Pennetreau, F., Tölle, F., Mülhaupt, R., Riant, O., Hermans, S., Barthel, J., Janiak, C., *Carbon* **2014**, *66*, 285-294.

[144] Marcos-Esteban, R., Schütte, K., Brandt, P., Marquardt, D., Meyer, H., Beckert, F., Mülhaupt, R., Kölling, H., Janiak, C., *Nano-Struct.&Nano-Objects*, **2015**, *1, in press.*

[145] Marcos-Esteban, R., Schütte, K., Marquardt, D., Barthel, J., Beckert, F., Mülhaupt, R., Janiak, C., *Nano-Structures & Nano-Objects* **2015**, *1*, in press

[146] Sheldon, R.A., *Chem. Commun.* **2008**, 3352-3365.

[147] Wasserscheid, P., and Welton, T., in *Ionic Liquid in Synthesis*, Vol. 1, Wiley-VCH, Weinheim, **2007**, pp. 325-350.

[148] Doorslaer, C.v. , Schellekens, Y., Mertens, P., Binnemanns, K., De Vos, D., *Phys. Chem. Chem. Phys.* **2010**, *12*, 1741-1749.

[149] Sawant, A.D., Raut, D.G., Darvatkar, N.B., Salunkhe, M.M., *Green Chem. Lett. Rev.* **2011**, *4*, 41-54.

[150] Astruc, D., *Nanoparticles and Catalysis*, Wiley-VCH, New York, **2007**.

[151] Dupont, J., de Souza, R.F., Suarez, P.A.Z., *Chem. Rev.* **2002**, *102*, 3667-3692.

[152] Mastrorilli. P., Monopoli, A., Dell'Anna, M.M., Latronico, M., Corugno, P., Nacci., A., in *Topics in Organometallic Chemistry*, Vol. 51 (Eds. J. Dupont, L. Kollar), Springer, Heidelberg, **2015**, pp. 237-286.

[153] Praetorius, J. M., and Crudden, C. M., *Dalton Trans.* **2008**, 4079-4094.

[154] Ertl, G., Knözinger, H., Weitkamp, J., in *Handbook of Heterogenous Catalysis,* Vol. 9, Wiley-VCH, Weinheim, **2008**.

3.4 Comparative synthesis of Cu and Cu_2O nanoparticles from different copper precursors in ionic liquid and propylene carbonate

R. Marcos Esteban, H. Meyer, J. Kim, C. Gemel, R. A. Fischer, C. Janiak
Eur. J. Inorg. Chem. **2015**, *submitted*.

Copper is cheaper in comparison with other noble metals, and together with its thermal and electrical conductivity properties is a very interesting material. In catalysis shows to be highly active and therefore is very attractive for the synthesis of copper nanoparticles. However, the small size of the nanoparticles and the fast oxidation of the copper (0) to copper (II) or (I) oxides, make the synthesis of Cu-NPs even more challenging.

Copper nanoparticles can be obtained from commercially metal salts such as $Cu(BF_4)_2$, $Cu(acac)_2$ or $Cu(AcO)_2$ monohydrate, or from organometallic compounds as $Cu(dmap)_2$ (acac= acetyl acetonate; AcO= acetate; dmap: (dimethylamino)propan-2-olate). To avoid the thermodynamic aggregation and agglomeration of the Cu-NPs usually need the presence of external capping agents or stabilizers when the reaction is carried out in common organic solvents or, conversely, using solvents such as ionic liquid (1-butyl-3-methylimidazolium tetrafluoroborate, [BMIm][BF_4]) or propylene carbonate (PC), which can stabilize and help to the nucleation and growth of the Cu-NPs. The reduction of the selected copper salts was done using the energy-saving microwave input.

The obtained Cu-NPs and Cu_2O-Nanocubes were characterized by TEM, PXRD and EDX. The Cu-NPs from the reduction of $Cu(BF_4)_2$ gave a size distribution of 45 nm in PC, while from $Cu(dmap)_2$ smaller nanoparticles showed size distributions of 3.1 ± 0.7 nm (in PC) and 3.7 ± 1.4 nm (in [BMIm][BF_4]). The reduction of $Cu(acac)_2$ achieved a size distribution of 3.3 ± 0.9 nm for Cu-NPs in [BMIm][BF_4]. By using the water content metal salt, $Cu(AcO)_2$ monohydrate, the reduction in [BMIm][BF_4] yielded to the synthesis of cuprite (cuprous oxide) copper(I) oxide nanocubes (Cu_2O-NCs) with a diameter of 43 ± 15 nm.

Author's contribution of the publications:*

- Previously bibliographic research, design of the synthetic procedures and application of the methods (laboratory work).
- Characterization of the samples by PXRD and interpretation of the EDX and TEM images.
- Writing of the manuscript together with the further corrections and edition according to the reviewer's comments.

* Detailed work of the co-authors in the manuscript:

-H. Meyer: measurements of TEM and EDX.

-J. Kim, Dr. C. Gemel, Prof. Dr. R. A. Fischer: synthesis of $Cu(dmap)_2$ within the priority program SPP 1708 (DFG).

Comparative synthesis of Cu and Cu_2O nanoparticles from different copper precursors in ionic liquid and propylene carbonate†

Raquel Marcos Esteban,[a] Hajo Meyer,[a] Jiyeon Kim, [b]Christian Gemel,[b] Roland A. Fischer,[b]* and Christoph Janiak[a]*

a Institut für Anorganische Chemie und Strukturchemie, Heinrich Heine Universität Düsseldorf, 40204 Düsseldorf. E-mail: janiak@uni-duesseldorf.de; Fax:+49-211-81-12287; Tel: +49-211-81-12286.

b Lehrstuhl Anorganische Chemie, II– Organometallics & Metallics, Ruhr-Universität Bochum, NC 2, Universitätsstr. 150, 44801 Bochum, Germany. E-mail: roland.fischer@rub.de; Fax: +49-234-32-14174; Tel: +49-234-32-24174

Abstract

Copper metal and copper(I) oxide (cuprite, cuprous oxide) nanoparticles (Cu-NPs and Cu_2O-NPs) were prepared from different copper salts by means of microwave irradiation (MWI) in propylene carbonate (PC) or in the ionic liquid, 1-butyl-3-methylimidazolium tetrafluoroborate ([BMIm][BF_4]). The nanostructures were studied by high-angle annular dark field-scanning transmission microscopy (HAADF-STEM), transmission electron microscopy (TEM), scanning electron microscopy (SEM) and powder X-ray diffraction (PXRD). Star-shaped agglomerated copper nanoparticles with about 45 nm diameter were formed from copper(II) tetrafluoroborate, $Cu(BF_4)_2$ using PC as solvent. Copper nanoparticles with smaller size distribution of 3.1 ± 0.7 nm and 3.7 ± 1.4 nm were obtained when copper(II) bis(1-(dimethylamino)propan-2-olate), $Cu(OCH(Me)CH_2NMe_2)_2$ was decomposed in PC and in [BMIm][BF_4]. Small Cu-NPs were also obtained from copper (II) acetylacetonate, $Cu(acac)_2$ in [BMIm][BF_4] with a diameter distribution of 3.3 ± 0.9 nm. Cubic cuprous oxide Cu_2O-nanocubes (NCs) of 43 ± 15 nm could be prepared using copper(II) acetate, $Cu(AcO)_2 \cdot H_2O$ together with [BMIm][BF_4]. The size of the Cu_2O-NCs increased when the nanoparticles are isolated from the neat ionic liquid by addition of acetonitrile, giving nanocubes of 0.1 to 0.5 μm.

Keywords: copper nanoparticles; copper(I) oxide nanoparticles; cuprite nanoparticles; cuprous oxide nanocubes; ionic liquids; propylene carbonate

1. Introduction

Synthesis and properties of metal, metal oxide and other nanoparticles (M-NPs) are continuous interest in areas like medicine, science or industry.[1] For applications M-NPs need to be synthesized reproducibly in a controllable reaction with defined size and small size distribution.[2,3,4,5,6] A "bottom-up" chemical synthesis typically uses the reduction of metal salts or organometallic compounds or their photolytic, sonolytic or thermal decomposition.[7] The synthesis conditions such as temperature, solvent, reducing and stabilizing agent can influence the size, size distribution and shape of metal nanoparticles.[8]

Copper and copper oxide nano- to micro-materials are studied for catalytic CO oxidation,[9,10,11,12,13,14] alkyne-azide cycloadditions,[15,16,17] aryl-sulfur bond formation,[18,19] or for amination of aryl halides[20,21,22,23] among others.[24,25,26] Copper(I) oxide, Cu_2O, is a metal oxide semiconductor with promising applications in solar energy conversion.[27,28,29] The preparation of copper nanoparticles (Cu-NPs) can be a challenge in comparison with more noble metals because less-noble Cu-NPs are easily oxidized in aqueous solution and quickly agglomerate under exposure to air. Because of this copper nanoparticles have to be synthesized under inert atmospheres and mostly together with a stabilizing agent such as polyvinylpyrrolidone (PVP)[30,31,32,33] or cetyltrimethylammonium bromide (CTAB)[34,35] to give a protective layer around the nanoparticle to prevent oxidation. However, the use of a capping ligand [36] or polymer micelles[37,38] to stabilize the nanoparticles will decrease the activity of the nanoparticles in catalysis.

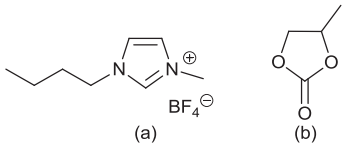

Scheme 1 (a) 1-Butyl-3-methyl-imidazolium tetrafluoroborate ([BMIm][BF_4]) and (b) propylene carbonate (PC).

Interest in "ligand-free" metal nanoparticles synthesis is growing in the last few years due their use for catalysis with the advantage of the absence of capping agents. Non-conventional solvents like ionic liquids (ILs) (Scheme 1) can kinetically stabilize M-NPs without the need of additional capping agent.[39,40,41,42,43,44,45]

Room temperature ionic liquids (RTILs) are defined as salts which are liquid at room temperature. Ionic liquids have almost no vapor pressure, a high ionic charge and dielectric constant, the ability to dissolve a variety of materials well as high thermal and chemical stability which are advantages in the preparation and stabilization of M-NPs.[43,47,48,49,50,51,52,53] Also, ILs have a very high absorption efficiency for microwave irradiation (MWI) because of their high ionic charge, polarity and dielectric

constant. This allows for rapid microwave heating during precursor decomposition for nanoparticle synthesis.[49,54,55,56]

Organic carbonates (Scheme 1) are considered as *green solvents* due to their low toxicity and low flammability. Properties like their low viscosity, their large range of liquid temperature (for propylene carbonate m.p. –49 °C, b.p. 243 °C) and also their low price should make them interesting, *inter alia*, for the synthesis of the metal nanoparticles.[44,57,58,59,60,61]

The synthesis of copper and copper oxide nanoparticles using methods such as metal vapor chemistry,[62] plasma electrochemistry,[63,64] photolysis,[65] microemulsion techniques[66,67] or by thermal reduction[68,69,70,71] have already been described.

Microwave irradiation was used to synthesize flower-like cuprite (Cu_2O) architectures.[72] The reaction was done in a aqueous solution (distilled water) using glucose as capping agent and several tests were done using different concentrations of ionic liquid ([BMIm][BF_4]). In the absence of the ionic liquid the Cu_2O-NPs crystallized in a cubic form with a size in the range of 50-100 nm. However, when a specified amount of [BMIm][BF_4] was added to replace the water, the structure changes from coral-like (300-1500 nm; 1.5 mL IL) to a sunflower-like structure (500-3500 nm; 5 mL IL) and finally to leaf-like Cu_2O-nanosheets when the amount of IL increases to 7.5 mL.[72]

Santini *et al*.[70] reported the easy synthesis of copper nanoparticles (Cu-NPs) in imidazolium based ionic liquids ($C_1C_nImNTf_2$, with n = 4 or 6) using copper mesitylene ([$(CH_3)_3C_6H_2$]Cu) as a precursor and H_2 as reducing agent. Variation of parameters such as stirring rate, pressure, temperature and time could generate different sizes of Cu-NPs in the neat ionic liquid. For example, reduction of the precursor at an H_2 pressure of 0.9 MPa at 100 ºC for 2 hours gave Cu-NPs nanoparticles of 4.5 nm diameter with a narrow size distribution.[70] Synthesis of Cu-NPs in functionalized imidazolium-based ionic liquids was also investigated by Chandra and co-workers,[73,74] to give nanoparticles of 50-60 nm. The Cu-NPs/IL dispersions were used as catalyst for coupling reactions such as the coupling between thiazolidine-2,4-dione, aromatic aldehydes and ammonium acetate, to give conversions of 95%.[74]

Copper nanoparticles without external capping ligands are difficult to synthesize and to handle due to their fast oxidation,[75] and therefore usually a capping agent, stabilizer or supports are involved in order to avoid the aggregation or agglomeration of the particles and he synthesis of naked and small Cu-NPs is even more challenging.[76]

Here we report the comparative synthesis of copper (Cu)- and cuprite (Cu_2O)-nanoparticles using the different copper sources $Cu(BF_4)_2$, $Cu(dmap)_2$, $Cu(AcO)_2{\cdot}H_2O$ or $Cu(acac)_2$ [dmap = 1-(dimethylamino)propan-2-olate, $^-OCH(Me)CH_2NMe_2$; AcO = acetate, acac = acetylacetonate] and the solvents propylene carbonate (PC) and the ionic liquid 1- butyl-3-methylimidazolium tetrafluoroborate, [BMIm][BF_4].

2. Results and discussion

2.1 Copper nanoparticles in propylene carbonate (PC) and 1-butyl-3-methylimidazolium tetrafluoroborate [BMIm][BF_4].

The blue solution of copper(II) tetrafluoroborate, $Cu(BF_4)_2$, in propylene carbonate turns to a deep red solution under microwave irradiation (5 min, 250 °C, 50 W) (Fig. 1) indicating that copper nanoparticles were formed. The synthesis was carried out with and without the presence of the base *n*-butyl imidazole (BIm).

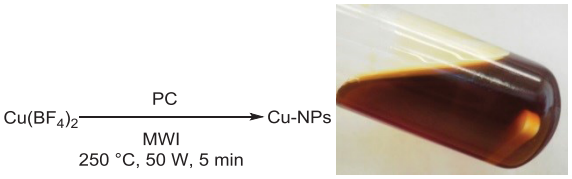

Fig. 1 Formation of copper nanoparticles using $Cu(BF_4)_2$ and *n*-butylimidazole in propylene carbonate (PC) (red solution) under microwave irradiation (MWI).

High-angle annular dark field–scanning transmission microscopy (HAADF-STEM) shows the formation of star-shaped particles which are agglomerated (Fig. 2). Hence a size and size dispersion cannot be reliably determined.

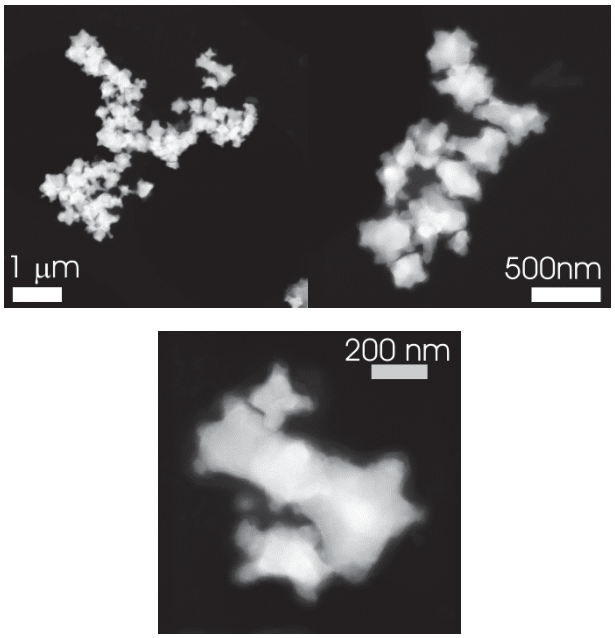

Fig. 2 HAADF-STEM images of Cu-NPs from $Cu(BF_4)_2$ in propylene carbonate (PC) in the presence of BIm (for more TEM images and EDX spectra see Fig. S1 and S2).

Composition, structure and phase purity of the Cu-NPs was verified by powder X-Ray diffraction (PXRD) (Fig. 3) and by energy-dispersive X-ray spectrometry (EDX) (Fig. S2). The peaks from the Cu-NPs in the PXRD after isolation can be positively matched to those of the face-centered cubic metal lattice of copper (crystallographic open database COD Nr. 7101269). The peaks from the crystal planes (111), (200), (220) and (311) are associated to the 2θ values of 42.9°, 50.1°, 73.8° and 89.6°, respectively. The size of the nanoparticles was calculated by the Debye-Scherrer formula,[82] which gave an average diameter of 45 nm related to the (111) reflection. From the PXRD no oxidation of the *solid* BIm-protected copper nanoparticles under air is apparent within five days (Fig. 3b). However in solution the red Cu-NPs (Fig. 1) are very unstable and immediately (within one hour) turn green upon contact to air,

indicating the oxidation of the nanoparticles to Cu^{2+} species.

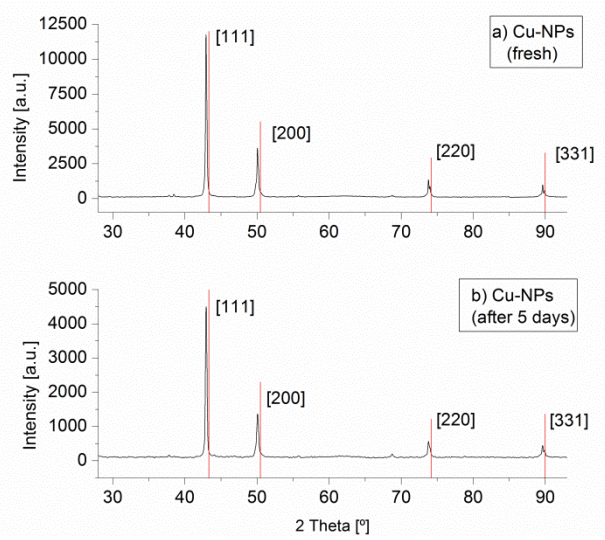

Fig. 3 Powder X-Ray diffractogram of Cu-NPs (top) freshly synthesized from $Cu(BF_4)_2$ in PC in the presence of BIm and separated by centrifugation, (down) after 5 days of contact with air; compared with the theoretical pattern of Cu (red bars, COD No. 7101269).

Copper nanoparticles can also be synthesized in PC without the presence of *n*-butyl imidazole. Again, the PXRD matches well with the theoretical pattern for Cu metal. An average diameter of 43 nm was determined for Cu-NPs based on the (111) reflection (Fig. 4 top). however after five days under air new peaks at 2θ 36.12°, 42.02° and 61.15° have developed which correspond to the lattice planes (111), (200) and (220), respectively, of copper(I) oxide (Fig. 4 bottom).

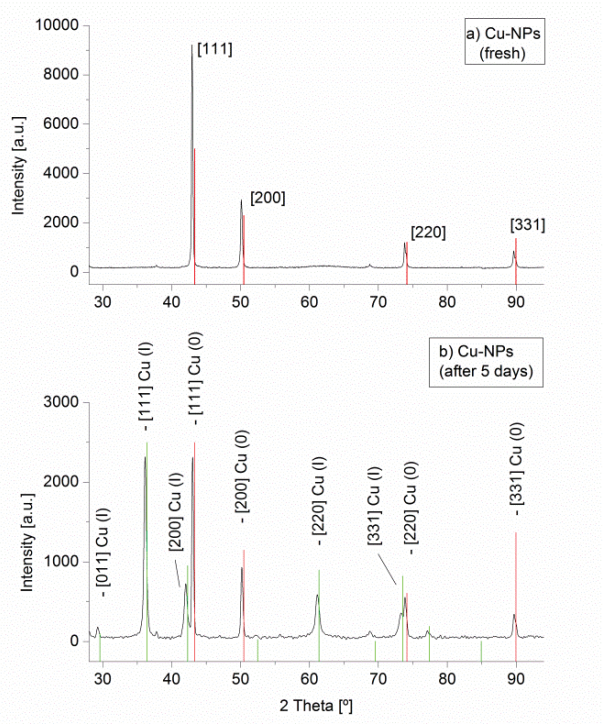

Fig. 4 PXRD for Cu-NPs synthesized from $Cu(BF_4)_2$ in PC without BIm, precipitated with CH_3CN, separated by centrifugation and measured under air (top) on the first day and (bottom) after five days. Red bars indicate the theoretical pattern for Cu (COD No. 7101269) and green bars for Cu_2O (COD No. 9005769).

Freshly prepared Cu-nanoparticles from PC without BIm are also much larger in size (or strongly agglomerated) as seen in Fig. 5. Again, from Fig. 5 a size and size dispersion cannot be reliably determined.

The same procedure was tried with $Cu(BF_4)_2$ in the ionic liquid [BMIm][BF_4] several times, albeit unsuccessfully. From the IL the TEM did not show the formation of nanoparticles.

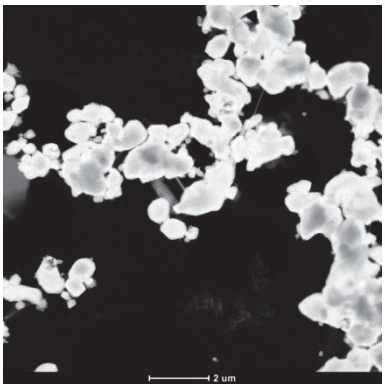

Fig. 5 HAADF-STEM images of Cu-NPs from $Cu(BF_4)_2$ in PC without BIm showing large particles (for more images see Fig. S3 in the Supp. Info).

Buhro and co-workers[77] observed that the pyrolysis of $Cu(dmap)_2$ $Cu(OCH(Me)CH_2NMe_2)_2$ formed pure copper metal without formation of Cu_2O or CuO, making this starting material very suitable for the synthesis of Cu-NPs. *Fischer* and co-workers already used this copper(II) dimethylamino alkoxide compound to obtain heterometallic copper-zinc compounds, such as Cu@ZnO composites in a single decomposition step and without using an external reducing agent.[78]

The blue $Cu(dmap)_2$ solution in PC or [BMIm][BF_4] turns red in PC or red-brown in IL after decomposition by means of microwave irradiation (15 min, 220 ºC, 50 W) (Fig. 6).

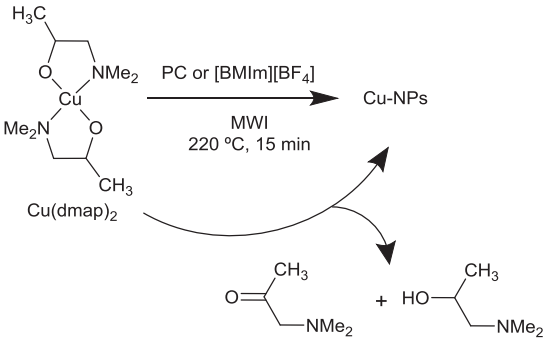

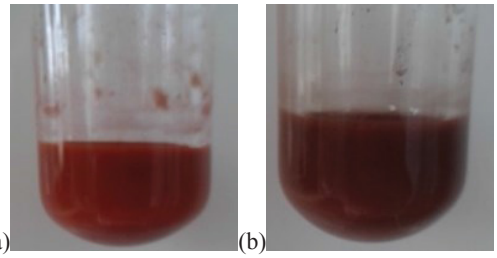

Fig. 6 Synthesis of copper nanoparticles after decomposition of $Cu(dmap)_2$ in PC (**a**) and in $[BMIm][BF_4]$ (**b**) by means of microwave irradiation. The reduction of the copper was described by *Young et al.* [79] The decomposition of the $Cu(dmap)_2$ occurs through a β-hydride elimination and reductive elimination.

PXRDs of the Cu-NPs from $Cu(dmap)_2$ show the typical reflections of Cu metal with the lattice planes (111), (200), (220) and (331) without the presence of copper oxides (Cu_2O or CuO) (Fig. 7).

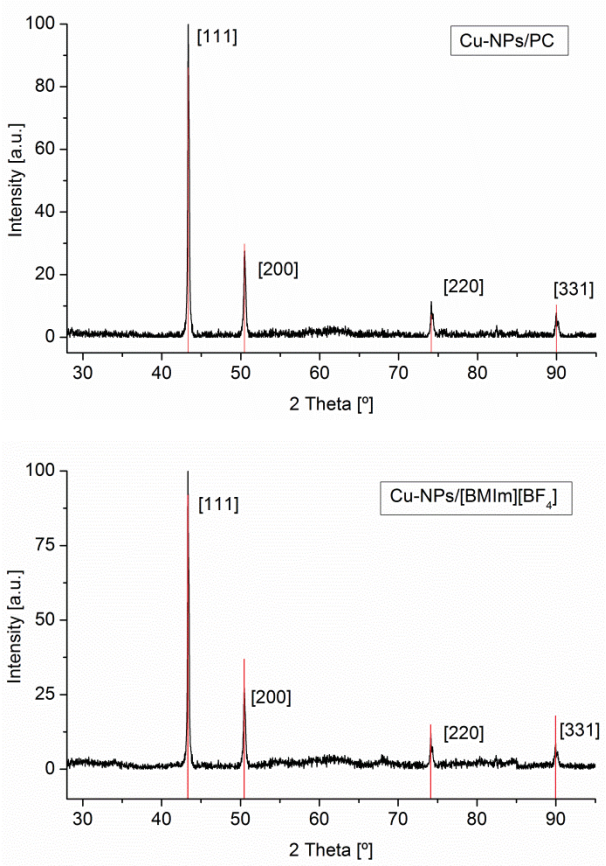

Fig. 7 PXRD for Cu-NPs from the decomposition of $Cu(dmap)_2$ in PC (top) or IL (bottom) by MWI, after precipitation with CH_3CN, separation by centrifugation and measured under air. Red bars indicate the theoretical pattern for Cu (COD No. 7101269).

The TEM images for Cu-NPs from $Cu(dmap)_2$ gave a diameter distribution, of 3.1 ± 0.7 nm in PC and of 3.7 ± 1.4 nm in in $[BMIm][BF_4]$ (Fig. 8).

The nucleation and growth of the nanoparticles depend on the precursor, the solvent and the capping ligands. We trace the formation of small nanoparticles from $Cu(dmap)_2$ compared to $Cu(BF_4)_2$ to the clean intramolecular reduction of the copper(II) alkoxide (Fig. 6).

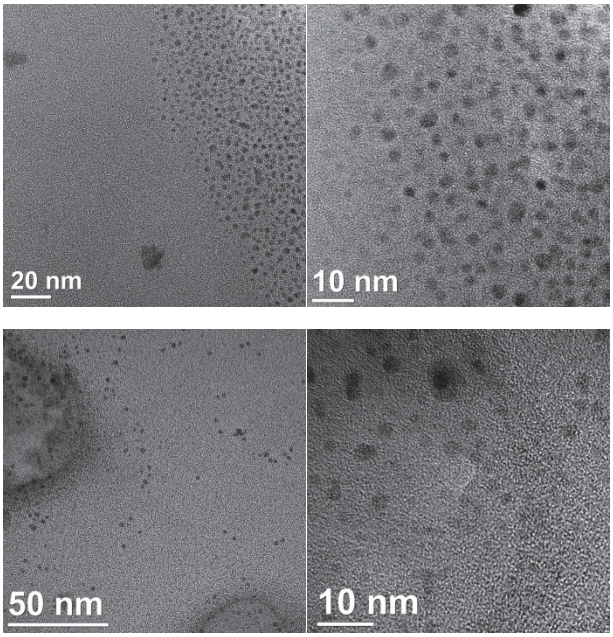

Fig. 8 TEM images of Cu-NPs after decomposition of $Cu(dmap)_2$ in PC (top) or IL (bottom) by MWI. Histogram in Fig. S7.

Copper(II) acetylacetonate, $Cu(acac)_2$ in the IL $[BMIm][BF_4]$ yielded a deep-red solution of copper nanoparticles under microwave irradiation for 15 minutes to 250 °C (200 W, 3 bar). TEM analysis of the Cu-NPs/IL dispersion yielded a diameter distribution of 3.3 ± 0.9 nm (Fig. 9) and PXRD shows the typical reflections of Cu metal (Fig. 10).

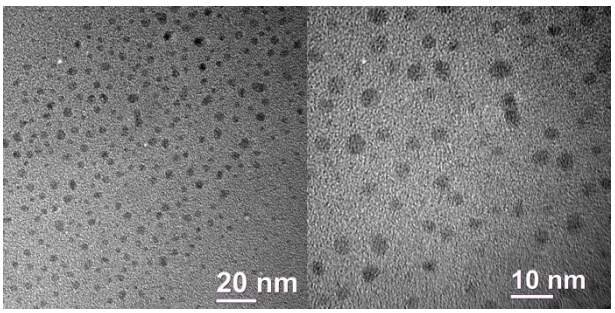

Fig. 9 HR-TEM images of Cu-NPs from MWI-induced decomposition of $Cu(acac)_2$ in $[BMIm][BF_4]$.

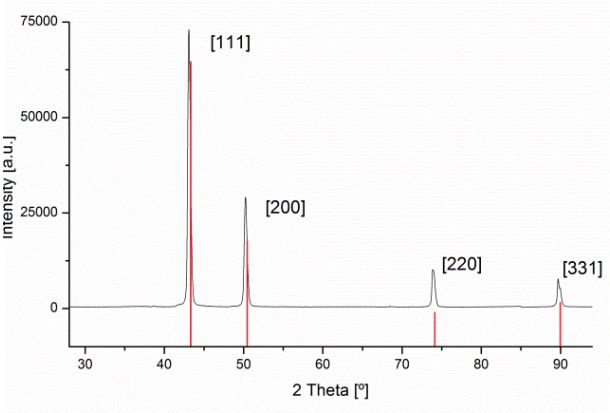

Fig. 10 PXRD of Cu-NPs from MWI-induced decomposition of $Cu(acac)_2$ in $[BMIm][BF_4]$. Red bars indicate the theoretical pattern for Cu (COD No. 7101269)

2.2 Copper(I) oxide nanocubes in $[BMIm][BF_4]$

The synthesis of copper(I) oxide nanocubes in ionic liquids is already described in the literature using phosphonium ionic liquids[80] or in combination with a capping agent[72] to stabilize the formed nanoparticles.

The blue dispersion of copper(II) acetate monohydrate, $Cu(AcO)_2 \cdot H_2O$ in $[BMIm][BF_4]$ turned to an orange suspension after microwave heating to 250 °C for 15 minutes (Fig. 11).

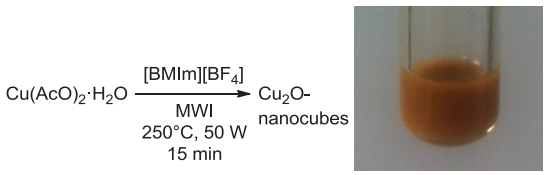

Fig. 11 Formation of Cu_2O-nanocubes from $Cu(AcO)_2 \cdot H_2O$ in $[BMIm][BF_4]$ under microwave irradiation (orange dispersion).

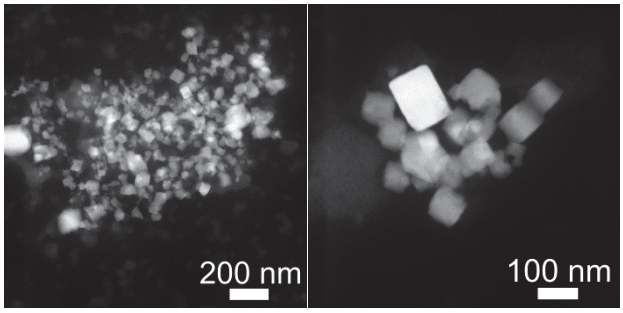

Fig. 12 HAADF-STEM images of Cu_2O-nanocubes synthesized from $Cu(AcO)_2 \cdot H_2O$ in $[BMIm][BF_4]$ under microwave irradiation (for more TEM images and histograms see Fig. S9, Fig. S10, and Fig. S11 for EDX).

HAADF-STEM (Fig. 12) shows particles with a cubic shape and a size of up to 100-150 nm, with the average diameter and distribution being 43 ± 15 nm. The composition of the sample was verified by PXRD (Fig. 13) with peaks at 2θ 29.21°, 36.08°, 41.97°,52.03°, 60.99°, 73.15° and 77.07° corresponding to the lattice planes (011), (111), (002), (112), (022), (113) and (222), respectively, of Cu_2O (cuprite, cuprous oxide). The interplanar distances are 3.05 and 2.49 Å for the planes (001) and (111), which fit well with the literature values (COD. No. 9005769). The (111) peak by the Scherrer equation yields a diameter of 35 nm.[82]

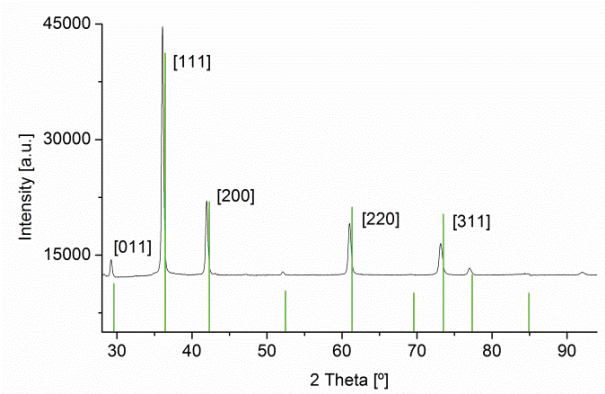

Fig. 13 PXRD of Cu_2O-nanocubes synthesized from $Cu(AcO)_2 \cdot H_2O$ in $[BMIm][BF_4]$ and comparison with the theoretical pattern (green) for Cu_2O (COD No. 9005769).

After centrifugation, washing with acetonitrile (3 x 5 mL) and isolation of Cu_2O as an orange powder the sample was measured again by HAADF-STEM (Fig. 14) and by SEM (Fig. 15). It is evident that that the Cu_2O-nanocubes (NCs) grew in the absence of the ionic liquid to microcubes, achieving a size of approx. 1 µm. This behavior supports the capability of ionic liquids to stabilize nanoparticles in their small size.

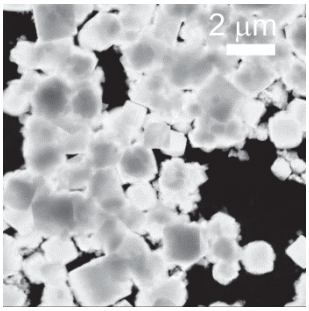

Fig. 14 HAADF-STEM images of Cu_2O-nanocubes synthesized from $Cu(AcO)_2 \cdot H_2O$ in $[BMIm][BF_4]$ after centrifugation from the ionic liquid and washing with acetonitrile (for more images and EDX see Fig. S12, S14 and S15).

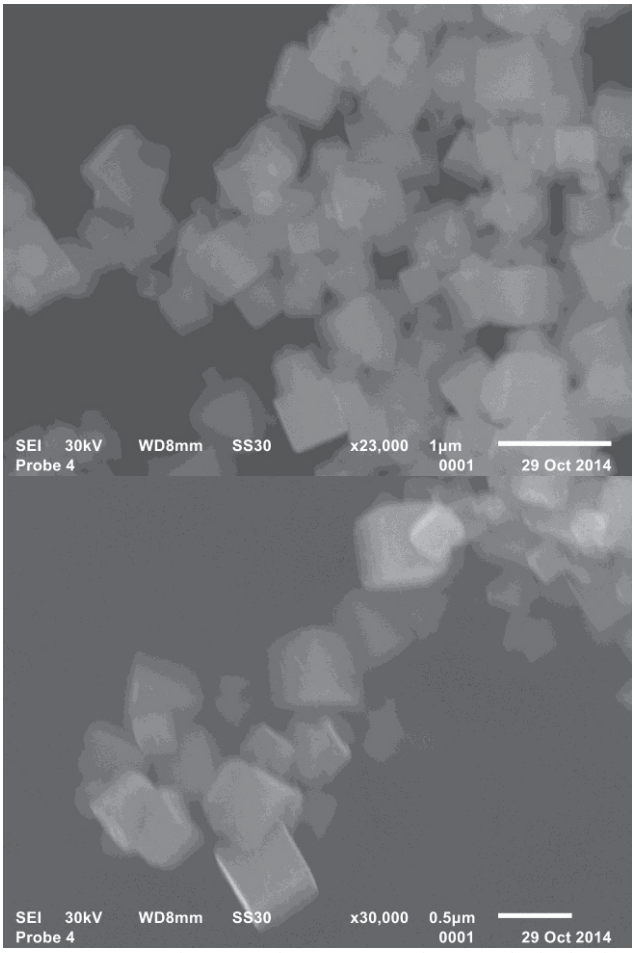

Fig. 15 SEM images of Cu_2O-nanocubes synthesized from $Cu(AcO)_2 \cdot H_2O$ in [BMIm][BF_4] after centrifugation from the ionic liquid and washing with acetonitrile (see Fig.S16 and S17 for additional SEM images).

Xie and co-workers reported the synthesis of such Cu_2O cubes in the absence and presence of IL and using glucose as capping agent. When the amount of [BMIm][BF_4] was increased, the cubic shape of the particles changed to flower-like arquitectures.[72] The aggregation and agglomeration of the nanocubes was also reported by Huang *et al.*[81] who reported five different shapes of Cu_2O nanocubes in aqueous solution depending on the amount of the surfactant sodium dodecyl sulfate sodium dodecyl sulfate (SDS).

Surprisingly our cubic structures were achieved when only ionic liquid was involved. This presents a new method of synthesizing Cu_2O nanocubes in the absence of any capping agent by just using the ionic liquid [BMIm][BF_4].

3. Conclusion

Synthesis of Cu- and Cu_2O-nanoparticles by means of microwave irradiation can be easily achieved from copper sources such as $Cu(BF_4)_2$, $Cu(dmap)_2$, $Cu(acac)_2$ or $Cu(AcO)_2$ H_2O together with an aprotic solvent such as propylene carbonate (PC) or with the ionic liquid 1-butyl-3-methylimidazolium tetrafluoroborate ([BMIm][BF_4]).

$Cu(BF_4)_2$ gave to star shaped Cu-NPs with a diameter of about 45 nm in PC while from $Cu(dmap)_2$ smaller nanoparticles were obtained in both solvents PC and [BMIm][BF_4] with size distributions of 3.1 ± 0.7 nm and 3.7 ± 1.4 nm diameter, respectively. Cu-NPs in the ionic liquid could also be achieved using the oxygen containing $Cu(acac)_2$ as precursor, giving nanoparticles with a narrow size distribution of 3.3 ± 0.9 nm. When $Cu(AcO)_2$ monohydrate was used, cuprite (cuprous oxide) copper(I) oxide nanocubes were formed, with a diameter of 43 ± 15 nm. Their isolation from neat ionic liquid by precipitation with acetonitrile led to particle growth up to 0.1 to 0.5 µm. This behavior illustrates the capability of the ionic liquids to function as a kinetic stabilizer for nanoparticles.

4. Experimental section

4.1 Methods and instrumentation

All manipulations were performing using Schlenk techniques. The solvents were dried using the MBraun solvent purification system. Copper(II) tetrafluoroborate hydrate, copper(II) acetylacetonate (> 99.9% trace metals basis) and propylene carbonate (purity 97%, H_2O free) were purchased from Sigma-Aldrich. Copper(II) acetate monohydrate was purchased from Merck and *n*-butylimidazole from Alfa Aesar. The synthesis of $Cu(dmap)_2$ (dmap = 1-(dimethylamino)propan-2-olate, $Cu(OCH(Me)CH_2NMe_2)_2$) was carried out as described by *Buhro et al.* [77,78]. All copper salts were dried under high vacuum (10^{-3} mbar). Propylene carbonate was dried for several days by 100°C under high vacuum (10^{-3} mbar).

The synthesis of the ionic liquid [BMIm][BF_4] was done as described elsewhere.[44]

Powder X-ray diffraction patterns data were measured on a Bruker D2 Phaser using a sample holder and Cu-Kα radiation (λ=1.54182Å, 35 kV) covering 2 theta angles 5-90° over a time of 8 h, that is 0.003 °/sec. All measurement was done under room temperature. The samples were precipitated with CH_3CN, washed with dry acetonitrile, and dried under vacuum (10^{-3} mbar). The size of the nanoparticles was calculated by the Debye-Scherrer formula.[82]

$$\beta_s(2\theta)_{hkl} = \frac{K_\lambda}{T\ cos\theta\ _{hkl}}$$

From the Scherrer equation PXRD often gave an average diameter (related to the (111) reflection) which was much larger (20-45 nm) then from TEM (3-4 nm). Hence, the acetonitrile precipitation and washing procedure apparently induces agglomeration by removing the stabilizing PC or IL. In turn, this illustrates the kinetic stabilizing effect of PC or the ionic liquid.

High-angle annular dark field-scanning transmission electron microscopy (HAADF-STEM) and high-resolution transmission electron microscopy (HR-TEM) images were obtained at room temperature on a FEI Tecnai G20 TEM operating at an accelerating voltage of 200 kV. Samples were deposited on 200 µm carbon-coated gold grids. Energy dispersive X-ray spectra (EDX) were taken on a FEI Tecnai f20, 136 k, the exposure time for individual EDX spectra is 3 min. For HAADF-STEM and HR-TEM the samples were prepared in two different procedures. The samples of Cu-NPs/PC or Cu-NPs/[BMIm][BF_4] were prepared by putting a drop of the dispersion on the gold-grid under inert atmosphere and allowed it to settle for 30 minutes. Afterwards the samples were quickly washed with 3-5

mL of dry acetonitrile before placed into the TEM.

For Cu_2O-NCs we used two different methods. The first one was done as described for Cu-NPs in PC or IL (Fig. 12). In the second one, the Cu_2O-NCs (Fig. 14, Fig. 15) were precipitated with dry acetonitrile and the *orange-solid* was dried under vacuum. Afterwards the solid was re-suspended under sonication with CH_3CN for about 5 min, and consecutively three drops of the Cu_2O-NPs/CH_3CN dispersion were put on the gold grid and let dried.

Scanning electron transmission (SEM) images were obtained on a Jeol JSM 6510 (LaB6 cathode, SDD detector) after being sputtered for 20 s with gold. Images in Fig. S15 were obtained on gold-coated samples using an ESEM Quanta 400 FEG SEM equipped with a secondary electron (SE) detector and operated at 20 keV. The Cu_2O-NC samples were prepared by precipitation with dry acetonitrile and dried under high vacuum (10^{-3} mbar).

4.2 Synthesis of copper nanoparticles from $Cu(BF_4)_2$ and $Cu(dmap)_2$.

In a typical experiment 52.5 mg $Cu(BF_4)_2$ (0.22 mmol), and ~3 equivalents of *n*-butyl imidazole (0.1 mL, 0.76 mmol, 0.95 g/mL) were dissolved and stirred for one hour under inert atmosphere together with 2 mL propylene carbonate (2.40 g, 23.59 mmol). The blue solution was placed in the microwave reactor (CEM discover, 50 W, 250 °C) for 5 min. The same procedure was repeated with 20 mg $Cu(dmap)_2$ (0.075 mmol) in 1 mL propylene carbonate (1.2 g, 11.79 mmol) or in 1 mL [BMIm][BF_4] The blue solution was placed in the microwave reactor at 220 ºC (50 W) for 10 min.

The attempted synthesis of Cu-NPs from $Cu(BF_4)_2$ in the IL was unsuccessful.

The resulting red copper nanoparticle solutions was centrifuged and washed with dry acetonitrile (3x 5mL). The (red) powder was dried under vacuum and stored under inert atmosphere for further analysis.

4.3 Synthesis of copper nanoparticles from $Cu(acac)_2$ in IL.

A solution of $Cu(acac)_2$ (50 mg, 0.19 mmol) in [BMIm][BF_4] (1 mL, 1.17 g, 5.78 mmol) was prepared under inert atmosphere and stirred for 24 hours to achieve a good dispersion. Reduction of the copper salt was initiated by microwave irradiation for 15 minutes (100 W, 250 °C). The red-brown solution was centrifuged and washed with dry acetonitrile (3 x 5 mL), dried under vacuum and stored under vacuum for further analysis.

4.4 Synthesis of copper(I) oxide nanoparticles in IL.

A dispersion of $Cu(AcO)_2 \cdot H_2O$ (26.8 mg, 0.13 mmol) in [BMIm][BF_4] (1 mL, 1.17 g, 5.78 mmol) was stirred for one hour under inert atmosphere. Decomposition was done with microwave irradiation for 15 minutes (50 W, 250 °C). The orange powder of Cu_2O-NCs was separated from the IL by centrifugation, washing with dry acetonitrile (3 x 5 mL), followed by drying under vacuum and storing under inert atmosphere.

Acknowledgements

Authors are thankful to the Deutsche Forschungsgemeinschaft (DFG) for grant Ja466/31-1 within the priority program SPP 1708 and to Dr. Juri Barthel and the Ernst Ruska-Centre (ER-C) for Microscopy and Spectroscopy with Electrons, Jülich Research Centre and RWTH Aachen University, 52425 Jülich (Germany) for help and access to the HR-TEM facilities. We thank Dr. Kai Schütte, Annika Herbst, Karsten Klauke, Dr. Harold Tanh Jeazet and Katrin Verlinden for help with the TEM and SEM measurements.

References.

[1] S.- H. Yu, L. R. MacGillivray, C. Janiak, *CrystEngComm*. **2012**, *14*, 7531–7534.
[2] A. H. Lu, E. L. Salabas, F. Schüth, *Angew. Chem. Int. Ed.* **2007**, *46*, 1222–1244.
[3] A. Gedanken, *Ultrasonics Sonochemistry* **2004**, *11*, 47–55.
[4] C. N. R. Rao, S. R. C. Vivekchand, K. Biswas, A. Govindaraj, *Dalton Trans.* **2007**, *34*, 3728–3749.
[5] Y. Mastai, A. Gedanken, *Chemistry of Nanomaterials* **2004**, *1*, 113–169.
[6] J. Park, J. Joo, S. G. Kwon, Y. Jang, T. Hyeon, *Angew. Chem. Int. Ed.* **2007**, *46*, 4630–4660.
[7] Z. Peng, H. Yang, *Nano Today* **2009**, *4*, 143–164.
[8] K. An, S. Alayoglu, T. Ewers, G. A. Somorjai, *J. Colloid Interface Sci.* **2012**, *373*, 1–13.
[9] U. R.Pillai, S. Deev, *Appl. Catal. B: Environ.* **2006**, *64*, 146–151.
[10] T.- J. Huang, D.- H. Tsai, *Catal. Lett.* **2003**, *87*, 173–178.
[11] G. G. Jernigan, G. A. Somorjai, *J. Catal.* **1994**, *147*, 567–577.
[12] D. A. Svintsitskiy, A. P. Chupakhin, E. M. Slavinskaya, O. A. Stonkus, A. I. Stadnichenko, S. V. Koscheev, A. I. Boronin, *J. Mol. Catal. A: Chem.* **2013**, 95–106.
[13] B. White, M. Yin, A. Hall, D. Le, S. Stolbov, T. Rahman, N. Turro, S. O'Brien, *Nano Lett.* **2006**, *6*, 2095–2098.
[14] G. Wu, N. Guan, L. Li, *Catal. Sci. Tech.* **2011**, *1*, 601–608.
[15] I. S. Park, M. S. Kwon, Y. Kim, J. S. Lee, J. Park, *Org. Lett.* **2008**, *10*, 497–500.
[16] T. Jin, M. Yan, Y. Yamamoto, *ChemCatChem* **2012**, *4*, 1217–1229.
[17] D. Raut, K. Wankhede, V. Vaidya, S. Bhilare, N. Darwatkar, A. Deorukhkar, G. Trivedi, M. Salunkhe, *Catalysis Communications* **2009**, *10*, 1240–1243.
[18] B. C. Ranu, A. Saha, R. Jana, *Adv. Synth. Catal.* **2007**, *349*, 2690–2696.
[19] C. Gonzalez-Arellano, R. Luque, D. J. Macquarrie, *Chem. Commun.* **2009**, 1410–1412.
[20] S. Sarkar , R. Pal, M. Roy, N. Chatterjee, S. Sarkar, A. Kumar Sen, *Tetrahedron Letters* **2015**, *56*, 623–626.
[21] M. T. Keßler, S. Robke, S. Sahler, M. H. G. Prechtl, *Catal. Sci. Technol.* **2014**, *4*, 102–108.
[22] M. Lakshmi Kantam, V. Neeraja, B. Kavita, B. Neelima, M. K. Chaudhuri, Sahid Hussain, *Adv. Synth. Catal*. **2005**, *347*, 763 –766.
[23] M. Lakshmi Kantam, B. Neelima, Ch. Venkat Reddy, *Journal of Molecular Catalysis A: Chemical* **2006**, *256*, 269–272.
[24] T. Mitsudome, Y. Mikami, K. Ebata, T. Mizugaki, K. Jitsukawa, K. Kaneda, *Chem. Commun.* **2008**, 4804–4806.
[25] M. Lakshmi Kantam, V. Neeraja, B. Kavita, Y. Haritha, *Synlett* **2004**, *3*, 525–527.
[26] C. Liu, J. Han, J. Wang, *Synlett* **2007**, *4*, 643–645.
[27] M. Yin, C.-K. Wu, Y. Lou, C. Burda, J. T. Koberstein, Y. Zhu, S. O'Brien, *J. Am. Chem. Soc.* **2005**, *127*, 9506–9511.
[28] J. J. Michael, S. Iniyan, *Energy Conversion and Management* **2015**, *95*, 160–169.
[29] A. Zamzamian, M. KeyanpourRad, M. KianiNeyestani, M. T. Jamal-Abad, *Renewable Energy* **2014**, *71*, 658–664.
[30] H. H. Huang, F. Q. Yan, Y. M. Kek, C. H. Chew, G. Q. Xu, W. Ji, P. S. Oh, S. H. Tang, *Langmuir* **1997**, *13*, 172–175.

[31] Y. Wang, T. Asefa, *Langmuir* **2010**, *26*, 7469–7474.
[32] Y. Wang, P. Chen, M. Liu, *Nanotechnology* **2006**, *17*, 6000–6006.
[33] V. Engels, F. Benaskar, D. A. Jefferson, B. F. G.Johnson, A. E.H. Wheatley, *Dalton Trans.* **2010**, *39*, 6496–6502.
[34] B. Bozzini, L. D'Urzo, M. Re, F. Riccardis, *J. Appl. Electrochem.* **2008**, *38*, 1561–1569.
[35] S. Wu, D. J. Chen, *Colloid Interface Sci.* **2004**, *273*, 165–169.
[36] J. L. C. Huaman, K. Sato, S. Kurita, T. Matsumoto, B. Jeyadevan, *J. Mater. Chem.* **2011**, *21*, 7062–7069.
[37] H. Lu, L. Yu, B. Yang, J. Si, J. Du, *RSC Adv.* **2014**, *4*, 14193–14196.
[38] I. Lisiecki, M. Bjoerling, L. Motte, B. Ninham, M. P. Pileni, *Langmuir* **1995**, *11*, 2385–2392.
[39] C. Vollmer, C. Janiak, *Coord. Chemistry Reviews* **2011**, *255*, 2039–2057.
[40] G. S. Fonseca, A. P. Umpierre, P. F. P. Fichtner, S. R. Teixeira, J. Dupont, *Chem. Eur. J.* **2003**, *9*, 3263–3269.
[41] C. Janiak, *Z. Naturforsch.* **2013**, *68b*, 1059–1089.
[42] C. Janiak, *Metal Nanoparticle Synthesis in Ionic Liquids, in Ionic Liquids (ILs) in Organometallic / Topics in Organometallic Chemistry*, *Vol. 51* (Eds. J. Dupont, L. Kollar), Springer, Heidelberg, **2015**, pp. 17–53.
[43] C. Janiak, *Metal Nanoparticle Synthesis in Ionic Liquids, in Catalysis in Ionic Liquids: From Catalyst Synthesis to Application*, *Chapter 11* (Eds. C. Hardacre, V. Parvulescu), RSC Publishing, Cambridge, **2014**, pp. 537–577.
[44] K. Schütte, A. Doddi, C. Kroll, H. Meyer, C. Wiktor, C. Gemel, G. van Tendeloo, R. A. Fischer, C. Janiak, *Nanoscale* **2014**, *6*, 5532–5544.
[45] a) R. Marcos Esteban, K. Schütte, P. Brandt, D. Marquardt, H. Meyer, F. Beckert, R. Mülhaupt, H. Kölling, C. Janiak, *Nano-Struct. & Nano-Objects* **2015**, *1*, XX–XX http://dx.doi.org/10.1016/j.nanoso.2015.07.001; b) K. Schütte, H. Meyer, C. Gemel, J. Barthel, R. A. Fischer, C. Janiak, *Nanoscale* **2014**, *6*, 3116–3126; c) E. Redel, J. Krämer, R. Thomann, C. Janiak, *J. Organomet. Chem.* **2009**, *694*, 1069–1075.
[46] a) E. Ahmed, J. Breternitz, M. F. Groh and M. Ruck, *CrystEngComm.* **2012**, *14*, 4874–4885; b) E. Ahmed, M. Ruck, *Dalton Trans.* **2011**, *40*, 9347–9357; c) M. F. Groh, U. Müller, E. Ahmed, A. Rothenberger, M. Ruck, *Z. Naturforsch.* **2013**, *68b*, 1108–1122
[47] P. Wasserscheid, W. Keim, *Angew. Chem. Int. Ed.* **2000**, *39*, 3773–3789.
[48] J. Krämer, E. Redel, R. Thomann, C. Janiak, *Organometallics* **2008**, *27*, 1976–1978.
[49] J. Dupont, J. D. Scholten, *Chem. Soc. Rev.* **2010**, *39*, 1780–1804.
[50] J. Dupont, *J. Brazil Chem. Soc.* **2004**, *15*, 341–350.
[51] M.- A. Neouze, *J. Mater. Chem.* **2010**, *20*, 9593–9607.
[52] C. S. Consorti, P. A. Z. Suarez, R. F. de Souza, R. A. Burrow, D. H.Farrar, A. J. Lough, W. Loh, L. H. M. da Silva , J. Dupont, *J. Phys. Chem. B* **2005**, *109*, 4341–4349.
[53] J. Dupont, P. A. Z. Suarez, R. F. de Souza, R. A. Burrow, J.- P. Kintzinger, *Chem. Eur. J.* **2000**, *6*, 2377–2381.
[54] P. Wasserscheid, W. Keim, *Angew. Chem. Int. Ed.* **2000**, *39*, 3773–3789.
[55] L. Taubert, Z. Li, *Dalton Trans* **2007**, 723–727.
[56] a) C. Vollmer, E. Redel, K. Abu-Shandi, R. Thomann, H. Manyar ,H. Hardacre, *Chem Eur J.* **2010**, *16*, 3849–3858; b) K. Klauke, B. Hahn, K. Schütte, J. Barthel, C. Janiak, *Nano-Struct. & Nano-Objects* **2005**, *1*, 24–31.
[57] B. Schäffner, F. Schäffner, S. P. Verevkin, A. Börner, *Chem. Rev.* **2010**, *110*, 4554–4581.
[58] J. Bayardon, J. Holz, B. Schäffner, V. Andrushko, S. Verevkin, A. Preetz, A. Börner, *Angew. Chem. Int. Ed.* **2007**, *46*, 5971–5974.
[59] S. P. Verevkin, V. N. Emel'yanenko, A. V. Toktonov, Y. Chernyak, B. Schäffner, A. Börner, *J. Chem. Thermodyn.* **2008**, *40*, 1428–1432.
[60] B. Schäffner, S. P. Verevkin, A. Börner, *Chem. Unserer Zeit* **2009**, *43*, 12–21.
[61] a) R. Marcos Esteban, K. Schütte, D. Marquardt, J. Barthel, F. Beckert, R. Mülhaupt, C. Janiak, *Nano-Struct. & Nano-Objects* **2015**, *1*, XX–XX http://dx.doi.org/10.1016/j.nanoso.2015.07.002; b) C. Vollmer, C. Janiak, *Dalton Trans.* **2012**, *41*, 9722–9727.
[62] A. A. Ponce, K. J. Klabunde, *J. Molecular Catalysis A: Chemical* **2005**, *225*, 1–6.
[63] M. Brettholle, O. Höfft, L. Klarhöfer, S. Mathes, W. Maus-Friedrichs, S. Zein El Abedina, S. Krischok, J. Janek, F. Endres, *Phys. Chem. Chem. Phys.* **2010**, *12*, 1750–1755.
[64] N. Kulbe1, O. Höff, A. Ulbrich,S. Zein El Abedin, S. Krischok, J. Janek, M. Pölleth, F. Endres, *Plasma Processes and Polymers* **2011**, *8*, 32–37.
[65] T.- Y. Chen, S.- F. Chen, H.- S. Sheu, C.- S. Yeh, *J. Phys. Chem. B* **2002**, *106*, 9717–9722.
[66] J. N. Solanki, R. Sengupta, Z. V. P. Murthy, *Solid State Sciences* **2010**, *12*, 1560–1566.
[67] L. M. Qi, J. M. Ma, J. L. Shen, *J. Colloid Interface Sci.* **1997**, *186*, 498–500.
[68] V. Engels, F. Benaskar, D. A. Jefferson, B. F. G. Johnson, A. E. H. Wheatley, *Dalton Trans.* **2010**, *39*, 6496–6502.
[69] P. Christian, M. Bromfield, *J. Mater. Chem.* **2010**, *20*, 1135–1139.
[70] P. Arquilliere, P. H. Haumesser, C. C. Santini, *Microelectronic Engineering* **2012**, *92*, 149–151.
[71] B. Mohan, H. Woo, S. Jang, S. Lee, S. Park, K. H. Park, *Solid State Sciences* **2013**, *22*, 16–20.
[72] S.- K. Li, X. Guo, Y. Wang, F.- Z. Huang, Y.- H. Shen, X.- M. Wang, A.- J. Xie, *Dalton Trans.* **2011**, *40*, 6745–6750.
[73] P. Singh, A. Katyal, R. Kalra, R. Chandra, *Tetrahedron Letters* **2008**, *49*, 727–730.
[74] P. Singh, A. Katyal, R. Kalra, R. Chandra, *Catalysis Communications* **2008**, *9*, 1618–1623.
[75] D. Mott, J. Galkowski, L. Wang, J. Luo, C. J. Zhong, *Langmuir* **2007**, *23*, 5740–5745.
[76] A. Umer, S. Naveed, N. Ramzan, M. S.Rafique, *NANO* **2015**, *7*, 1230005-1/ 1230005-18; DOI: 10.1142/S1793292012300058
[77] S. C. Goel, K. S. Kramer, M. Y. Chiang, W. E. Buhro, *Polyhedron* **1990**, *9*, 611.
[78] R. Becker, J. Weiß, M. Winter, K. Merz, A. Fischer, *Journal of Organometallic Chemistry* **2001**, *630*, 253–262.
[79] V. L. Young, D. F. Cox, M. E. Davis, *Chem. Mater.* **1993**, *5*, 1701–1709.
[80] M. T. Keßler, C. Gedig, S. Sahler, P. Wand, S. Robke, M. H. G. Prechtl, *Catal. Sci. Technol.* **2013**, *3*, 992–1001.
[81] C.- H. Kuo, C.- H. Chen, M. H. Huang, *Adv. Funct. Mater.* **2007**, *17*, 3773–3780.
[82] P. Scherrer, N. G. W. Gottingen, *Math-Pys. Kl.* **1918**, *2*, 96–100.

Supporting Information (SI)

Comparative synthesis of Cu and Cu_2O nanoparticles from different copper precursors in ionic liquid and propylene carbonate

Raquel Marcos Esteban,[a] Hajo Meyer,[a] Jiyeon Kim, [b]Christian Gemel,[b] Roland A. Fischer,[b]* and Christoph Janiak[a]*

a Institut für Anorganische Chemie und Strukturchemie, Heinrich Heine Universität Düsseldorf, 40204 Düsseldorf. E-mail: janiak@uni-duesseldorf.de; Fax:+49-211-81-12287; Tel: +49-211-81-12286.

b Lehrstuhl Anorganische Chemie, II– Organometallics & Metallics, Ruhr-Universität Bochum, NC 2, Universitätsstr. 150, 44801 Bochum, Germany. E-mail: roland.fischer@rub.de; Fax: +49-234-32-14174; Tel: +49-234-32-24174

E-mail:

Raquel Marcos Esteban: raquel.marcos.esteban@hhu.de

Hajo Meyer: hajo.meyer@hhu.de

Jiyeon Kim: jiyeon.kim@rub.de

Christian Gemel: christian.gemel@rub.de

Roland A. Fischer: roland.fischer@rub.de

Christoph Janiak: janiak@hhu.de

1. Synthesis of Cu-NPs in propylene carbonate and [BMIm][BF_4].

1.1 $Cu(BF_4)_2$ with 1-butylimidazole in PC.

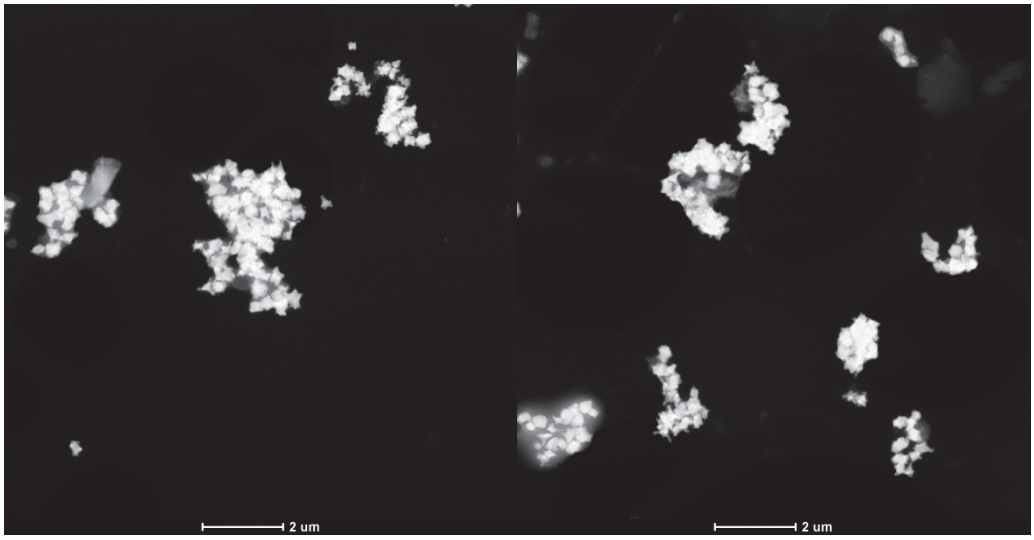

Fig. S 4 HAADF-STEM images of Cu-NPs synthetized in PC with 1-butylimidazole.

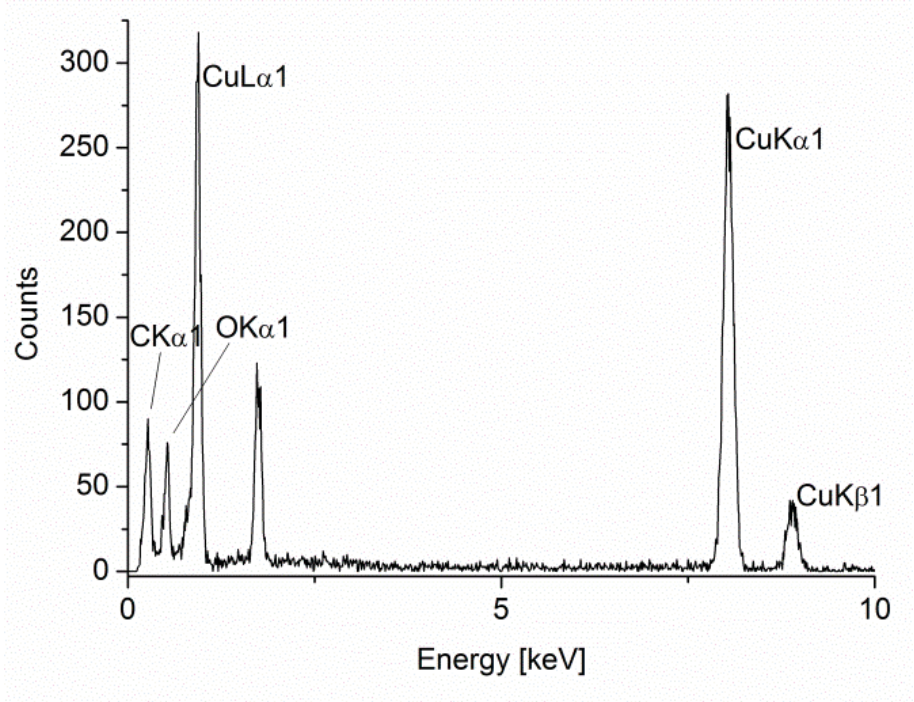

Fig. S 5 EDX of Cu-NPs in PC with 1-butylimidazole.

1.2 $Cu(BF_4)_2$ without 1-butylimidazole in PC.

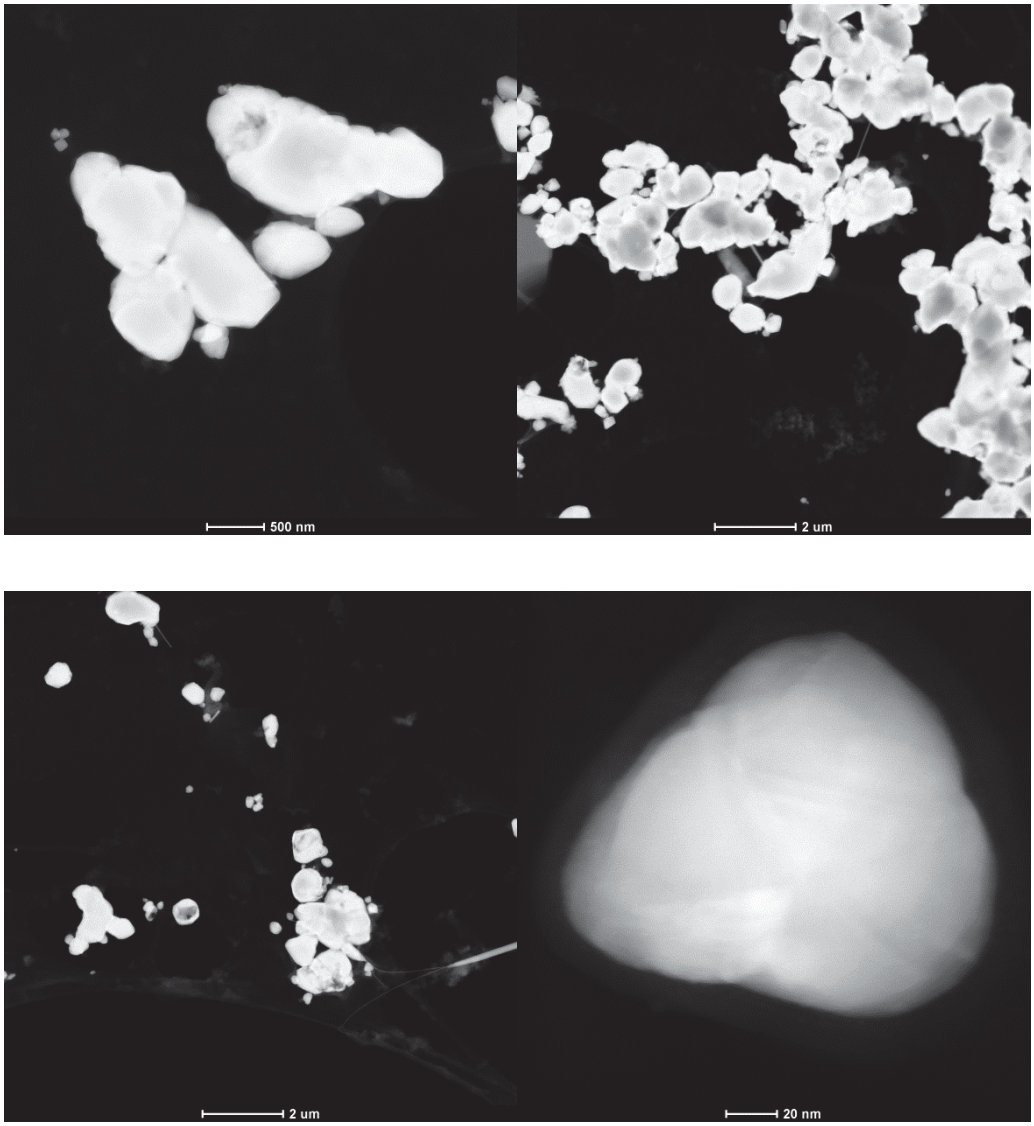

Fig. S 6 HAADF-STEM images of Cu-particles from $Cu(BF_4)_2$ in PC.

1.3 $Cu(dmap)_2$ $\{Cu(OCH(Me)CH_2NMe_2)_2\}$ in PC.

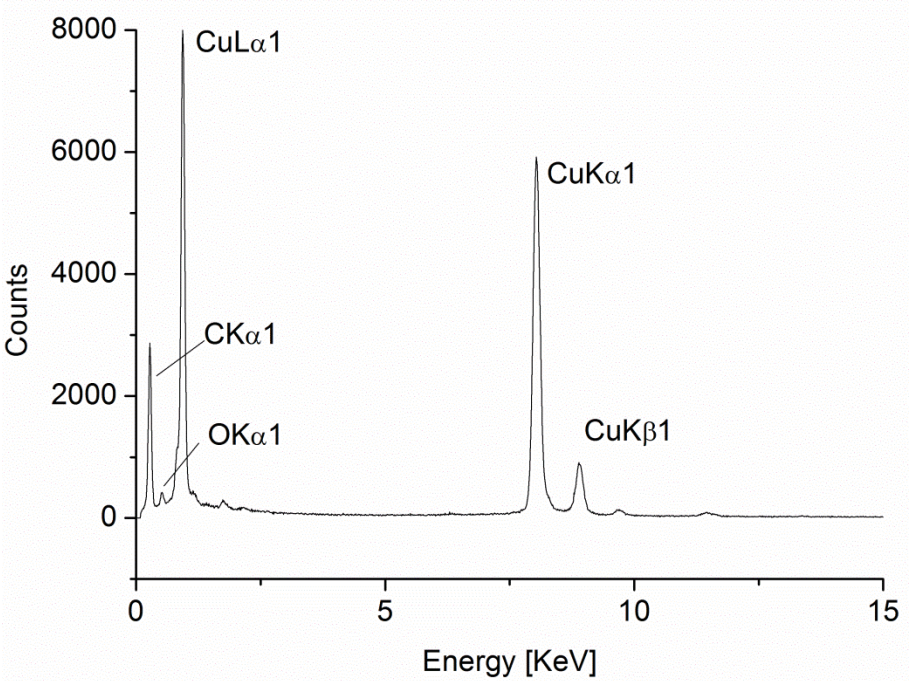

Fig. S 7 EDX of Cu-NPs from the decomposition of $Cu(dmap)_2$ by microwave irradiation in propylene carbonate.

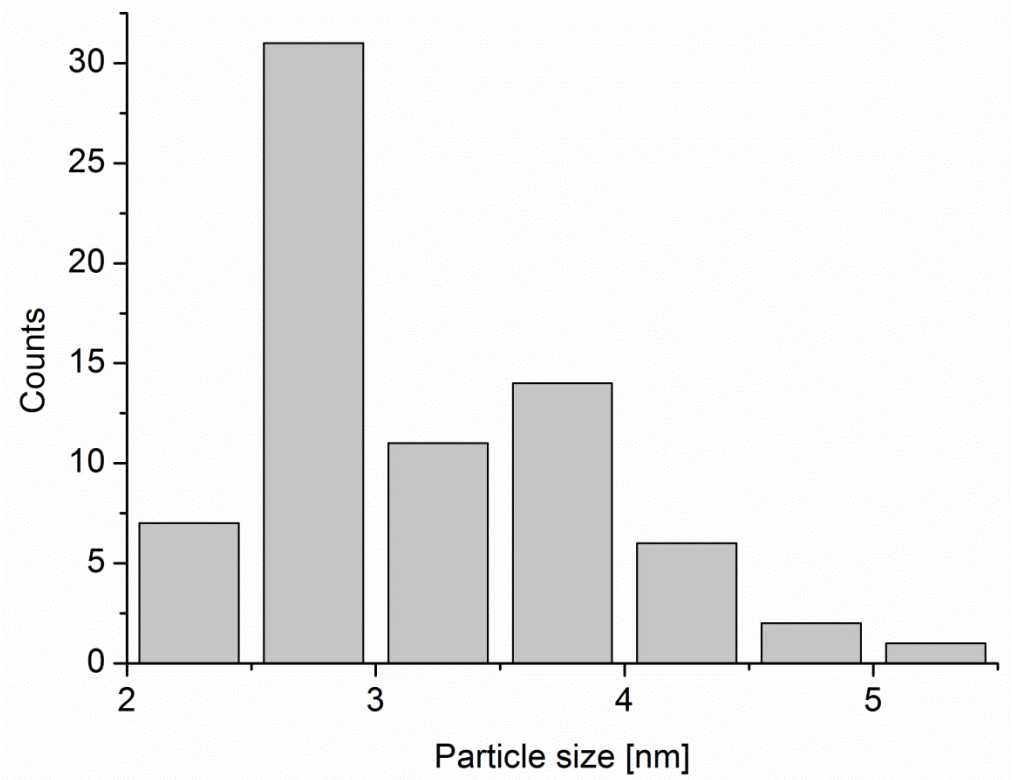

Fig. S 8 Histogram of Cu-NPs obtained from the decomposition of $Cu(dmap)_2$ by microwave irradiation with a size distribution of 3.1 ± 0.7 nm from 72 selected nanoparticles in the 10 nm scale image (Fig. 8-top right). The nanoparticles were measured manually.

1.4 $Cu(dmap)_2$ {$Cu(OCH(Me)CH_2NMe_2)_2$} in [BMIm][BF_4].

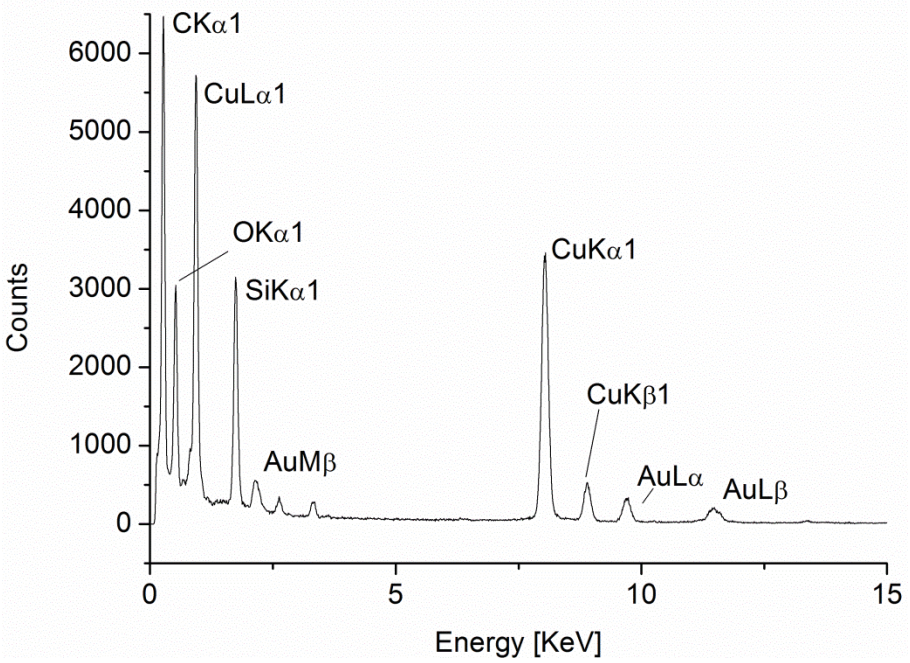

Fig. S 9 EDX of Cu-NPs from the decomposition of $Cu(dmap)_2$ by microwave irradiation in IL.

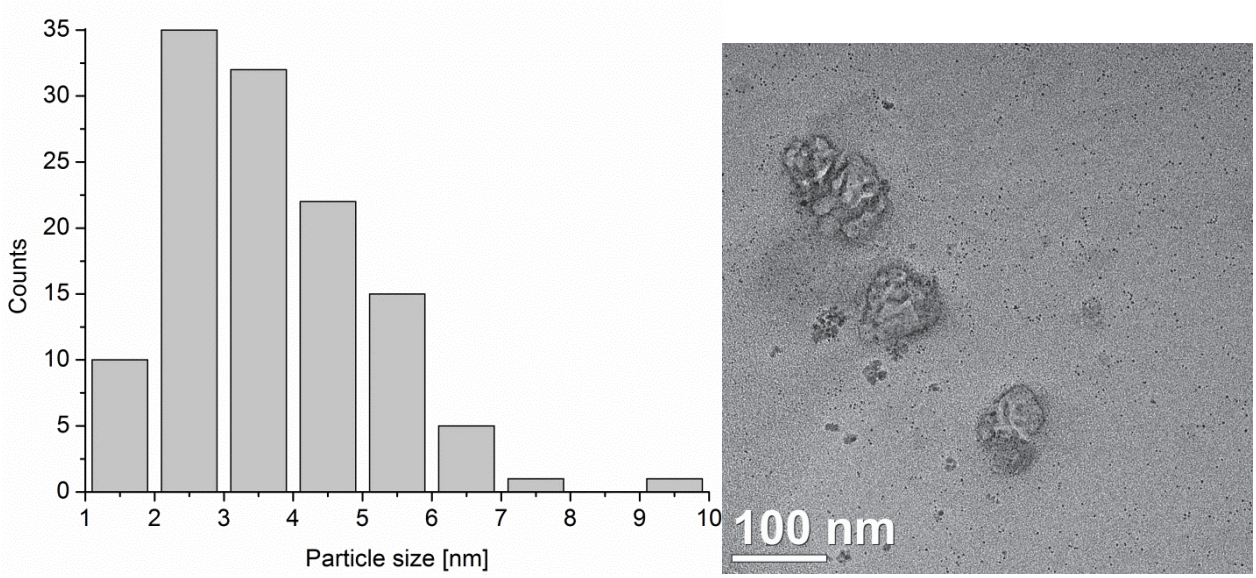

Fig. S 10 Histogram of Cu-NPs from the decomposition of $Cu(dmap)_2$ by microwave irradiation in [BMIm][BF_4]. The nanoparticles have a size distribution of 3.7 ± 1.4 nm calculated from 121 nanoparticles by the software Digital micrograph (Gatan).

2. Synthesis of Cu-NPs from $Cu(acac)_2$ in the ionic liquid $[BMIm][BF_4]$.

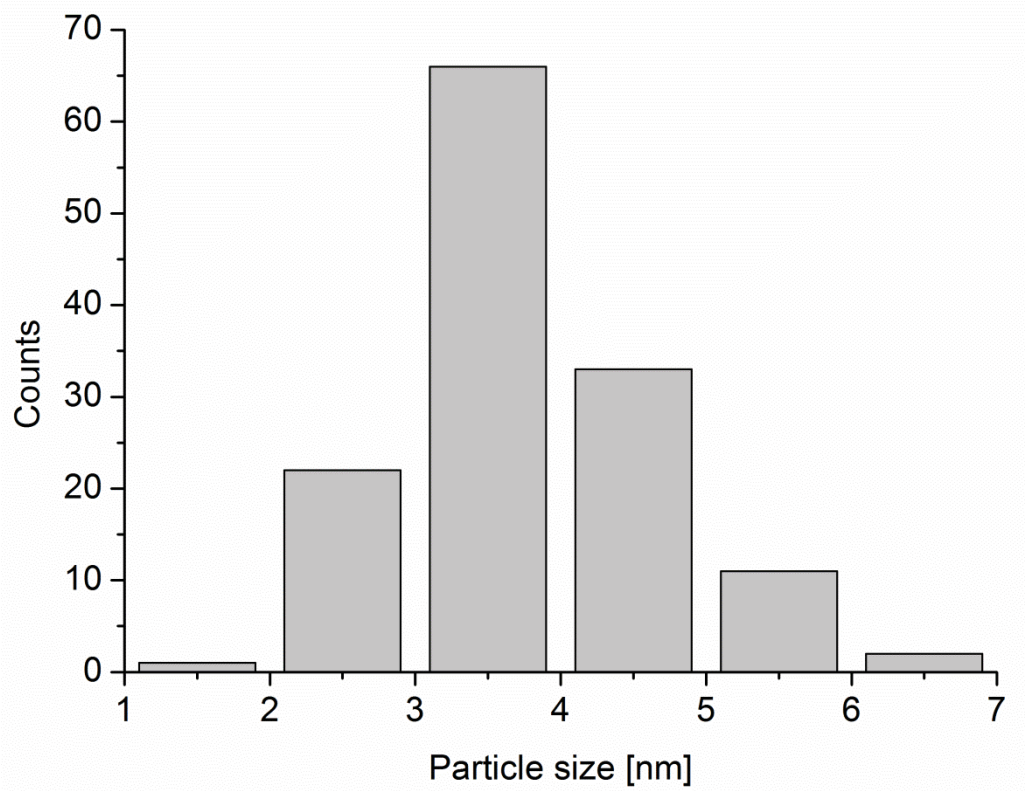

Fig. S 11 Histogram of Cu-NPs from the decomposition of $Cu(acac)_2$ by microwave irradiation in $[BMIm][BF_4]$ with a size of 3.3 ± 0.9 nm from 135 manually selected nanoparticles from the TEM image with the 20 nm scale (Fig 9-left).

3. Synthesis of Cu_2O-NCs from $Cu(AcO)_2$ H_2O in ionic liquid, [BMIm][BF_4].

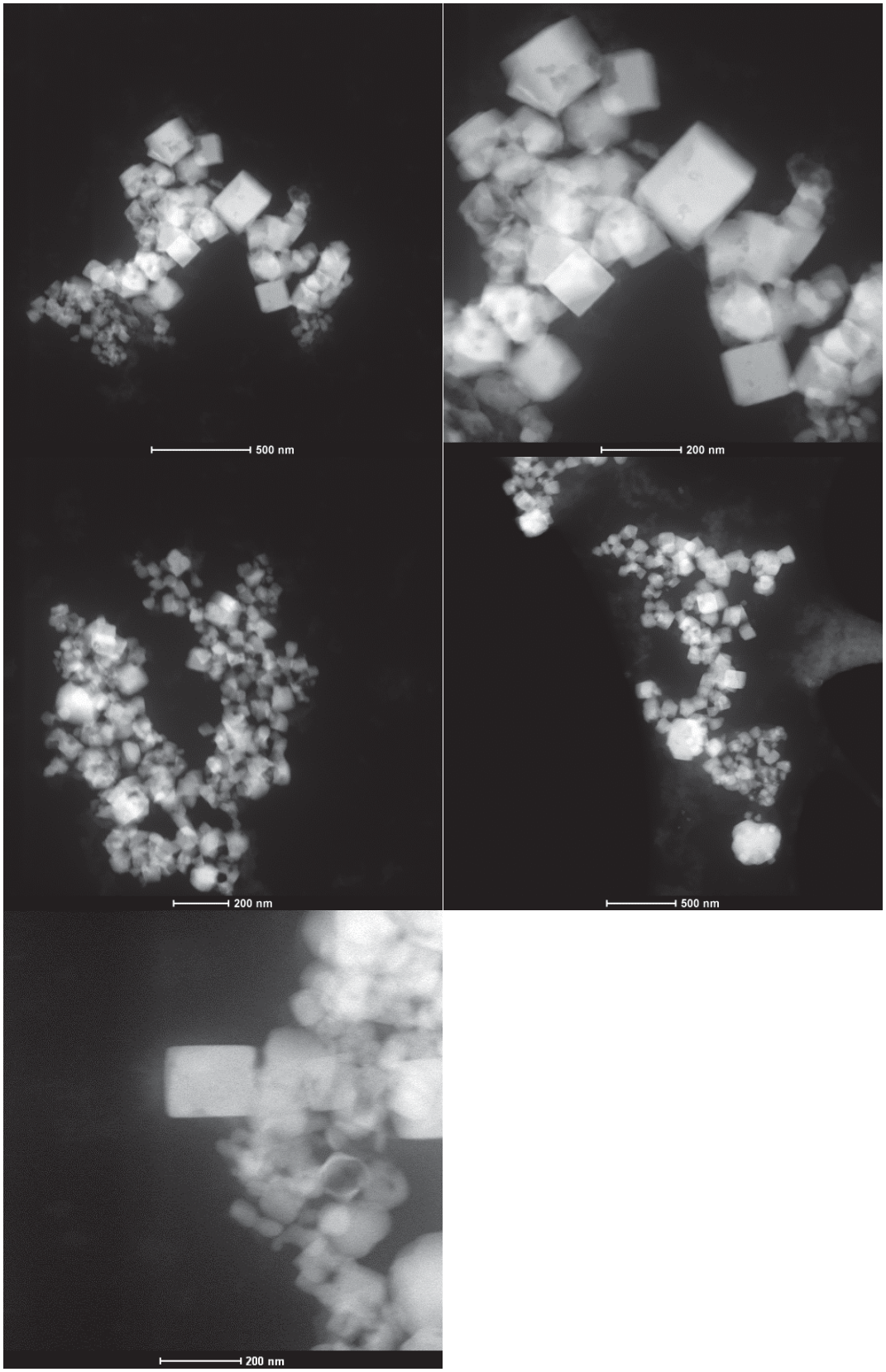

Fig. S 12 HAADF -STEM images of Cu_2O-NCs from $Cu(AcO)_2 \cdot H_2O$ by MWI in [BMIm][BF_4].

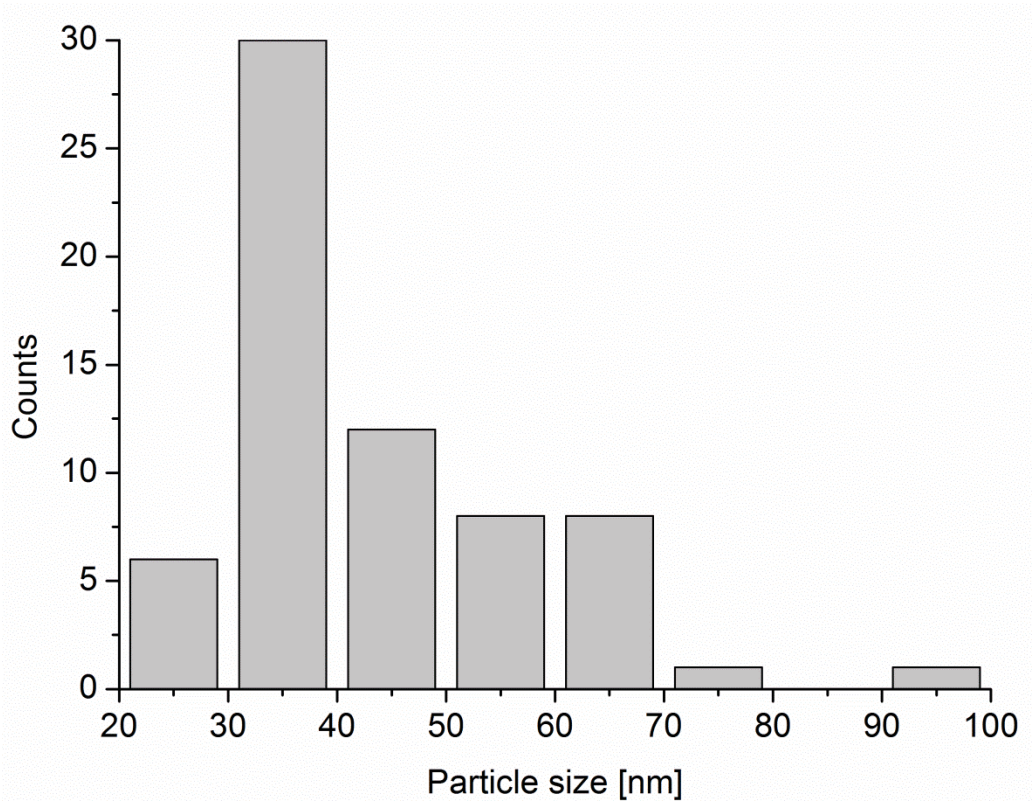

Fig. S 13 Histogram of Cu_2O-nanocubes from $Cu(AcO)_2 \cdot H_2O$ by MWI in [BMIm][BF_4] with a size distribution of 43 ± 15 nm from 66 selected nanoparticles related to the Fig.12-left with the 200 nm scale.

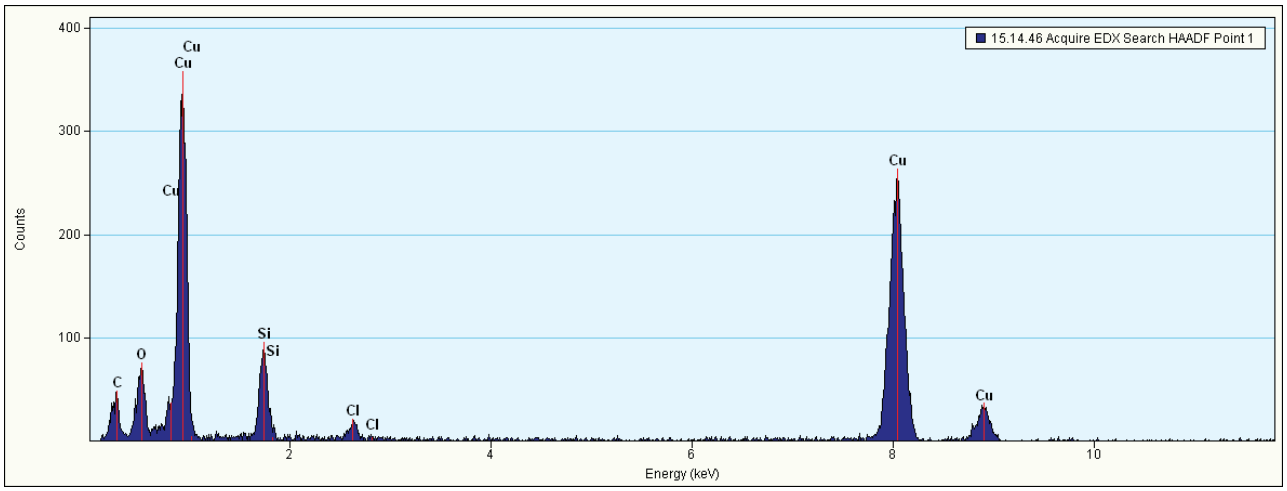

Fig. S 14 EDX of Cu_2O-NCs from $Cu(AcO)_2 \cdot H_2O$ by MWI in [BMIm][BF_4].

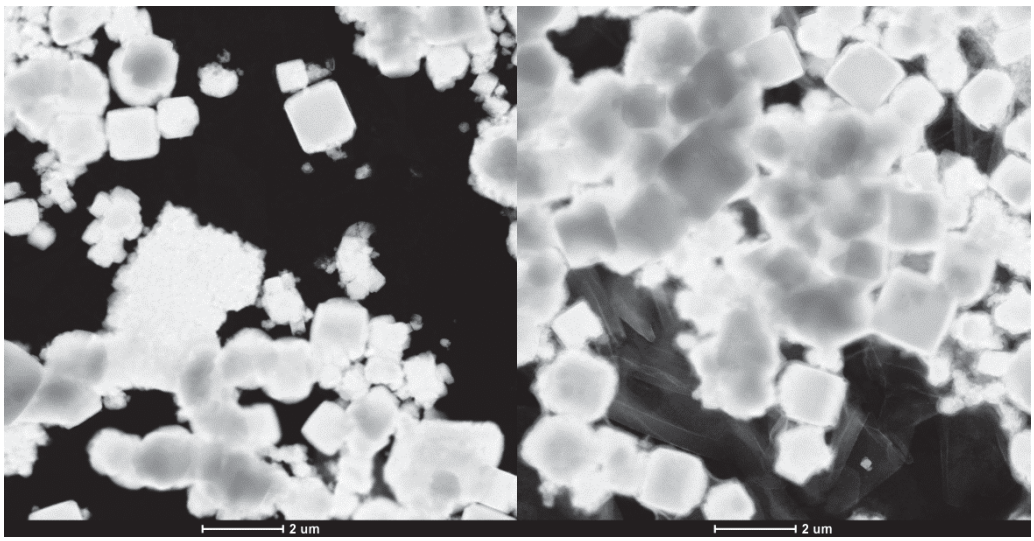

Fig. S 15 HAADF-STEM of Cu_2O-NCs from $Cu(AcO)_2 \cdot H_2O$ by MWI in $[BMIm][BF_4]$ after washing with acetonitrile.

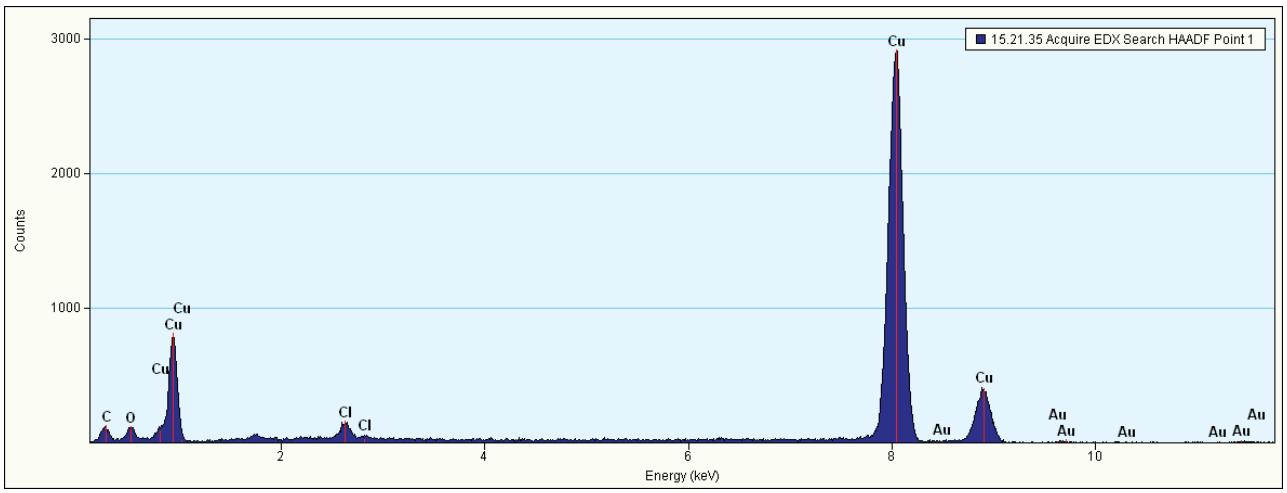

Fig. S 16 EDX of Cu_2O-NCs from $Cu(AcO)_2 \cdot H_2O$ by MWI in $[BMIm][BF_4]$ after washing with acetonitrile.

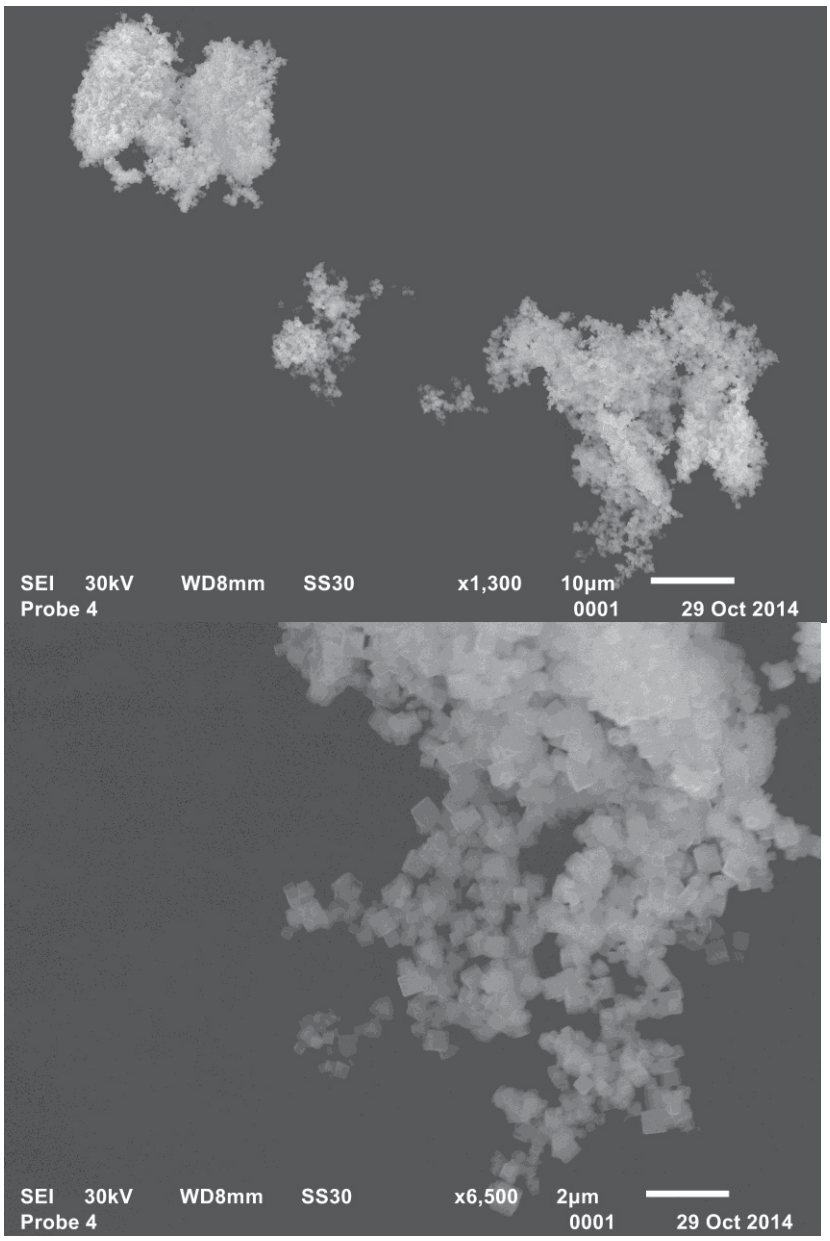

Fig. S 17 SEM micrographs of Cu_2O-nanocubes from $Cu(AcO)_2 \cdot H_2O$ by MWI in [BMIm][BF_4] after washing with acetonitrile. Images taken on Jeol JSM 6510.

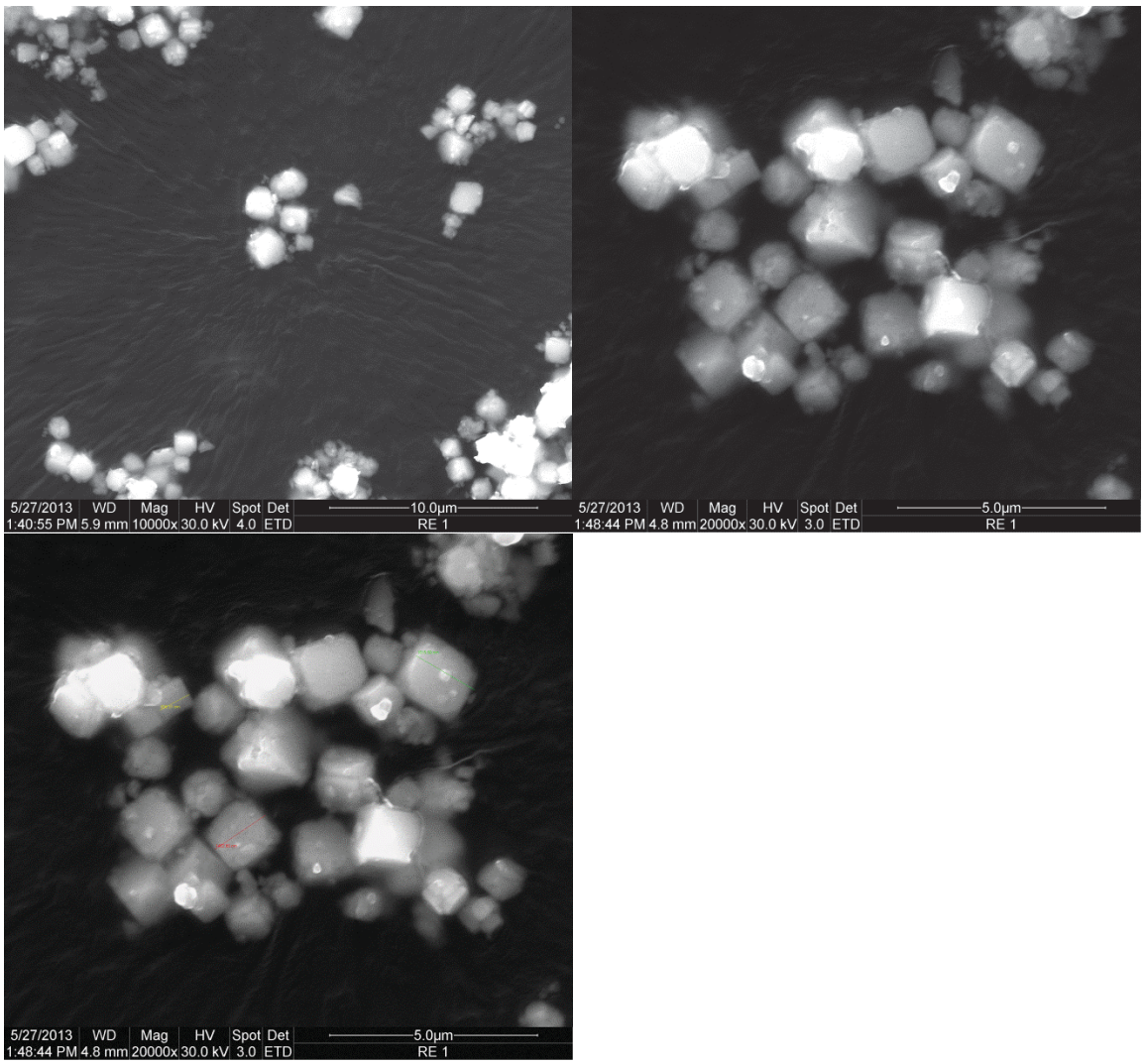

Fig. S 18 SEM micrographs of Cu_2O-NCs from $Cu(AcO)_2 \cdot H_2O$ by MWI in [BMIm][BF_4] after washing with acetonitrile. Images takes on ESEM Quanta 400 FEG SEM equipped with a secondary electron (SE) detector and operated at 20 keV.

4. Unpublished work

In this section are described the unpublished results, which were also done during the doctoral thesis from January 2012 until November 2015.

Iridium@graphene nanomaterials and their application as a catalyst.

In the section 3.1 was already discussed the synthesis and deposition of iridium nanoparticles on thermally reduced graphite oxide (Ir@TRGO) in 1-butyl-3-methylimidazolium tetrafluoroborate ([BMIm][BF_4]) by decomposition of the corresponding metal carbonyl, $Ir_4(CO)_{12}$, by the energy-saving microwave irradiation.

In the following sections are described the synthesis of Ir@TRGO nanomaterials in propylene carbonate, and the used of the already characterized Ir@TRGO nanomaterials (section 3.1) as catalyst for the hydrogenation of levulinic acid to γ-valerolactone.

4.1 Iridium@graphene nanomaterials in propylene carbonate

The synthesis of Ir@TRGO nanomaterials in ionic liquids achieved small Ir-NPs and narrow size distributions of 1.0 ± 0.4 and 2.7 ± 0.7 nm by the microwave decomposition of $Ir_4(CO)_{12}$.[85] However, the use of ionic liquids is expensive. An alternative to ILs are organic carbonates, which in comparison to ILs are commercially available and cheaper. Propylene carbonate (PC) is an aprotic and dipolar solvent with a low (eco-) toxicity, low volatility and flammability, and with a wide liquid temperature range (mp –49 ºC, bp 243 ºC). M-NPs/PC dispersions were also reported, as well as the synthesis of Ru@TRGO nanomaterials in PC (see section 3.2).[49,50]

Here is described an attempt for the deposition of Ir-NPs on TRGO using PC as a solvent. The tetrairidium dodecarbonyl, $Ir_4(CO)_{12}$, was suspended together with TRGO in propylene carbonate and the thermal decomposition was done by the energy-saving microwave input (250 ºC, 50 W). The residual CO was removed under vacuum and the black powder, "Ir@TRGO/PC" was washed, centrifuged and dried for their further characterization.

The composition and phase purity of the Ir@TRGO nanomaterials was analyzed by powder X-ray diffraction (PXRD) (Fig. 26). As in Fig. 26 shows, the characteristic reflexes corresponding to the Ir-bulk materials are not visible in the PXRD diffractogram (red bars, Fig. 26), indicating a non-crystalline structure of the nanomaterials.

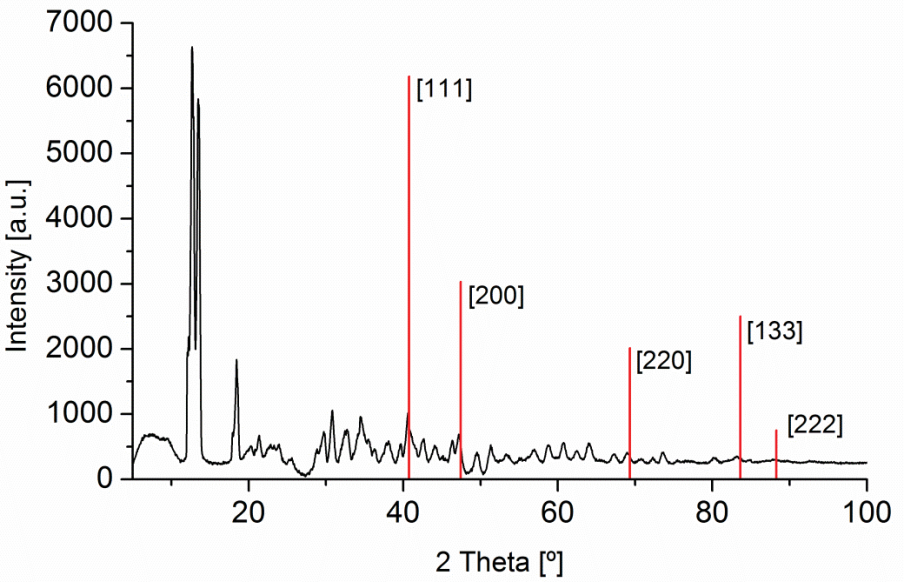

Fig. 26 PXRD of Ir@TRGO nanomaterials synthetized in propylene carbonate by means of microwave decomposition in comparison with the Ir pattern (red bars, COD 9008470)

The “Ir@TRGO” nanomaterials were also measured by transmission electron microscopy (TEM) and non-defined Ir-NPs were found, and just dispersed Ir-NPs with a size average of about 5-10 nm were founded (Fig. 27).

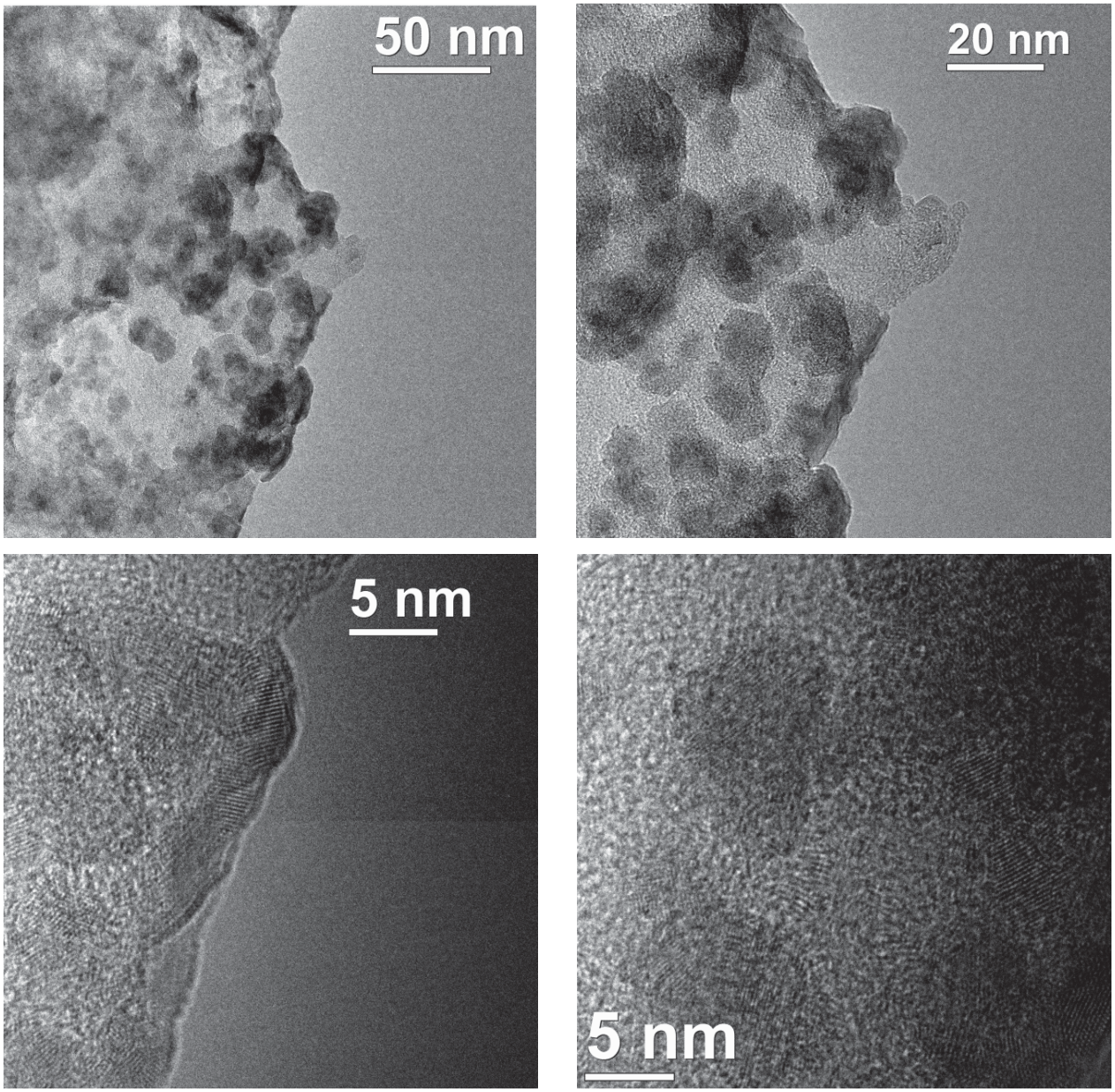

Fig. 27 TEM images of Ir@TRGO nanomaterials synthetized in propylene carbonate.

The synthesis of Ir@TRGO nanomaterials was not successfully achieved in comparison with the synthesis in ionic liquids. Propylene carbonate is a suitable solvent for microwave reactions and for the synthesis of M-NPs, but their weekly coordinative properties might not be enough to help in the nucleation, growth and formation of Ir-NPs.

4.2 Hydrogenation of levulinic acid with Ir@TRGO nanomaterials.

The levulinic acid (LA) is one of the products obtained from the biomass-derived lignocellulose. LA can be upgraded by hydrogenation reactions to different products such as γ-valerolactone (GVL), valeric fuels, pentanoic acid (PA), 5-nonanone or methyltetrahydrofuran (MTHF).[284,285,289]

The described Ir@TRGO nanomaterials in the section 3.1 were synthetized in [BMIm][BF_4], synthesis which yielded to a size distribution of 2.7 ± 0.7 nm after the microwave decomposition of $Ir_4(CO)_{12}$. Here, we tested the Ir@TRGO as a catalyst for the hydrogenation of levulinic acid to γ-valerolactone (Scheme 5). The hydrogenation reaction of LA involves not only the hydrogenation of C=C bonds but also the C=O groups should be hydrogenated. Ir@TRGO nanomaterials were synthetized with the same procedure as explain in the section 3.1 and characterized by TEM, which gives a size distribution of 2.7 ± 0.7 nm (Fig. 28, for IR, PXRD, Histograms and EDX see Appendix 7.1).

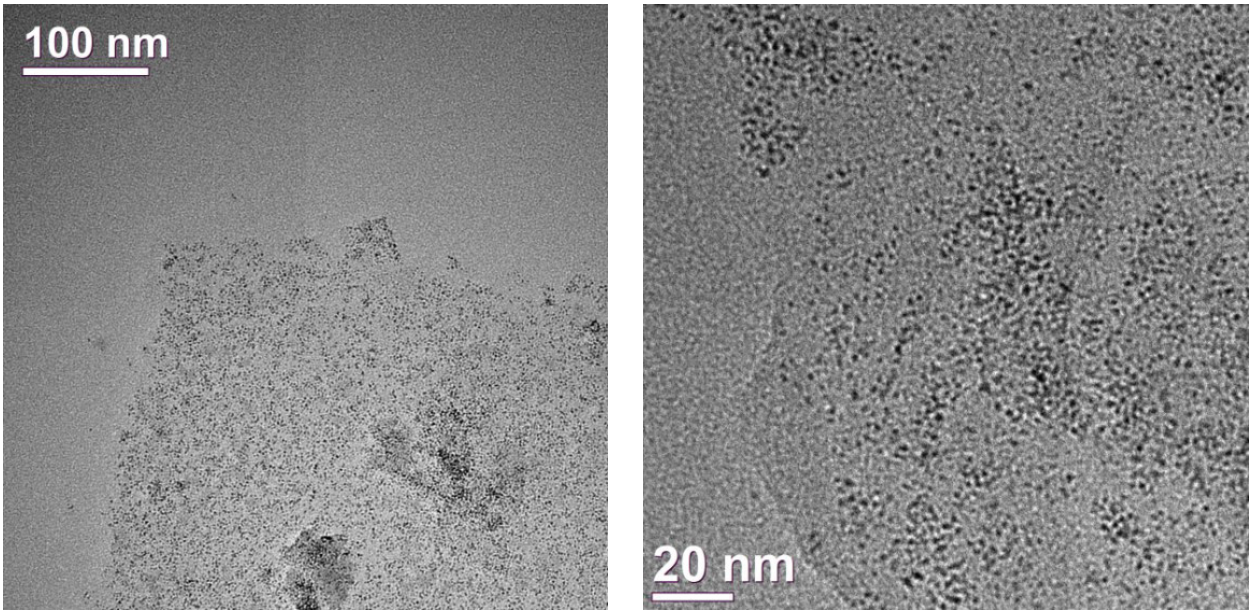

Fig. 28 TEM images of Ir@TRGO nanomaterials synthetized in [BMIm][BF_4] under microwave irradiation, with a size distribution of 2.7 ± 0.7 nm for 242 selected nanoparticles.

All catalytic reactions were done using a stainless-steel autoclave provided with a glass inlay to avoid any interference of the steel surface. The autoclave was re-filled three times with H_2 before to charge it to the H_2 pressure.

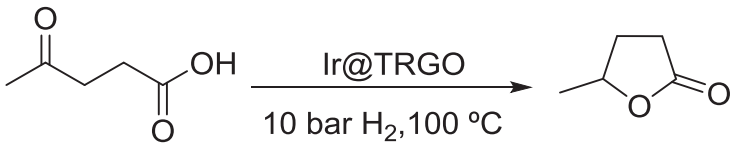

Levulinic acid (LA) — g-Valerolactone (GVL)

Scheme 5 Hydrogenation of Levulinic acid (LA) to g-Valerolactone (GVL).

The Ir@TRGO catalyst (5 mg, 3.6 % Ir, 0.18 mg, 9.36 x 10^{-4} mmol Ir, molar ratio 1998) was placed together with the desired amount of LA (0.22 g, 1.87 mmol, 191 μL, 116.11 g/mol, 1.14 g/mL) in the autoclave. The autoclave was heated to 100 ºC, charged with 10 bars of H_2 and stirred (800 rpm) for 3 h and the reaction was carried under solvent–free conditions. Once the time was consumed the autoclave was cooled down, and the products were separated by centrifugation. The catalyst could be recovered after washing with MeOH (3 x1 mL), and used for 4 consecutive hydrogenation runs (Table 3).

Table 3 Hydrogenation of levulinic acid to γ-valerolactone using Ir@TRGO nanomaterials under solvent-free conditions.[a]

Catalyst	Conversion[%][d]	TON[e]	TOF [h^{-1}][f]
$Ir_4(CO)_{12}$[b]	-	-	-
Ir@TRGO[c]			
run 1	55.1	370	1100
run 2	57.1	380	1140
run 3	71.3	408	1430
run 4	38.4	260	770

[a] The hydrogenation of LA was done by 100ºC, 10 bar H_2, 3 h and 800 rpm; [b] a blind experiment was done to verify the no catalytic activity of the precursor for the synthesis of Ir-NPs; [c] molar ratio = mol levulinic acid / mol Ir = 1998; [d] determined by GC; [e] Turn over number, TON=(mol GVL)/(mol Ir); [f] turn over frequency, TOF= (mol GVL) x (mol Ir) $^{-1}h^{-1}$

The analysis of the products by GC shows GVL as main product for the hydrogenation of LA without the presence of other intermediates. The highest conversion was reached up in the third run with a TOF of 1430 h^{-1}. During the thermally hydrogenation reactions, the surface of the Ir@TRGO nanomaterials is sputtered from CO traces proceeding from the starting material, $Ir_4(CO)_{12}$, and this exfoliation can generate more active centers on the surface, which might explains the increase on the activity in the first third runs (Fig. 29), but the consecutive re-use, washing procedure and traces of subtrates or products might also deactivate the Ir-NPs centers, which a decrease in the activity (Fig. 29).

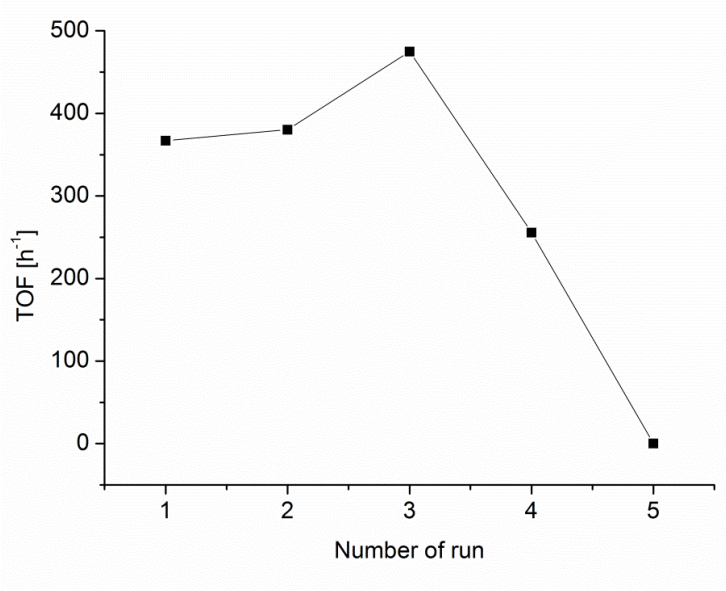

Fig. 29 Turn over frequency [(mol GVL) x (mol Ir)$^{-1}$ x h^{-1}] over the number of run for the hydrogenation of levulinic acid with Ir@TRGO nanomaterials (100ºC, 10 bar H_2, 3h).

Ir@TRGO nanomaterials were analyzed by TEM to give a size distribution of 7.8 ± 4.4 nm (Fig. 30) (for histograms and EDX see Appendix 7.1). The definition on the shape and form of Ir-NPs after the catalysis is not well defined, a possible effect due to of the several washing procedure and the traces from the substrates or products.

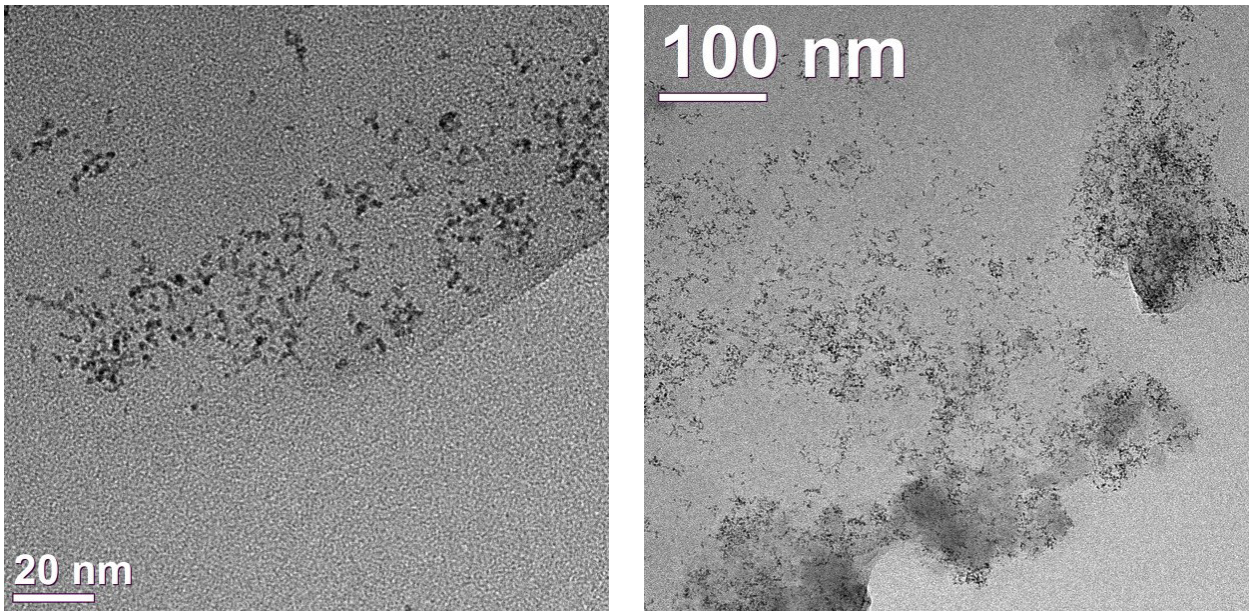

Fig. 30 TEM images of Ir@TRGO nanomaterials after five runs of hydrogenation of levulinic acid to γ-valerolactone with a size distribution of 7.8 ± 4.4 nm from 109 nanoparticles (for histogram see Appendix 7.1).

Ir@TRGO nanomaterials were characterized by IR after the first and third hydrogenation run. Typical -CO bands from the starting material $Ir_4(CO)_{12}$ (at 2021 and 2058 cm^{-1}) can be observed in the fresh Ir@TRGO nanomaterials with a slightly decreased after their use in the hydrogenation reactions. PXRD patterns of Ir@TRGO after catalysis showed the typical peaks for iridium at the 2θ values 40.7 º, 47.7 º, 69.4 º and 83.5 º corresponding with the respectively planes [111], [200], [220] and [331] (Fig. 32).

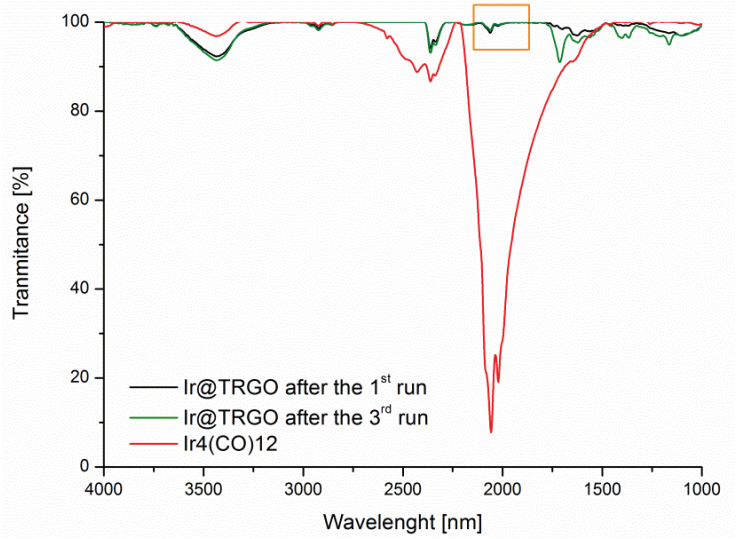

Fig. 31 IR spectra of used Ir@TRGO nanomaterials after the first (black) and third (green) hydrogenation runs for the hydrogenation of levulinic acid to γ-valerolactone in comparison with the starter material $Ir_4(CO)_{12}$ (red).

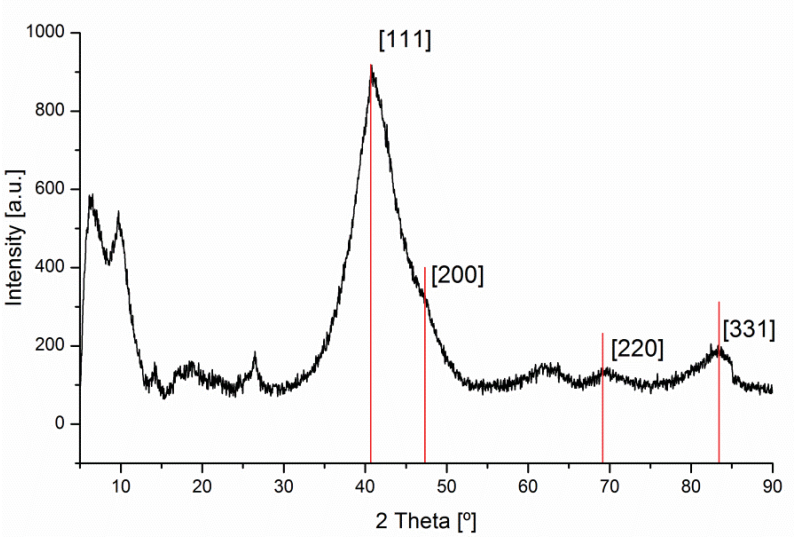

Fig. 32 PXRD of Ir@TRGO nanomaterials after five runs of hydrogenation of levulinic acid to γ-valerolactone at 100ºC, 10 bars H_2 and 3 hours.

In the literature have been reported different catalyst and conditions for the hydrogenation of levulinic acid (Table 4). *Fu et al.* described the used of iridium–pincer complexes, in which the selection of the stronger electron-donating substituents has an influence in the selectivity and activity in the hydrogenation of LA, being the metoxy-substituents which achieves the higher TOF of 78000 h^{-1} at 120 ºC and 20 bar H_2 in aqueous solutions.[311] *Weckhuysen et al.* observed the effect on the character of the support (TiO_2, Nb_2O_3, H-β and H-ZSM5) for ruthenium-based catalysts.[303] The non-acidic materials, such as Ru/TiO_2, achieved the production of GVL as main product with a selectivity of 97.5 %, meanwhile zeolite materials, such as Ru/H– or Ru–ZMS5, were able to upgrade the hydrogenation of LA to obtain pentanoic acid with a selectivity of 45.8 % in dioxane.[303]

Table 4 Comparison of different catalyst for the hydrogenation of levulinic acid.

Catalyst	Solvent	T [ºC]	pH_2 [bar]	time [h]	Conversion [%]	Selectivity [%][a]	TON	Ref.
Ir@TRGO	-	100	10	4	71.3	100	408	this work
Ir/CNT	water	50	20	1	100	99	-	[314]
	-	50	20	20	100	97	-	
Ru-NPs	-	130	12	24	100	99		[300]
Ru/TiO_2	dioxane	150	40	4	92.3	95.8	590.4	[303]
Ru/H-ZMS5	dioxane	150	40	3	100	45.8[b]	734.4	
Ru/Carbon	dioxane	265	1	50	100	98.6	-	[294]
Ru/TiO_2	water	150	35	5	100	93	247	[312]
Pd/SiO_2	water	180	90		88.1		780.8	[304]
Pt/HMFI [c]	-	200	8	6	100%[c]	99 [c]	-	[313]

[a] to γ-valerolactone, [b] conversion to pentanoic acid; [c]conversion to valeric acid.

In comparison to our solvent-free system, only a few examples are already reported. *Yong et al.* described the synthesis of supported iridium nanoparticles on carbon-nanotubes (Ir/CNTs) by using molecular hydrogen as a reductant with a pressure of 20 bar H_2 and at 50 ºC for 20 h of reaction. The conversion of LA to GVL was near to 100 % with a selectivity of 99 % to GVL.[314] Supported platinum-nanoparticles (Pt–NPs) on HMFI materials also achieved conversions of 100 % with a high selectivity of 99 % to GVL (200 ºC, 6 h, 2–8 bar H_2).[313] Similar conditions to our system were used by *Garcia et al.* using Ru–NPs as catalyst. Conversions of 100 % (selectivity to 99 % GVL) were achieved

after 24 h, by a pressure of 12 bar H_2, at 120 ºC, and in the absence of solvents.[300]

In contrast our catalyst, Ir@TRGO, achieved lower catalytic activities (Table 4). However, lower pressures of H_2 (10 bar) and low temperatures (100 ºC) were used. Furthermore, the selected mild conditions helps for the selectivity to GVL as main product in the of hydrogenation of LA with conversions of 71.3 % and a maximal TOF of h^{-1}.

5. Experimental

5.1 General

All experiments were done under inert atmosphere using Schlenk techniques and the solvents were dried using the MBraun solvent purification system.

The synthesis of the ionic liquid 1-butyl-3-methylimidazolium tetrafluroborate ([BMIm][BF_4]) ,Thermally Reduced Graphite Oxide (TRGO) and $Cu(dmpa)_2$ are described in the section 3.1, 3.2 and 3.4. Propylene carbonate was dried under vacuum (10^{-3} mbar) by 100 ºC for 3 days and stored over molecular sieves 4 Å before used it. The starting materials for the hydrogenation reactions (benzene and cyclohexene) were dried with sodium, distilled and stored over 4 Å molecular sieves. Levulinic acid was used without further purification.

All the chemicals and solvents are listed on the Table 5.

Table 5. Chemicals and solvents.

Chemicals	Purity [%]	Source
Acetonitrile [a]	HPLC grade	Sigma Aldrich
Aluminium oxide	≥98	Sigma-Aldrich
Benzene [b]	p.A	VWR
Chlorbutane	≥99.5	Sigma-Aldrich
Chloroform-d	99.8	euriso-top
$Cu(acac)_2$	> 99.9	Sigma-Aldrich
$Cu(AcO)_2$ H_2O		Merck
$Cu(BF_4)_2$ xH_2O		Sigma-Aldrich
$Cu(dmpa)_2$ [c]		
Cyclohexene [b]	>99.9	Merck
Dichloromethane	≥99.8	Sigma-Aldrich
Ethylacetate	≥99.5	Sigma-Aldrich
Hydrochloric acid	37	Sigma Aldrich
Hydrogen (H_2)	99.999	Alphagaz
$Ir_4(CO)_{12}$	98	STREM/ABCR Chemicals
Levulinic acid	98	Sigma-Aldrich
Methanol		Sigma Aldrich
n-Butylimidazole		Alfa Aesar
n-Dodecane	>99	TCI
Nitric acid	65	Sigma Aldrich
Phenylacetylene	98	Sigma-Aldrich
Propylene carbonate	99.7, H_2O free	Sigma-Aldrich
$Ru_3(CO)_{12}$	99	STREM/ABCR Chemicals
Tetrafluorborsäure	>98	TCI
TRGO-400[d]		

[a] dried on MBraun solvent purification system; [b] dried with Na and stored under 4 Å molecular sieves; [c] $Cu(dmap)_2$ was given to us from the working group of Prof. R. A. Fischer, Bochum, within priority program SPP 1708 (DFG);[d] TRGO was given to us in cooperation with the university of Freiburg.

5.2 Instrumentation and analytical methods

5.2.1. CEM Discover microwave

The thermal reduction or decomposition of the starting materials for synthesis of metal nanoparticles was carried out on a CEM Discover microwave. Each reaction was adapted and carried out at a determined temperature (ºC), pressure (bar), power (W) and time (h).

5.2.2. Büchi pressflow gas controller

All catalytic reactions were done using stainless-steel autoclaves together with a glass inlay to avoid any interference of the steel surface. The autoclave was purged with H_2 three times and heated to the desire temperature before the reaction was started. Once the temperature was reached, the autoclave was charged with the desire pressure of H_2 (3-10 bar), heated at the chosen temperature and stirred (800 rpm).

For hydrogenation reactions of benzene and cyclohexene, the H_2 uptake was measured with an interval of Δ1 s from the BPC, and the data was analyzed with origin 8.5 and Excel. In the case of the hydrogenation of levulinic acid, H_2-consumption was not detected and the products were analyzed by GC.

5.2.3. Transmission electron microscopy and energy dispersive X-ray spectrometry

All the measurements were done at the Ernst Ruska-Centre (ER-C) for 110 Microscopy and Spectroscopy with Electrons in the Jülich Research Centre from the RWTH Aachen University, 52425 Jülich (Germany).

High-resolution transmission electron microscopy (HR-TEM), transmission electron microscopy (TEM) and high-angle annular dark field-scanning transmission electronmicroscopy (HAADF-STEM) images were taken on a FEI Tecnai G20 TEM operating at an accelerating voltage of 200 kV. Samples were deposited on 200 μm carbon-45 coated copper or gold grids (3.025 mm copper-grids with a 200 mesh and coated with 10 nm carbon film) from PLANO GmbH. Energy dispersive X-ray (EDX) spectra were taken on a FEI Tecnai f20, detector voltage 136 kV; the exposure time for 50 individual EDX spectra was 3 min.

The sample can be prepared by three different methods:

Method 1: A drop of the dispersion was deposited on the copper or gold grid and let it “dry” for 30 minutes. Afterwards the sample was washed with acetonitrile (3-5 mL), dried and stored under inert atmosphere.

Method 2: The sample was previously precipitated in acetonitrile to wash out the solvent (IL or PC). The dried solid (0.5- 1 mg) was sonicated with 0.5 mL ACN and deposited on the grid, dried, washed with 1 mL of ACN, dry and store under inert atmosphere.

Method 3: The sample (0.1 mL) was prepared *in situ* (inside the syringe) and diluted with 0.5 mL ACN. Three-four drops of the solution were deposited on the grid, dried and washed with 2 mL of ACN. Once the grid was dried, the sample was stored under inert atmosphere.

The size distribution was determined using Gatan Digital Micrograph software for at least 150 selected nanoparticles or measured by hand.

HR-TEM images were measured by D. Juri Barthel. TEM images were measured by Dr. Kai Schütte, H. Meyer, K. Klauke and S. Wegner.

5.2.4. Powder-X Ray diffraction

Powder X-Ray diffraction patterns were taken on a Brucker D Phaser with a Cu-Kα radiation (λ=1.54182Å, 35 kV) covering 2 theta angles 5-90° over a time of 8 h, that is 0.003 °/sec. The samples were measured using a flat low background holder and, in the case of the cooper nanoparticles, the holder was previously closed in the glove box. All measurements were done at room temperature. The results were edited with the STOE WinXPOW 1.10 and Match! software.

5.2.5. Fourier transform infrared spectroscopy

Infrared spectra was measured on a Brucker TENSOR 37 IR spectrometer in a range from 4000 to 500 cm^{-1} in form of KBr disks.

5.2.6. Atomic absorption spectrometry

The metal content on the M@TRGO and on the catalysis products were analyzed by flame atomic absorption spectrometry (ASS) on a Vario 6 from Analytic Jena. The samples were measured with the help of Annette Ricken. The sample (5 or 10 mg) were digested in *aqua regia* (3 HCl: HNO_3) three times. Afterwards the samples were stirred in 5 mL of *aqua regia* overnight, filtered and added to a final volumina of 25 mL.

5.2.7. Gas chromatography

The conversion of the catalytic products was determined by gas chromatograpy (GC).

The hydrogenation of benzene to cyclohexene was done using a Perkin Elmer 8500 HSB 6 (equipped with a DB-5 film capillary column, 60 m × 0.32 mm, film thickness 25 µm, oven temperature 40 °C, N2 carrier flow 120 L/min and a flame ionization detector (FID), 250 °C detector temperature). The samples were analyzed by putting a drop of the product into a GC sample vial together with 1 mL of distilled water.

The hydrogenation of cyclohexene and levulinic acid were determined using the Shimadzu, GC-2014. The measurements were done in two steps. The first heating ramp was done from 50ºC to 150ºC with a flow rate of 15°C/min, and the second one from 150°C to 250°C, with a flow rate of 50^0C/min. The N_2 total flow was 53.7 mL/min and the flame ionization detector (FID) temperature was 250°C.

All the measurements were calculated using as a reference the pure substrate. Conversions were calculated through the integration of the peaks.

5.3 Synthesis

Here are described all the synthetic procedures which are related to the unpublished results. The syntheses from the cumulative part are described in the corresponding publications or supporting information attachments (sections 3.1-3.3).

5.3.1. Synthesis of Thermally Reduced Graphite Oxide

Natural graphite (type KFL 99.5 from Kropfmühl AG, Passau, Germany) was used as a raw material for the synthesis of the thermal reduced graphite oxide (TRGO) based on the two-steps oxidation/thermal reduction process according to the procedure described by Hummers and Offeman [58]. The graphite oxidation to graphite oxide (GO) is done by oxidation with HNO_3 and $KMnO_4$ in concentrated H_2SO_4. The GO was subjected to a rapid heating above 400 ºC where the functional groups decomposed into CO and CO_2 gas which exfoliated the layered GO structure into functionalized graphene sheets and lead to the formation of the thermally reduced graphite oxide (TRGO).

5.3.2. Synthesis of 1-butyl-3-methylimidazolium tetrafluoroborate

The ionic liquid, [BMIm][BF_4], was synthesized by reacting 1-methylimidazole with 1-chlorobutane to yield first [BMIm]Cl which was further reacted with HBF_4 to give [BMIm][BF_4]. The IL was dried under high vacuum (10^{-7} mbar) at 80 °C for several days. Quantitative anion exchange and, thus, IL purity was assessed by ion chromatography (ICS-1100, with Ion-Pac® AS22, 4 x 250 mm column) to be >99 %. The water content determined by coulometric Karl Fischer titration (ECH/ANALYTIKJENA AQUA 40.00) was less than 10 ppm.

5.3.3. Synthesis of TRGO-supported iridium nanoparticles in propylene carbonate

Iridium dodecacarbonyl, $Ir_4(CO)_{12}$ (39.2 mg, 0.035 mmol) was suspended with 4.8 mg of TRGO (0.2 wt.% related to 2.41 g of PC) in 2 mL of propylene carbonate (2 mL, 2.41 g), sonicated for 6 hours and stirred overnight (800 rpm). Afterwards the sample was heated in microwave reactor (250ºC, 15 min, 50W, 4 bars) and the volatiles (-CO) were removed under vacuum (10^{-3} mbar). The black suspension was washed with distilled H_2O (5 x 5 mL), centrifuged (10 min x 6000 rpm) and dried under vacuum. The Ir@TRGO was stored under inert atmosphere and stored for further analysis (Fig. 26, Fig. 27).

5.3.4. Hydrogenation of levulinic acid with Ir@TRGO nanomaterials

The hydrogenation reaction was carried out in a stain-less Steel autoclave (for more details see Section 5.2).The Ir@TRGO catalyst (5 mg, 3.6 % Ir, 0.18 mg, 9.36 x 10^{-4} mmol Ir, molar ratio 1998) and the desire amount of levulinic acid (0.22 g, 1.87 mmol, 191 μL, 116.11 g/mol, 1.14 g/mL) were placed in the autoclave and the air/N_2 atmosphere was replaced and re-fill with H_2. The autoclave was heated to 100 ºC, charged with 10 bar H_2, and stirred (800 rpm) for 3 hours.

Once the autoclave was cooled down, the products and the catalyst (Ir@TRGO) were separated by centrifugation. The products were analyzed by GC (see Section 5.2.7). Ir@TRGO nanomaterials were washed with MeOH (3x 1mL) and dried before the next hydrogenation run. A further analysis of the products was done by AAS, finding less than 1ppm content of Iridium in the samples. The same procedure was repeated for at least five consecutive runs (with the same Ir@TRGO catalyst). The size distribution of Ir-NPs were measured by TEM, finding an average of 2.7 ± 0.7 nm before to 7.8 ± 4.4 nm after 5 consecutive hydrogenation runs.

6. Summary and outlook

Metal carbonyls are commercially available, easy to handle and a good alternative to organometallic compounds in the synthesis of metal nanoparticles. The already zero-oxidation state of metal carbonyls reduces the use of extra reducing agents, which provide a cleaner method for the synthesis of metal nanoparticles.

The deposition of iridium- and ruthenium-nanoparticles (Ir-, Ru-NPs) on the thermally derived graphite oxide (also named *graphene* or TRGO) could be easily prepared by the thermal decomposition of $Ir_4(CO)_{12}$ and $Ru_3(CO)_{12}$ in the ionic liquid 1-butyl-3-methylimidazolium tetrafluoroborate ([BMIm][BF_4]) and propylene carbonate (PC) respectively.

Iridium@graphene (Ir@TRGO) nanomaterials could be prepared in the ionic liquid 1-butyl-3-mtheyltetrafluoroborate ([BMIm][BF_4]) by decomposition of $Ir_4(CO)_{12}$ using the saving-energy microwave input (MWI) and electron-beam irradiation (IBA Rhodotron accelerator). Small nanoparticles for the Ir-NPs were achieved, with size distributions of 1.0 ± 0.4 and 2.7 ± 0.7 nm for the microwave reactions and 3.6 ± 1.0 nm for the Ir–NPs obtained from the e-beam irradiation. The stable Ir@TRGO nanomaterials were tested as catalyst for the hydrogenation of benzene to cyclohexane, reaching catalytic activities up to 10 000 h^{-1} after ten consecutive runs, by the microwave-obtained Ir@TRGO catalyst, and up to 4582 h^{-1} after five consecutive runs, in the case of the e-beam nanomaterial. After several hydrogenation reactions, the size distributions of the Ir-NPs were determined by TEM, which show an increment of ~1 nm for the Ir-NPs, achieving a size distribution of 3.6 ±1.1 nm for the MWI Ir@TRGO and of 4.6 ±1.5 nm for the e-beam irradiation Ir@TRGO nanomaterials.

The hydrogenation of cyclohexene to cyclohexane was also tested with the MWI Ir@TRGO nanomaterials, to obtain a TOF of ~68 000 h^{-1} after five consecutive hydrogenation runs. Furthermore, the solvent-free hydrogenation of the biomass-derived levulinic acid was also possible with Ir@TRGO, which showed a TOF 1430 h^{-1} with γ-valerolactone as a main product for four consecutive hydrogenation reactions.

Supported ruthenium nanoparticles on thermally reduced graphite oxide (Ru@TRGO) could be also prepared by decomposition of $Ru_3(CO)_{12}$ using the microwave irradiation in propylene carbonate. The obtained Ru-NPs achieved a size distribution of 4.3 ± 1.4 nm. Ru@TRGO nanomaterials showed a turn over frequencies of 34000 h^{-1} for the

hydrogenation of benzene to cyclohexane (< 20 min, 100 ºC, 10 bar H_2) after ten consecutive hydrogenation runs without loss of activity. The Ru-NPs showed a slightly increase after catalysis to achieve a size distribution of 6.7 ± 2.4 nm.

Copper-nanoparticles (Cu-NPs) and cuprite-nanocubes (Cu_2O-NCs) were also prepared in [BMIm][BF_4] and PC. As starting materials diverse copper sources were selected, using different commercially available copper salts, such as $Cu(BF_4)_2$, $Cu(acac)_2$ or $Cu(AcO)_2$ monohydrate, and the organometallic compound copper (II) bis- (dimethylamino)propan-2-olate) ($Cu(dmap)_2$). The different copper sources were subjected to reduction by means of microwave irradiation. The obtained Cu-NPs from $Cu(BF_4)_2$ in PC, and $Cu(acac)_2$ in [BMIm][BF_4] achieved size distributions of 45 nm and 3.3 ± 0.9 nm, respectively. However, the reduction of $Cu(dmap)_2$ gave smaller size distributions in both solvents, of 3.1 ± 0.7 nm in PC, and of 3.7 ± 1.4 nm [BMIm][BF_4]. Cuprite-nanocubes (Cu_2O-NCs) were also obtained by microwave reduction of $Cu(AcO)_2$ monohydrate in [BMIm][BF_4], which yielded to the formation of Cu_2O-NCs, with a size distribution of 43 ± 15 nm.

The explained methods for the deposition of M-NPs on thermally reduced graphite oxide is definitely a valid and elegant method for future works by using other available metal carbonyls such as $W(CO)_6$, $Mo(CO)_6$, $Rh_6(CO)_{16}$, $Co_2(CO)_9$, or $Fe_3(CO)_9$ to obtain new metal@TRGO nanomaterials. The M-NPs synthesis in ionic liquids provides in front of organic solvents the absence of stabilizers due to their intrinsic nanostructured arrangements, which allow the inclusion of small molecules and particles such as M–NPs. As well, propylene carbonate seems to be an effective option for the synthesis of M@TRGO nanomaterials, with the advantage that PC is cheaper and easy to remove from the M@TRGO dispersions as ILs. These methods in combination with the microwave irradiation for the thermal decomposition of metal carbonyls afford easy procedures, which can be applied not only for the synthesis of monometallic graphene materials but also for the synthesis of bimetallic nanoparticles.

In terms of catalysis, the substrates such as levulinic acid, hydroxymethylfurfural or furfural, derived from the biomass lignocellulosic, are attractive for hydrogenation routes and to use the M@TRGO nanomaterials as catalyst (Fig. 21). Levulinic acid can be upgraded for the synthesis of γ-valerolactone, important for their application on food additives or as solvents, or it can be further hydrogenated to valeric esters, which are used for the synthesis of bio-fuels.

7. Appendix

7.1 Hydrogenation of levulinic acid to g-valerolactone with Ir@TRGO.

Before catalysis

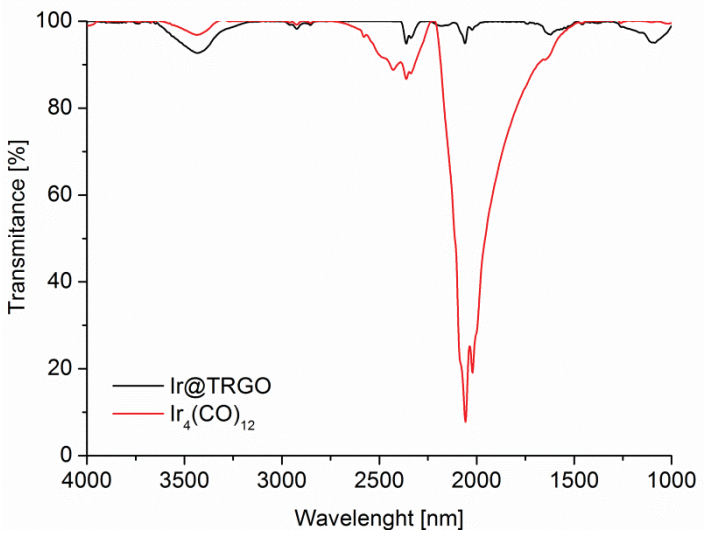

Fig. 33 IR spectrum of Ir@TRGO nanomaterials after microwave synthesis (red spectrum) in comparison with the pure starter material, $Ir_4(CO)_{12}$ (black)

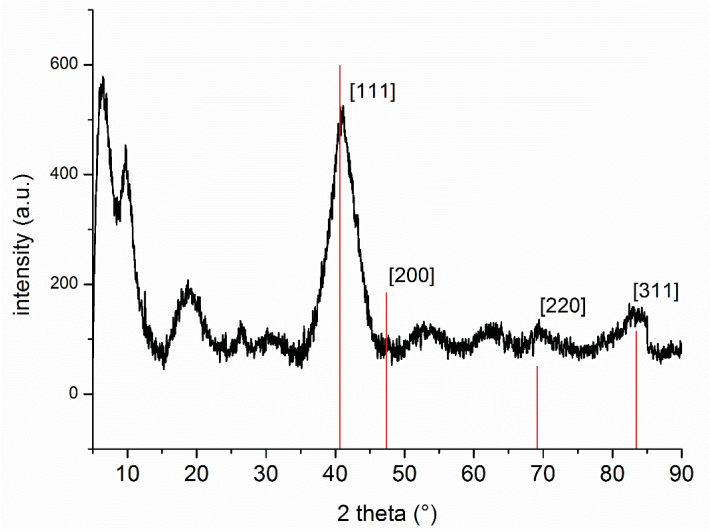

Fig. 34 PXRD pattern of Ir@TRGO nanomaterials before catalysis in comparison (red bars) with the bulk material Ir, with reference COD: 9008470.

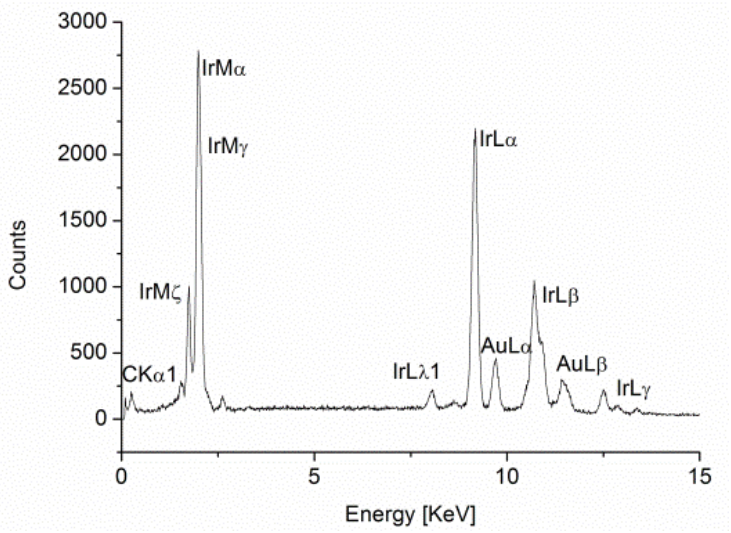

Fig. 35 EDX of Ir@TRGO nanomaterials synthetized in [BMIm][BF_4] and used for the hydrogenation of levulinic acid.

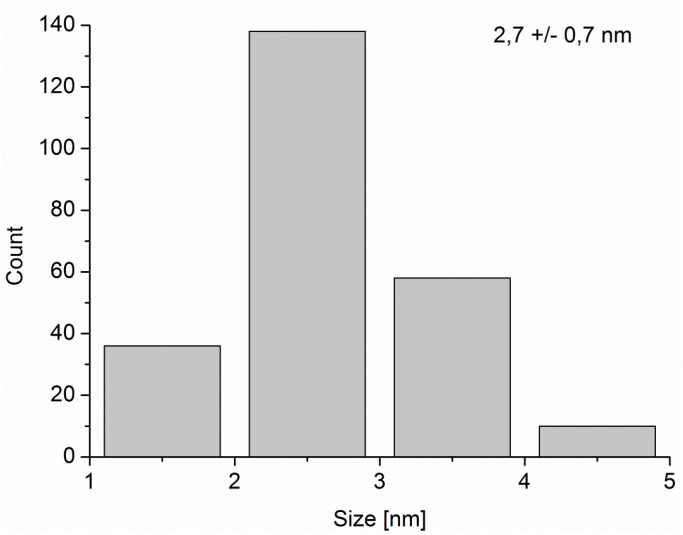

Fig. 36 Histogram of Ir@TRGO nanomaterials determined with the GATAN software for 242 nanoparticles and related to the Fig. 28 (left, 100 nm scale).

After catalysis (solvent-less conditions)

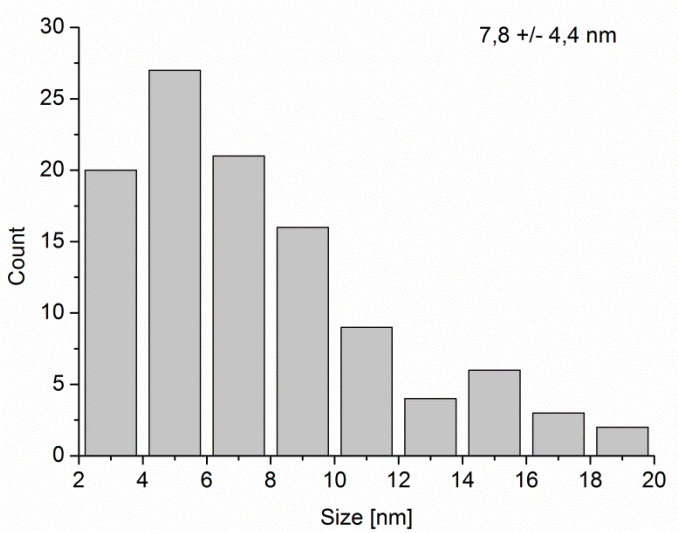

Fig. 37 Histogram of Ir@TRGO nanomaterials after the hydrogenation of levulinic acid, determined with the GATAN software for 109 nanoparticles and related to the (left, 20 nm scale, Fig. 30).

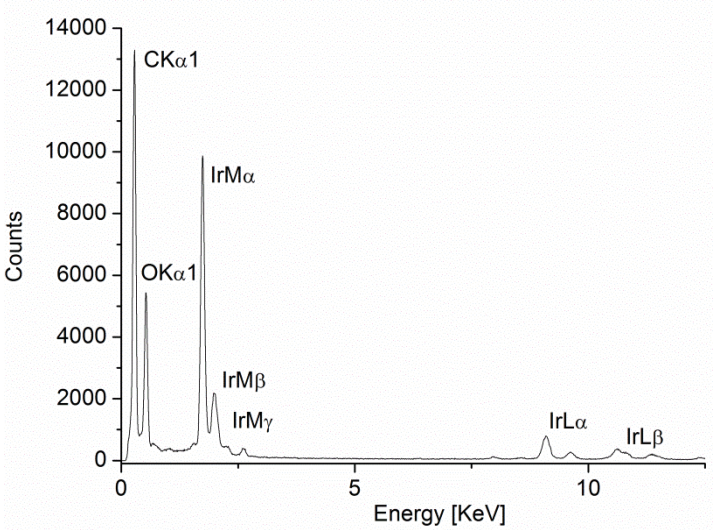

Fig. 38 EDX Spectra of Ir@TRGO nanomaterials after the hydrogenation of levulinic acid to γ-valerolactone.

8. References

[1] N. V. Plechkova, K. R. Seddon, *Chem. Soc. Rev.* **2008**, *37*, 123–150.

[2] T. L. Greaves, C. J. Drummond, *Chem. Rev.* **2008**, *108*, 206–237.

[3] C. Janiak, Metal Nanoparticle Synthesis in *Ionic Liquids*, *Ionic Liquids (ILs) in Organometallic Catalysis/ Topics in Organometallic Chemistry*, *Vol. 51* (Eds.: J. Dupont, L. Kollar) Springer, Heidelberg, **2015**, pp. 17–53.

[4] M. Galinski, A. Lewandowski, I. Stepniak, *Electrochim. Acta* **2006**, *51*, 5567–5580.

[5] F. v. Rantwijik, R. A. Sheldon, *Chem. Rev.* **2007**, *107*, 2757–2785.

[6] J. Lua, F. Yana, J. Texter, *Prog. Polym.Sci.* **2009**, *34*, 431–448.

[7] T. Welton, *Chem. Rev.* **1999**, *99*, 2071–2083.

[8] R. E. Morris, *Chem. Commun.* **2009**, 2990–2998.

[9] E. R. Cooper, C. D. Andrews, P. S. Wheatley, P. B. Webb, P. Wormald, R. E. Morris, *Nature* **2004**, *430*, 1012–1016.

[10] D. Freudenmann, S. Wolf, M. Wolff, C. Feldmann, *Angew. Chem. Int. Ed.* **2011**, *50*, 11050–11060.

[11] H. L. Ngo, K. LeCompte, L. Hargens, A. B. McEwen, *Thermochim. Acta* **2000**, *357–358*, 97–102.

[12] J. Dupont, P. A. Z. Suarez, *Phys. Chem. Chem. Phys.* **2006**, *8*, 2441–2452.

[13] J. Dupont, *J. Braz. Chem. Soc.* **2004**, *15*, 341–350.

[14] R. Sheldon, *Chem. Commun.* **2001**, 2399–2407.

[15] V. I. Pârvulescu, C. Hardacre, *Chem. Rev.* **2007**, *107*, 2615–2665.

[16] P. Wasserschied, W. Keim, *Angew. Chem. Int. Ed.* **2000**, *39*, 3772–3789.

[17] J. D. Holbrey, K. R. Seddon, *Clean Products and Processes* **1999**, *1*, 223–226.

[18] K. Dong, S. Zhang, D. Wang, X. Yao, *J. Phys. Chem. A* **2006**, *110*, 9775–9782.

[19] J. Łuczak, J. Hupka, J. Thöming, C. Jungnickel, *Colloids and Surfaces A: Physicochem. Eng. Aspects* **2008**, *329*, 125–133.

[20] H. Weingärtner, *Angew. Chem. Int. Ed.* **2008**, *47*, 654–670.

[21] H. Weingärtner, *Angew. Chem.* **2008**, *120*, 664–682.

[22] J. Dupont, J. D. Scholten, *Chem. Soc. Rev.* **2010**, *39*, 1780–1804

[23] C. S. Consorti, P. A. Z. Suarez, R. F. de Souza, R. A. Burrow, D. H. Farrar, A. J. Lough, W. Loh, L. H. M. da Silva, J. Dupont, *J. Phys. Chem. B* **2005**, *109*, 4341–4349.

[24] S. Fukuoka, M. Kawamura, K. Komiya, M. Tojo, H. Hachiya, K. Hasegawa, M. Aminaka, H. Okamoto, I. Fukawa, S. Konno, *Green Chem.* **2003**, *5*, 497–507.

[25] B. Schäffner, F. Schäffner, S.P. Verevkin, A. Börner, *Chem. Rev.* **2010**, *110*, 4554–4581.

[26] B. Schäffner, J. Holz, S.P. Verevkin,A. Börner, *ChemSusChem* **2008**, *1*, 249–253.

[27] J. Simonet, *Electrochem. Commun.* **2012**, *19*, 93–96.

[28] J. H. Clements, *Ind. Eng. Chem. Res.* **2003**, *42*, 663–674.

[29] JEFFSOL ®; Huntsman: Conroe, TX, **2008**.

[30] T. Sakakura, K. Kohno, *Chem. Commun.* **2009**, 1312–1330.

[31] L. Zhang, D. Niu, K. Zhang, G. Zhang, Y. Luo, Ji. Lu, *Green Chem.* **2008**, *10*, 202–206.

[32] A. M. Z. Paquin, *Naturforsch.* **1946**, *1*, 518–523.

[33] P. Ball, H. Fullmann, R. Schwalm, W. C. Heitz, *C. Mol. Chem.* **1984**, *1*, 95.

[34] Ger. Pat. 109,933 (Chemische Fabrik von Heyden) 1900 Friedl 5 (**1901**).

[35] Ger. Pat. 116,386 (Chemische Fabrik von Heyden) 1900 Friedl, 6 (**1904**) 1160.

[36] A.-A. G. Shaikh, S. Sivaram, *Chem. Rev.* **1996**, *96*, 951–975.

[37] A. Dibenedetto, A. Angelini in *Advances in Inorganic Chemistry*, *Vol. 66*, Elsvier Inc., New York, USA, **2013**, pp. 25–82 (chapter 2).

[38] M. Selva, P. Tundo, A. Perosa, *J. Org. Chem.* **2003**, *68*, 7374–7378.

[39] W.-C. Shieh, S. Dell, O. Repič, *Org. Lett.* **2001**, *3*, 4279–4281.

[40] J. Mak, D. Nielsen, D. Schulte, LRGCC Conf. Proc. 57, 267–280, **2007**.

[41] A. L. Kohl, P. A. Buckingham, *Oil Gas J.* **1960**, *58*, 146–155.

[42] J. Roger, Cécile Verrier, R. Le Goff, C. Hoarau, H. Doucet, *ChemSusChem* **2009**, *2*, 951–956.

[43] J. Bayardon, J. Holz, B. Schäffner, V. Andrushko, S. Verevkin, A. Preetz, A. Börner, *Angew. Chem. Int. Ed.* **2007**, *46*, 5971–5974.

[44] K. N. Gavrilov, S. V. Zheglov, P. A. Vologzhanin, M. G. Maksimova, A. S. Safronov, S. E. Lyubimov, V. A. Davankov, B. Schäffner, A. Börner, *Tetrahedron Lett.* **2008**, *49*, 3120–3123.

[45] M. Reetz, G. Lohmer, *Chem. Commun.* **1996**, *16*, 1921–1922.

[46] A. Behr, H. Schmidke, *Chem. Ing. Tech.* **1993**, *65*, 568–569.

[47] J. Demel, J. Čejka, S. Bakardjieva, P. Štěpnička, *J. Mol. Catal. A* **2007**, *263*, 259–265.

[48] A. Behr, N. Döring, S. Durowicz-Heil, B. Ellenberg, C. Kozik, C. Lohr, H. Schmidke, *Fat Sci. Technol.* **1993**, *95*, 2–12.

[49] C. Vollmer, R. Thomann, C. Janiak, *Dalton Trans.* **2012**, *41*, 9722–9727.

[50] R. Marcos Esteban, K. Schütte, D. Marquardt, J. Barthel, F. Beckert, R. Mülhaupt, C. Janiak, *Nano-Structures & Nano-Objects* **2015**, *2*, 28–34.

[51] K. Schütte, H. Meyer, C. Gemel, J. Barthel, R.A. Fischer, C. Janiak, *Nanoscale* **2014**, *6*, 3116–3126.

[52] V. Singh, D. Joung, L. Zhai, S. Das, S.I. Khondaker, S. Seal, *Prog. Mater. Sci.* **2011**, *56*, 1178–1271.

[53] C. N. R. Rao, A. K. Sood, K. S. Subrahmanyam, A. Govindaraj, *Angew. Chem. Int. Ed.* **2009**, *48*, 7752–7777.

[54] M. I. Katsnelson, *Materi. tod.* **2007**, *10*, 20–27.

[55] K. S. Novoselov, K. Geim, S. V. Morozov, D. Jiang, Y. Zhang, V. Dubonos, I. V. Grigorieva, A. A. Firsov, *Science* **2004**, *306*, 666–669.

[56] B. C. Brodie, *Phil. Trans. Roy. Soc. London Ser. A.* **1895**, *149*, 249–259.

[57] L. Staudenmaier, *Ber. DeutschenChem.Ges.* **1898**, *31*, 1481–1487.

[58] W. S. Hummers, R. E. Offeman, *J. Am. Chem. Soc.* **1958**, *6*, 1339–1339.

[59] B. C.Brodie, *Liebigs Ann. Chem.* **1860**, *114*, 6–24

[60] H.-P.Boehm, W. Scholz, *Liebigs Ann. Chem.* **1965**, *691*, 1–8.

[61] D.R.Dreyer, S. Park,C. W. Bielawski, R. S. Ruoff, *Chem. Soc. Rev.* **2010**, *39* 228–240.

[62] F. J. Tölle, Fabritius, M., Mülhaupt, R., *Adv. Funct. Mater.* **2012**, *22*, 1136–1144.

[63] C. Lee, X. Wei, J. W. Kysar, J. Hone, *Science* **2008**, *321*, 385–388.

[64] A.H. Castro Neto, F. Guinea, N. M. R. Peres, N. S. Novolesov, A. K. Geim, *Rev. Mod. Phys.* **2009**, *81*, 109–162.

[65] J. K. Lee, K. B. Smith, C. M. Hayner, H. H. Kung, *Chem Commun.* **2010***, 46*, 2025–2027.

[66] S. Yang, X. Feng, S. Ivanovici, K. Müllen, *Angew. Chem. Int. Ed.* **2010**, *49*, 8408–8411.

[67] J. D. Roy-Mayhew, D. J. Bozym, C. Punckt, I. A. Aksay, *ACS Nano* **2010**, *4*, 6203–6211.

[68] N. Mohanty, V. Berry, *Nano Letters* **2008**, *8*, 4469–4476.

[69] L. Ganhua, L. E. Ocola, J. Chen, *Nanotechnology* **2009**, *20*, 445502/1–445502/9.

[70] B. Dai, K. Chen, Y. Wang, L. Kan, M. Zhu, *ACS Catal.* **2015**, *5*, 2541–2547.

[71] V. Georgakilas, M. Otyepka, A. B. Bourlinos, V. Chandra, N. Kim, K. C. Kemp, P. Hobza, R. Zboril, K. S. Kim, *Chem. Rev.* **2012**, *112*, 6156–6214.

[72] N. A. Kumar, H.-J. Choi, Y. R. Shin, D. W. Chang, L. Dai, J.-B. Baek, *ACS Nano* **2012**, *6*, 1715–1723.

[73] L. Rodríguez-Pérez, M. Á. Herranz, N. Martín, *Chem. Commun.* **2013**, *49*, 3721–3735

[74] E. Bekyarova, M. E. Itkis, P. Ramesh, C. Berger, M. Sprinkle, W. A. de Heer, R. C Haddon, *J. Am. Chem. Soc.* **2009**, *131*, 1336–1337.

[75] M. Fang, K. Wang, H. Lu, Y. Yanga, S. Nutt, *J. Mater. Chem.* **2010**, *20*, 1982–1992.

[76] M. Fang, K. Wang, H. Lu, Y. Yanga, S. Nutt, *J. Mater. Chem.* **2009**, *19*, 7098–7105.

[77] L. Rodriguez Perez, M. Ángeles Herranz, N. Martín, *Chem. Commun.* **2013**, *49*, 3721–3735.

[78] J. Shen, M. Shi, B. Yan, H. Ma, N. Li, M. Ye, *J. Mater. Chem.* **2011**, *21*, 7795–7801.

[79] M. Fu, Q. Jiao, Y. Zhao, *J. Mater. Chem. A.* **2013**, *1*, 5577–5586.

[80] R. Muszynski, B. Seger, P. V. Kamat, *J. Phys. Chem. C.* **2008**, *112*, 5263–5266.

[81] F. Li, J. Chai, H. Yang, D. Han, L. Niu, *Talanta* **2010**, *81*, 1063–1068.

[82] J.-S.Lee, T.Lee, H.-K.Song, J. Cho, B.-S. Kim, *Energy Environ. Sci.* **2011**, *4*, 4148–4154.

[83] J. Lu, J.-x. Yang, J. Wang, A. Lim, S. Wang, K. P. Loh, *ACS Nano* **2009**, *3*, 2367–2375.

[84] D. Marquardt, F. Beckert, F. Pennetreau, F. Tölle, R. Mülhaupt, O. Riant, S. Hermans, J. Barthel, C. Janiak, *Carbon* **2014**, *66*, 285–294.

[85] R. Marcos Esteban, K. Schütte, P. Brandt, D. Marquardt, H. Meyer, F. Beckert, R. Mülhaupt, H. Kölling, C. Janiak, *Nano-Structures & Nano-Objects* **2015**, *2*, 11–18.

[86] R. Marcos Esteban, C. Janiak in *Synthesis and application of metal nanoparticle catalysts in ionic liquid media using metal carbonyl complexes as precursors*, *Nanocatalysis in Ionic Liquids* (Eds.: M. Prechtl) Wiley-VCH, Weinheim, **2015**.

[87] J. A. Dahl, B. L. S. Maddux, J. E. Hutchison, *Chem. Rev.* **2007**, *107*, 2228–2269.

[88] S.-H. Yu, L. R. MacGillivray, C. Janiak, *CrystEngComm* **2012**, *14*, 7531–7534.

[89] K. Saha, S. S. Agasti, C. Kim, X. Li, V. M. Rotello, *Chem. Rev.* **2012**, *112*, 2739–2779.

[90] P. K. Jain, X. Huang, I. H. El-Sayed, M. A. El-Sayed, *Acc. Chem. Res.* **2008**, *41*, 1578–1586.

[91] H. Goesmann, C. Feldmann, *Angew. Chem. Int. Ed.* **2010**, *49*, 1362–1395.

[92] K. Eric Drexler, *Proc. Nad Acad. Sci. USA* **1981**, *78*, 5275–5278.

[93] N. Toshima, T. Yonezawa, *New J. Chem.* **1998**, 1179–1201.

[94] H. Birol, C. Renato Rambo, M. Guiotoku, D. Hotza, *RSC Adv.* **2013**, *3*, 2873–2884.

[95] S. Mende, F. Stenger, W. Peukert, J. Schwedes, *Chem. Ing. Tech.* **2002**, *74*, 994–1000.

[96] M. S. Sibbald, G. Chumanov, T. M. Cotton, *J. Phys. Chem.* **1996**, *100*, 4672–4678.

[97] Z. Peng, H. Yang, *Nano Today* **2009**, *4*, 143–164.

[98] K. An, S. Alayoglu, T. Ewers, G. A. Somorjai, *J. Colloid Interface Sci.* **2012**, *373*, 1–13.

[99] M. Kim, V. N. Phan, K. Lee, *CrystEngComm* **2012**, *14*, 7535–7548.

[100] J. D. Scholten, B. C. Leal, J. Dupont, *ACS Catal.* **2012**, *2*, 184–200.

[101] N. Yan, C. Xiao, Y. Kou, *Coord. Chem. Rev.* **2010**, *254*, 1179–1218.

[102] A. Welther, J. Jacobi von Wangelin, *Curr. Organic Chem.* **2013**, *17*, 326–335.

[103] T. N. Gieshoff, A. Welther, M. T. Kessler, M. H. G. Prechtl, A. Jacobi von Wangelin, *Chem. Commun.* **2014**, *50*, 2261–2264.

[104] P. S. Campbell, M. H. G. Prechtl, C. C. Santini, P. H. Haumesser, *Curr. Organic Chem.* **2013**, *17*, 414–429.

[105] M. Guerrero, N. T. Than-Chau, S. Noël, A. Denicourt-Nowicki, F. Hapiot, A. Roucoux, E. Monflier, K. Philippot, *Curr. Organic Chem.* **2013**, *17*, 364–399.

[106] J. D. Scholten, *Curr. Organic Chem.* **2013**, *17*, 348–363.

[107] W. Ostwald, *Phys. Chem.* **1901***,37*, 385–385.

[108] W. Ostwald in *Lehrbuch der Allgemeinen Chemie*, *Vol. 2*, Leipzig, Germany,**1986**.

[109] H. Goesmann, C. Feldmann, *Angew. Chem.* **2010**, *122*, 1402–1437.

[110] P. Arquilliere, P. H. Haumesser, C. C. Santini, *Microelectron. Eng.* **2012**, *92*, 149–151.

[111] C. J. Murphy, T. Sau, A. M. Gole, C. J. Orendorff, J. Gao, L. Gou, S. E. Hunyadi, T. Li, *J. Phys. Chem. B* **2005**, *109*, 13857–13870.

[112] M. Zahmakiran, S. Özkar, *J. Alloys Compd.* **2005**, *728*, 404–406.

[113] M. Zahmakiran, S. Özkar, *J. Mol. Catal. A: Chem.* **2006**, *258*, 95–103.

[114] H. Bönnemann, R. M. Richards, *Eur. J. Inorg. Chem.* **2001**, 2455–2480.

[115] S. Bauer, C. Hunger, M. Bodensteiner, W.- S. Ojo, Ar. Cros-Gagneux, B. Chaudret, C. Nayral, F. Delpech, M. Scheer, *Inorg. Chem.* **2014**, *53*, 11438−11446.

[116] C. Vollmer, C. Janiak, Coord. *Chem. Rev.* **2011**, *255*, 2039–2057.

[117] D. Marquardt, C. Vollmer, R. Thomann, P. Steurer, R. Mülhaupt, E. Redel, C.Janiak, *Carbon* **2011**, *49*, 1326–1332.

[118] N. Dahal, S. García, J. Zhou, S. M. Humphrey, *ACS Nano* **2012**, *6*, 9433–9446.

[119] B. Zhang, X. Ni, W. Zhang, L. Shao, Q: Zhang, F. Girgsdies, C. Liang, R. Schlögl, D. Sheng Su, *Chem. Commun.* **2011**, *47*, 10716–10718.

[120] C. Vollmer, E. Redel, K. Abu-Shandi, R. Thomann, H. Manyar, C. Hardacre, C. Janiak, *Chem. Eur. J.* **2010**, *16*, 3849–3858.

[121] K. V. P. M. Shafi, S. Wizel, T. Prozorov, A. Gedanken, *Thin Solid Films* **1998**, *318*, 38–41.

[122] K. S. Suslick, J. W. Goodale, P. F. Schubert, H. H. Wang, *J. Am. Chem. Soc.* **1983**, *105*, 5781–5785.

[123] N. Du, H. Zhang, B. Chen, J. Wu, X. Ma, Z. Liu, Y. Zhang, D. Yang, X. Huang, J. Tu, *Adv. Mater.* **2007**, *19*, 4505–4509.

[124] V. Amendola, M. Meneghetti, *Phys. Chem. Chem. Phys.* **2009**, *11*, 3805–3821.

[125] J. M. Zhu, Y. H. Shen, A. J. Xie, L. G. Qiu, Q. Zhang, X. Y. Zhang, *J. Phys. Chem. C* **2007**, *111*, 7629–7633.

[126] M. A. Firestone, M. L. Dietz, S. Seifert, S. Trasobares, D. J. Miller, N. J. Zaluzec, *Small* **2005**, *1*, 754–760.

[127] M. Platt, R. A. W. Dryfe, *Phys. Chem. Chem. Phys.* **2005**, *7*, 1807–1814.

[128] U. Kolb, S. A. Quaiser, M. Winter, M. T. Reetz, *Chem. Mater.* **1996**, *8*, 1889–1894.

[129] D. Astruc, F. Lu, J. R. Aranzaes, *Angew. Chem. Int. Ed.* **2005**, *44*, 7852–7872.

[130] C. Pan, K. Pelzer, K. Philippot, B. Chaudret, F. Dassenoy, P. Lecante, M.–J. Casanove, *J. Am. Chem. Soc.* **2001**, *123*, 7584–7593.

[131] J. D. Aiken III, R. G. Finke, *J. Am. Chem. Soc.* **1999**, *121*, 8803–8810.

[132] J. Krämer, E. Redel, R. Thomann and C. Janiak, *Organometallics* **2008**, *27*, 1976–1978.

[133] M.-A. Neouze, *J. Mater. Chem.* **2010**, *20*, 9593–9607.

[134] J. Dupont, P. A. Z. Suarez, R. F. de Souza, R. A. Burrow, J.-P. Kintzinger, *Chem. Eur. J.* **2000**, *6*, 2377–2381.

[135] C. Janiak, *Z. Naturforsch.* **2013**, *68b*, 1056–1089.

[136] P. Wasserscheid, W. Keim, *Angew. Chem. Int. Ed.* **2000**, *39*, 3772–3789.

[137] M. Larhed, C. Moberg, A. Hallberg*, Acc. Chem. Res.* **2002**, *35*, 717–727.

[138] D. Bogdal in *Microwave-Assisted Organic Synthesis*, *Vol. 25*, Tetrahedon Organic Chemistry Series, Elsevier, New York, USA, **2006**, pp. 47–189.

[139] D. M. P Mingos, D. R. Baghurst, *Chem. Soc. Rev.* **1991**, *20*, 1–47.

[140] S. A. Galema, *Chem. Soc. Rev.* **1997**, *26*, 233–238.

[141] M. F. Groh, M. Heise, M. Kaiser, M. Ruck, *Nachr. Chemie* **2013**, *61*, 26–29.

[142] A. L. Buchachenko, E. L. Frankevich in *Chemical Generation and Reception of Radio- and Microwaves*, Wiley-VCH, Weinheim, Germany, **1993**, pp. 41–56.

[143] V. K. Ahluwulia in *Alternative Energy Processes in Chemical Synthesis*, Alpha Science International LTD, Oxford, United Kingdom, **2008**.

[144] I. Bilecka, M. Niederberger, *Nanoscale* **2010**, *2*, 1358–1374.

[145] C. Janiak in *Catalysis in Ionic Liquids: From Catalyst Synthesis to Application* (Eds.: C. Hardacre, V. Parvulescu) RSC Publishing, Cambridge, **2014**, pp. 537–577 (chapter 11).

[146] H. Zhang, H. Cui, *Langmuir* **2009**, *25*, 2604–2612.

[147] E. J. W. Verwey, J. T. G. Overbeek in Theory of the Stability of Lyophobic Colloids, Dover Publications Mineola, New York, **1999**, pp. 1–218.

[148] E. J. W. Verwey, J. T. G. Overbeek in *Theory of Stability of Lyophobic Colloids*, Elsevier, Amsterdam, **1948**.

[149] J.-P. Hansen, H. Löwen, *Annu. Rev. Phys. Chem.* **2000**, *51*, 209–242.

[150] B. W. Ninham, *Adv. Colloid Interface Sci.* **1999**, *83*, 1–17.

[151] A. Taubert, Z. Li, *Dalton Trans.* **2007**, 723–727.

[152] E. Redel, R. Thomann, C. Janiak, *Inorg. Chem.* **2008**, *47*, 14–16.

[153] L. S. Ott, R. G. Finke, *Inorg. Chem.* **2006**, *45*, 8382–8393.

[154] G. S. Fonseca, A. P. Umpierre, P. F. P. Fichtner, S. R. Teixeira, J. Dupont, *Chem. Eur. J.* **2003**, *9*, 3263–3269.

[155] Z. Li, A. Friedrich, A. Taubert, *J. Mater. Chem.* **2008**, *18*, 1008–1014.

[156] P. Migowski, D. Zanchet, G. Machado, M. A. Gelesky, S. R. Teixeira, S.R., J. Dupont, *Phys. Chem. Chem. Phys.* **2010**, *12*, 6826–6833.

[157] P. Migowski, G. Machado, S. R. Teixeira, M. C. M. Alves, J. Morais, A. Traverse, J. Dupont, *Phys. Chem. Chem. Phys.* **2007**, *9*, 4814–4821.

[158] M. Ruta, G. Laurenczy, P.J. Dyson, L. Kiwi-Minsker, *J. Phys. Chem. C* **2008**, *112*, 17814–17819.

[159] R. R. Deshmukh, R. Rajagopal, K. V. Srinivasan, *Chem. Commun.* **2001**, 1544–1545.

[160] K. Anderson, S. C. Fernández, C. Hardacre, P. C. Marr, *Inorg. Chem. Commun.* **2004**, *7*, 73–76.

[161] K. Peppler, M. Polleth, S. Meiss, M. Rohnke, J. Janek, *Z. Phys. Chem.* **2006**, *220*, 1507–1527.

[162] A. Safavi, N. Maleki, F. Tajabadi, E. Farjami, *Electrochem. Commun.* **2007**, *9*, 1963–1968.

[163] K. Kim, C. Lang, P. A. Kohl, *J. Electrochem. Soc.* **2005**, *152*, E9–E13.

[164] E. Ahmed, J. Breternitz, M. F. Groh, M. Ruck, *CrystEngComm* **2012**, *14*, 4874–4885.

[165] E. Ahmed, M. Ruck, *Dalton Trans.* **2011**, *40*, 9347–9357.

[166] M. F. Groh, U. Müller, E. Ahmed, A. Rothenberger, M. Ruck, *Z. Naturforsch.* **2013**, *68b*, 1108–1122.

[167] E. R. Parnham, R. E. Morris, *Acc. Chem. Res.* **2007**, *40*, 1005–1013.

[168] C. N. R. Rao, H. S. S. R. Matte, R. Voggu, A. Govindaraj, *Dalton Trans.* **2012**, *41*, 5089–5120.

[169] T. Gutel, J. Garcia-Anton, K. Pelzer, K. Philippot, C. C. Santini, Y. Chauvin, B. Chaudret, J.-M. Basset, *J. Mater. Chem.* **2007**, *17*, 3290–3292.

[170] G. Salas, A. Podgorsek, P. S. Campbell, C. C. Santini, A. A. H. Pádua, M. F. Costa-Gomes, K. Philippot, B. Chaudret, M. Turmine, *Phys. Chem. Chem. Phys.* **2011**, *13*, 13527–13536.

[171] C. Janiak in *Moderne Anorganische Chemie*, *Vol. 4* (Eds.: H.-J. Meyer) Walter de Gruyter, Berlin, **2012**, pp. 645–661 (chapter 3-4).

[172] D. G. E. Kerfoot, X. Nickel, E. Wildermuth, H. Stark, G. Friedrich, F. L. Ebenhöch, B. Kühborth, J. Silver, R. Rituper in *Ullmann's Encyclopaedia of Industrial Chemistry*, Wiley (online), **2008**.

[173] T. Hyeon, *Chem. Commun.* **2003**, 927–934.

[174] P. H. Hess, P. H. Parker Jr., *J. Appl. Polym. Sci.* **1966**, *10*, 1915–1927.

[175] J. R. Thomas, *J. Appl. Phys.* **1966**, *37*, 2914–2915.

[176] E. Papirer, P. Horny, H. Balard, R. Anthore, C. Petipas, A. Martinet, *J. Colloid Interface Sci.* **1983**, *94*, 207–219.

[177] E. Papirer, P. Horny, H. Balard, R. Anthore, C. Petipas, A. Martinet, *J. Colloid Interface Sci.* **1983**, *94*, 220–228.

[178] K. S.Suslick, S.-B.Choe, A. A. Cichowlas, M. W. Grinstaff, *Nature* **1991**, *353*, 414–416.

[179] K. S. Suslick, M. Fang, T. Hyeon, *J. Am. Chem. Soc.* **1996**, *118*, 11960–11961.

[180] K. S. Suslick, T. Hyeon, M. Fang, *Chem. Mater.* **1996**, *8*, 2172–2179.

[181] T. Hyeon, M. Fang, K. S. Suslick, *J. Am. Chem. Soc.* **1996**, *118*, 5492–5493.

[182] J.-I. Park, J. Cheon, *J. Am. Chem. Soc.* **2001**, *123*, 5743–5746.

[183] G. H. Lee, S. H. Huh, H. I. Jung, *J. Mol. Struct.* **1998**, *440*, 141–145.

[184] S. Sun, C. B. Murray, D. Weller, L. Folks, A. Moser, *Science* **2000**, *287*, 1989–1991.

[185] V. F. Puntes, K. M. Krishnan, A. P. Alivisatos, *Appl. Phys. Lett.* **2001**, *78*, 2187–2189.

[186] V. F. Puntes, P. Gorostiza, D. M. Aruguete, N. G. Bastus, A. P. Alivisatos, *Nat. Mater.* **2004**, *3*, 263–268.

[187] E. V.Shevchenko, D. V.Talapin, A. L. Rogach, A. Kornowski, M. Haase, H. Weller, *J. Am. Chem. Soc.* **2002**, *124*, 11480–11485.

[188] M. Rutnakornpituk, M. S. Thompson, L. A. Harris, K. E. Farmer, A. R. Esker, J. S. Riffle, J. Connolly, T. G. St. Pierre, *Polymer* **2002**, *43*, 2337–2348.

[189] H. Bönnemann, W. Brijoux, R. Brinkmann, N. Matoussevitch, N. Waldöfner, N. Palina, H. Modrow, *Inorg. Chim. Acta* **2003**, *350*, 617–624.

[190] N. Matoussevitch, A. Gorschinski, W. Habicht, J. Bolle, E. Dinjus, H. Bönnemann, S. Behrens, *J. Magn. Magn. Mater.* **2001**, *311*, 92–96.

[191] H. Zhang, N. Du, P. Wu, B. Chen, D. Yang, *Nanotechnology* **2008**, *19*, 315604/1–315604/6.

[192] A. H. Lu, E. L.Salabas, F. Schüth*, Angew. Chem. Int. Ed.* **2007**, *46*, 1222–1244.

[193] A. Gedanken, *Ultrason. Sonochem.* **2004**, *11*, 47–55.

[194] R. H. Kodama, *J. Magn. Magn. Mater.* **1999**, *200*, 359–372.

[195] S. Laurent, D. Forge, M. Port, A, Roch, C. Robic, L. V. Elst, R. N. Muller, *Chem. Rev.* **2008**, *108*, 2064–2110.

[196] S.-W. Kim, S. U. Son, S. S. Lee, T. Hyeon, Y. K. Chung, *Chem. Commun.* **2001**, 2212–2213.

[197] M. V. Landau, S. V. Savilov, M. N. Kirikova, N. B. Cherkasov, A. S. Ivanov, V. V. Lunin, Y. Koltypinc, A. Gedanken, *Mendeleev Commun.* **2011**, *21*, 125–128.

[198] X. Ma, L. Liu, N. Aronhime, M. R. Zachariah, *Energy Fuels* **2011**, *25*, 3925–3933.

[199] T. W. Chamberlain, T. Zoberbier, J. Biskupek, A. Botos, U. Kaiser, A. N. Khlobystov, *Chem. Sci.* **2012**, *3*, 1919–1924.

[200] T. W. Chamberlain, J. H. Earley, D. P. Anderson, A. N. Khlobystova, R. A. Bourne, *Chem. Commun.* **2014**, *50*, 5200–5202.

[201] S. Cao, Y. Chen, C.-C. Hou, X.-J. Lva, W.-F. Fu, *J. Mater. Chem. A.* **2015**, *3*, 6096–6101.

[202] S. Cao, Y. Chen, C. J. Wang, P. He, W. F. Fu, *Chem.Commun.* **2014**, *50*, 10427–10429.

[203] J. He, Y. Zhang, E. Y.-X. Chen, *ChemSusChem* **2013**, *6*, 61–64.

[204] D. Marquardt, Z. Xie, A. Taubert, R. Thomann, C. Janiak, *Dalton Trans.* **2011**, *40*, 8290–8293.

[205] J.-M. Andanson, S. Marx, A. Baiker, *Catal. Sci. Technol.* **2012**, *2*, 1403–1409.

[206] D. O. Silva, J. D. Scholten, M. A. Gelesky, S. R. Teixeira, A. C. B. Dos Santos, E. F. Souza-Aguiar, J. Dupont, *ChemSusChem* **2008**, *1*, 291–294.

[207] M. Scariot, D. O. Silva, J. D. Scholten, G. Machado, S. R. Teixeira, M. A. Novak, G. Ebeling, J. Dupont, *Angew. Chem. Int. Ed.* **2008**, *47*, 9075–9078.

[208] S. Behrens, S. Essig, *J. Mater. Chem.* **2012**, *22*, 3811–3816.

[209] C. Vollmer, M. Schröder, Y. Thomann, R. Thomann, C. Janiak, *Appl. Catal. A: General* **2012**, *425-426*, 178–183.

[210] E. Redel, R. Thomann, C. Janiak, *Chem. Commun.* **2008**, 1789–1791.

[211] E. Redel, J. Krämer, R. Thomann, C. Janiak, *J. Organomet. Chem*. **2009**, *694*, 1069–1075.

[212] P. Lignier, in *Topics in Organometallic Chemistry*, *Vol. 51* (Eds.: J. Dupont, L. Kollar) Springer, Heidelberg, **2015**, pp. 55–78.

[213] R. Fernandes, N. Patel, E. Edla, N. Bazzanella, D. C. Kothari, A. Miotello, *Appl. Catal. A: General* **2015**, *495*, 23–29.

[214] N. Cao, W. Luo, G. Cheng, *Int. J. Hydrogen Energy* **2013**, *38*, 11964–11972.

[215] Y. Ma, Y. Huang, Y. Cheng, L. Wang, X. Li, *Appl. Catal. A: General* **2014**, *484*, 154–160.

[216] L. Wang, J. Chen, L. Ge, V. Rudolph, Z. Zhu, *J. Phys. Chem. C.* **2013**, *117*, 4141–4151.

[217] L. Foppa, L. Luza, A. Gua, D. E. Weibel, D. Eberhardt, S. R. Texeira, J. Dupont, *Dalton Trans.* **2015**, *44*, 2827–2834.

[218] S. Schauermann, N. Nilius, S. Shaikhu, H.-J. Freund, *Acc. Chem. Res.* **2013**, *46*, 1673–1681.

[219] P. D. Kent, J. E. Mondloch, R. G. Finke, *J. Am. Chem. Soc.* **2014**, *136*, 1930–1941.

[220] C. N. R. Rao, A. K. Sood, R. Voggu, K. S. Subrahmanyam, *J. Phys. Chem. Lett.* **2010**, *1*, 572–580.

[221] H. P. Boehm, E. Stumpp, *Carbon* **2007**, *45*, 1381–1383.

[222] H. Park, *Mater. Chem. Phys.* **2012**, *133*, 1050–1054.

[223] H. Park, J. S. Kim, B. G. Choi, S. M. Jo, D. Y. Kim, W. H. Hong, S.-Y. Jang, *Carbon* **2010**, *48*, 1325–1330.

[224] Y. Gao, S. Li, B. Zhao, Q. Zhai, A. Lita, N. S. Dalal, H. W. Kroto, S. F. A. Acquah, , *Carbon* **2014**, *77*, 705–709.

[225] G. M. Scheuermann, L. Rumi, P. Steurer, W. Bannwarth, R. Mülhaupt, *J. Am. Chem. Soc.* **2009**, *131*, 8262–8270.

[226] S. Stankovich, D. A. Dikin, G. H. B. Dommett, K. M. Kohlhaas, E. J. Zimney, E. A. Stach,R. D. Piner, S. T. Nguyen, R. S. Ruoff, *Nature* **2006**, *442*, 282–286.

[227] A. K. Geim, K.S. Novoselov, K.S., *Nature Mater.* **2007**, *6*, 183–191.

[228] D. Li, R. B. Kaner, *Science* **2008**, *320*, 1170–1171.

[229] P. Steurer, R. Wissert, R. Thomann, R. Mülhaupt, *Macromol. Rapid Commun.* **2009**, *30*, 316–327.

[230] M. J. McAllister, J. L. Li, D. H. Adamson, H. C. Schniepp, A. A. Abdala, J. Liu, M. Herrera-Alonso, D. L. Milius, R. Car, R. K. Prud'homme, I. A. Aksay, *Chem. Mater.* **2007**, *19*, 4396–4404.

[231] H. C. Schniepp, J. L. Li, M. J. McAllister, H. Sai, M. Herrera-Alonso, D. H. Adamson, R. K. Prud'homme, R. Car, D. A. Saville, I. A. Aksay, *J. Phys. Chem. B* **2006**, *110*, 8535–8539.

[232] D. Haag, H. H. Kung, *Top. Catal* **2014**, *57*, 762–773.

[233] J. Zhu, A. Holmen, D. Chen, *ChemCatChem* **2013**, *5*, 378–401.

[234] Y. Cheng, Y. Fan, Y. Pei, M. Qiao, *Catal. Sci. Technol.* **2015**, *5*, 3903–3916.

[235] G. Goncalves, P. A. A. P. Marques, C. M. Granadeiro, H. I. S. Nogueira, M. K. Singh, J. Grácio, *Chem. Mater.* **2009**, *21*, 4796–4802.

[236] H. B. Li, W. J. Kang, B. J. Xi, Y. Yan, H. Y. Bi, Y. C. Zuhu, Y. T. Qian, *Carbon* **2010**, *48*, 464–469.

[237] D. N. Ventura, R. A. Stone, K. S. Chen, H. H. Hariri, K. A. Riddle, T. J. Fellers, C. S. Yun, G. F. Strouse, H. W. Kroto, S. F. A. Acquah, *Carbon* **2010**, *48*, 987–994.

[238] S. Kudo, T. Maki, K. Miura, K. Mae, *Carbon* **2010**, *48*, 1186–1195.

[239] K. Scholz, J. Scholz, A. J. McQuilla, G. Wagner, O. Klepel, *Carbon* **2010**, *48*, 1788–1798.

[240] Y. H. Kim, Y. T. Kim, H. Kim, D. Lee, *Carbon* **2010**, *48*, 2072–2084.

[241] V. Tzitzios, V. Georgakilas, E. Oikonomou, M. Karakassides, D. Petridis, *Carbon* **2006**, *44*, 848–853.

[242] R. A. Sheldon, *Chem. Commun.* **2008**, 3352–3365.

[243] P. Wasserscheid, T. Welton, in *Ionic Liquid in Synthesis*, *Vol. 1*, Wiley-VCH, Weinheim, **2007**, pp. 325–350.

[244] C. v. Doorslaer, Y. Schellekens, P. Mertens, K. Binnemanns, D. De Vos, *Phys. Chem. Chem. Phys.* **2010**, *12*, 1741–1749.

[245] A. D. Sawant, D. G. Raut, N. B. Darvatkar, M. M. Salunkhe, *Green Chem. Lett. Rev.* **2011**, *4*, 41–54.

[246] D. Astruc in *Nanoparticles and Catalysis*, Wiley-VCH, New York, **2007**.

[247] J. Dupont, R. F. de Souza, P. A. Z. Suarez, *Chem. Rev.* **2002**, *102*, 3667–3692.

[248] P. Mastrorilli, A. Monopoli, M. M. Dell'Anna, M. Latronico, P. Corugno, A. Nacci. in *Topics in Organometallic Chemistry*, *Vol. 51* (Eds.: J. Dupont, L. Kollar), Springer, Heidelberg, **2015**, pp. 237–286.

[249] J. M.Praetorius, C. M. Crudden, *Dalton Trans.* **2008**, 4079–4094.

[250] G. Ertl, H. Knözinger, J. Weitkamp in *Handbook of Heterogenous Catalysis*, *Vol. 9*, Wiley-VCH, Weinheim, **2008**.

[251] D. Martin Alonso, J. Q. Bond, J. A. Dumesic, *Green Chem.* **2010**, *12*, 1493–1513

[252] D. Tilman, R. Socolow, J. A. Foley, J. Hill, E. Larson, L. Lynd, S. Pacala, J. Reilly, T. Searchinger, C. Somerville, R. Williams, *Science* **2009**, *325*, 270–271.

[253] G.W. Huber, S. Iborra, A. Corma, *Chem. Rev.* **2006**, *106*, 4044–4098.

[254] A. Corma, S. Iborra, A. Velty, *Chem.Rev.* **2007**, *107*, 2411–2502.

[255] A. J. Ragauskas, C. K. Williams, B. H. Davison, G. Britovsek, J. Cairney, C. A. Eckert, W. J. Frederick Jr., J. P. Hallett, D. J. Leak, C. L. Liotta, J. R. Mielenz, R. Murphy, R. Templer, T. Tschaplinski, *Science* **2006**, *311*, 484–489.

[256] R. D. Perlack, L. L.Wright, A. Turhollow, R. L.Graham, B.Stokes, D. C. Erbach in *Biomass as Feedstock for a Bioenergy and Bioproducts Industry: The Technical Feasibility of a Billion-Ton Annual Supply*, Report No. DOE/GO-102995-2135; Oak Ridge National Laboratory: Oak Ridge, TN, **2005**. http://www.osti.gov/bridge.

[257] F. Goudriaan, B. v. d.Beld, F. R. Boerefijn, G. M. Bos, J. E. Naber, S. v. d. Wal, J. A. Zeevalkink in *Progress in Thermochemical Biomass Conversion*, Tyrol, Austria, **2000**.

[258] L. E. Manzer in *Biomass DeriViatiVes: A Sustainable Source of Chemicals*; *National Science Foundation Workshop: Catalysis for Renewables Conversion*,Washington, DC, 2004.

[259] L. E. Manzer, US 2005/0210738 A1, DuPont, **2005**.

[260] Homgren, J. American Chemical Society Annual Meeting, Atlanta, GA (2006).

[261] G. W. Huber, J. N. Chheda, C. J. Barrett, J. A. Dumesic, *Science* **2005**, *300*, 2075–2077.

[262] P. McKendry, *Bioresour. Technol.* **2002***, 83*, 37–46.

[263] T. A. Hsu, M. R. Ladisch, G. T. Tsao, *Chem. Technol.* **1980**, *10*, 315–319.

[264] N. Mosier, C. E. Wyman, B. E. Dale, R. T. Elander, Y. Y. Lee., M. Holtzapple, M. R. Ladisch, *Bioresour. Technol.* **2005**, *96*, 673–686.

[265] F. S. Chakar, A. J. Ragauskas, *Ind. Crops Prod.* **2004**, *20*, 131–141.

[266] A. Aden, T. Foust, *Cellulose* **2009**, *16*, 535–545.

[267] F. Carvalheiro, L. C. Duarte, F. M. Girio, *J. Sci. Ind. Res.* **2008**, *67*, 849–864.

[268] J. Zaldivar, J. Nielsen, L. Olsson, *Appl. Microbiol. Biotechnol.* **2001**, *56*, 17–34.

[269] B. C. Saha, *J. Ind. Microbiol. Biotechnol.* **2003**, *30*, 279–291.

[270] C. E. Wyman, S. R. Decker, M. E. Himmel, J. W. Brady, C. E. Skopec, L. Viikari in *Hydrolysis of cellulose and hemicellulose in Polysaccharides: Structural Diversity and Functional Versatility*, Marcel Dekker INC., New York, **2005**, pp. 995–1033.

[271] R. Rinaldi, F. Schuth, *ChemSusChem.* **2009**, *2*, 1096–1107.

[272] A. T. W. M. Hendriks, G. Zeeman, *Bioresour. Technol.* **2009**, *100*, 10–18.

[273] D. Sutton, B. Kelleher, J. R.H. Ross, *Fuel Process. Technol.* **2001**, *73*, 155–173.

[274] J. D. Holladay, J. Hu, D. L. King, Y. Wang, *Catal.Today* **2009**, *139*, 244–260.

[275] D. Mohan, C. U. Pittman Jr., P. H. Steele, *Energy & Fuels* **2006**, *20*, 848–889.

[276] A. Demirbas, *Prog. Energy Combust. Sci.* **2007**, *33*, 1–18.

[277] A. V. Brigdwater, *Chem. Eng. J.* **2003**, *91*, 87–102.

[278] D. Lai, L. Deng, Q.-X. Guo, Y. Fu, *Energy Environ. Sci.* **2011**, *4*, 3552–3557.

[279] M. Mascal, S. Dutta, I. Gandarias, *Angew. Chem. Int. Ed.* **2014**, *53*, 1854–1857.

[280] Y. Yu, X. Lou, H. Wu, *Energy Fuels* **2008**, *22*, 46–60.

[281] F. Guo, Z. Fang, C. Charles Xub, R. L. Smith Jr, *Prog. Energy Combust. Sci* **2012**, *38*, 672–690.

[282] D. J. Hayes, S. Fitzpatrick, M. H. B. Hayes, J. R. H. Ross in *Biorefineries: Industrial Processes and Products*, *Vol. 1* (Eds.: B. Kamm, P. R. Gruber, M. Kamm) Wiley–VCH, Weinheim, **2006**, pp. 139–164.

[283] B. Girisuta, L. P. B. M. Janssen, H. J Heeres, *Chem. Eng. Res. Des.* **2006**, *84*, 339–349.

[284] A. M. Raspolli Galletti, C. Antonetti, E. Ribechini, M. Perla Colombini, N. N. o Di Nasso, E. Bonari, *Appl. Energy* **2013**, *102*, 157–162.

[285] I. T. Horvath, H. Mehdi, V. Fabos, L. Boda, L.T. Mika, *Green Chem.* **2008**, *10*, 238–242.

[286] J.-P. Lange, E. v. d. Heide, J. v. Buijtenen, R. Price, *ChemSusChem* **2012**, *5*, 150–166.

[287] M. S. Holm, S. Saravanamurugan, E. Taarning, *Science* **2010**, *328*, 602–605.

[288] H. Mehdi, V. Fabos, R. Tuba, B. Robert, M. Andrea, T. Laszlo, I. T. Horvath, *Top. Catal.* **2008**, *48*,49–54.

[289] J. C. Serrano-Ruiz, D. Wang, J. A. Dumesic, *Green Chem.* **2010**, *12*, 574–577.

[290] E. L. Kunkes, D. A. Simonetti, R. M. West, J. C. Serrano-Ruiz, C. A. Gärtner, J. A. Dumesic, *Science* **2008**, *322*, 417–421.

[291] D. Martin Alonso, S. G. Wettstein, J. A. Dumesic, *Green Chem.* **2013**, *15*, 584–595.

[292] C. E. Chan-Thaw, M. Marelli, R. Psaro, N. Ravasio, F. Zaccheria, *RSC Adv.* **2013**, *3*, 1302–1306.

[293] I. T. Horvath, V. Fabos, L. T. Mika, PCT Int. Appl., WO 2009136213 A1 20091112, **2009**.

[294] P. P. Upare, J.- M. Lee, D. W. Hwang, S. B. Halligudi, Y. K. Hwang, J.-S. Chang, *J. Ind. Eng. Chem.* **2011**, *17*, 287–292.

[295] Z.-P. Yan, L. Lin, S. Liu, *Energy & Fuels* **2009**, *23*, 3853–3858.

[296] K. Yan, A. Chen, *Fuel* **2014**, *115*, 101–108.

[297] A. M. Hengne, C. V. Rode, *Green Chem.* **2012**, *14*, 1064–1072.

[298] S. G. Wettstein, J. Q. Bond, D. Martin Alonso, H. N. Pham, A. K. Datye, J. A. Dumesic, *Applied Catal., B: Environmental* **2012**, *117–118*, 321–329.

[299] M. Chia, J. A. Dumesic, *Chem. Commun.* **2011**, *47*, 12233–12235.

[300] C. Ortiz-Cervantes, J. J. García, *Inorg. Chim. Acta* **2013**, *397*, 124–128.

[301] I. Podolean, V. Kuncser, N. Gheorghe, D. Macovei, V. I. Parvulescu, S. M. Coman, *Green Chem.* **2013**, *15*, 3077–3082.

[302] K. Yan, C. Jarvis, T. Lafleur, Y. Qiao, X. Xie, *RSC Adv.* **2013**, *3*, 25865–25871.

[303] W. Luo, U. Deka, A. M. Beale, E. R. H. van Eck, P. C. A. Bruijnincx, B. M. Weckhuysen, *J. Catal.* **2013**, *301*, 175–186.

[304] K. Yana, T. Lafleur, G. Wu, J. Liao, C. Ceng, X. Xie, *Applied Catalysis A: General* **2013**, *468*, 52–58.

[305] K. Yan, T. Lafleur, C. Jarvis, G. Wu, *J. Cleaner Prod.* **2014**, *72*, 230–232.

[306] G. Chieffi, C. Giordano, M. Antonietti, D. Esposito, *J. Mater. Chem. A.* **2014**, *2*, 11591–11596.

[307] Y Yang, G. Gao, X. Zhang, F. Li, *ACS Catal.* **2014**, *4*, 1419−1425.

[308] A. Stanislaus, B.H. Cooper, *Catal. Rev.* **1994**, *36*, 75–123.

[309] R. C. Larock, *Comprehensive Organic Transformations*, Wiley-VCH, New-York, **1999**.

[310] D. Marquardt, PhD Thesis, Heinrich-Heine Universität Düsseldorf (Gemany), **2012**.

[311] J. Deng, Y. Wang, T. Pan, Q. Xu, Q.-X. Guo, Y. Fu, *ChemSusChem* **2013**, *6*, 1163 –1167.

[312] A. Primo, P. Concepción, A.Corma, *Chem. Commun.* **2011**, *47*, 3613–3615

[313] K. Kon, W. Onodera, K. Shimizu, Catal. *Sci. Technol.* **2014**, *4*, 3227–3234.

[314] D. Xianlong, L. Yongmei, W. Jianqiang, C. Yong, F. Kangnian, *Chin. J. Catal* **2013**, *34*, 993–1001.